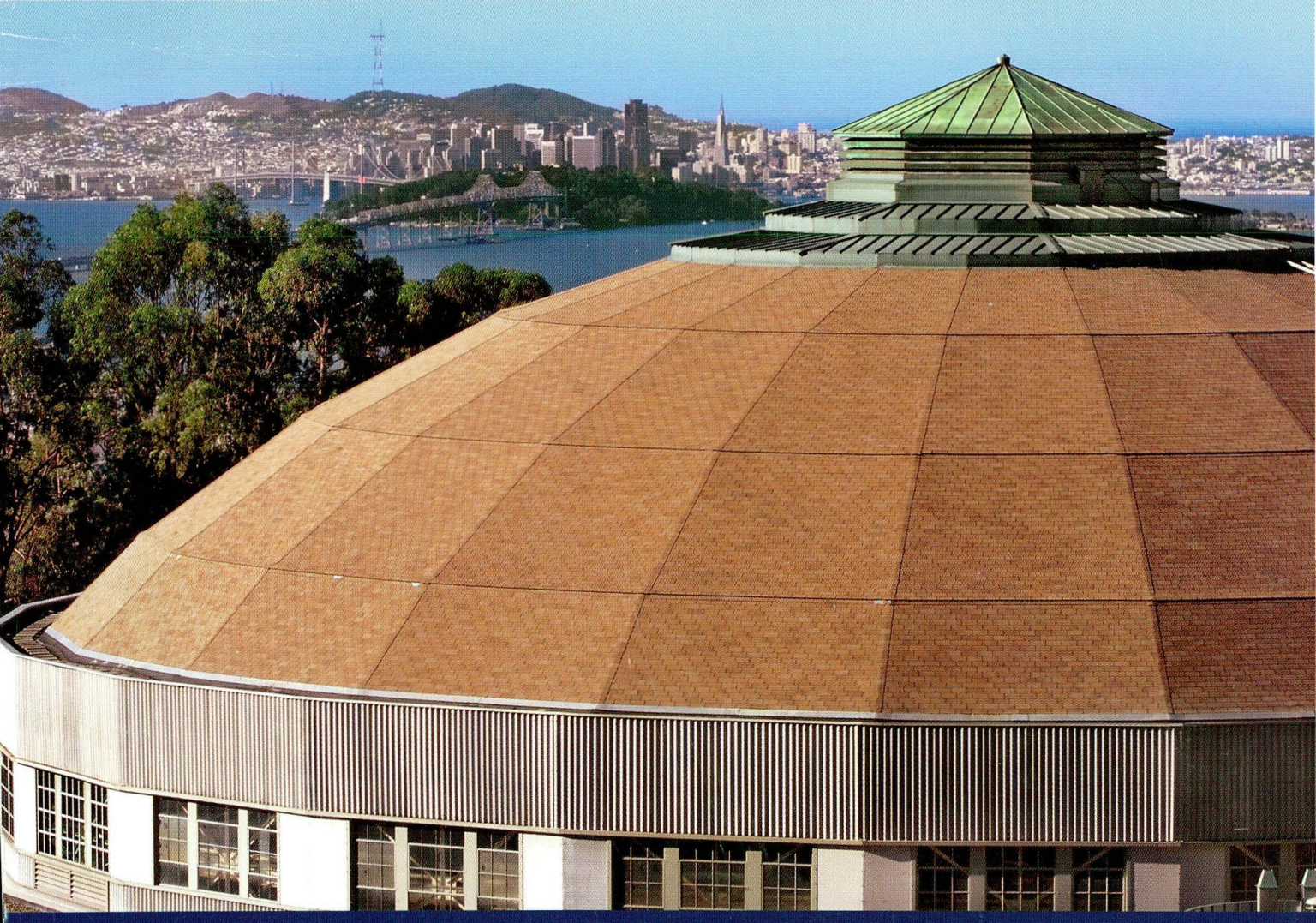

ADVANCED LIGHT SOURCE

ACTIVITY REPORT 2000

April 2001
Ernest Orlando Lawrence Berkeley National Laborato
University of California · Berkeley, California, 9472
LBNL-47783

EDITORS
Annette Greiner
Elizabeth Moxon
Arthur L. Robinson
Lori Tamura

DESIGN, LAYOUT
PHOTOGRAPHY
Berkeley Lab's,
Technical and Electronic Information
Department (TEID) Creative Services

Available to DOE and DOE Contractors from the Office of Scientific and Technical Communication, P.O. Box 62, Oak Ridge, TN 37831. Prices available from (615) 576-8401.

Available to the public from the National Technical Information Service, U.S. Department of Commerce, 5285 Port Royal Road, Springfield, VA 22161.

The editors gratefully acknowledge the ALS users and staff for their contributions, advice, and patience.

DISCLAIMER

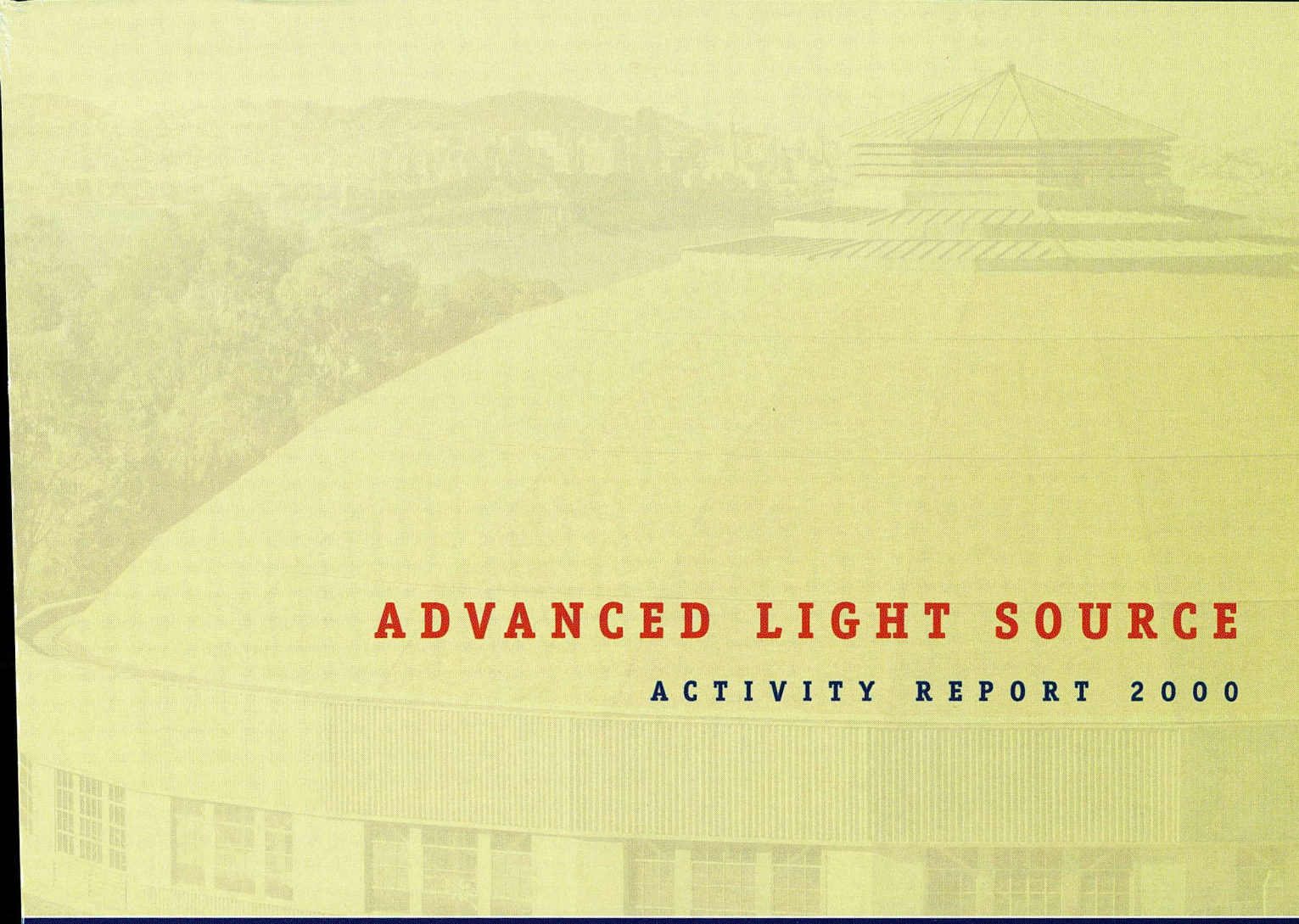

ADVANCED LIGHT SOURCE

ACTIVITY REPORT 2000

This work was supported by the Director, Office of Science, Office of Basic Energy Sciences, Materials Sciences Division, of the U.S. Department of Energy under Contract No. DE-AC03-76SF00098.

April 2001
Ernest Orlando Lawrence Berkeley National Laboratory
University of California · Berkeley, California, 94720
LBNL-47783

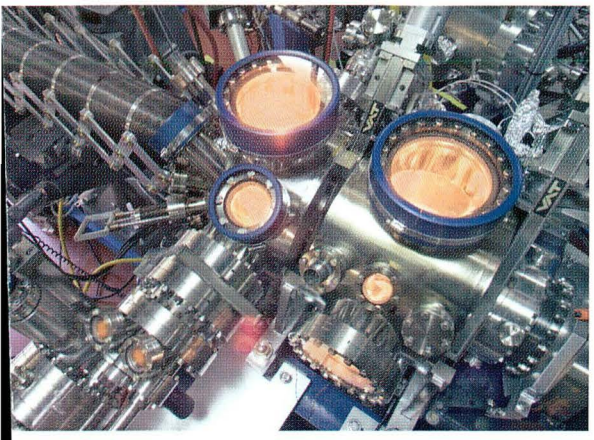

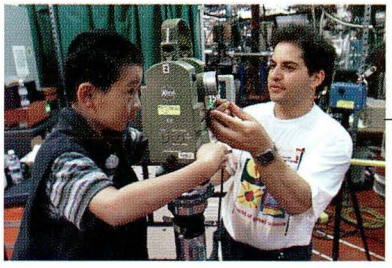

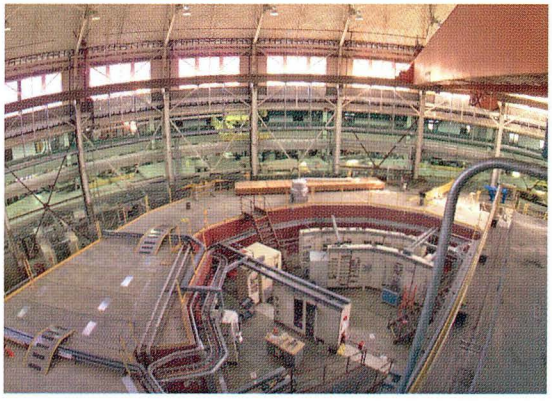

CONTENTS

INTRODUCTION

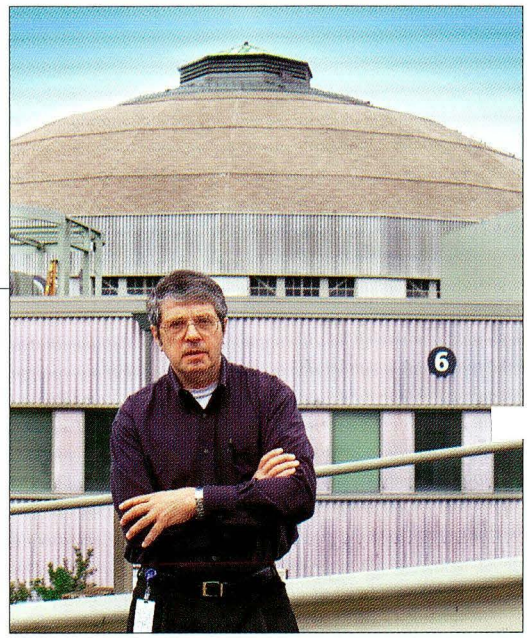

Daniel Chemla
ALS Director

Now that the ALS has passed a series of reviews by the Department of Energy (DOE) and the University of California with flying colors, our challenge is to maintain momentum and avoid complacency. The frequencies of reviews and meetings of the Scientific Advisory Committee are tapering down to a more bearable level, releasing our energies for the implementation of the scientific priorities that have been identified. Through these reviews and consultations with our users, we have formulated an ambitious plan that will keep the ALS at the state of the art for many years to come. Knowing precisely which facilities should be constructed and what new instrumentation should be developed is only a first step. We have now to work with the community and the funding agencies to actually realize this dream. So strategic planning is, and will continue to be, a major activity. As I learned on the streets of Paris in 1968, it is essential to sustain a "permanent revolution."

Our budget situation is much improved, resulting in a significant increase in direct support to our users. This is in recognition of glowing reviews, but none of the improvement would have been possible without the vigorous efforts of the scientific community in making its needs known to Congress. We thank all of you who wrote letters. It definitely made a difference. We are especially indebted to Nora Berrah (Users' Executive Committee Chair for 2000) and Harald Ade (Chair for 2001), who personally went to Washington and spoke directly with members of Congress and their staffers. Once again, we must not drop into complacency. With a new administration in Washington, there is no guarantee that these gains will be remembered. In this Activity Report, you will read of the continuing strong scientific accomplishments of our users, improvements in machine performance, and progress on many construction projects. The Superbend Project (installation of superconducting bend magnets into the storage ring to make more hard-x-ray beams available to users) is well advanced and is on schedule to start operations in late 2001. This development will have a profound effect on life at the ALS, if only in the number and demographics of our users. We have been working closely with Graham Fleming, Director of the Physical Biosciences Division of Berkeley Lab, in the creation of the Berkeley Center for Structural Biology (BCSB), an umbrella organization that will coordinate the activities of the many new protein crystallography beamlines and their interactions with the ALS. I look forward to the development of a world-class program in this strategic area of life sciences.

When wearing my other hat as Director of the Materials Sciences Division of Berkeley Lab, I have been heavily involved with the DOE Office of Basic Energy Sciences plans within the National Nanotechnology Initiative. The centerpiece of the Berkeley Lab part is a proposal to establish the

"Molecular Foundry," a unique, state-of-the-art collaborative research facility for the design, synthesis, and characterization of nanostructures. If funded, this facility will be hosted in a new building just up the hill from the ALS. It will be available to qualified researchers at no charge. We have emphasized the synergistic advantages of proximity to the ALS, including integration with the numerous activities and interests of our users in nanoscale materials and phenomena. The Foundry will provide new and much needed laboratory space for users and will include a new beamline at the ALS. The response from the DOE has so far been very encouraging but, again, we must keep up the pressure.

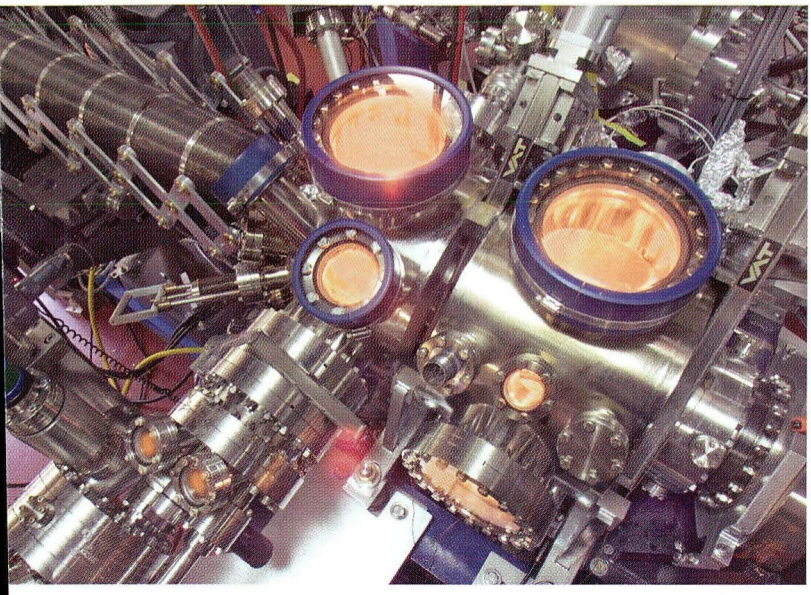

SCIENCE

HIGHLIGHTS

Overview

Neville Smith
Division Deputy for Science

As customary, we offer here a selection of highlights of scientific work done in the past year at the ALS. The number of experiments performed each year is steadily increasing, and yet the size of this volume stays much the same. The selection is therefore becoming progressively more painful, so we are continuing our practice of enlisting the help of the Users' Executive Committee with this delicate task. We also continue to emphasize high-profile-journal quality while maintaining a balance over the various disciplines practiced at the ALS. We trust that you will find the selection interesting. For a more complete sampling, we recommend our Compendium of User Abstracts (see the CD on the inside back cover of this report) and the publication list beginning on page 111.

Because beamtime at the ALS is at a premium, we must also exercise selectivity in determining which studies can be carried out. Proposals from independent investigators—those users who are not part of a Participating Research Team (PRT)—are evaluated for scientific merit by our two Proposal Study Panels (PSPs): the General Sciences PSP and the Macromolecular Crystallography PSP. The work of the PSPs is very important since it directly contributes to the scientific productivity and excellence of the ALS. Using the scientific rankings generated by the PSPs, ALS management works with beamline scientists and PRT members to develop a schedule for beamtime allocation on each beamline. The process has evolved over the years and, with the help of PSP members, we are still refining it.

In 2000, the charter members of the General Sciences PSP, David Ederer, Dennis Lindle, and Piero Pianetta, rotated off after having served five years.

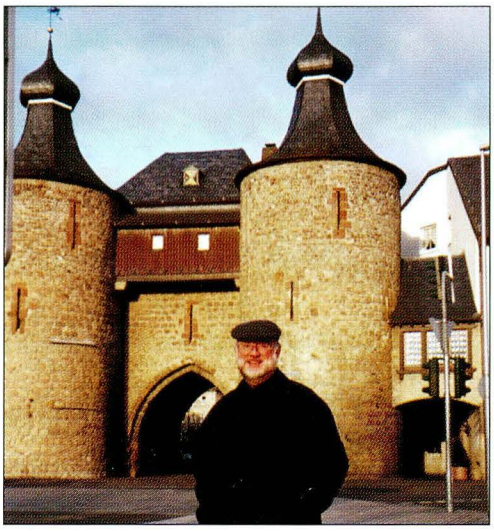

Neville Smith spent a portion of the year at the Forschungszentrum in Jülich, Germany, as a recipient of the Humboldt Research Award for Senior U.S. Scientists. He is shown here at the Hexenturm, or "Witches' Tower."

Back in 1995, we had only a few beamlines and very little independent investigator time to hand out. I chose to approach Dave, Dennis, and Piero for their help for three reasons. First, they had all served as Users' Executive Committee Chair and so were familiar with the ALS. Second, each had served on a very similar panel at the Synchrotron Radiation Center in Wisconsin. Third, they had a range of scientific expertise that covered the independent investigator activities at the ALS at that time. After a couple of years, the panel was expanded to five members and then, in 2000, expanded again to eight members. It is a pleasure on behalf of the ALS to thank Dave, Dennis, and Piero for setting the PSP process in motion and for formulating its basic procedures. Nora Berrah also rotated off in 2000 after a three-year term, and we offer her our thanks as well.

Our Macromolecular Crystallography PSP has three members at present and is ripe for expansion and rotation. The review of the wiggler-based protein crystallography beamline revealed the need for an evaluation and allocation process that is responsive to faster turnaround. We expect to have a modified procedure in place before the new superbend beamlines come into operation. If the work of PSP members thus far is any indication, we can look forward to a still more robust scientific program as we enhance our ability to accommodate users of higher-energy beams.

Complex Materials

The Electronic Structure of Quasicrystals Is Similar to That of Normal Metals

Ever wonder why nobody covers their kitchen floor with only pentagonal tiles? Five-sided tiles can't cover a flat surface without leaving gaps. Ten-sided tiles (decagons) suffer from the same limitation. For similar reasons, until the early 1980s, pentagonal and decagonal crystals were considered structurally impossible, since a crystal was defined as a material with a periodic arrangement of atoms. Imagine the stir, then, when scientists began to see evidence for crystals with such forbidden symmetries. The very definition of a crystal had to change. Now, as scientists begin to directly probe the behavior of electrons in these "quasicrystals," they are again having to reexamine their theories. Their best guesses about electrons in quasicrystals supposed that they would be localized to groups of atoms, but the research reported here demonstrates that at least some of the electrons are delocalized, moving freely through the atomic lattice like electrons in normal metals.

Weirdness. It's the stock in trade of those uncannily regular yet aperiodic alloys known as quasicrystals. Though these materials' intriguing atomic structures have been closely scrutinized since their discovery almost 20 years ago, scientists have only recently taken a solid step toward directly probing their electronic structure. In work carried out at Beamline 7.0.1, we have discovered that the electrons in quasicrystals behave surprisingly like electrons in normal metals. This development runs counter to the most promising theories of how electrons should move in these unpredictable alloys.

Atoms in a quasicrystal, like those in a more familiar crystal, have perfect long-range order. The twist is that the order is not based on a repeating unit cell but on a regular, predictable series of a different type. A one-dimensional analogy can be found in the Fibonacci sequence, where each value is the sum of the two previous values. The resulting series is regular but not periodic. Such rules of order generate crystals with rotational symmetries that, were the crystals periodic, would not allow their unit cells to fill space without overlapping. In spite of the lack of periodicity, these crystals have perfectly sharp diffraction patterns that are as crisp as those imaged for the best ordinary, periodic crystals.

In addition to their bizarre geometries, quasicrystals have counterintuitive properties. For example, though composed of elements that are good conductors in their pure form, they are themselves poor conductors that conduct more poorly as the lattice becomes more perfect. At low temperatures, they have magnetoresistances similar to those observed in giant magnetoresistive materials. Potentially useful properties include durability, stability, low stickiness, and the ability to store hydrogen at high density.

Our experiments focused on an AlNiCo alloy ($Al_{71.8}Ni_{14.8}Co_{13.4}$), a member of the decagonal family of quasicrystals, which is aperiodic in two dimensions and periodic in the third (Figure 1). These crystals have tenfold symmetry in the aperiodic plane. The crystals were analyzed by acquiring a series of angle-resolved photoemission spectra at the Ultra-ESCA endstation. These spectra collectively form an energy–momentum map that looks strikingly like the electronic bandmap of a conventional crystal but with several intriguing aspects. For example, we were able to track a single electronic state in both the aperiodic and periodic directions, showing that the same electronic state in the quasicrystal displayed both periodic and aperiodic character (Figure 2).

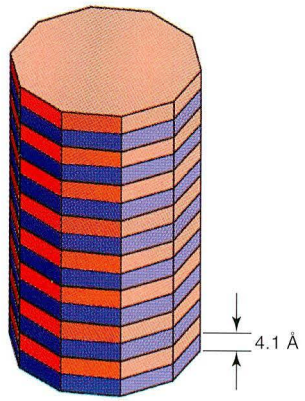

Figure 1 AlNiCo alloy has aperiodic order in two dimensions (axes parallel to the surface studied) and periodic order in the third. The aperiodic plane has tenfold rotational symmetry.

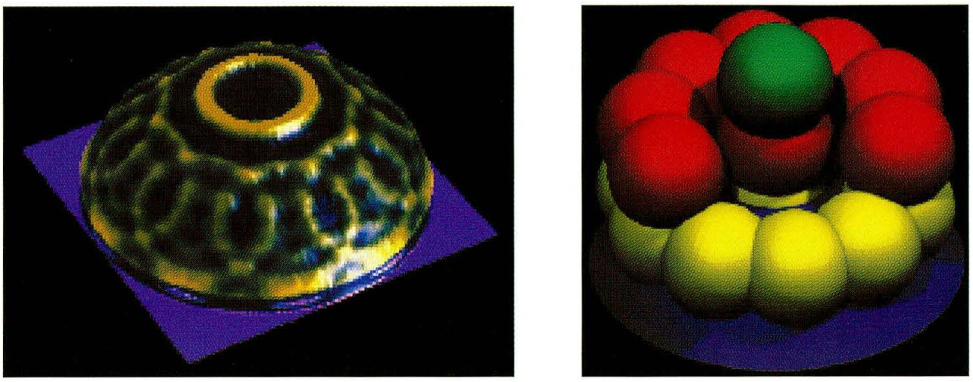

Figure 2 Photoemission data (*left*) showed that the material contains nearly free electrons confined to spheres in momentum space. The model (*right*) based on that data shows that these spheres are arranged in tenfold rings that are stacked periodically, reflecting the mixed periodic/aperiodic quasicrystalline character.

In particular, we noted three important similarities to the band structure of ordinary metals (Figure 3). First, this work shows clear evidence of delocalized states (i.e., the electrons are not all confined to localized groups that move around a small cluster of atomic nuclei, as was predicted). Second, the electrons also have an effective mass (a measure of how difficult it is for an electron to move through the crystal) comparable to a free electron's mass, rather than the nearly infinite mass predicted for electrons in quasicrystals. Finally, we observed that the Fermi surface of a quasicrystal consists of well-defined contours. The topology of the Fermi surface should determine the electron transport properties of the material. That these features are related to the aperiodic order is evidenced by the fact that the band structure reflected the tenfold structure of the aperiodic crystal plane.

These new findings begin to answer the much-asked question of how electrons in quasicrystals move. They showed that electrons behave much more like those in ordinary metals than previously thought.

INVESTIGATORS

E. Rotenberg (ALS), W. Theis (Freie Universität Berlin), K. Horn (Fritz-Haber-Institut, Berlin), and P. Gille (Ludwig-Maximilians-Universität, Munich).

FUNDING

U.S. Department of Energy, Office of Basic Energy Sciences; and Deutsche Forschungsgemeinschaft.

PUBLICATION

1. E. Rotenberg, W. Theis, K. Horn, and P. Gille, "Quasicrystalline valence bands in decagonal AlNiCo," *Nature* **406**, 602 (2000).

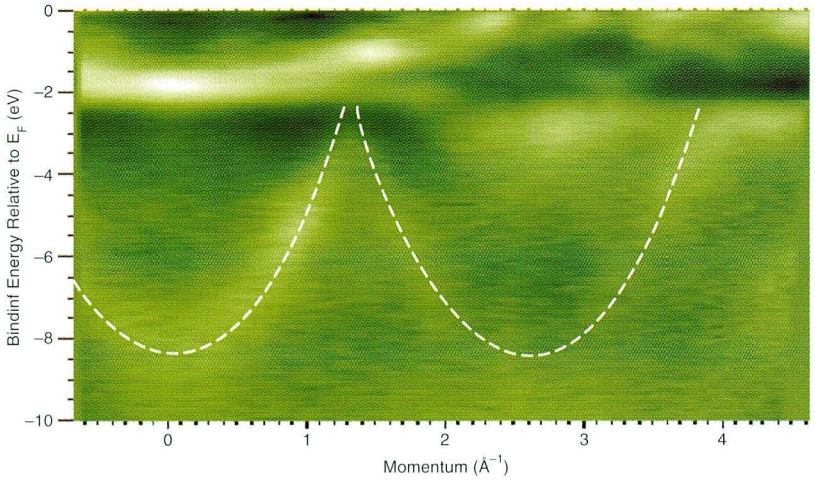

Figure 3 Collecting valence band spectra as a function of electron momentum in the aperiodic plane reveals features that are very similar to those seen in the band structures of ordinary periodic metals: a set of shallow d bands, some of which clearly cross the Fermi level, and a pair of deeper, parabolic s-p bands (*dashed lines*) with free-electron-like character. These bands give strong evidence for the existence of delocalized states in quasicrystals.

Evidence for an Energy Scale for Quasiparticle Dispersion in the High-Temperature Superconductor $Bi_2Sr_2CaCu_2O_8$

Why superconductivity—the resistanceless flow of electricity in certain materials when cooled to a sufficiently low temperature, usually within a few degrees of absolute zero—occurs in metals and alloys is well established. The same cannot be said for "high-temperature" superconductivity, which persists in certain ceramic oxide compounds at temperatures above the boiling point of liquid nitrogen (77 Kelvin), and understanding high-temperature superconductivity remains toward the top of any list of important unsolved problems in condensed-matter physics. The body of the wide variety of research conducted to date, both experiments and theory, supports the contention that the mechanism driving high-temperature superconductivity is quite different from the interaction between electrons and lattice vibrations that causes conventional superconductivity. However, recent research at the ALS suggests that some form of this type of interaction may yet play an important role in resolving the high-temperature superconductivity conundrum.

The mechanism responsible for high-temperature superconductivity remains elusive. In a conventional metal, the observation of spectral features occurring at a characteristic energy (an energy scale) often provides significant insight into physical processes in the material. The most noted example is the observation of phonon anomalies in strong-coupling superconductors such as lead, which had a far-reaching impact on understanding the mechanism of conventional superconductivity. In this highlight, we present evidence from high-resolution angle-resolved photoemission spectroscopy (ARPES) for an energy scale in the high-temperature superconductor $Bi_2Sr_2CaCu_2O_8$.

With its ability to directly measure energy–momentum relationships for electron excitations near the Fermi energy (quasiparticle dispersions) and lifetimes, ARPES provides a unique opportunity to look for energy scales that manifest themselves in the quasiparticle dynamics. We recorded angle-resolved photoemission data at ALS Beamline 10.0.1.1 on two types of $Bi_2Sr_2CaCu_2O_8$: one with a lower concentration of holes than needed for the maximum superconducting transition temperature (T_c) and the other with slightly more, i.e., underdoped (UD) and slightly overdoped (OD), respectively. The single-crystal samples were grown by the floating-zone method and oriented and cleaved in situ at low temperature. The measurements were made at photon energies of 22 eV, 33 eV, and 55 eV. The angular (momentum) resolution of ± 0.1 degrees, which is about an order of magnitude better than in the previous studies of this material, made the results reported here possible.

Figure 4 shows raw ARPES data collected at a photon energy of 33 eV along the (0,0) to (π,π) (nodal) direction across the Brillouin zone boundary in momentum space (see inset) from the OD sample (T_c = 91 K) at 30 K. In Figure 5A, we plot the energy–momentum dispersion determined from numerical fits to the momentum distribution curves (MDCs) obtained from angle scans at a constant binding energy (i.e., horizontal line scans of the photoemission intensity in Figure 4). MDC

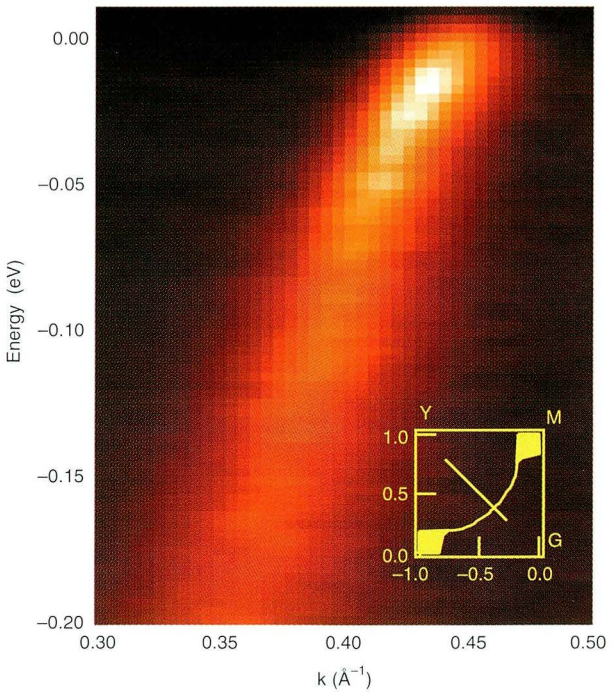

Figure 4 Raw ARPES data showing the photoemission intensity collected along the (0,0) to (π,π) (nodal) direction in momentum space from overdoped $Bi_2Sr_2CaCu_2O_8$ at 30 K and a photon energy of 33 eV. The inset shows the location of the momentum scan in a quadrant of the Brillouin zone.

plots show a peak on a constant background that can be fitted very well with a simple Lorentzian line shape to obtain momentum and energy values, as illustrated in Figure 5B. The data clearly show a feature dispersing towards the Fermi energy ($E = 0$ in the figure) but with an obvious kink in the slope near a binding energy of 50 meV. A similar kink in the dispersion was also observed at photon energies 22 eV and 55 eV. Data for all three photon energies are plotted in Figure 5C.

Figure 6 shows the locations in the two-dimensional Brillouin zone where the kink is experimentally observed by taking data in other directions through momentum space. It demonstrates that the effect is present in all directions and closely follows the Fermi surface. A similar effect is observed for underdoped samples, where the kink in the slope appears to be larger. The effect persists above T_c, where the kink becomes rather broad. Because a calculation of the electronic structure for this material predicts a linear dispersion in this energy range, this result represents an important effect in

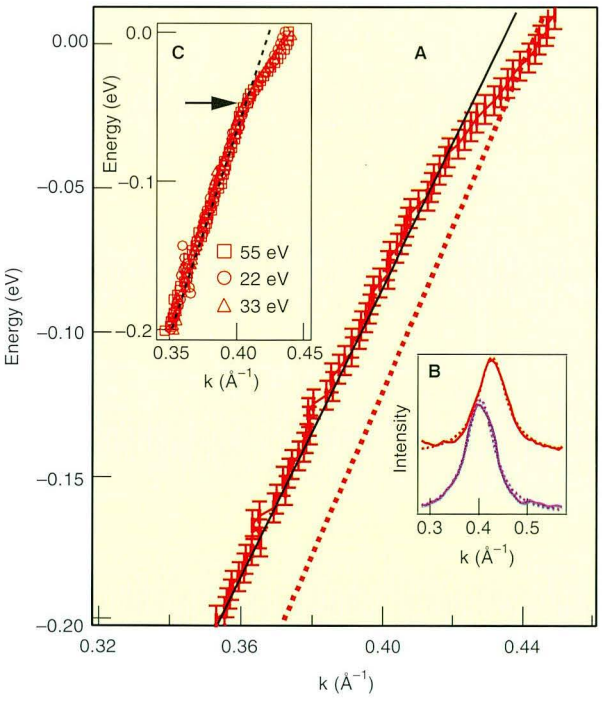

Figure 5 *A*, the energy–momentum dispersion determined from numerical fits to the momentum distribution curves (MDCs) obtained from angle scans at a constant binding energy. The dotted line is the linear dispersion curve predicted by theory. *B*, typical MDCs. *C*, superimposed data from other photon energies shows the same kink in the dispersion curve.

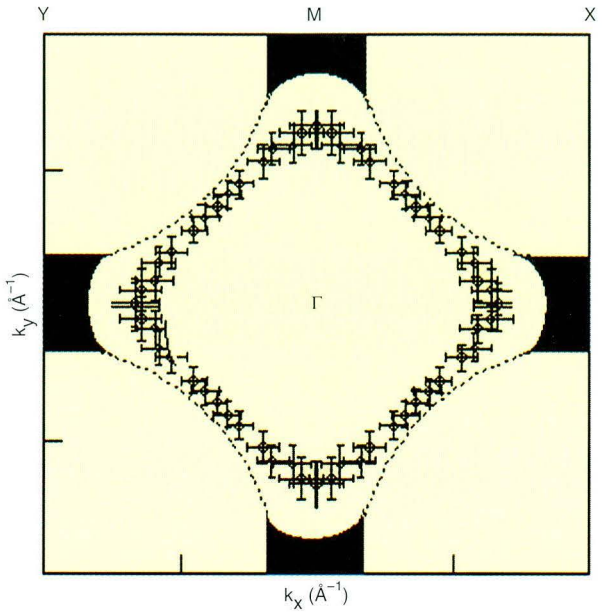

Figure 6 Locations in the two-dimensional Brillouin zone of $Bi_2Sr_2CaCu_2O_8$ where the kink in the quasiparticle dispersion is experimentally observed. Error bars in momentum and energy are determined from the fit uncertainty and energy resolution, respectively. The dashed line is the Fermi surface.

the real part of the quasiparticle self-energy with a scale near 50 ± 15 meV.

Kinks in quasiparticle dispersions are also observed in other high-temperature superconductors. In materials with vastly different transition temperatures and gap sizes, such as $Bi_2Sr_2CaCu_2O_8$, $Bi_2Sr_2CuO_6$, and $La_{2-x}Sr_xCuO_4$, a kink in dispersion occurs at roughly the same energy with comparable slope changes. Universality of the feature in hole-doped materials and its uniformity in momentum space strongly suggest that the observed feature is a signature of a very strong electron–phonon coupling. Direct observation of the kink in the electronic spectra of high-temperature superconductors brings the electron–phonon interaction back as an important player in the high-temperature superconductivity puzzle.

INVESTIGATORS

P. V. Bogdanov, S.A. Kellar, X.J. Zhou, W. Zheng, and Z.X. Shen (Stanford University); A. Lanzara (Stanford University and ALS); E. D. Lu and Z. Hussain (ALS); G. Gu (University of New South Wales, Kensington, Australia); and J.-I. Shimoyama and K. Kishio (University of Tokyo).

FUNDING

National Science Foundation and U.S. Department of Energy, Office of Basic Energy Sciences.

PUBLICATION

1. P.V. Bogdanov et al., "Evidence for an energy scale for quasiparticle dispersion in $Bi_2Sr_2CaCu_2O_8$," *Phys. Rev. Lett.* **85**, 2581 (2000).

Interaction of Copper 3d and Oxygen 2p States in $Mg_{1-x}Cu_xO$ Solid Solutions with the NaCl Structure

One of the important problems of physics is discovering how to increase the transition temperature below which superconductors carry electrical current without any resistance. A superconductor that operated at room temperature rather than today's maximum of 125 Kelvin, for example, would not need refrigeration, thereby making it much more attractive for a wide range of applications from power lines for transmitting electricity to tiny microdevices. One approach to this problem is to study the interaction between copper and oxygen atoms, which seems to underlie the properties of today's high-temperature superconductors, in materials with different arrangements of atoms (crystal structures) in the hope that a new structure might be more conducive to superconductivity. An international group working at the ALS has taken just this approach and discovered that, in at least one case, the crystal structure does not seem to be the dominant factor in the character of the copper–oxygen interaction.

Copper monoxide (CuO) exists in nature with a monoclinic crystal structure. While it has been proposed that CuO with a cubic NaCl structure might be a superconductor with a high transition temperature (T_c), so far it has not been possible to prepare the material in this form. One can test the interaction between copper and oxygen, which plays a key role in determining electronic properties, in the NaCl structure by studying solid solutions of $Mg_{1-x}Cu_xO$, where x is smaller than 0.20. To this end, we present results of x-ray emission (XES) and x-ray photoelectron (XPS) spectroscopy studies that allowed us to investigate copper 3d and oxygen 2p partial states in copper–oxygen bonds. The main differences between CuO and $Mg_{1-x}Cu_xO$ do not appear to be due to the crystal structure.

Solid solutions of $Mg_{1-x}Cu_xO$ ($x = 0.10$, 0.12, 0.15, 0.20) were prepared by a solid-state reaction from powders of MgO and CuO. XES measurements included photon-excited oxygen Kα spectra with a resolution of about 0.3 eV at ALS Beamline 8.0.1 and electron-excited copper Lα spectra. XPS spectra were obtained with monochromatic aluminum Kα radiation.

Figure 7 shows valence-band XPS spectra of $Mg_{1-x}Cu_xO$ (x = 0.10, 0.15, and 0.20) together with copper Lα and oxygen Kα x-ray emission spectra

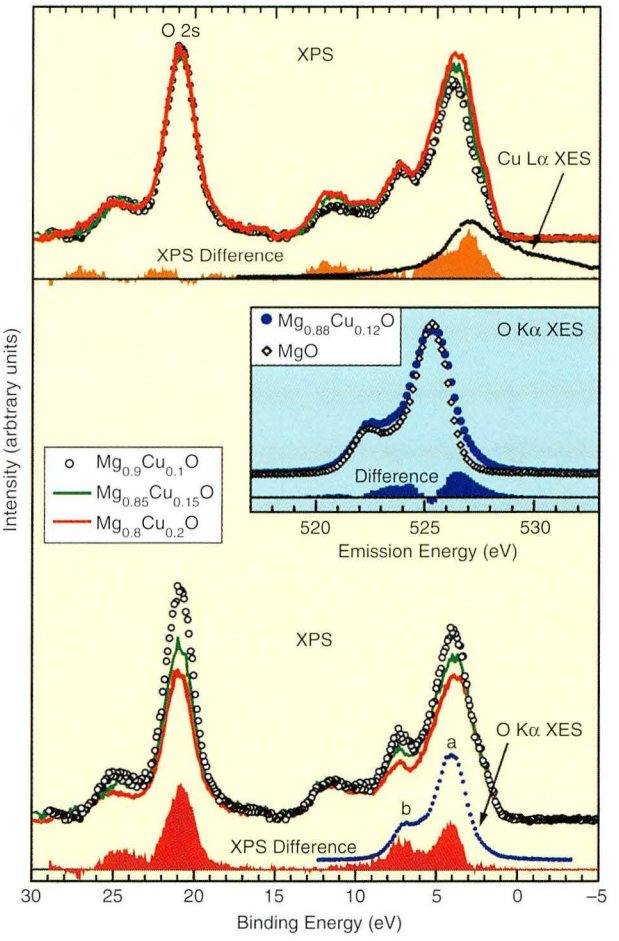

Figure 7 X-ray photoelectron valence-band spectra (XPS) of $Mg_{1-x}Cu_xO$. *Upper panel*, the separation of the copper 3d partial states. The copper L XES spectrum of $Mg_{0.80}Cu_{0.20}O$ is also shown. *Lower panel*, the separation of the oxygen 2p states hybridized with the magnesium 3(s,p,d) states. An oxygen Kα x-ray emission spectrum is also shown. *Inset*, oxygen Kα x-ray emission spectra of $Mg_{0.88}Cu_{0.12}O$ and MgO. The shaded area is the difference spectrum.

for $Mg_{0.88}Cu_{0.12}O$. The spectra in the upper panel are normalized to the oxygen 2s peak. The difference spectrum obtained by subtracting the spectrum of $Mg_{0.90}Cu_{0.10}O$ from that of $Mg_{0.80}Cu_{0.20}O$ should reflect mainly the copper 3d states. The spectra in the lower panel are normalized to the copper 3p peak (not shown). The difference spectrum obtained in the way just described should give information about the oxygen 2p states hybridized with the magnesium 3(s,p,d) states.

The inset in Figure 7 shows the oxygen Kα x-ray emission spectra of MgO and $Mg_{0.88}Cu_{0.12}O$ obtained at an excitation energy of 550 eV to avoid high-energy satellites. The oxygen Kα spectrum for a solid solution of $Mg_{1-x}Cu_xO$ can be regarded as a superposition of the oxygen spectra corresponding to the magnesium–oxygen and copper–oxygen bonds, taken in the ratio of $(1-x):x$. The blue area corresponds to the copper–oxygen bond and was obtained by subtracting the MgO spectrum from that of $Mg_{0.88}Cu_{0.12}O$.

In Figure 8, the difference spectra for $Mg_{1-x}Cu_xO$ reflecting copper 3d states and partial oxygen 2p states of the copper–oxygen bond are compared with XPS (upper panel) and oxygen Kα XES (lower panel) spectra for CuO. The feature A (singlet ^1A) is less pronounced and the maximum B (triplets ^3E, $^3B_1$) is shifted towards the Fermi level compared to the XPS spectrum of CuO. The oxygen 2p difference spectrum exhibits two peaks, a and b, that coincide with those in the oxygen Kα x-ray emission spectrum of CuO. These results show that the crystal structure (the monoclinic structure in CuO or the NaCl structure in $Mg_{1-x}Cu_xO$) does not play a strong role in the electronic structure.

An exchange splitting observed in the copper 3s core-level XPS (not shown) allowed us to find quantitative changes of the strength of the copper–oxygen interaction in $Mg_{1-x}Cu_xO$ in comparison with that in CuO. The degree of covalency and the occupancy of copper 3d states in $Mg_{1-x}Cu_xO$ solid solutions are less than those in CuO (9.2 and 9.3 3d electrons, respectively). The decrease in the interatomic copper–oxygen interaction leads, probably, to a decreasing splitting of the hybridized copper 3d–oxygen 2p valence band and, therefore, to its narrowing (see Figure 8).

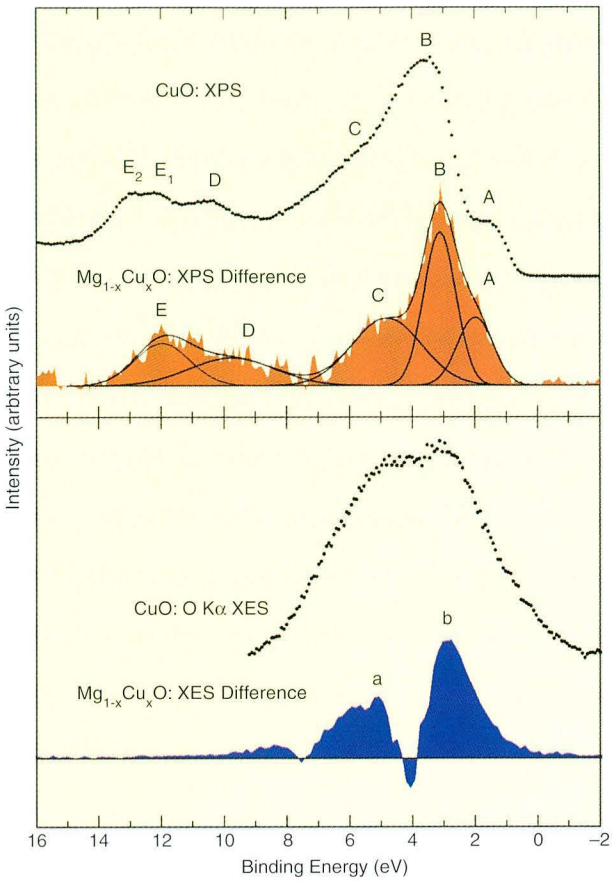

Figure 8 *Upper panel*, x-ray photoelectron valence-band spectrum of CuO and the difference spectrum showing the copper 3d states in $Mg_{1-x}Cu_xO$ solid solutions. *Lower panel*, oxygen Kα x-ray emission spectrum of CuO, and the partial contributions of oxygen 2p states in the copper–oxygen bond in $Mg_{1-x}Cu_xO$ solid solutions.

INVESTIGATORS

V.R. Galakhov and E.Z. Kurmaev (Institute of Metal Physics of the Russian Academy of Sciences, Yekaterinburg, Russia); A. Moewes (University of Saskatchewan, Canada); and M. Demeter, S. Bartkowski, and M. Neumann (University of Osnabrück, Germany).

FUNDING

Russian Science Foundation for Fundamental Research and NATO.

PUBLICATION

1. V.R. Galakhov et al., "Interaction of Cu 3d and O 2p states in $Mg_{1-x}Cu_xO$-solid solutions with the NaCl-structure: X-ray photoelectron and x-ray emission study," *Phys. Rev. B* **62**, 4922 (2000).

Magnetism and Magnetic Materials

Imaging Spin Alignment in Magnetic Layers

At the frontier of advanced magnetic devices are tiny structures comprising multiple layers, each with dimensions measured in nanometers, hence the name magnetic nanostructures. These devices are based on the giant magnetoresistance (GMR) effect, in which an external magnetic field dramatically changes the electric current flowing through the device. In the newest computer disks, the high- and low-current states are used to represent the digital states (0 and 1) in the read head that skims over the disk surface sensing the magnetic fields associated with the stored bits. The magnetic storage industry is developing similar devices as random access memory (RAM) for computers. One of the unsolved puzzles associated with GMR-based devices is a phenomenon called exchange biasing. A team of IBM, ALS, and academic researchers has used an improved x-ray microscope (an x-ray photoemission electron microscope, or PEEM) to directly observe exchange biasing in action, thereby opening the door to a definitive understanding of how this effect works.

Our group has taken a major step toward the solution of a long-standing problem in magnetic multilayers: identifying the mechanism of directional coupling between spins in an antiferromagnet and those in an adjacent ferromagnet. Known as exchange bias, this coupling plays a key role in magnetic devices based on the giant magnetoresistance (GMR) effect. Using the photoemission electron microscope at the ALS (PEEM2), we obtained x-ray magnetic dichroism images that revealed the magnetic structure on both sides of the interface between a thin layer of ferromagnetic cobalt and a layer of antiferromagnetic lanthanum iron oxide ($LaFeO_3$) on which it was grown, as well as local remanent hysteresis loops for individual ferromagnetic domains. The experiments may lead to a definitive understanding of the elusive mechanism of exchange biasing.

Devices based on the GMR effect consist of a sandwich of a nonmagnetic metal layer a few atoms thick between two thin ferromagnetic layers, the bottom layer of which is grown on top of an antiferromagnetic substrate. An external magnetic field can switch the magnetization direction of the outer ferromagnetic layer, but the magnetization of the layer grown on the antiferromagnet is pinned in one position by exchange biasing. The flipping of the magnetization orientation of the two ferromagnetic layers from parallel to antiparallel changes the resistance state of the material from low to high. Although exchange bias is important to a multibillion- dollar industry, the basic physics is not well understood, largely because of the lack of techniques capable of studying in detail the magnetic moments near interfaces.

To attack this problem, our "PEEM team" combined polarized synchrotron radiation from Beamline 7.3.1.1 at the ALS with the new PEEM2 microscope with a spatial resolution as good as 20 nm. For some years, experimenters have been able to image ferromagnetic domains in thin layers by means of x-ray magnetic circular dichroism (XMCD), in which the absorption of circularly polarized x rays depends on the relative orientation of the polarization and the magnetization of the domain, thereby providing magnetic contrast.

Antiferromagnetic materials have typically posed a bigger problem because the alternating orientations of the spins at each atom result in no net magnetic moment. Recently, we showed that use of x-ray magnetic linear dichroism (XMLD) could be employed to image antiferromagnetic domains in $LaFeO_3$. Here the contrast arises at an absorption edge that splits into two peaks (multiplets) with heights that depend in opposite ways on the angle between the x-ray polarization and the antiferromagnetic axis.

Putting it all together, we studied a sample comprising a thin (1.2-nm) cobalt layer on a 40-nm-thick layer of $LaFeO_3$. Owing to the thinness of the

cobalt, electrons emitted from the underlying layer were able to escape, and the magnetic structure on both sides of the interface could be imaged. XMLD images made at the split L_3 edge of iron resulted in a pattern of dark and light areas, according to the orientation of the antiferromagnetic axis (Figure 1). XMCD images made at the $L_{3,2}$ edge of cobalt resulted in a pattern highly correlated with that from $LaFeO_3$ (Figure 2). Horizontally oriented domains, which showed up as light areas in the $LaFeO_3$, appear as gray areas in the cobalt. Vertically oriented domains, which showed up as dark areas in $LaFeO_3$, appear either dark or light in the cobalt, depending upon spin orientation (up or down, respectively).

These results and the local remanent hysteresis loops recorded in individual ferromagnetic domains imply that the alignment of the ferromagnetic spins is determined, domain by domain, by the spin orientation in the antiferromagnetic layer.

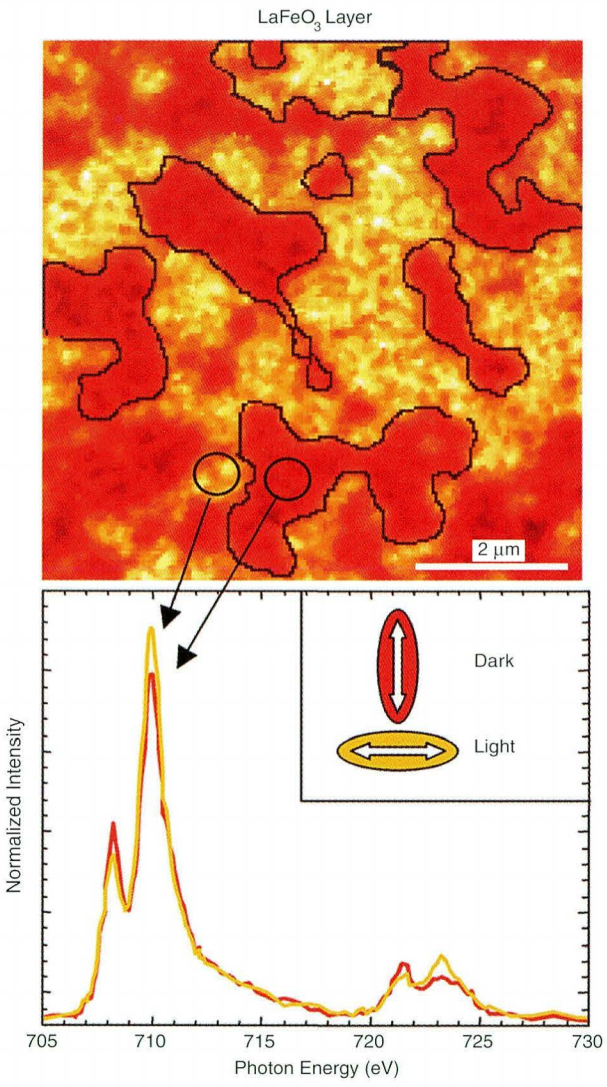

Figure 1 Linear dichroism at iron L_3 edge images antiferromagnetic domains in the $LaFeO_3$ layer. Light and dark orange regions correspond to domains with the projections of the antiferromagnetic axes in the plane of the layer in the vertical and horizontal directions shown by the arrows.

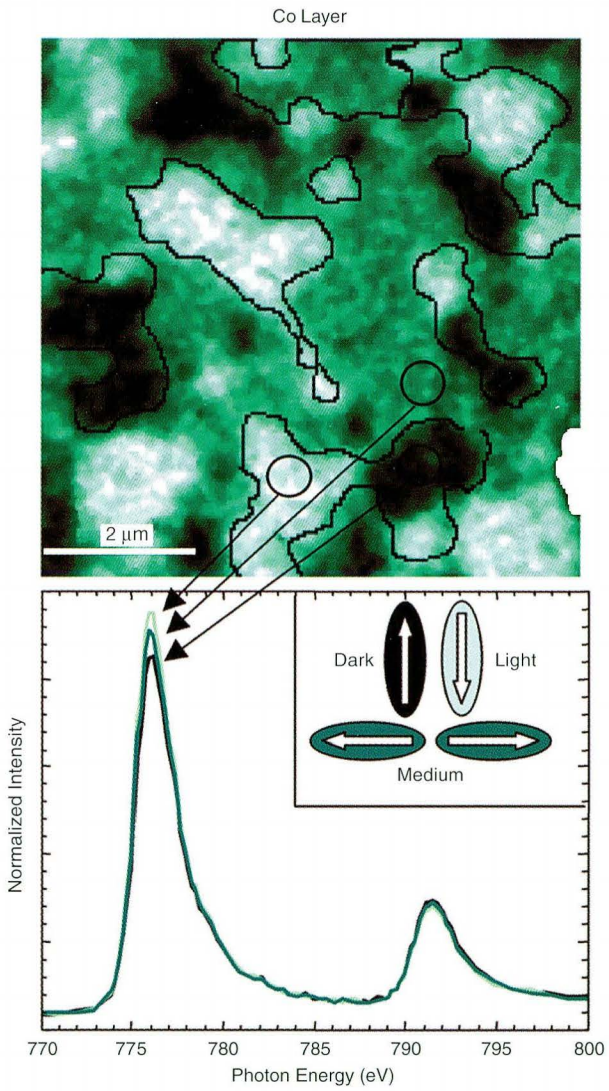

Figure 2 Circular dichroism at cobalt $L_{3,2}$ edge images ferromagnetic domains in the cobalt layer. Light and dark green regions correspond to domains with the magnetization in the down and up vertical directions shown by the arrows. The medium green regions represent domains with the magnetization in the left and right horizontal directions shown by the arrows. In the geometry of the experiment, there is no contrast between left and right horizontally oriented domains.

INVESTIGATORS

F. Nolting, A. Scholl, and H.A. Padmore (ALS); J. Stöhr and J. Lüning (Stanford Synchrotron Radiation Laboratory); S. Anders, E.E. Fullerton, and M.F. Toney (IBM Almaden Research Center); J.W. Seo (University of Neuchâtel and IBM Zürich Research Laboratory); J. Fompeyrine, H. Siegwart, and J.-P. Loquet (IBM Zürich Research Laboratory); and M.R. Scheinfein (Arizona State University).

FUNDING

U.S. Department of Energy, Office of Basic Energy Sciences; and Swiss National Science Foundation.

PUBLICATIONS

1. F. Nolting et al., "Direct observation of the alignment of ferromagnetic spins by antiferromagnetic spins," *Nature* **405**, 767 (2000).
2. A. Scholl et al., "Observation of antiferromagnetic domains in epitaxial thin films," *Science* **287**, 1014 (2000).

Depth-Resolved Study of Magnetization Reversal in Exchange-Coupled Bilayers with the X-Ray Magneto-Optical Kerr Effect (XMOKE)

Pull on a spring and it expands, but as soon as you let go, it bounces back to its normal length. The stretching and springing back is reversible—you can do it over and over again. Scientists studying magnetic materials recently discovered an intriguingly similar behavior in certain structures consisting of two different kinds of magnets, soft and hard. Soft magnets permanently change their magnetization (from North to South, for example) easily just by immersing them in a weak external magnetic field, whereas hard magnets require much larger external fields to change their magnetization. When a thin layer of soft magnet rests on a layer of hard magnet, the magnetization of the soft layer does not permanently change in a weak external field but instead springs back when the field is removed. Researchers from IBM and Berkeley Lab have used the ALS to explore how the hard layer brings about this "exchange-spring" behavior.

There is tremendous interest in exchange-coupled magnetic films that are artificially structured at the atomic level. Such structures not only provide new scientific challenges but are the basis for many of today's magnetic storage devices. One class of coupled films is the exchange-spring magnet comprising a soft magnetic layer that is ferromagnetically coupled to a magnetically hard layer. These films often display reversible magnetic switching, as shown schematically in Figure 3. In small external fields, the magnetization of the soft film is pinned at the interface with the hard layer, but at the surface it is free to rotate to align with the field. The angle of rotation increases with increasing distance from the hard layer, as in a Bloch wall. Because the magnetization will rotate back when the applied field is reduced, this is described as an exchange spring process, in analogy with the elastic motion of a mechanical spring.

This behavior is currently being studied as an approach for designing permanent magnets with energy products that are higher than currently available, tuning the high-frequency response of magnetic devices, and manipulating domain walls

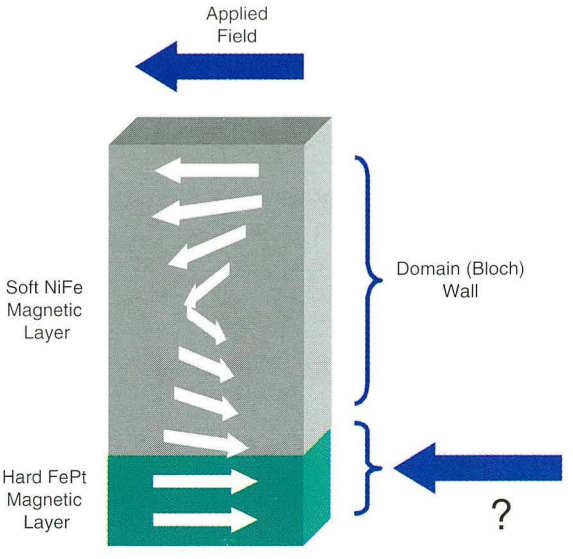

Figure 3 The exchange-spring bilayer system studied consists of a magnetically soft NiFe layer (50 nm thick) grown on top of a magnetically hard, polycrystalline FePt layer (20 nm thick). This magnetization twist in the soft layer is analogous to a Bloch wall, and if the applied field is removed the magnetization in the soft layer will reversibly spring back into alignment with the hard layer. Only for applied fields sufficient to reverse the hard layer does the magnetization of the entire structure switch irreversibly.

in ferromagnetic films. The simple picture in which the soft layer is pinned at the interface with the hard layer can qualitatively describe the low-field magnetic behavior. However, a quantitative understanding depends on the mechanism by which the hard layer is perturbed by the soft layer. For increasing applied fields, a domain wall is thought first to compress against the hard layer and then to propagate into and irreversibly switch the hard layer. Controlled by the microstructure of the hard magnetic layer, this irreversible behavior is not well understood and until now has been difficult to experimentally determine.

To explore in detail the interfacial behavior of exchange-spring magnets, we have developed element-specific soft x-ray magneto-optical techniques to measure the soft and hard layers individually. Recently, we exploited the element specificity of resonant soft x-ray techniques to directly measure the local magnetic response of FePt/NiFe exchange-spring magnets. We inserted 20-Å-thick cobalt marker layers at different depths within the structure (see Figures 4 and 5) and then measured the cobalt magnetization by using the soft x-ray magneto-optical Kerr effect (XMOKE) at the cobalt L_3 resonance at ALS undulator Beamline 8.0.1. XMOKE is an extension of the conventional Kerr effect at visible wavelengths and is made possible by the use of tunable soft x-ray linear polarizers developed at Berkeley Lab. We also measured more traditional hysteresis

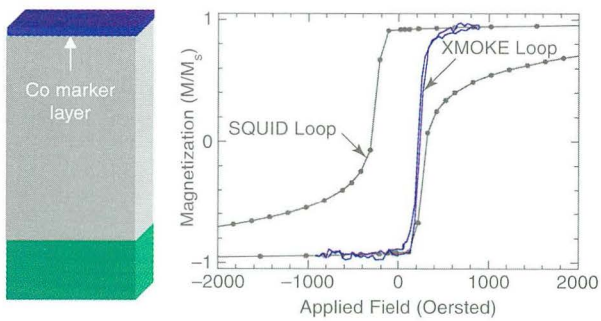

Figure 4 XMOKE loop for the cobalt marker layer at the top of the sample superimposed with the more traditional hysteresis loop that averages over the entire structure. The XMOKE loop is a minor loop in which the applied field is reversed before the entire structure switches irreversibly. This loop shows that the top of the NiFe layer does indeed exhibit nearly completely reversible switching at these low fields. The SQUID loop is a major loop in which the applied field is increased until the magnetization of the entire structure has reversed in both directions.

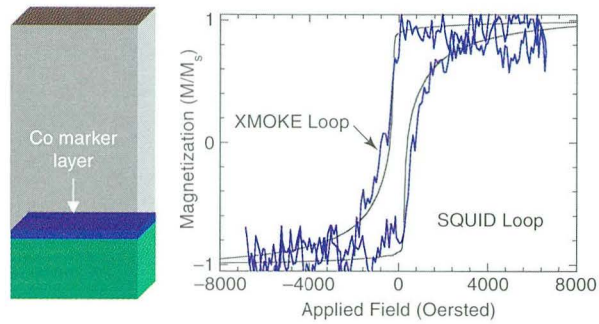

Figure 5 The XMOKE loop for the bottom marker is also a major loop and shows that the interfacial region between the hard and soft layers begins to reverse soon after the top of the soft layer reverses. This means that the top of the hard layer itself switches at very low fields, and that the hard layer stores a significant portion of the reversible exchange-spring energy in this structure as the domain-wall region pushes well into the hard FePt layer.

loops with a superconducting quantum interference device (SQUID) that averages over the entire structure. By comparing XMOKE and SQUID loops, we can understand how different regions of the coupled film respond to applied films.

By monitoring the cobalt XMOKE signal, we locally probe the reversal process. The sample with cobalt at the top of the NiFe layer shows the reversible switching expected for an exchange-spring magnet. The cobalt layer at the FePt/NiFe interface reveals that the twist is not pinned rigidly at the interface but rather propagates significantly into the hard magnetic layer in low fields. As a consequence, the reversible magnetization is not stored only in the soft layer as often assumed. Instead, the results show that the hard layer is an active component of the structure even in weak fields. The results also demonstrate that XMOKE, in conjunction with ultrathin marker layers, provides an effective technique to study depth-resolved magnetic reversal in complex heterostructures.

INVESTIGATORS

O. Hellwig, K. Takano, and E.E. Fullerton (IBM Almaden Research Center) and J.B. Kortright (Berkeley Lab).

FUNDING

U.S. Department of Energy, Office of Basic Energy Sciences.

PUBLICATION

1. O. Hellwig, J.B. Kortright, K. Takano, and E.E. Fullerton, "Switching behavior of Fe-Pt/Ni-Fe exchange-spring films studied by resonant soft x-ray magneto-optical Kerr effect," *Phys. Rev. B* **62**, 11694 (2000).

Oscillatory Decay of Magnetization Induced by Domain-Wall Stray Fields

The silicon microcircuits that power today's computers include memory chips. Different technologies are needed according to the particular attributes desired, such as speed and density. Perhaps the most ubiquitous memory chip today is the dynamic random access memory (DRAM), which is dense and comparatively inexpensive. However, DRAMs do have drawbacks. Based on tiny capacitors that must be regularly recharged, not only do they consume considerable power, but they are volatile: when the power goes out, all the information is lost. Consequently, researchers are turning to a novel nonvolatile memory technology, known as magnetic random access memory (MRAM), based on recent advances in thin-film magnetic structures. So attractive are the features of MRAMs that they have stimulated an outpouring of work. In the research reported here, an IBM/ALS team used several techniques to obtain a surprising explanation for a magnetic failure mechanism of one proposed type of MRAM structure.

With the emergence of magnetoelectronic devices based on magnetic multilayer structures, it has become increasingly important to identify and understand mechanisms leading to the indirect coupling of magnetic layers through thin nonmagnetic spacer layers. Indeed, the most promising structures, which exhibit magneto-tunneling or giant magnetoresistance (GMR) effects, are formed with stacks of magnetic layers, separated by extremely thin (about 1 nm thick) insulating or metallic nonmagnetic spacers. For metallic spacer layers, a spectacular oscillatory interlayer exchange coupling was discovered in the early 1990s, which led to an enormous amount of experimental and theoretical work over the past decade. For insulating spacer layers, such as in magnetic tunnel junctions (MTJs), the same coupling mechanism is not operative. However, the ferromagnetic layers may nevertheless be coupled through magnetostatic interactions. In this work, we address the influence of an unusual magnetostatic coupling associated with the presence of domain walls in the magnetic layers.

We have prepared by dc magnetron sputtering magnetic sandwiches consisting of a magnetically "hard" $Co_{75}Pt_{12}Cr_{13}$ layer (about 5 nm thick), a nonmagnetic chromium spacer (about 1.5 nm thick), and magnetically soft $Co_{84}Fe_{16}$ layer (about 10 nm thick). Since the two magnetic layers have very different coercive fields (about 1.5 kOe and 50 Oe for the hard and soft layers, respectively), it is possible to switch the magnetization of the soft layer in fields (less than 100 Oe) that are much too small to themselves modify the magnetic state of the hard layer. Thus, two magnetically stable states may be obtained at zero applied field, with the magnetization of the two magnetic layers parallel or antiparallel to one another. Thanks to the GMR effect or magnetic tunneling effects, these two states have different resistances, thereby making it possible to use such a structure as a memory cell for MRAMs.

While one might anticipate that the magnetic layers in such hard/soft sandwiches are essentially uncoupled (by suitable choice and thickness of the spacer layer), we discovered that repeated cycling of the soft layer magnetization in moderate fields (much smaller than the hard layer's coercive field) induces the progressive demagnetization of the hard layer. This unexpected behavior is of significant importance for MRAM applications since it would imply that such a device would not endure repeated writing.

The demagnetization process of the hard layer was studied in more detail using a combination of SQUID magnetometry, high-resolution photoemission electron microscopy (PEEM) on ALS Beamline 7.3.1.1, and micromagnetic simulations. PEEM microscopy images, which allowed us to observe magnetic domains at a microscopic scale, were consistent with macroscopic magnetometry results. As the number of cycles was increased, an increasing number of reversed domains nucleated randomly

within the hard layer. Moreover, detailed analysis of the images taken for the first few cycles exhibited a striking oscillating behavior.

The six images shown in Figure 6 present the evolution of the same 5×5 mm^2 area of the sample. While the yellow strands (corresponding to reversed magnetization) progressively expand, some parts of the sample clearly switch back and forth (see for example within the white rectangle). This observation is in excellent agreement with the oscillatory behavior observed at the macroscopic scale by magnetometry. This oscillating behavior was also well reproduced using micromagnetic simulations in which a complex domain wall structure, including vortex-like singularities, develops within the soft layer.

INVESTIGATORS

L. Thomas, J. Lüning, J. Stöhr, and S.S.P. Parkin (IBM Almaden Research Center) and A. Scholl and F. Nolting (ALS).

FUNDING

Defense Advanced Research Projects Agency and Office of Naval Research (Multidisciplinary Research Program of the University Research Initiative); and U.S. Department of Energy, Office of Basic Energy Sciences.

PUBLICATION

1. L. Thomas et al., "Oscillatory decay of magnetization induced by domain-wall stray fields," *Phys. Rev. Lett.* **84**, 3462 (2000).

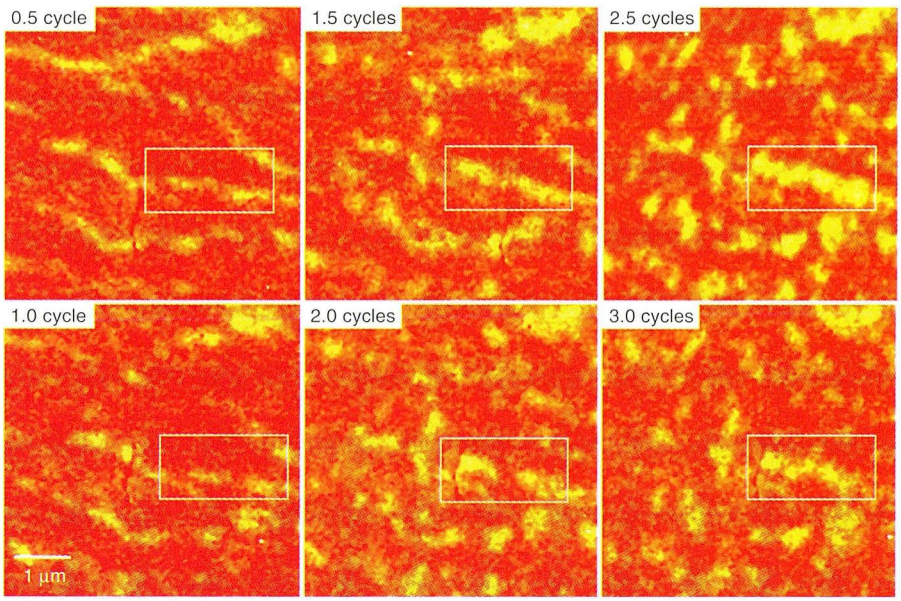

Figure 6 PEEM images showing the magnetization state of the hard layer of a magnetic trilayer consisting of a hard $Co_{75}Pt_{12}Cr_{13}$ layer (5 nm thick), a nonmagnetic chromium spacer (1.5 nm thick), and a soft $Co_{84}Fe_{16}$ layer (10 nm thick). The images illustrate the locally oscillating but progressively decreasing net magnetization in the hard layer as the the soft layer's magnetization is switched back and forth by a small external field.

Polymers, Biomaterials, and Soft Matter

Vibronic Features Seen in Polystyrene NEXAFS Spectrum

The amount of x-ray light a polymer absorbs at different wavelengths reveals surprising detail about the chemistry of the material. In fact, the shape of a plot of these absorptions (an x-ray absorption spectrum) is so characteristic that it is often referred to as a chemical fingerprint. Recent advances in wavelength resolution have improved the sensitivity of x-ray absorption spectroscopy, and now comes evidence that these improvements are bringing another kind of effect into view—vibronic features, caused by vibrations within the polymer molecule. Until now the effect was considered irrelevant for larger molecules, such as complex polymers. But a study conducted by academic researchers at the ALS on polystyrene shows an unambiguous difference between the spectra of two polymers whose only practical difference is the vibration of their atoms. The result is that spectroscopists can now expect the study of vibronic effects to yield new insights into polymer chemistry.

While conducting polymer analyses with the Scanning Transmission X-Ray Microscope (STXM) on Beamline 7.0.1, we have observed a phenomenon not previously considered relevant to the spectra of polymers. Our work has shown that vibronic effects—the combination of electronic and vibrational changes—have a significant effect on the near-edge x-ray absorption fine structure (NEXAFS) spectra of polystyrene. The observation of vibronic features in this polymer suggests that the phenomenon affects spectra of other large, complex molecules. This information will be crucial in interpreting future spectra as finer resolutions make smaller spectral features observable.

Our group came to the ALS after preliminary work at the National Synchrotron Light Source's Beamline X1A. The ALS STXM offered a high photon flux with a resolving power of 5700, enabling us to study subtle differences in the fine structures of polystyrene spectra. In order to isolate the vibronic effect from the chemical shifts known to affect the shapes of NEXAFS peaks, we collected spectra from regular (protonated) polystyrene (H-PS) and polystyrene in which the hydrogen was replaced by deuterium (D-PS). In D-PS, the deuterium atoms that replace the hydrogen atoms differ from the hydrogen atoms in mass only. The mass difference leads to a dramatic change in the C–H stretch energies without introducing a difference in chemical state. These stretches translate to vibronic features in the NEXAFS spectra. Thus, any real differences between the spectra for H-PS and D-PS could be attributed to vibronic effects.

We took advantage of STXM's spatial resolution to provide a control for the inevitable differences between sets of data taken in separate sessions. We mounted two samples, one of H-PS and one of D-PS, on the same sample mount less than one micron apart (Figure 1). We then captured a series

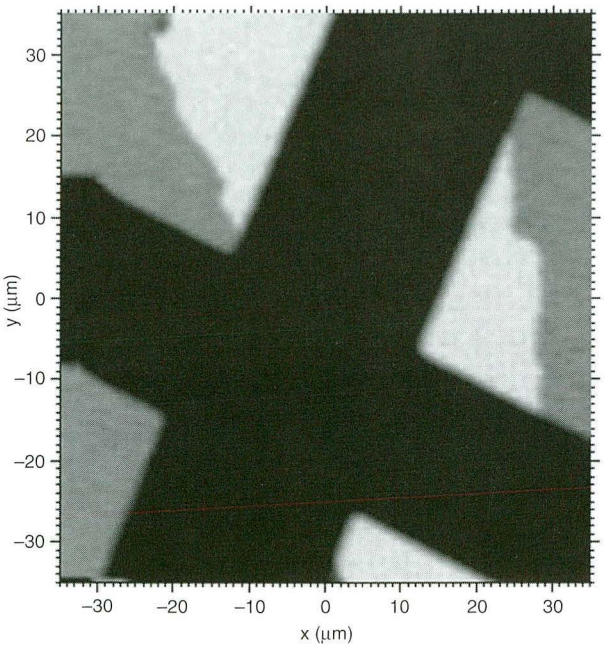

Figure 1 Samples of deuterated polystyrene (D-PS, *left*) and protonated polystyrene (H-PS, *right*) mounted next to each other, as imaged in the scanning transmission x-ray microscope. The black areas are a supporting grid, and the light gray is the area between samples.

of x-ray transmission images of the samples, scanning across a typical range of energies. From this we could measure x-ray transmission and incident photon flux (needed to normalize the data) for both samples at each energy in the scan. By taking the data for both samples concurrently, we minimized low-frequency noise, mechanical drift, and electron beam decay factors and exactly matched the relative energy scales for the two samples.

The resulting carbon 1s spectra for H-PS and D-PS clearly differed (Figure 2). Moreover, the differences between them corresponded well to the vibronic shift seen in previous studies of benzene, which consists of a ring structure that is analogous to that in the repeating unit of polystyrene. Correlations were also seen with vibronic effects in calculated spectra for toluene (an even closer analog to polystyrene's repeating structure). This, together with the much wider peak width seen for the polystyrene spectrum than predicted by chemical shift alone, suggests that vibronic effects have a notable effect on the carbon $1s \rightarrow 1\pi^*$ transition in all aromatic polymers.

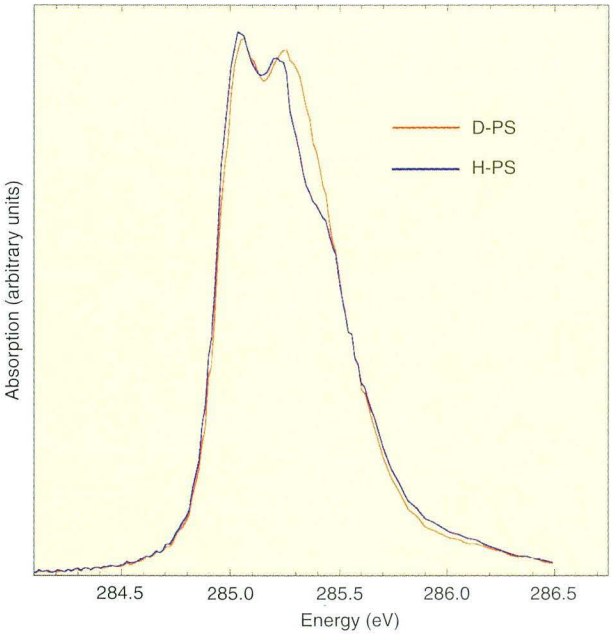

Figure 2 Comparison of high-resolution carbon 1s NEXAFS spectra from H-PS and D-PS, showing a clear shape difference attributable to vibronic effects.

This study is the first to report vibronic effects in the carbon 1s NEXAFS spectrum of a high-molecular-weight polymer. Though current theories of polymer spectroscopy hold that only changes in chemical state are relevant to the spectra of such large molecules, this work has shown clearly that vibronic effects must be considered in these analyses.

INVESTIGATORS

S.G. Urquhart and H. Ade (North Carolina State University) and M. Rafailovich, J.S. Sokolov, and Y. Zhang (State University of New York, Stony Brook).

FUNDING

U.S. Department of Energy, Offices of Basic Energy Sciences and Biological and Environmental Research; and National Science Foundation.

PUBLICATION

1. S.G. Urquhart, H. Ade, M. Rafailovich, J.S. Sokolov, and Y. Zhang, "Chemical and vibronic effects in the high-resolution near-edge x-ray absorption fine structure spectra of polystyrene isotopomers," *Chem. Phys. Lett.* **322**, 412 (2000).

Nanostructures and Semiconductors

Effect of Interfacial Roughness on the Phase of Quantum-Well States in Cu/Co(001) and Cu/Ni(001) Systems

In very thin films only a few atomic layers thick, the surfaces of the film act like the walls of a deep well, confining the electrons to a small volume. Accordingly, the resulting quantum-mechanical electron wave functions, which describe the electrons' behavior, go by the name quantum-well states. Quantum-well states are more than an intriguing curiosity to physicists because they play a key role in controlling the magnetic properties of advanced data-storage and memory devices consisting of multiple thin layers of magnetic and nonmagnetic materials. It was believed that the leading theoretical model explaining how the quantum-well states exert their influence required that the interface (boundary) between magnetic and nonmagnetic layers be atomically smooth. In the work reported here, researchers from the University of California, Berkeley, and the ALS show that the model works even when the interfaces are not so sharp, thereby further clarifying the action of the quantum-well states.

We have been using photoemission to study quantum wells in systems related to the magnetic thin-film structures that exhibit the giant magnetoresistance effect. Comprising magnetic layers separated by a nonmagnetic metallic spacer layer, these structures exhibit an oscillatory interlayer exchange coupling that is at the root of the giant magnetoresistance (GMR) effect. Quantum-well (QW) states have been of intense interest since they were first discovered in metallic thin films and their connection to the oscillatory interlayer magnetic coupling was subsequently revealed.

Currently, the origin of the QW states and its relation to the interlayer coupling are reasonably well understood. For example, QW states in magnetic layered structures can be well described by a phase-accumulation model (PAM) in which the phase is calculated by assuming a perfectly sharp interface. However, real systems invariably possess interfacial roughness due to interlayer mixing of the metallic constituents, a roughness that has until now mostly been ignored. Our goal in these experiments was to study the effects of interfacial roughness on the phase of the QW states, thereby testing the validity of the sharp interface assumption in the PAM. For this purpose, Cu/Co(001) and Cu/Ni(001) systems have been investigated. In sum, we found that the interfacial roughness only decreases the strength of the interlayer coupling but has little effect on the phase of the QW states.

The experiment was carried out on ALS Beamline 7.0.1.2. The small beam size (50–100 μm) and high photon flux ($> 10^{12}$ photons per second at a resolving power of 10^4) enabled our photoemission experiments to be performed with monolayer thickness resolution by moving wedged samples under the beam, because the thickness of the illuminated portion of the wedge is effectively constant. The resulting photoemission patterns (Figure 1) clearly show the periodic modulation of the copper quantum well states as a function of the copper thickness for both the Cu/Co(001) and Cu/Ni(001) systems. Notice that the QW states line up nicely between the two systems, showing that the phases of QW states are the same. Considering that the growth of copper on nickel results in a much rougher interface than copper on cobalt, Figure 1 suggests that the roughness has little effect on the QW phase.

In order to further investigate the role of interfacial mixing on the QW phase, the two systems are capped with three monolayers of cobalt. The two magnetic layers of each system, the top and bottom cobalt layers in the Co/Cu/Co(001) system or the top cobalt layer and the bottom Ni layer in the Co/Cu/Ni(001) system, experience interlayer oscillatory coupling as the thickness varies, which reflects the oscillations of the QW states inside the copper layer imaged in Figure 1. Thus by monitoring the coupling, we can also observe the QW states.

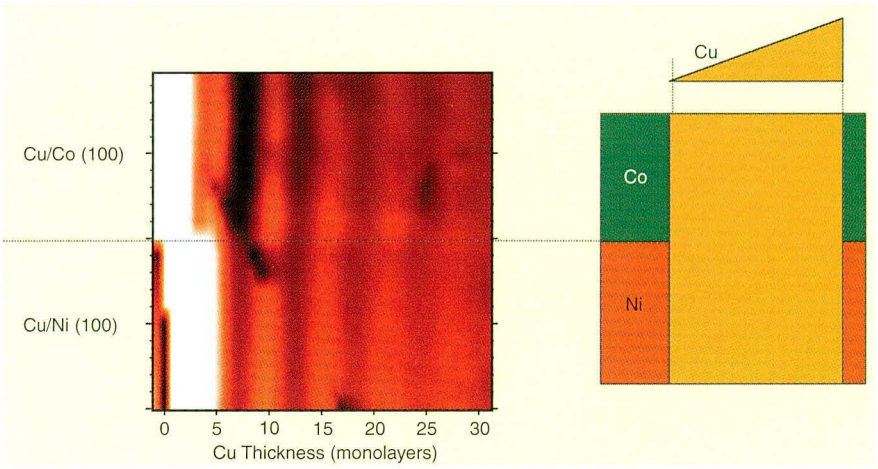

Figure 1 Photoemission measurements of the Cu/Co(001) and Cu/Ni(001) systems show the periodic modulation of the copper quantum-well states as a function of the copper thickness. Notice that the quantum-well peak positions occur at the same copper thickness in both systems, demonstrating that the phases of quantum-well states are the same in both systems.

The samples were then gradually annealed to increase the interlayer mixing while we observed the positions of the coupling peaks or, equivalently, the phase of the QW states. Figure 2 shows the results for the Co/Cu/Ni(001) system. As seen clearly in Figure 2, annealing does not change the antiferromagnetic coupling peak positions, although it does reduce the coupling, as indicated by the disappearance of the peaks. Similar results are obtained in the Co/Cu/Co(001) system.

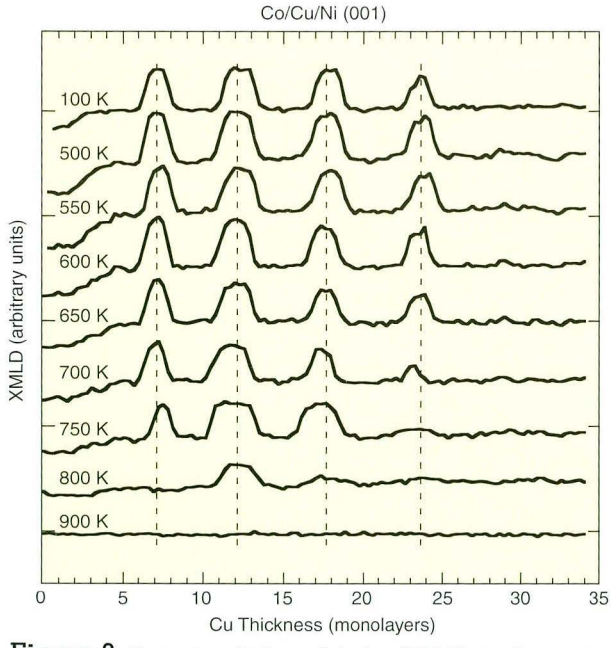

Figure 2 X-ray magnetic linear dichroism (XMLD) coupling measurements after annealing a Co/Cu/Ni(001) trilayer system at various temperatures. While XMLD peaks decrease with increasing annealing temperature, their position as a function of copper thickness remains unchanged, indicating that the phases of the quantum-well states are not affected by the annealing.

Thus one can conclude that in these two systems studied, atomic mixing at the interface does not change the phase of the QW states and can be ignored, thereby validating the sharp interface assumption in the PAM.

INVESTIGATORS

H.J. Choi, R.K. Kawakami, U. Bovensiepen, J.H. Wolfe, and Z.Q. Qiu (University of California, Berkeley) and E. Rotenberg and N.V. Smith (ALS).

FUNDING

U.S. Department of Energy, Office of Basic Energy Sciences; National Science Foundation; and University of California.

PUBLICATION

1. H.J. Choi et al., "Effect of interfacial roughness on the phase of quantum well states in Cu/Co(001) and Cu/Ni(001) systems," *Phys. Rev. B* **62**, 6561 (2000).

Out-Diffusion and Precipitation of Copper in Silicon: An Electrostatic Model

As designers cram ever more transistors onto microcircuit chips, they place a heavy burden on the tiny wires that carry electrical current between the devices. To optimize the current-carrying capacity, circuit designers are turning to copper, which has a higher electrical conductivity than previously used materials. But use of copper has a down side, because individual copper atoms can diffuse into the silicon chip far more easily than before,

especially at the temperatures of several hundred degrees at which some chip-processing steps take place. Whether this is a problem depends critically on where the free-roaming copper atoms migrate. Up to now, analytical techniques to answer this question have been sorely lacking. Now, researchers from Berkeley Lab and the ALS have combined two techniques that, when used together, provided the data needed to construct a model for copper in silicon. The model explains where the copper goes under various conditions.

The introduction of copper interconnects in silicon integrated-circuit technology has drastically increased the danger of unintentional contamination of silicon substrates with copper, since copper has the highest solid solubility in the silicon lattice at high temperatures. While at room temperature the equilibrium concentration of interstitial copper drops to a negligible level, it remains highly mobile. Therefore, the defect reactions of copper do not stop when the wafer is cooled down to room temperature, but proceed towards a thermodynamically stable defect configuration at an appreciable rate. Two major defect reactions of copper are reported in the literature: formation of copper silicide precipitates in the bulk, where it drastically degrades performance, and out-diffusion to the surface, where it is easily removed. However, the conditions under which copper diffuses out to the surface or agglomerates and precipitates in the bulk were unknown.

In our study, we investigated the behavior of copper in silicon by combining two unique experimental techniques, transient ion drift (TID), which measures the interstitial copper concentration by detecting the drift of copper ions as a change of capacitance of a reverse-biased Schottky diode, and high-sensitivity x-ray fluorescence (XRF) analysis, available at ALS Beamline 10.3.1. The high brightness of the x-ray beam combined with an optimized optics design enabled us to achieve a sensitivity level for copper better than 10^{16} cm^{-3}, i.e., in the 10-ppb range. This sensitivity limit is several orders of magnitude better than can be reached with conventional x-ray sources. XRF enabled us to measure the total concentration of copper that remained in the bulk of a sample after out-diffusion was complete, i.e., the copper that had precipitated. This combination of electrical characterization and fluorescence analysis of the same samples allowed us to quantitatively identify for the first time the preferred defect reactions of copper in silicon.

The out-diffusion/precipitation behavior of copper was studied in silicon samples with different boron doping levels and with different starting copper concentrations. The experimental data were compared with our earlier studies of the electrical activity of copper silicide precipitates in n-type silicon. All our observations could be explained by an electrostatic model of copper precipitation in silicon, illustrated in Figure 3. The idea of this model is as follows: interstitial copper is a shallow donor in silicon, which is always positively charged. Copper silicide precipitates form bandlike states in the upper half of the silicon bandgap. These precipitates are amphoteric, so they are positively charged if the Fermi level lies below the electroneutrality level of the precipitates and are negatively charged or neutral if the Fermi level lies above the electroneutrality level.

The position of the Fermi level depends on the temperature, total concentration of shallow donors/acceptors, and interstitial copper concentration. In n-type silicon, where the Fermi level lies close to the conduction band edge, copper precipitates are neutral or negatively charged and electrostatically attract interstitial copper. Consequently, copper easily precipitates in n-type silicon, and its out-diffusion is insignificant. In contrast, in p-type silicon, the Fermi level lies in the lower half of the band gap, if the copper concentration is not too

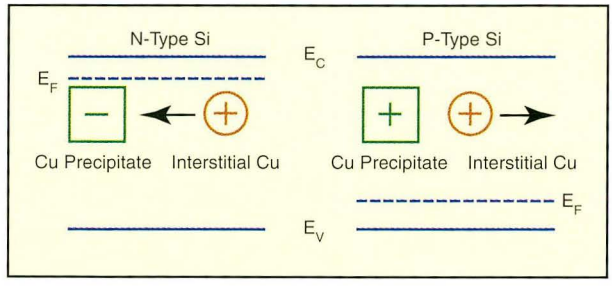

Figure 3 Schematic representation of the electrostatic model of copper precipitation in silicon. In n-type silicon, negatively charged copper silicide precipitates attract positively charged copper interstitials, thereby promoting further copper precipitation. In p-type silicon, the precipates are positively charged, repel the copper interstitials, and promote copper out-diffusion to the surface.

high compared to the doping level. In this case, copper precipitates are positively charged and electrostatically repel interstitial copper. Hence, precipitation is suppressed and out-diffusion of copper to the wafer surface is dominant.

This model is a key to understanding the reaction paths of copper, the major impurity in silicon. This finding is instrumental in predicting the behavior of copper in silicon and in developing techniques for its detection and removal. Additionally, to the best of our knowledge, it is the first demonstration of the significance of electrostatic effects in defect reactions of impurities in silicon.

INVESTIGATORS

C. Flink, H. Feick, W. Seifert, H. Hieslmair, T. Heiser, A.A. Istratov, and E.R. Weber (University of California, Berkeley, and Berkeley Lab), and S.A. McHugo (ALS).

FUNDING

Silicon Wafer Engineering and Defect Science Consortium (SiWEDS), the National Science Foundation, the National Renewable Energy Laboratory (NREL), and the U.S. Department of Energy, Office of Basic Energy Sciences.

PUBLICATIONS

1. A.A. Istratov et al, "Electrical and recombination properties of copper silicide precipitates in silicon," *J.Electrochem. Soc.* **145**, 3889 (1998).
2. C. Flink et al., "Out-diffusion and precipitation of copper in silicon: An electrostatic model," *Phys. Rev. Lett.* **85**, 4900 (2000).

Surface and Interface Science

Coupling between Adsorbate Vibrations and an Electronic Surface State

Electrons at surfaces often have unique features that set them apart from the "bulk," or interior. While in the past it has been both computationally convenient and scientifically fruitful to treat electrons as independent particles, this is not the situation at the frontiers of solid-state physics where exotic effects resulting from the collective action of electrons interacting with each other and with other excitations, such as vibrating atoms, predominate. Combining these two themes, scientists from the ALS and the University of Oregon have shown that the electrons at the surface of tungsten are modified by a strong interaction between the electrons and vibrating hydrogen atoms deposited on the surface. This work demonstrates directly how vibrational energy of surface atoms (and molecules) is dissipated into electronic excitations on a metal, a finding that may benefit those studying catalysis of chemical reactions on surfaces, reactions of considerable industrial import.

For metals at very low temperatures, exotic states (e.g., superconductivity, charge-density waves, and spin-density waves) driven by "many-body" effects replace the ground (lowest energy) state predicted by conventional "one-electron" theory. Since many-body effects are often more prominent in low-dimensional metallic systems, such as two-dimensional surfaces and interfaces, our group has engaged in a continuing series of experiments to explore metal surfaces covered with one atomic layer (monolayer) or less of adsorbate atoms. In our most recent investigation of tungsten covered with one monolayer of hydrogen, we have demonstrated a many-body effect in which there is a strong coupling between the tungsten surface electrons and vibrating hydrogen atoms that splits a surface electronic band.

Metals at room temperature are traditionally described by the one-electron approximation, in which the electrons act independently and have a spectrum of energies and momenta that form energy bands. Among metals, tungsten has a particularly long history as a subject for surface science and therefore provides a well-characterized starting point for the investigation of many-body effects at surfaces by the technique of angle-resolved photoemission (ARPES). With ARPES, researchers can create energy–momentum "maps" of the energy bands for both "bulk" electrons with momenta in three dimensions and surface electrons with momenta in two dimensions parallel to the surface.

In earlier ARPES studies, we discovered that the momenta of electrons at the Fermi energy for two-dimensional energy bands on the (110) surface of tungsten were highly sensitive to the amount of hydrogen on the surfaces. It is one of these surface bands that our new ARPES measurements show is altered by the hydrogen atomic vibrations. In the one-electron model, the creation and destruction of lattice-vibrational quanta (phonons) is a principal mechanism for driving transitions between quantum states as electrons relax or are thermally excited. But in the new experiments, the connection between lattice vibrations and electrons is much more intimate, and it is necessary to think of the two entities forming a composite, many-body system with its own spectrum of energies.

The telltale sign of the electron–phonon interactions involving hydrogen is that the energy for the onset of the band splitting matches the energy of the symmetric hydrogen stretching vibration mode. The electron vacancy (hole) left as a result of photoemission has two possible characters depending on its energy. If the hole energy is sufficiently large, its lifetime is short because it can decay into phonons, whereas holes with energies closer to the Fermi energy cannot decay into real phonons. Instead, these holes are longer lived and carry a cloud of "virtual" phonons that effectively raise the mass of the hole. The hydrogen vibration frequency

sets the energy scale that divides these two characteristic behaviors.

The critical test of this explanation is that substituting deuterium (which is heavier than hydrogen and consequently has a smaller vibrational frequency) for hydrogen decreased the onset energy for band splitting (Figures 1 and 2). Moreover, among the various surface and bulk bands present, only the particular surface band that is most strongly confined to the surface shows a strong electron–phonon coupling effect, evidence that the interaction is confined to the hydrogen surface layer.

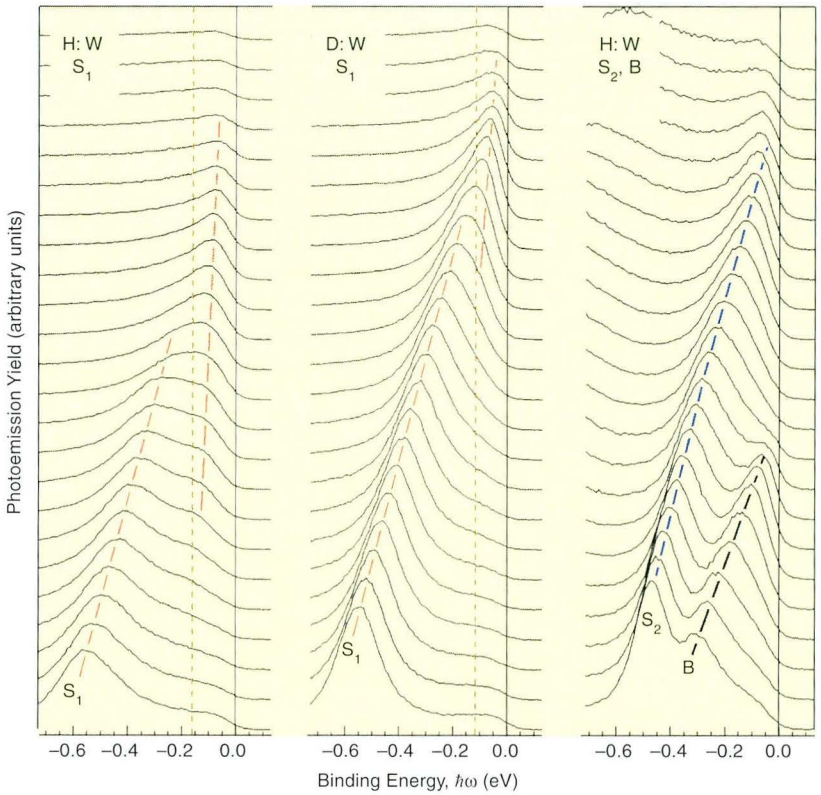

Figure 1 *Left*, for hydrogen on tungsten(110), the splitting of the S_1 surface band near the energy of the symmetric hydrogen stretching mode (*dashed line*) is clearly visible in ARPES spectra. *Center*, on substituting deuterium for hydrogen, the vibrational energy decreases because of the H-D isotope effect, and the splitting becomes smaller. *Right*, in less surface-localized bands (S_2 and B) having poorer overlap to the surface phonon modes, the effects for H disappear altogether.

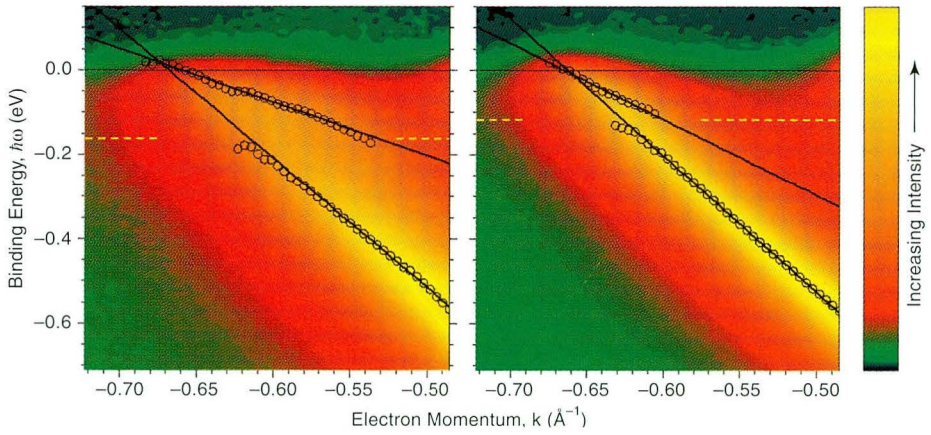

Figure 2 ARPES intensity maps of surface band S_1 in the presence of (*left*) hydrogen and (*right*) deuterium with the fitted positions (*circles*) of the two peaks, the best-fit lines through these data, and the known hydrogen and deuterium symmetric stretch vibrational energies (*horizontal dashed lines*). From the slopes of these lines, one can derive the electron–phonon coupling parameters.

The results have potential practical implications. That electrons and holes can decay to phonons also implies the reverse: that phonons can decay by excitation of electron–hole pairs. This is an important dissipation channel for energy and will affect chemical reactions at surfaces, such as reactions on catalysts. Another interesting implication is the possibility of an electron-phonon-mediated superconductivity that is confined to the surfaces of metals and has a greatly enhanced critical temperature as compared to ordinary superconductors.

INVESTIGATORS

E. Rotenberg (ALS) and J. Schaefer and S.D. Kevan (University of Oregon).

FUNDING

U.S. Department of Energy, Office of Basic Energy Sciences.

PUBLICATION

1. E. Rotenberg, J. Schaefer, and S.D. Kevan "Coupling between adsorbate vibrations and an electronic surface state," *Phys. Rev. Lett.* **84**, 2925 (2000).

How Carbon Monoxide Adsorbs at Different Sites

Surface science is where the rubber hits the road, so to speak. All materials have surfaces, and like a tire that grips or slips depending on its surface properties, a material's surface properties (mechanical, optical, magnetic, electronic, and chemical) determine how it interacts with the outside world. Chemical surface behavior in particular is central to a wide variety of technologies, including the catalytic converters used in cars to reduce carbon monoxide (CO) emissions. Such applications depend on CO adsorption (where the CO molecule attaches to a surface but does not penetrate). In surface science, CO is often used as a prototypical adsorbate because it displays a wide variety of surface behaviors and is relatively easy to study by various methods. In this work, Swedish researchers observed how the electronic orbitals of CO change depending on the adsoption site's geometry, an interaction that is of fundamental importance for understanding many surface phenomena.

Deep within an ideal crystalline solid, every atom has a full complement of neighboring atoms, held in place by chemical bonds in all three dimensions. In contrast, atoms on the two-dimensional surface remain partially unattached, leaving unsaturated bonds that are available for chemical reactions with external substances. An understanding of how simple molecules bond to such surfaces is important for many different fields of science, including heterogeneous catalysis, electrochemistry, biomaterials, and molecular environmental science. A basic question is why molecules preferentially bond to sites with a particular geometry. Our research group has combined x-ray emission spectroscopy experiments on carbon monoxide and *ab initio* electron-density calculations to explore the subtle interplay between the electronic and geometric structures of adsorbates.

Carbon monoxide (CO) is known for its ability to populate different adsorption sites, depending on the substrate, CO coverage, temperature, and influence from coadsorbate species. In this work, we compared the electronic bond structures of CO adsorbed onto a nickel substrate in three different configurations. The objective was to study how the electronic structure of the CO changes when it is brought into direct contact with one, two, and four atoms at the surface (i.e., with increasing coordination with the substrate atoms).

The electronic structure of the CO–nickel complex results from the mixing of the CO electron orbitals with those of the nickel substrate. This hybridization creates new orbitals that can be characterized as having either π or σ symmetry, depending on the shape of the resulting orbitals' electron distribution. A study of how electrons are shared and redistributed upon adsorption of a molecule at different sites requires an experimental method that allows the determination of atom- and symmetry-specific electronic structures. Furthermore, the information from the small number of adsorbed molecules must be separated from the information from the huge number of substrate atoms.

At ALS Beamline 8.0.1, atom-specific valence electrons can be selectively probed by x-ray emission spectroscopy where only the valence electrons in proximity to the core hole localized on either the carbon or oxygen atom participate in the x-ray

decay process (Figure 3). By varying the detection angle of the x rays emitted upon decay, one can distinguish between electron states of π and σ symmetry. The resulting carbon and oxygen K-edge spectra show, most notably, a strong adsorption-induced band (d_π) and different CO molecular states, both with significant intensity variations (Figure 4). From this data, several orbital contour plots were generated (Figures 5 and 6). To compare the experimental results with theory, orbital contour plots were generated based on *ab initio* electron density calculations (using density functional theory). Analysis shows that the σ interaction is repulsive (antibonding) while the π interaction is attractive (bonding) and also weakens the internal CO bond. Both the π and σ interactions increase with higher coordination, but the two contributions partly offset each other.

With this information, we can better understand the rich chemistry of CO adsorbed on metals and the variety of behaviors arising from the different possible adsorption sites. The small differences in adsorption energies previously observed for the different sites had been interpreted as an indication of rather similar bonding. In addition, it was known from vibrational spectroscopy that the CO stretch frequency decreases with increasing coordination

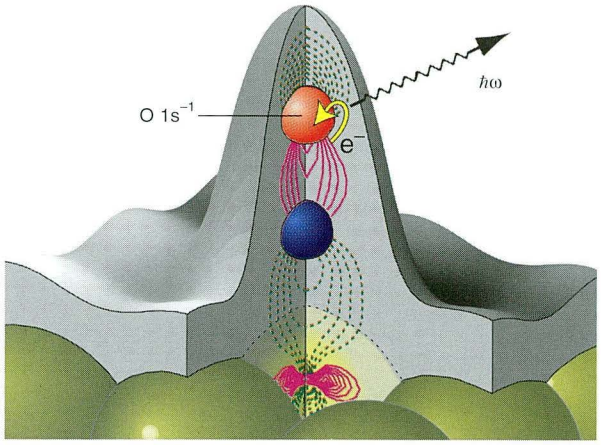

Figure 3 Schematic diagram of the local probe character of selectively excited x-ray emission from CO/Ni. From the total charge density (*gray envelope*), valence electrons with p-angular momentum (*contour lines*) decay into the oxygen 1s core-hole. Because of the core-hole localization, the outgoing x-ray emission gives a measure of the atom-specific projection of the electron density with p-angular momentum. By selective excitation, this projection can be performed around the oxygen or carbon atoms.

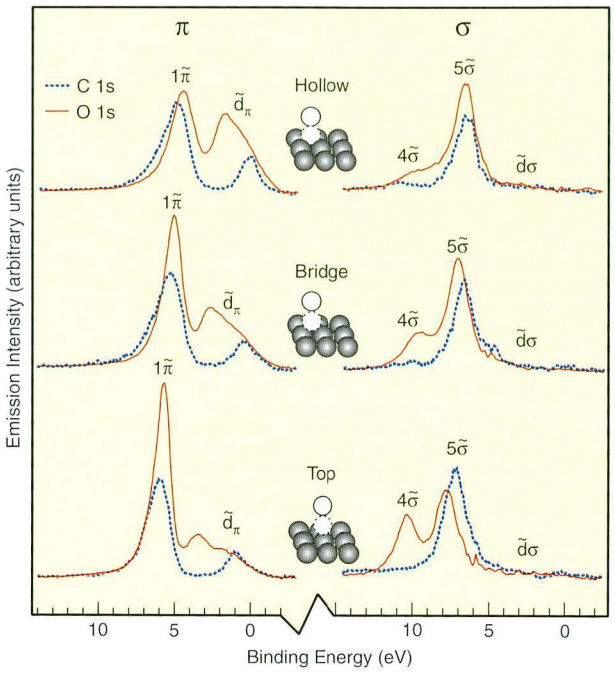

Figure 4 Carbon and oxygen K-edge x-ray emission spectra of CO adsorbed on Ni(100) on top, bridge, and hollow sites. The energy scale is relative to the Fermi level.

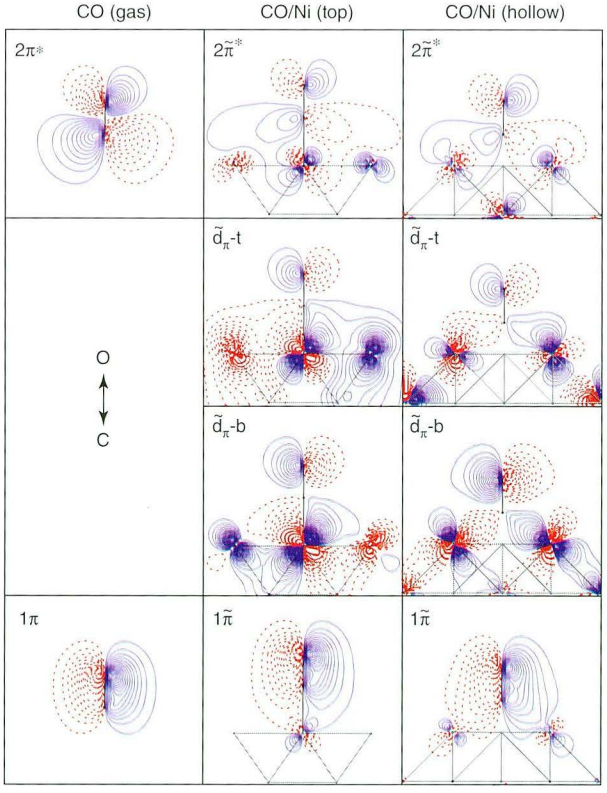

Figure 5 Contour plots of π orbitals for CO in the gas phase and adsorbed on Ni(100) in the top and hollow sites. The strong modifications to the CO orbital structure for different adsorption sites are apparent, in line with the experimental observations.

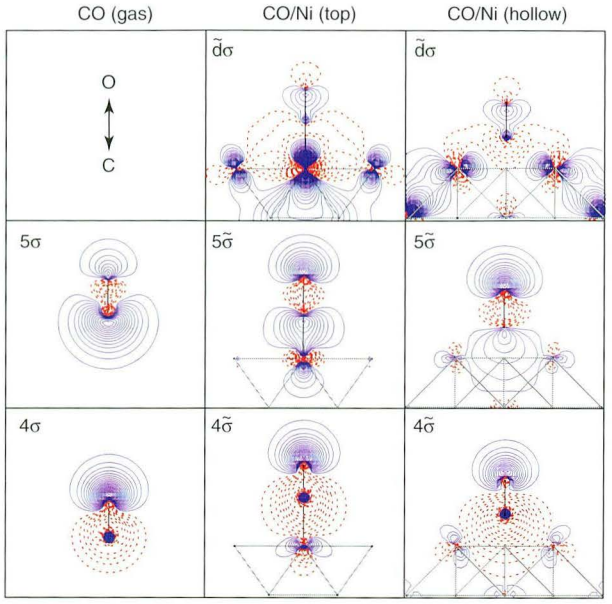

Figure 6 Contour plots of σ orbitals for CO in the gas phase and adsorbed on Ni(100) in the top and hollow sites, again showing strong modifications to the CO orbital structure for different adsorption sites, in line with the experimental observations.

to the substrate. Based on the findings reported here, such phenomena can be understood in terms of the interplay between the π and σ interactions. The π interaction weakens the internal CO bond, decreasing the CO stretch frequency as coordination increases, and the balance between π bonding and σ repulsion leads to small differences in adsorption energies despite very large differences in electronic structure.

INVESTIGATORS

A. Föhlisch, J. Hasselström, O. Karis, P. Bennich, and A. Nilsson (Uppsala University, Sweden) and M. Nyberg, L. Triguero, and L.G.M. Pettersson (University of Stockholm, Sweden).

FUNDING

Swedish Natural Science Research Council (NFR) and the Göran Gustafsson Foundation for Research in Natural Sciences and Medicine.

PUBLICATIONS

1. A. Föhlisch et al., "How carbon monoxide adsorbs in different sites," *Phys. Rev. Lett.* **85**, 3309 (2000).
2. A. Föhlisch et al., "The bonding of CO to metal surfaces," *J. Chem. Phys.* **112**, 1946 (2000).

Photoelectron Diffraction Imaging Reveals a New Bonding Configuration for C_2H_2 and C_2H_4 Chemisorbed on Si(100)

Determining the atomic structure (where the atoms are) of crystalline solids (metals, semiconductors, ceramics, and so on) is comparatively easy with the technique of x-ray diffraction. Solving the same problem for the atoms at a surface is not so easy, in part because the surface structure is only one or a few atomic layers thick, so that the x-ray diffraction signal is weak compared to that from the rest of the sample. Electron techniques have the advantage of being surface sensitive, but interpreting experimental data in terms of atomic positions is extremely challenging. Photoelectron holography is a new method based on the use of electron rather than light waves for directly imaging surface atomic structure. Researchers from Montana State University and their colleagues have used this technique to image the local structure of ethylene and acetylene molecules on a silicon surface and found some surprising results that contradicted the prevailing thinking.

The adsorption of small hydrocarbons on silicon surfaces is of particular interest because of the role that silicon plays in technology. For example, ethylene (C_2H_4) and acetylene (C_2H_2) groups are commonly used to attach larger molecules with specialized functional groups to a silicon surface. It has long been believed that both ethylene and acetylene bond with the same site symmetry to a pair of silicon atoms on the silicon(100) surface via the silicon dangling bonds. The pair of silicon atoms is that formed when the clean silicon (100) surface reconstructs by forming dimer pairs (2×1 reconstruction). Our photoelectron diffraction experiments, however, show that acetylene unexpectedly can bond to four silicon surface atoms, while ethylene, as expected, bonds to two silicon surface atoms.

To image the molecule's site position (symmetry), we inverted carbon 1s photoelectron diffraction oscillations to generate direct real-space images of silicon atoms neighboring the carbon emitters. Ball-and-stick representations of the local atomic structures obtained in this way are shown in Figure 7. We used the photon-energy-scanned, constant-initial-energy spectra (CIS) technique. Representative CIS are shown in Figure 8. The oscillations in the

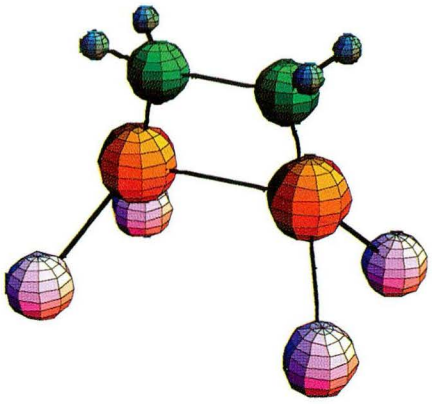

di-σ ethylene/Si(100)-2 × 1

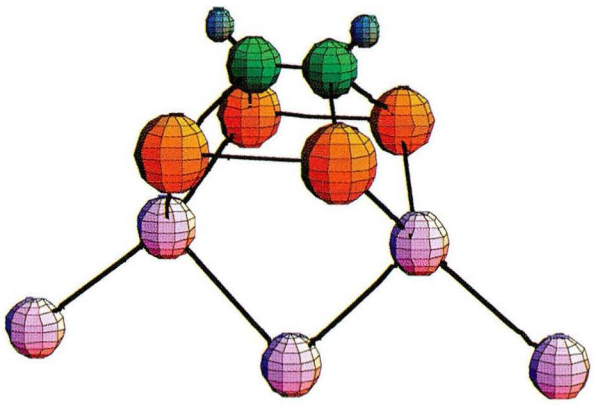

tetra-σ acetylene/Si(100)-2 × 1

Figure 7 Ball-and-stick sketches of the silicon (100) adsorption sites for (*top*) ethylene (C_2H_4) and (*bottom*) acetylene (C_2H_2) obtained by holographically inverting carbon 1s photoelectron diffraction oscillations. Ethylene bonds to two silicon atoms, whereas acetylene unexpectedly bonds to four. The large green balls are carbon atoms, the orange balls are first-layer silicon atoms, and the pink balls are second- and third-layer silicon atoms. The small blue balls represent likely positions for hydrogen atoms.

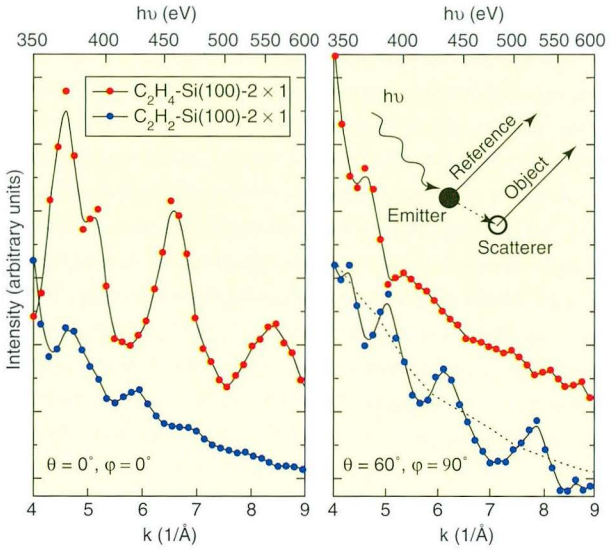

Figure 8 Constant-initial-energy photoelectron diffraction spectra for ethylene and acetylene in two different photoelectron emission directions. The oscillations in the spectra for ethylene and acetylene have different frequencies, already indicating that the adsorption sites are different. The inset illustrates the internal-reference holographic principle in which a photoelectron wave from a carbon emitter atom serves as both the reference wave and, when scattered from a neighboring silicon, the object wave.

photoelectron diffraction spectra for ethylene and acetylene have different frequencies in Figure 8, already indicating that the sites are different.

The inversion is based on the internal-reference-beam holographic principal, where the reference wave and the scattered wave come from the same source, namely, the photoelectron-emitting carbon atoms. Inversion involves a transform first against the set of wave numbers (photon energies) and then the set of directions. The latter organizes the measured beam directions into collections of small cones, which span all directions (small cone method).The holographic-based inversion generates an "image function" represented by an intensity value for every point in space.

The image can be displayed in a number of ways. Choosing gray-scale, horizontal planar cuts through the second layer of silicon atoms, we see immediately that the images are quite different in that ethylene (Figure 9) shows four intense spots centered at a depth 2.8 Å below the carbon emitters, while acetylene (Figure 10) shows only two spots at a depth of 1.6 Å. The distance values may be in error by several tenths of an angstrom. The second-layer spots together with first- and third-layer spots contained in the image function establish the local atomic structure shown in Figure 7.

The image structure and the local atomic structure are not the same. Since each emitting atom sends out its own reference beam, the inversion places all emitters at the same place in the image (the origin). If every emitter has the same site symmetry, the image and the atomic structure are the same, but in these molecules, the two carbon atoms are in inequivalent sites. As a result, both emitters appear at the origin of the composite image, giving the image a kinship to a double-exposed photo. To extract the local structure from the image, one looks

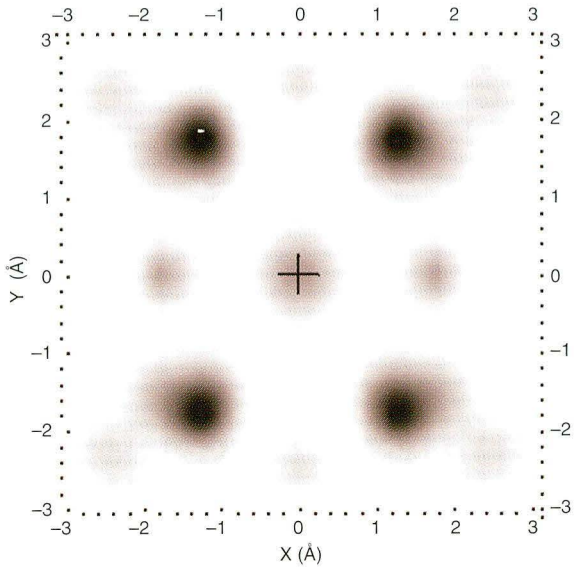

Figure 9 Horizontal, planar cut of the ethylene image function through the second layer of silicon atoms (pink balls in top structure in Figure 7). The image intensity is indicated by the gray scale. The positions of the two carbon emitter atoms are the same in the image, directly above the center of the cut. The value of the stretch in the *X* (dimer) direction needed to make the rectangular into a square pattern is the value for the C–C separation in the actual molecule.

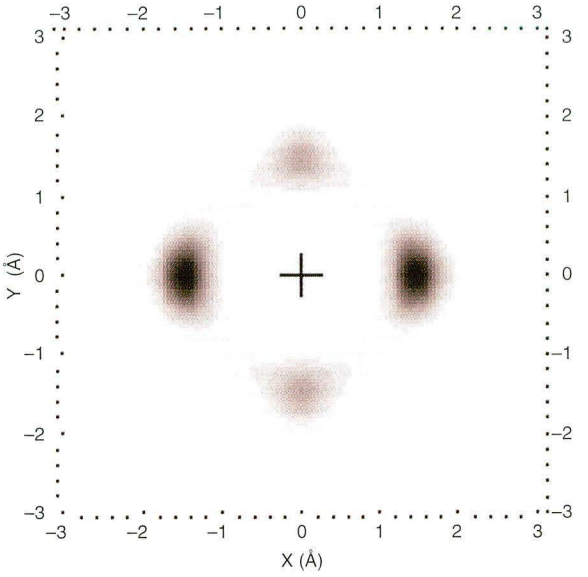

Figure 10 Horizontal, planar cut of the acetylene image function through the second layer of silicon atoms (pink balls in bottom panel of Figure 7). The positions of the carbon emitter atoms in the image are again identical, directly above the center of the cut. To obtain a value for the C–C separation in the actual molecule, it is necessary to examine a planar cut for the third layer of silicon atoms.

for features in the image that can be used to determine the C–C separation.

The square unit cell of a bulk (100) plane is taken to be a reasonable description for the second and third silicon layers after adsorption. For ethylene, notice that the spots in the horizontal cut containing the second-layer silicon atoms form a rectangular pattern (Figure 9). To make the spots into a square, the pattern has to be extended in the *X* direction by a distance 1.4 Å that represents the value of the C–C separation. The value also be used to infer a first-layer Si–Si (dimer) separation of 2.0 Å. For acetylene, a C–C separation of 1.2 Å is found when the third-layer image spots are used for the determination. In neither case does the value of the Si–Si distance suggest that the dimer bond has been severed but rather only modified.

INVESTIGATORS

S.H. Xu, M. Keeffe, Y. Yang, C. Chen, M. Yu, and G.J. Lapeyre (Montana State University); E. Rotenberg and J. Denlinger (ALS); and J.T. Yates, Jr. (University of Pittsburgh).

FUNDING

U.S. Department of Energy, Office of Basic Energy Sciences; Office of Naval Research (DEPSCoR), and National Science Foundation.

PUBLICATION

1. S.H. Xu, et al., "Photoelectron diffraction imaging for C_2H_2 and C_2H_4 chemisorbed on Si(100) reveals a new bonding configuration," *Phys. Rev. Lett.* **84**, 939 (2000).

Environmental and Earth Science

Probing Individual Living Cells with Synchrotron-Based FTIR Spectromicroscopy

Can infrared light from a synchrotron be used to study changes in single, living human cells? If so, it would open up possibilities for the eventual use of synchrotron infrared light in medical diagnostics or environmental health research. Some day, it may be routine to study a tiny sample of tissue from a patient and, by using synchrotron infrared spectroscopy, identify a single cell that has been subtly altered by exposure to a chemical. The two experiments reported here by a Berkeley Lab/ALS team, infrared microscopy studies of human cells throughout their life cycle and of cells exposed to the toxic chemical dioxin, bring this day closer. However, using a scientific technique in a way in which it hasn't been used before calls for verification by comparison with other methods. The strong correlation the researchers observed between infrared and known biochemical techniques shows that the group was indeed measuring real changes associated with the cell cycle and with dioxin.

In this highlight, we first report the use of synchrotron-radiation-based Fourier-transform-infrared (SR-FTIR) spectromicroscopy to observe distinct spectral changes that occur in individual living human lung cells as they progress through the normal cell cycle and finally die. Second, we demonstrate that SR-FTIR spectromicroscopy can be useful for examining dioxin-induced changes in individual living human liver cells, thereby providing new clues about what happens to human cells exposed to dioxins (polychlorinated aromatic hydrocarbons that can cause cancer, birth defects, and altered hormone levels, among other things). For all work, we used the FTIR microscope at ALS Beamline 1.4.3.

For the cell-cycle studies, we used living human lung fibroblast cells that had been placed onto gold-coated glass slides (Figure 1). We found that these cells showed clearly different infrared spectra throughout the cell cycle. Figure 2 shows spectra in the 1800 to 900 cm^{-1} region for typical individual cells in three cell-cycle phases. During the S phase, the DNA is undergoing replication and we observe that the absorption in the DNA/RNA spectral region increases relative to the G1 phase spectra by approximately a factor of two. When a G2/M-phase cell is measured, we observe a large increase in the overall absorbance, as is expected since the cell has roughly doubled in material in preparation for mitosis. Absorption in the DNA/RNA region is significantly increased relative to the protein peaks.

Occasionally some cells exhibited signs of dying or death even though visually the cells' morphology did not appear different. The spectrum of one such cell is shown in Figure 3 along with the spectrum of a normal living G1 phase cell. The "dying" cell shows two characteristic spectral signatures indicative of death. First, the centroids of the protein Amide I and II peaks shift from 1644 to 1633 and from 1542 to 1531 cm^{-1}, respectively, indicating a change in the overall protein conformational states within the cell. Second, we observe the appearance of a peak around 1743 cm^{-1}. These observations can now be used as signatures of cell death in future studies.

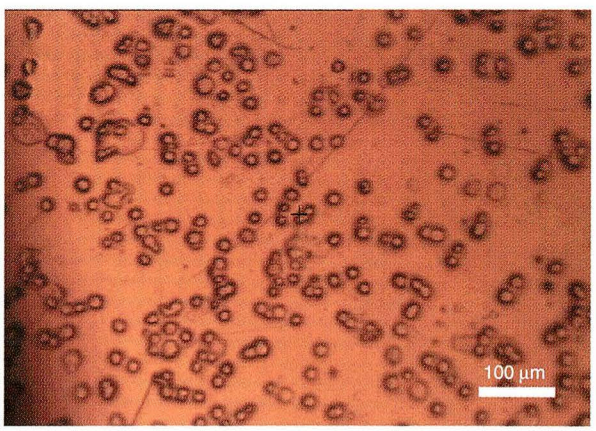

Figure 1 Cells placed on gold-coated slides ready for SR-FTIR analysis. Spot sizes for spectromicroscopy were10 µm or less, allowing study of individual cells.

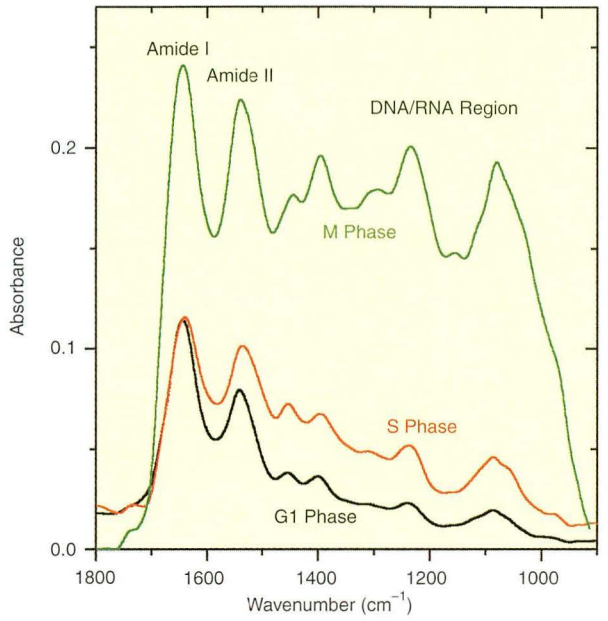

Figure 2 IR spectra in the 1800 to 900 cm^{-1} region for typical individual cells in the gap 1 (G1), synthesis (S), gap 2/Mitosis (G2/M) phases of the cell cycle showing clearly different infrared spectra. Spectra were not normalized, but a linear baseline was subtracted over the range of 2000 to 650 cm^{-1}.

For the dioxin studies, we examined the effects of 2,3,7,8-tetrachlorodibenzo-p-dioxin (TCDD) on liver cells. In the body, particularly in liver cells, TCDD induces increased production of cytochrome P4501A1, which is involved in metabolizing foreign compounds, such as aromatic hydrocarbons. In the study, three experimental groups of human hepatocellular carcinoma (HepG2) cells (cells from a liver tumor) were exposed to TCDD at different concentrations for 20 hours, while cells in a control group were kept in an incubator for 20 hours with no TCDD exposure.

In the mid-IR spectra we recorded, significant absorption differences between the treated samples and the control samples were evident for wavelengths associated with stretching vibrations in two bond types, phosphate and C–H. For phosphate (Figure 4), the intensity for the symmetric stretch band increased relative to that for the asymmetric stretch band with increased TCDD concentration but did not shift in wavelength. The band representing methylene (CH_2) stretch decreased and that

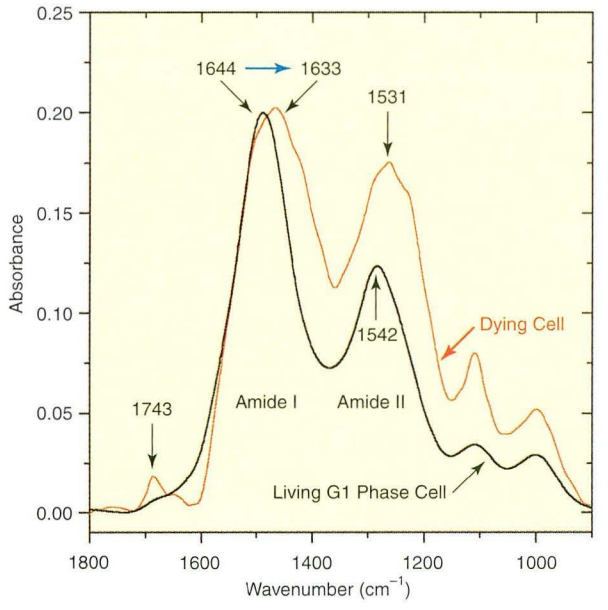

Figure 3 IR spectra comparison of a cell exhibiting signs of dying along with the spectrum of a normal living G1-phase cell. Spectra were normalized to the Amide I peak, and a linear baseline was subtracted from 1800 to 1350 cm^{-1}. Changes in the spectra can now be used as signatures of cell death in future studies.

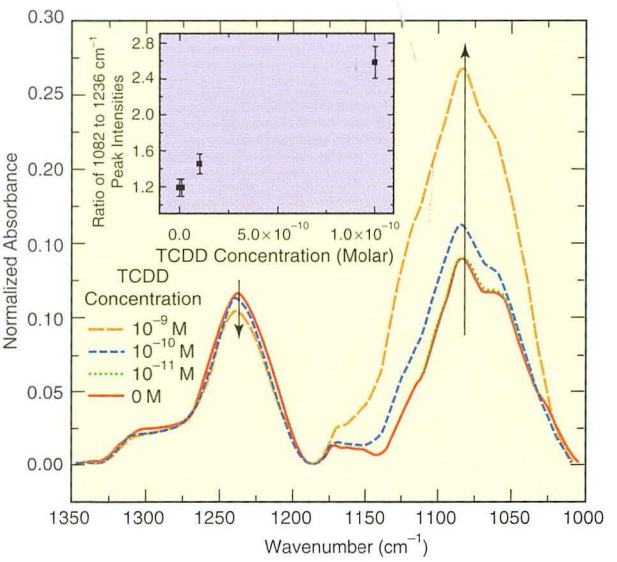

Figure 4 Infrared spectra of HepG2 cells near phosphate bands at 1236 cm^{-1} (asymmetric stretch) and 1082 cm^{-1} (symmetric stretch) show intensity differences for cells treated with varying concentrations of TCDD. The unchanging wavelengths at which the phosphate vibrations were found show that phosphate has weak hydrogen bonding that does not change with TCDD exposure.

for methyl (CH_3) stretch increased with increasing TCDD concentration. The increasing number of methyl groups relative to the number of methylene groups with TCDD exposure may indicate increased DNA methylation, which some researchers have suggested may cause gene inactivation—one possible mechanism by which TCDD could take its toxic toll.

Some cells from each group were analyzed by reverse transcriptase polymerase chain reaction (RT-PCR) to track the effect of TCDD on expression of the CYP1A1 gene. The RT-PCR results did in fact show the expected increase in CYP1A1 gene expression with increasing exposure to TCDD. This strong correlation between spectroscopic and RT-PCR data shows that the spectromicroscopy measurements succeeded in tracking real changes that are associated with induction of the CYP1A1 gene.

INVESTIGATORS

H.-Y.N. Holman, E.A. Blakely, R. Goth-Goldstein, M.L. Russell, and K. Bjornstad (Berkeley Lab) and M.C. Martin and W.R. McKinney (ALS).

FUNDING

U.S. Department of Energy, Office of Basic Energy Sciences and National Petroleum Technology Office; U.S. Army Corps of Engineers; and the National Aeronautics and Space Administration.

PUBLICATIONS

1. H.-Y.N. Holman, M.C. Martin, E.A. Blakely, K. Bjornstad, and W.R. McKinney, "Infrared spectroscopic characteristics of cell cycle and cell death probed by synchrotron-based FTIR spectromicroscopy," *Biopolymers (Biospectroscopy)*, **57**(6), 329 (2000).
2. H.-Y.N. Holman, R. Goth-Goldstein, M.C. Martin, M.L. Russell, and W. R. McKinney, "Low-dose responses to 2,3,7,8-tetrachlorodibenzo-p-dioxin in single living human cells measured by synchrotron infrared spectromicroscopy," *Env. Sci. & Technol.* **34**(12), 2513 (2000).

Extended X-Ray Absorption Fine Structure from Hydrogen Atoms in Water

In almost any circumstance where water plays a role, which includes most biological and environmental processes, as well as in many chemical reactions, hydrogen is ubiquitous. So, it stands to reason that locating the hydrogen atoms within molecules would be a high-priority task. It is highly unfortunate, therefore, that hydrogen with only one electron has been virtually impossible to detect with the conventional x-ray tools for measuring atomic structure (determining where the atoms are). As a result, experimenters often have to resort to supplementary measurements with other techniques that are more hydrogen sensitive to obtain information that can then be melded with their x-ray data to provide a complete structure picture. But now a multi-institutional group working at the ALS has demonstrated the ability to not only detect hydrogen by means of x-ray absorption but also measure its position in water-vapor molecules, a first step toward studying more complex samples.

X-ray scattering is one of the principal tools used for modern structure determination in chemistry and biology. It is conventional wisdom that hydrogen atoms remain "invisible" to traditional x-ray and electron diffraction techniques. As a result, x-ray studies of many important chemical and biological systems yield only partial structure functions. For example, the atom-pair-correlation function for liquid water can be obtained only by the synthesis of x-ray and neutron diffraction measurements. Clearly, techniques that directly probe hydrogen atoms in covalent and intermolecular hydrogen bonds could significantly enhance the scope of structure determination in aqueous solutions and biological systems. Here we report the first definitive measurements of the covalently bound hydrogen atom in water vapor by extended x-ray absorption fine structure (EXAFS).

EXAFS refers to small-amplitude oscillations in the x-ray absorption coefficient that can extend hundreds of electron volts above a core-level absorption edge. These oscillations arise from final-state

interference effects of backscattered photoelectrons from neighboring atoms. In contrast, an isolated atom exhibits a smooth and essentially structureless absorption background corresponding to the photoionization process induced by a core-level excitation. The well-known utility of EXAFS as a structural probe arises from the ability to selectively excite individual atomic species, thereby allowing the local environment (e.g., solvent cage) around a selected absorbing atom to be directly characterized. Since hydrogen possesses a single core electron, the cross section for scattering a photoelectron for a neighboring atom is small, and inter- and intramolecular hydrogen is generally thought to be undetectable in state-of-the-art experiments.

In our measurements, however, we have now demonstrated that EXAFS experiments on water vapor at the oxygen K edge, conducted on ALS Beamline 9.3.2, have the ability to detect scattering from hydrogen atoms. Experiments were conducted in a typical gas cell backfilled with about 20 mTorr of water vapor. Argon-filled cells were used as control samples. The measured EXAFS oscillations from hydrogen in water vapor are shown in Figure 5 along with the calculated values of the oscillations for isolated water molecules obtained with multiple-scattering theory and the FEFF8 *ab intio* electronic structure code. There is remarkable agreement between experiment and theory, which conclusively demonstrates a single scattering distance arising from the covalent O–H bond in water vapor. In reanalysis of an earlier experiment by others, we have used our measured O–H scattering phase shift to demonstrate that O–H bonds can be quantitatively measured in more complex liquids like water.

In sum, we have illustrated the general utility of hydrogen EXAFS as a new structural tool in the elucidation of hydrogen bonds in complex condensed-phase samples. Advances in synchrotron x-ray spectroscopy, coupled with existing computational techniques, imply that observation of hydrogen EXAFS is likely to become routine. The phase-shift function determined in this work can be used to extract quantitative O–H bond distances in other systems, thus becoming a useful complement to existing structural methods in chemistry, biology, and materials science.

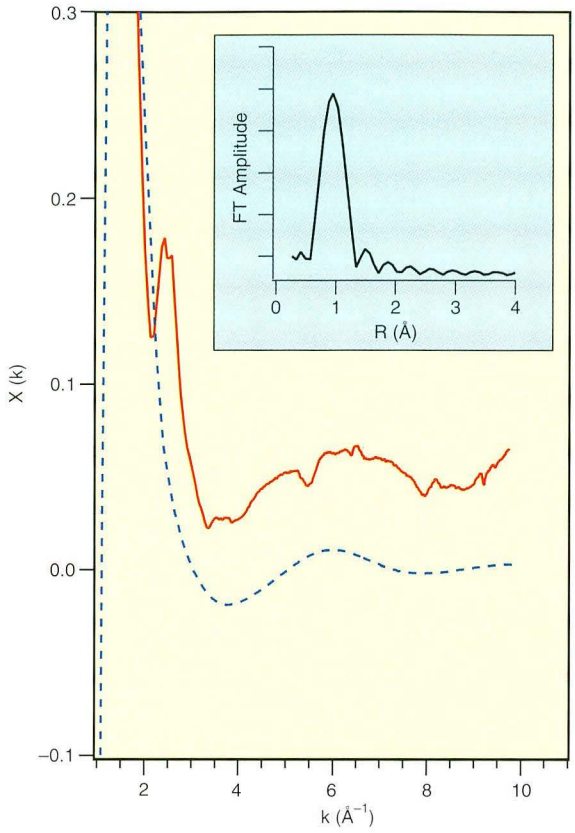

Figure 5 EXAFS oscillations for hydrogen in water vapor. The solid curve is the experimental data, and the dashed curve is calculated for isolated water molecules using multiple-scattering theory and the FEFF8 *ab intio* electronic structure code. The inset is the fast Fourier transform of the experiment data and shows a single scattering distance arising from the covalent O–H bond in water vapor.

INVESTIGATORS

K.R. Wilson and R.J. Saykally (University of California, Berkeley); J.G. Tobin (Lawrence Livermore National Laboratory); and A.L. Ankudinov and J.J. Rehr (University of Washington).

FUNDING

National Science Foundation.

PUBLICATION

1. K.R.Wilson, J.G. Tobin, A.L. Ankudinov, J.J. Rehr, and R.J. Saykally, "Extended x-ray absorption fine structure from hydrogen atoms in water," *Phys. Rev. Lett.* **85**, 4289 (2000).

Protein Crystallography

Architecture of RNA Polymerase II: Structural Clues Help Unravel Intricacies of DNA Transcription

Encoded into the double-helical strands of DNA, the human genome is the complete set of instructions required to make a human being. But mapping the human genome (roughly three billion components) is only the first step. Scientists must next understand how that blueprint gets interpreted, or "expressed" as an individual with unique traits. The pol II enzyme is the catalyst for a major step in this process. As a pol II molecule slides along a DNA molecule, it "unzips" the strands of the DNA double helix, synthesizes a complementary strand of RNA (which will carry the genetic information to where it is needed), and verifies that no mistakes have occurred. An academic team led by researchers from Stanford University has now obtained details of the structure of pol II, details expected to provide valuable insight into the detailed mechanisms underlying the flow of genetic information from DNA to RNA to protein, which is necessary for life and health.

Before a cell can begin to divide or differentiate, the genetic information within the cell's DNA must be copied, or "transcribed," onto complementary strands of RNA. RNA polymerase II (pol II) is an enzyme that, by itself, can unwind the DNA double helix, synthesize RNA, and proofread the result. When combined with other molecules that regulate and control the transcription process, pol II is the key to successful interpretion of an organism's genetic code. However, the size, complexity, scarcity, and fragility of pol II complexes have made analysis of these macromolecules by x-ray crystallography a formidable challenge. Our team of structural biologists has now met this challenge, obtaining a high-resolution model of a 10-subunit pol II complex that suggests roles for each of the subunits and will allow researchers to begin unraveling the intricacies of DNA transcription and its role in gene expression.

In this work, we studied the pol II enzyme from the yeast *Saccharomyces cerevisiae*, which is likely to be an excellent model for the human enzyme in light of its highly similar gene sequences. It is also the best-characterized form of the pol II enzyme. To obtain a high-resolution structure, we drew on our team's considerable expertise in the preparation of protein crystals. Two-dimensional crystals of pol II were used as seeds for growing three-dimensional crystals in an inert atmosphere to prevent oxidation. The addition of a final soaking procedure to produce uniform crystals resulted in a resolution of 3.0 Å in data obtained from both the Stanford Synchrotron Radiation Laboratory and the Macromolecular Crystallography Facility at ALS Beamline 5.0.2.

The current results bring into focus the somewhat fuzzy features previously observed in or inferred from earlier experiments. More important, the structural details suggest possible explanations for some of the unusual characteristics of this enzyme, which include a high processivity (the ability to synthesize very long strands of RNA) and the tendency to work in periodic spurts separated by pauses. While it is known that additional proteins (transcription factors) play a role in controlling the activity of pol II, scientists have yet to understand how such proteins interact with pol II binding sites to perform their various functions. The pol II model reported here establishes the positions of the various subunits and provides detailed information about the DNA/RNA binding domains (Figure 1).

The data reveal two main subunits (Rpb1 and Rpb2) separated by a deep cleft where DNA can enter the complex. At the end of the cleft is the active site, where the DNA can be unwound for a short distance (the "transcription bubble") and a DNA/RNA hybrid can be produced. Two prominent grooves lead away from the active site, either of which could accommodate the exiting RNA transcript. An opening below the active site may allow the entry of nucleotides (for manufacturing RNA) and transcription factors (for regulating the

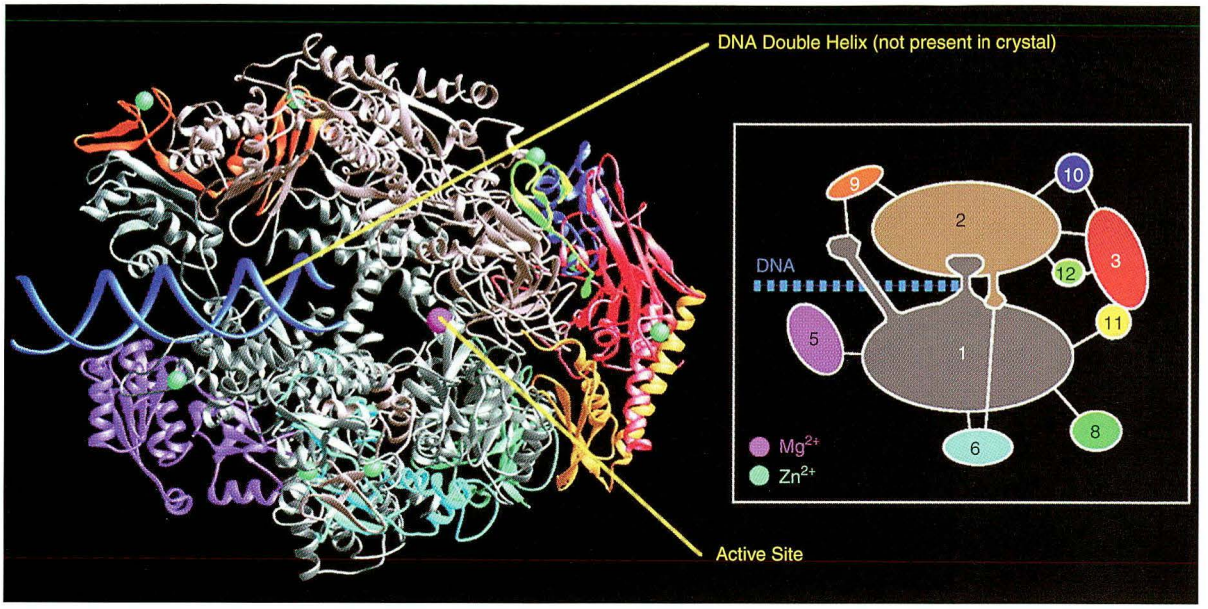

Figure 1 Ribbon diagram of RNA polymerase II backbone model (*left*), and a color-coded schematic of the 10 subunits and their interactions (*right*). Analysis of the structure suggests roles for each of the subunits and is allowing researchers to begin unraveling the intricacies of DNA transcription and its role in gene expression.

process). The same opening may provide room for the leading end of the RNA strand during "backtracking" maneuvers, which are important for proofreading and for traversing obstacles such as DNA damage. Other notable features that might help account for the great stability of this transcribing complex include a pair of "jaws" that appear to grip the DNA strands as they enter the complex and, closer to the active site, a clamp on the DNA that could possibly be locked in the closed position by the presence of RNA.

Our findings pull together threads from numerous diverse research efforts into a cohesive whole. Further study should yield many new insights into the detailed mechanisms of pol II and its transcription factors. Construction of an atomic model is already well under way.

INVESTIGATORS

P. Cramer, D.A. Bushnell, J. Fu, A.L. Gnatt, B. Maier-Davis, P.R. David, and R.D. Kornberg (Stanford University); N.E. Thompson and R.R. Burgess (University of Wisconsin-Madison); and A.M. Edwards (University of Toronto).

FUNDING

U.S. Department of Energy, Office of Basic Energy Sciences; National Institutes of Health; Deutsche Forschungsgemeinschaft; American Cancer Society; and U. S. Association of Medical Research Charities.

PUBLICATION

1. P. Cramer et al., "Architecture of RNA Polymerase II and Implications for the Transcription Mechanism," *Science* **288**, 640 (2000).

The Crystal Structure of the Rev Binding Element of HIV-1 Reveals Novel Base Pairing and Conformational Variability

The human immunodeficiency virus type 1 (HIV-1) is the primary form of HIV found worldwide. In recent years, great progress has been made in finding drug mixtures ("cocktails") that slow the advance of the illness. Each drug in a cocktail interferes in a different way with a different stage of the virus's life cycle, a

strategy necessitated by HIV's high mutation rate. The more drugs we have in our arsenal, the better the odds. The Rev binding element (RBE) of HIV-1 is an attractive target for such a drug. Just as a key must be inserted and turned to open a lock, a critical viral protein (Rev) must bind to the RBE before the virus can begin reproducing itself. Berkeley Lab researchers have now obtained a high-resolution structure of RBE in the hope that understanding the structure and mechanism of the RBE "lock" will help them find a drug that can deliver a molecule that will bind to the RBE in place of the Rev protein, thus effectively locking it out.

One of the most promising strategies for treating infection by human immunodeficiency virus type 1 (HIV-1) is to interfere with the replication of the virus at the genetic level. To this end, our group has analyzed the structure of a portion of the HIV-1 gene (the Rev binding element, or RBE) that plays a key role in the virus's life cycle. The high-resolution (2.1-angstrom) structure obtained indicates a greater degree of flexibility in the RBE than previously thought. Such details about the molecular structure of HIV-1 will help facilitate the design of drugs capable of throwing a metaphorical wrench into the virus's genetic machinery.

A virus reproduces itself by co-opting its host cell's own replicating mechanisms. Essentially, the virus enters the cell nucleus and splices its own DNA into that of the host. The modified host DNA now contains instructions for producing not only the proteins needed by the cell, but the proteins required to assemble a new virus particle as well. In the case of HIV-1, one of these viral proteins, the Rev protein, must fit (bind) like a key into the RBE "lock" before viral replication can proceed. If this binding can be blocked, perhaps by a different molecular key of the right shape, the infected cell will no longer be able to produce new virus particles, thus slowing the spread of the infection.

The RBE is a highly structured region in the virus's messenger RNA, which is a mobile copy of the genetic information stored in DNA. Previous studies have shown that the RBE takes the form of a double helix that includes two "noncanonical" base pairs of nucleotides: guanine-adenine (G-A) and guanine-guanine (G-G). Normally, guanine will pair only with cytosine (G-C). The two noncanonical base pairs are separated by a single (unpaired) uracil (U). This arrangement distorts the double helix and presents a unique, high-affinity binding site for the Rev protein.

To study the structure of the RBE crystallographically, we used synthetic RBE molecules. Solutions containing RNA strands that were chemically synthesized to have the requisite nucleotides in the proper order were first heated and then purified, concentrated, and crystallized. A brominated derivative (where 5-bromouridine replaced one of the uracils) was also produced and used for crystallographic phasing. Analysis of the data, obtained by using multiwavelength anomalous diffraction (MAD) techniques at ALS Beamline 5.0.2, revealed four unique RBE structures that could be grouped into two types (I and II) distinguishable by structural deviations of up to several angstroms. The largest deviations (and thus the greatest flexibility) occurred at the "internal loop" where the noncanonical base pairs create an asymmetrical bulge in the double helix.

The four structural variants were found to differ in several respects from models previously derived by nuclear magnetic resonance (NMR) techniques (Figure 2). For example, in the type II crystal structures, the bonding between the noncanonical G-A base pair was unexpectedly bridged by water molecules. Furthermore, in both the type I and type II structures, the noncanonical G-G pair formed a novel asymmetrical bond, in contrast with the symmetrical bond indicated by NMR-based models of the RBE in complex with (i.e., bound to) the Rev protein (Figure 3). This means that the G-G bonds would have to be broken and re-formed to accommodate Rev protein binding. The observed flexibility of the bulged internal loop region may facilitate this kind of extensive structural change. These results suggest that the NMR model provides only a partial picture of how Rev binding occurs. More detailed studies will be needed before we can begin identifying or designing potential drugs to exploit the RBE-Rev interaction.

INVESTIGATORS

L.W. Hung, E.L. Holbrook, and S.R. Holbrook (Berkeley Lab).

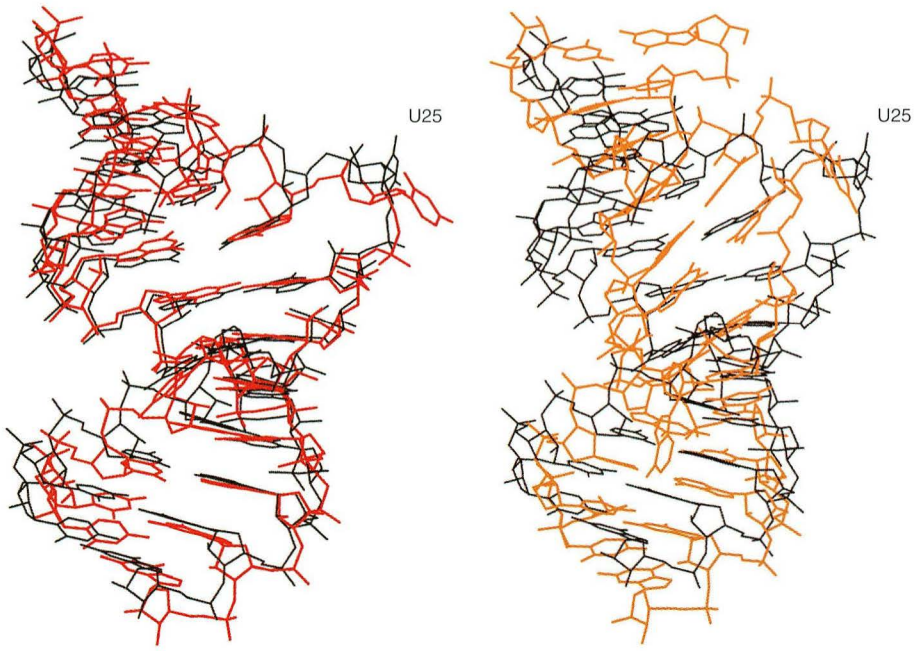

Figure 2 *Left*, superposition of type I (*black*) and type II (*red*) RBE structures. *Right*, superposition of type I RBE structure (*black*) and NMR model of unbound RBE (*orange*). The unpaired uracil (U25) is located between two noncanonical base pairs in an asymmetrical bulge in the double-helix structure.

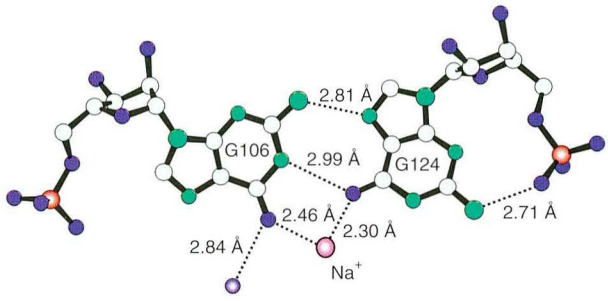

Figure 3 Asymmetrical bonding between noncanonical G–G base pair means that the G–G bonds would have to be broken and reformed to accommodate Rev protein binding.

FUNDING

National Institutes of Health and U.S. Department of Energy, Office of Biological and Environmental Research.

PUBLICATION

1. L.W. Hung, E.L. Holbrook, and S.R. Holbrook, "The crystal structure of the Rev binding element of HIV-1 reveals novel base pairing and conformational variability," *Proc. Natl. Acad. Sci. USA* **97**, 5107 (2000).

Crystal Structure of Poly(A) Polymerase

DNA tells cells how to produce the many kinds of proteins that do the actual work of building and operating an organism. Rather than interacting directly with the cellular machinery, however, DNA sequences are first copied into new, messenger RNA (mRNA) molecules that travel to ribosomes outside the cell nucleus and relay the message encoded by the DNA. Ribosomes are like tiny factories that use the coded information in the messenger RNA to transform raw materials into functional proteins. During the mRNA's trip out of the nucleus, certain chemical structures are added to ensure that it travels smoothly to its ribosomal destination and performs correctly once it arrives there. One of these structures is called a poly(A) tail. A team of researchers mainly from the Boston area has solved the crystal structure of the protein (enzyme) responsible for the tail addition and used the structure to generate a model for how the enzyme might do its work.

The information stored within our DNA is chemically rewitten as RNA before it leaves the nucleus and is translated into protein by the ribosome. The messenger RNA (mRNA) that carries the message

from the genome to the ribosome undergoes extensive modification before it exits the nucleus: nonsense regions within the message are spliced out; a chemical cap is added to the 5' end of the RNA; and a long tail of adenosine residues known as a poly(A) tail is added to the 3' end of the RNA. Our work concerns the last of these modifications. Poly(A) tails provide a handle by which cellular machinery can recognize and physically manipulate mRNAs. The tail facilitates the transport of mRNA from the nucleus, helps regulate the lifetime of mRNA in the cytoplasm, and facilitates translation of the encoded message into protein. Mutations that affect polyadenylation of specific messages have been linked to a number of human diseases.

Using multiwavelength anomalous diffraction (MAD) data collected near the selenium edge (12.65 keV) at ALS Beamline 5.0.2, we solved the crystal structure of yeast poly(A) polymerase, the enzyme at the heart of the machinery that adds the poly(A) tail. This polymerase is quite different from the other nucleic acid polymerases that have been solved to date. Whereas most polymerases are concerned with copying a DNA or RNA strand and use a nucleic acid template to position each new nucleotide as it is added to the chain, poly(A) polymerase simply elongates a chain, and though it performs the same chemical reaction, it does so without a template. Moreover, while most polymerases require additional proteins to prevent substrate release between elongation cycles, the poly(A) polymerase that we solved has a built-in mechanism for maintaining a grip on the mRNA while the newly added base moves within the active site from the position of the incoming nucleotide to the position of the 3' end of the mRNA.

The general architecture of poly(A) polymerase immediately suggested how the enzyme might work. The protein is composed of three globular domains, each containing approximately two hundred amino acids (Figure 4). The first domain contains the catalytic machinery; the second interacts with the adenosine triphosphate that is to be added to the RNA chain; and the third is known to interact with the RNA chain itself. Our crystals contain two independent copies of poly(A) polymerase that differ in the orientation of the second two domains relative to the first. Intramolecular movements that would

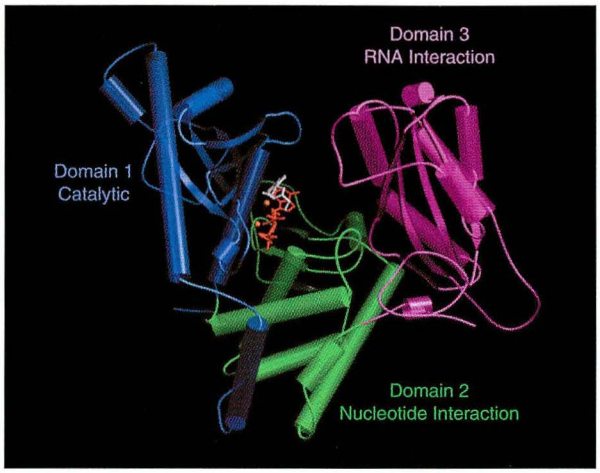

Figure 4 Domain structure of poly(A) polymerase. The active site of the enzyme is located in a cleft between the first and second domains. The first domain (*blue*) contains the residues of the active site. The second domain (*green*) interacts with the phosphates of the incoming nucleotide. The third domain (*purple*) is known to bind single-stranded RNA.

give rise to such conformational differences can account for the polymerase's ability to move itself along the RNA as the chain is extended. Movements of this type are known to occur between the functionally analogous domains of template-directed nucleic acid polymerases. In our model, the second domain serves as a lever that converts small atomic motions resulting from the catalytic event into larger motions in domain 3 (Figure 5). We believe these

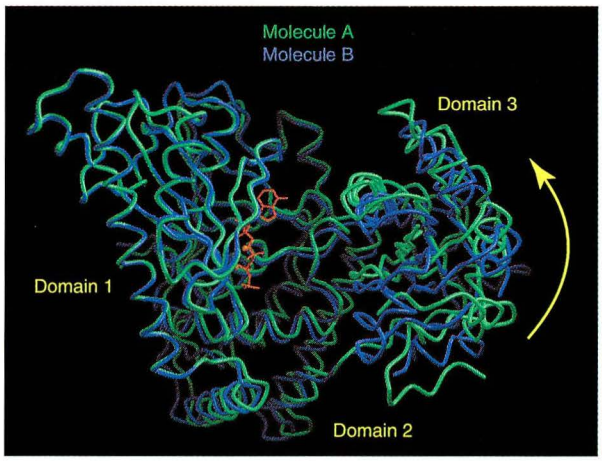

Figure 5 Superposition of the catalytic domains from the two crystallographically independent molecules reveals an intrinsic flexibility in the region that connects the first and second domains. Since the substrate sits at the interface of these domains, it is reasonable to expect that in solution, the global conformation of the molecule may undergo changes in response to the various chemical moieties occupying the active site during the catalytic cycle.

motions translate the RNA into position so that the next cycle of nucleotide addition can occur.

INVESTIGATORS

Joel Bard and Andrew Bohm (Boston Biomedical Research Institute); A.M. Zhelkovsky, S. Helmling, and C.L. Moore (Tufts University Medical School); and Thomas Earnest (Berkeley Lab).

FUNDING

National Institutes of Health and the American Cancer Society.

PUBLICATION

1. J. Bard et al., "Structure of yeast poly(A) polymerase alone and in complex with 3'-dATP," *Science* **289**, 1346 (2000).

Structure of a Glycerol Conducting Channel and the Basis for its Selectivity

The cell membrane defines the cell as a separate entity with an inside comprising the cellular constituents and an outside consisting of the rest of the cell's universe. As important as this boundary function is, however, the membrane must also allow numerous molecules to enter and leave (food enters and waste leaves, for example). Membrane proteins are the structures that open and close the gates and channel the selected molecules across the membrane. Researchers from the University of California, San Francisco, have determined the structure of one of these membrane proteins, the glycerol-conducting channel, from the common bacterium Escherichia coli. *This is the first high-resolution structure obtained for a membrane channel protein of this type. As similar channels are found in a wide variety of species, including humans, scientists expect to use the structure to help explain the mechanisms and regulation of this and the other members of the same family of channels, which are highly selective in what molecules they allow to pass.*

Found in species from bacteria to yeast, plants, and humans, membrane channel proteins of the aquaporin family are highly selective for permeation of specific small molecules. They also preserve the electrochemical potential across the cell membrane by sharp selectivity that excludes all ions and charged solutes, including hydroxide and hydronium ions, a potential that would otherwise be short circuited even by a line of hydrogen-bonded water molecules. Members of the aquaporin family are composed of functionally distinct subgroups that include transmembrane water-conducting channels (aquaporins) and glycerol-conducing channels (acquaglyceroporins), such as the *Escherichia coli* glycerol facilitator (GlpF).

We have determined the crystal structure of the glycerol-conducting channel GlpF with its primary permeant substrate, glycerol, inside the channel. GlpF was cloned from *E. coli* K12 strain, purified, and crystallized. Three heavy-metal derivatives were used to obtain the phases to 3.0-Å resolution. All crystallographic data for native crystals and heavy-metal derivatives were collected at ALS Beamline 5.0.2.

In the structure we determined, glycerol molecules (CH_2OH–$CHOH$–CH_2OH) line up single file in a 28-Å-long narrow region of a highly amphipathic channel (Figure 6). In the narrow selectivity filter of the channel, the glycerol alkyl backbone is wedged against a hydrophobic corner formed from the planes of two perpendicular aromatic rings of tryptophan (Trp) and phenylalanine (Phe). Each of the successive OH groups acts both as a hydrogen-bond acceptor from successive NH groups in the guanidinium group of an arginine (Arg) and as a hydrogen-bond donor to carbonyl oxygens. Surrounding each glycerol-conducting channel are six membrane-spanning and two half-membrane-spanning α helices (M1 to M8) arranged in a right-handed supertwisted fashion. The N-terminus and C-terminus lie on the cytoplasmic surface.

The protein is constructed as two segments, representing the genetic duplication, that are related by a quasi twofold axis that would pass through the center of the bilayer and almost intersects the fourfold axis of the tetramer. Two conserved asparagine (Asn)–proline (Pro)–alanine (Ala) motifs form a key interface between the N-terminal ends of the half helices that meet in the center of the bilayer. These two half-spanning helices (M3 and M7) form an intimate contact between their N-terminal ends on the opposite side of the channel, related by the

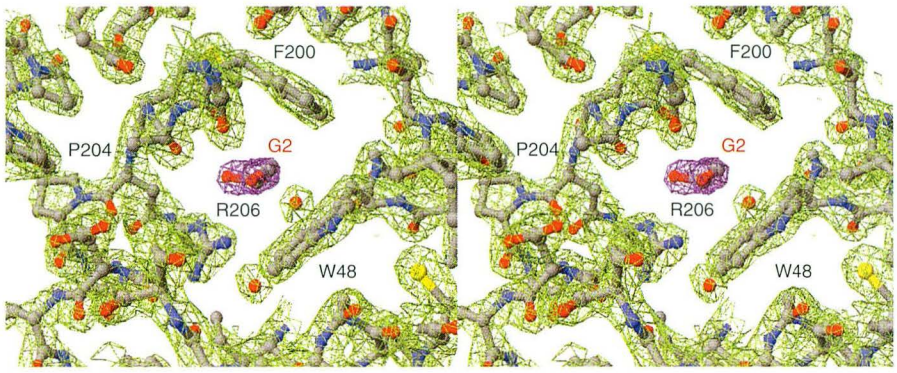

Figure 6 The essence of selectivity in the GlpF channel illustrated by a stereo view of the experimental electron density ($2F_o$–F_c) in the selectivity region of the channel viewed from the periplasmic side of the cell membrane (region outside the membrane but inside the cell wall of a bacterium). The orientation of G2 is defined in the amphipathic channel.

quasi twofold axis to form a coaxial bend. This unique, dimeric contact plays a key role in maintaining a glycerol binding site in the center of the bilayer. The conserved interface places the proline rings in Van der Waals contact against each other and cups each prolyl side chain between the proline and alanine side chains of the opposite helix. Each asparagine side chain is constrained by two hydrogen bonds that precisely orient the side-chain NHs toward acceptors on the permeant substrate. This structure elucidates the mechanism of selective permeability for linear carbohydrates and suggests how ions and water are excluded (Figure 7).

This is the first high-resolution structure of any member of the aquaporin family of integral membrane protein channels, a large family with at least

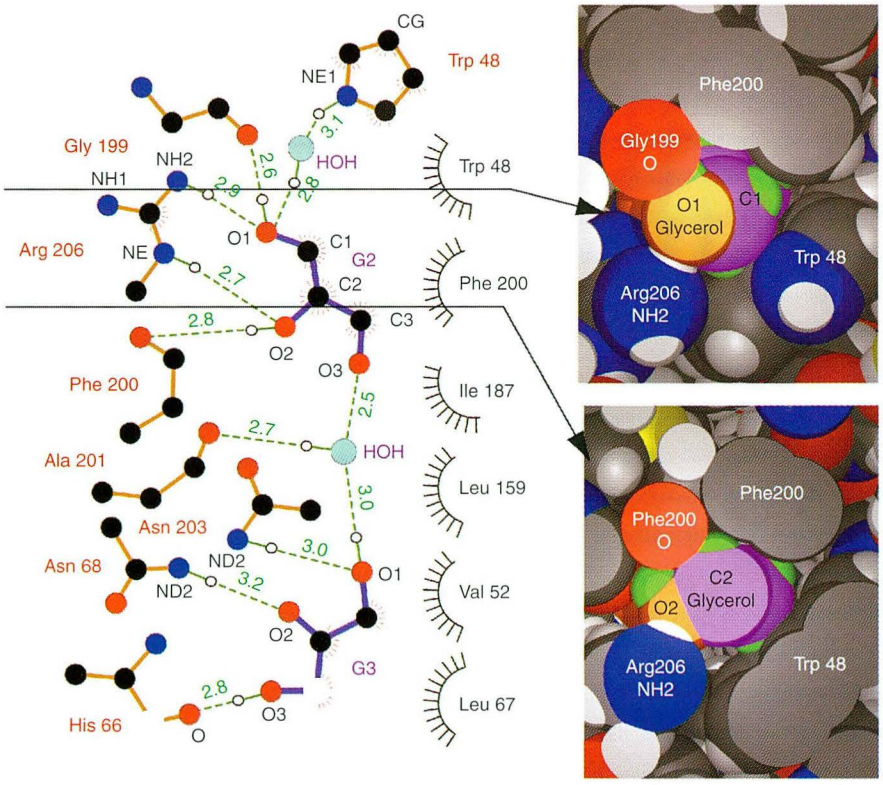

Figure 7 *Left*, the hydrogen bonding network (*dotted lines*) showing interactions of G2, G3, and associated water molecules with the selectivity filter. The view is rotated 90° about a horizontal axis from the density in Figure 6. Distances are in angstroms between heavy atoms. *Right*, two cross sections at positions indicated by the arrows show interactions with G2OH1, O1 (*orange*) and its associated CH2 group (C1, *purple*) and hydrogens (*green*). *Top right*, the donor NH2 of Arg206, acceptor carbonyl oxygen of Gly199, and hydrophobic corner formed by Trp48 and Phe200 viewed edge-on to the aromatic rings, as in the density figure. *Bottom right*, cross section through the channel at G2OH2 shows interactions with the donor NE of Arg206, acceptor carbonyl oxygen of Phe200, and the hydrophobic corner.

10 human orthologs. The high sequence conservation implies that many aspects of the structure will be essentially the same in all aquaporins, thus it instructs us directly as to the mechanisms and regulation of this and the other aquaporin family members. Based on substitution positions, we expect that the carbonyls that line the way into the channel will be common to all the family members. The unique "tripathic" nature of the channel, which presents two hydrophobic sides, one polar hydrogen-bond-accepting side, and one hydrogen-bond-donating side explains the remarkable selectivity of the aquaporin family and why they so tightly exclude passage of all ions through the channels.

INVESTIGATORS

D. Fu, A. Libson, L.J. Miercke, C. Weitzman, P. Nollert, J. Krucinski, and R.M. Stroud (University of California, San Francisco).

FUNDING

National Institutes of Health and the Human Frontiers Research Science Organization.

PUBLICATION

1. D. Fu et al., "Structure of a glycerol conducting channel and the basis for its selectivity," *Science* **290**, 481 (2000).

Structure and Function of a Human $TAF_{II}250$ Double Bromodomain

On one step of the journey from genetic code in a segment of DNA to functioning molecule in a cell, information is transcribed from the DNA to messenger RNA with the help of a protein (enzyme) called RNA polymerase II (pol II), as described in the first highlight in this section. Pol II does not work alone but combines with other molecules to form a very large multiprotein assembly that regulates and controls the transcription process. One of these molecules is itself a multisubunit complex, of which the largest subunit is the protein $TAF_{II}250$. In the work reported here by researchers from the University of California, Berkeley, the structures of two "motifs" known as bromodomains within $TAF_{II}250$ have been solved. Bromodomains are also found in many other kinds of proteins. The details of the structure led the authors to propose roles for the bromodomains in the DNA-to-RNA transcription process.

The goal of our work involved the structural characterization of a fragment of the human protein, $TAF_{II}250$, by means of multiwavelength anomalous dispersion (MAD) x-ray diffraction. Combining the structural information with biochemical characterization that examined the interactions between the bromodomains and acetylated histone peptides, we demonstrated that this region of $TAF_{II}250$ might play a part in nucleosome recognition and may mediate acetylation-dependent increases in transcriptional activity. These results are important for developing models of how gene expression is regulated and point to an unexpected role for the basal transcription machinery.

RNA transcription of class II genes in eukaryotes requires the assembly of a very large multiprotein apparatus composed of RNA polymerase II along with a complement of accessory factors. One important component required for pol II transcription is TFIID (RNA Polymerase II transcription factor D), a multisubunit complex that contains the TATA binding protein (TBP) along with at least eight additional subunits known as TAFs (TBP associated factors). TFIID contains the sequence-specific DNA binding activities necessary for recognition of class II promoters and also functions as a mediator of regulatory signals from many upstream activators. Until recently most in vitro transcription studies have utilized naked DNA templates, restricting such analyses to examination of direct interactions between TFIID, other basal factors, and DNA. However, in eukaryotic cells the template is wrapped around the nucleosomal histone proteins H2A, H2B, H3, and H4 to form chromatin. This packaging greatly alters the template accessibility by large protein complexes, such as TFIID, required for transcriptional initiation.

Studies of transcription in chromatin-containing systems have suggested that transcriptional activity is correlated with acetylation of specific lysine residues in the N-termini of histone molecules. However, the mechanisms underlying the modulation of transcriptional activity by these modifications

are not understood at a molecular level. The discovery that $TAF_{II}250$ (the largest subunit of TFIID), contained an intrinsic histone-acetyltransferase (HAT) activity raised the possibility that the basal machinery also plays an active role in chromatin targeting and or remodeling. In addition to the HAT domain, $TAF_{II}250$ also contains a tandem pair of about 120 residue motifs known as bromodomains. This motif is present in a variety of proteins, including nuclear histone-acetyltransferases, kinases, and chromatin remodeling factors.

Our studies resulted in the determination of the crystal structure of the double bromodomain module of human $TAF_{II}250$ (residues 1359–1638). The $hTAF_{II}250$ double bromodomain was expressed and purified from *E. coli*, and single crystals were obtained. Crystals of a selenomethionine-containing variant were used for phasing. MAD data were collected from single crystals at 100 K using the CCD detector at Beamline 5.0.2. Data were processed and scaled, and subsequent phase refinement was carried out with the CCP4 set of crystallographic programs. Our structure model was built with O and subsequently refined with CNS.

In our structure model, the two bromodomains each consist of a four-helix bundle with left-handed topology (Figure 8). Linking the helices within the domains are long well defined ZA loops and shorter BC loops (bottom of figure) that are responsible for recognition of acetyl-lysine moieties. The binding pockets are separated by approximately 25Å, making them ideally positioned to recognize histone tails containing two Nε-acetyl-lysine residues separated by 7–8 amino acids. Thus, this region of $TAF_{II}250$ may play a part in nucleosome recognition and may mediate acetylation-dependent increases in transcriptional activity.

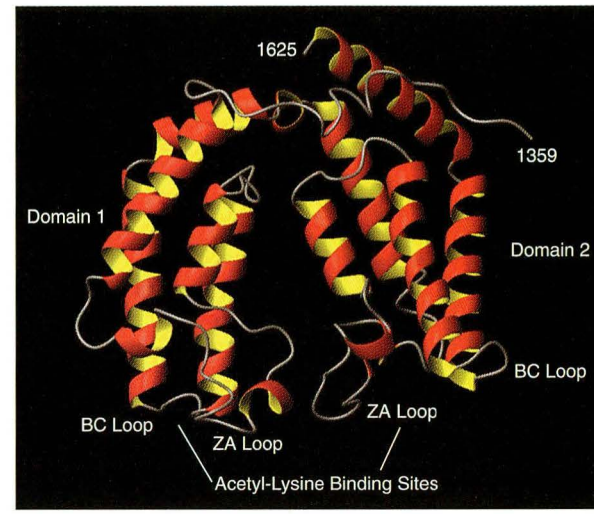

Figure 8 Ribbon representation of the $hTAF_{II}250$ double bromodomain calculated with Molmol. The two bromodomains each consist of a four-helix bundle with left-handed topology. Linking the helices within the domains are long, well-defined ZA loops and shorter BC loops (*bottom of figure*). The binding pockets are separated by approximately 25Å.

INVESTIGATORS

R.H. Jacobson, A.G. Ladurner, D.S. King, and R. Tjian (Howard Hughes Medical Institute and University of California, Berkeley).

FUNDING

National Institutes of Health, Howard Hughes Medical Institute, The Wellcome Trust, and the Burroughs Wellcome Fund.

PUBLICATION

1. R.H. Jacobson, A.G. Ladurner, D.S. King, and R. Tjian, "Structure and function of a human $TAF_{II}250$ double bromodomain module," *Science* **288**, 1422 (2000).

Soft X-Ray Microscopy

High-Resolution Protein Localization Using Soft X-ray Microscopy

Microscopy is a natural candidate for investigating what the proteins in cells do: if we can see where the proteins are and what cellular structures they are near, we have some clues about how they go about their business. Unfortunately, the two main kinds of microscopy for imaging cells and their constituents have limitations that restrict their usefulness for tracking proteins. The light microscope cannot see objects much smaller than the wavelength of the light used, and visible light waves are too long to image tiny proteins effectively. The electron microscope can easily see objects as small as proteins, but electrons cannot penetrate far into samples and so require time-consuming sample-preparation procedures that can also introduce artifacts into the images. The comparatively new technique of x-ray microscopy with shorter wavelengths than visible light offers a possible solution. Scientists at Berkeley Lab report here the use of two x-ray microscopy techniques that allow high-resolution localization of proteins in cells.

Currently, the light microscope is the quintessential tool for monitoring the dynamics of live cells, whereas the transmission electron microscope (TEM) provides high-resolution information about the structural organization of cells that have been fixed at a precise moment in time. The pressing need to understand the functions of specific proteins in cells has motivated a search for new techniques to obtain high-resolution information about protein location in cells. Here we show that soft x-ray microscopy, which achieves better than 50-nm resolution, can be used to localize proteins in several types of whole, hydrated cells and can, therefore, bridge the existing gap between light and electron microscopy.

Immunocytochemistry of antibody-labeled proteins has been carried out in whole, hydrated cells with light microscopy, but the spatial resolution attainable is often insufficient to answer questions regarding the precise location and size of proteins and protein complexes. Although TEM provides superb resolution, it requires extensive processing, including dehydration, embedding in plastic, and preparation of ultrathin sections (50–100 nm). These procedures are extremely time-consuming and can introduce artifacts and loss of antigenicity. An alternative immunocytochemistry approach for TEM that better preserves the epitope is labeling of glucose-treated frozen sections with gold-labeled antibodies (immunogold). This approach is generally successful but is extremely tedious and, therefore, infrequently used. Thus, there is a distinct need for a high-throughput approach that provides better resolution than light microscopy with minimal processing of the cells.

Soft x-ray microscopy has unique capabilities that make it a very useful tool for filling this niche. Specimens are imaged in the "water window," with x rays at photon energies between the K-shell absorption edges of carbon (284 eV) and oxygen (543 eV). In this energy range, organic matter absorbs approximately an order of magnitude more strongly than water. Operating at photon energies just below the oxygen edge (e.g., 517 eV, which corresponds to a wavelength of $\lambda = 2.4$ nm) enables examination of thick (up to 10 μm), hydrated cells. A conventional transmission x-ray microscope equipped with a zone-plate condenser and objective, such as XM-1 at ALS Beamline 6.3.2, can obtain high-contrast images of whole, hydrated labeled cells at better than 50-nm resolution. The use of a cryostage enables examination of rapidly frozen cells that are not exposed to chemical fixatives or contrast enhancement agents and therefore more closely resemble their native state.

Here we report imaging whole, hydrated 3T3 cells (Figure 1), the labeled microtubule network in a whole, hydrated mouse mammary epithelial cell (EPH4) (Figure 2), and the nuclei of human mammary epithelial tumor cells (T4) labeled for nuclear pore complex proteins (Figure 3). All specimens were fully hydrated and mounted between two thin (100-nm), low-absorption silicon nitride membranes. Images

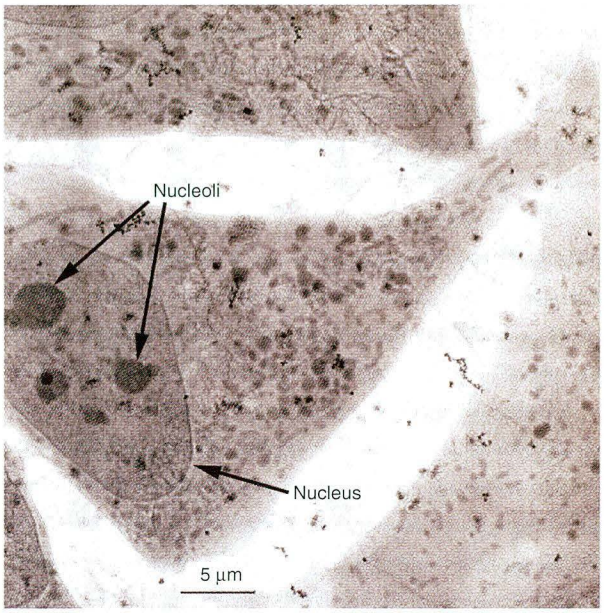

Figure 1 Cryo x-ray microscopy of whole, hydrated 3T3 cells. The cells were initially living, then rapidly frozen and examined under liquid nitrogen temperatures in the cryostage. No chemical fixatives or contrast enhancement agents were used. The image is 2035 × 2033 pixels with a pixel size of 20 nm. The image is a composite of a series of 144 individual x-ray microscope images.

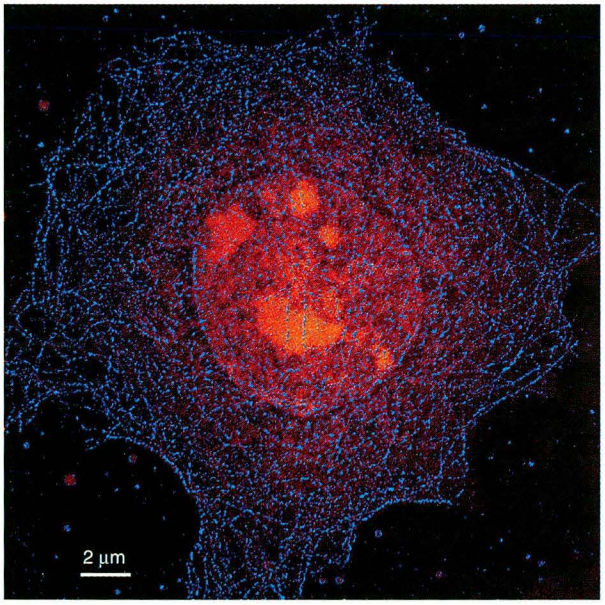

Figure 2 X-ray microscope image of the labeled microtubule network (*blue*) in a whole, hydrated mouse mammary epithelial cell (EPH4). The cell nucleus containing several nucleoli (*orange*) is seen in the center of the cell. The image is 2035 × 2033 pixels with a pixel size of 20 nm. The image is a tiled composite of a series of 144 individual, 10-µm × 10-µm, x-ray microscope images.

Figure 3 Nuclei of human mammary epithelial tumor cells (T4) labeled for nuclear pore complex proteins. This image is a montage compiled from four individual x-ray microscope images.

were formed by Fresnel-zone-plate condenser and objective lenses. The spatial resolution is largely determined by the width of the outermost zone of the objective zone plate and was on the order of 30–45 nm, depending on the zone plate used, the sample contrast, and the attainable signal-to-noise ratio. The magnified image was recorded on a Peltier-cooled, back-illuminated, 1024 × 1024 soft x-ray CCD camera.

To identify the subcellular distribution of proteins, we used the gold-labeled antibodies developed for localizing proteins in electron microscopy. In order to image intracellular proteins with the x-ray microscope, we used small (1.4-nm) gold particles, which readily penetrate the plasma membrane of the cell after it has been triton-permeabilized. We then used a silver enhancement technique to increase the gold to a size approximately equal to the resolution of the microscope. The silver particles are easily identified by the x-ray microscope.

INVESTIGATORS

W. Meyer-Ilse, D. Hamamoto, A. Nair, S.A. Lelièvre, G. Denbeaux, L. Johnson, A. Lucero, D. Yager, and M.A. LeGros (Berkeley Lab) and C.A. Larabell (Berkeley Lab and University of California, San Francisco).

FUNDING

U.S. Department of Energy, Offices of Basic Energy Sciences and Biological and Environmental Research; National Institutes of Health; Army Research Office; Office of Naval Research; and the Air Force Office of Scientific Research.

PUBLICATION

1. W. Meyer-Ilse, et al., "High resolution protein localization using soft x-ray microscopy," *J. Microscopy* **201** (part 3), 395 (2001).

Atomic and Molecular Science

More Trouble for the Dipole Approximation: Second-Order Corrections Found in Soft X-Ray Photoemission

Scientists studying atoms and molecules use x rays to determine the "electronic structure" comprising the electron orbitals and their characteristics. Photoemission is a good example. From the spectrum of kinetic energies and directions of travel of photoelectrons emitted after absorbing x rays, investigators can work backwards to reconstruct the electronic structure. For this purpose, they use as much as possible a simplification of the x-ray interaction with the atom or molecule called the dipole approximation. However, in the last few years, scientists have found that in surprising circumstances the dipole approximation is not sufficiently accurate. A more accurate approximation with extra "first-order" corrections helped but did not eliminate the discrepancies between theory and experiment in every case. Now an international collaboration of theorists and experimentalists has calculated the effects of even more sophisticated "second-order" corrections, which researchers in several fields may now need to take into account.

Our multi-institutional collaboration comprising both theorists and experimentalists has made the first measurements of second-order nondipole terms in the angular dependence of the cross section for neon valence photoemission. The finding potentially applies to a wide variety of x-ray photoemission studies, including gas-phase, surface-science, and materials-science work, where researchers may now need to account for the influence of higher order nondipole terms beyond the standard dipole approximation conventionally applied to the interaction of x rays with matter.

Expanded as a series, the exponential factor describing the x-ray radiation field at the absorbing atom or molecule has the form $1 + O(k) + O(k^2) + \ldots$, where k is the x-ray wave vector $(2\pi/\lambda)$ and $O(k^n)$ comprises terms proportional to the nth power of k. The dipole (or electric dipole) approximation refers to keeping only the 1, so it is also the zeroth-order approximation.

The resulting differential cross section (cross section per unit solid angle) for angle-resolved photoemission with linearly polarized x rays is described by three quantities: the total cross section, $\sigma(h\nu)$; the angular-distribution parameter, $\beta(h\nu)$; and the angle (θ) of the photoelectron trajectory relative to the polarization vector (Figure 1). When extracted from angular distribution measurements, $\sigma(h\nu)$ and $\beta(h\nu)$ provide information about the electronic structure of the atom and the molecule and the dynamics of the photoionization process. For example, at the "magic angle" $\theta = 54.7°$, the angular term disappears and the total cross section is obtained.

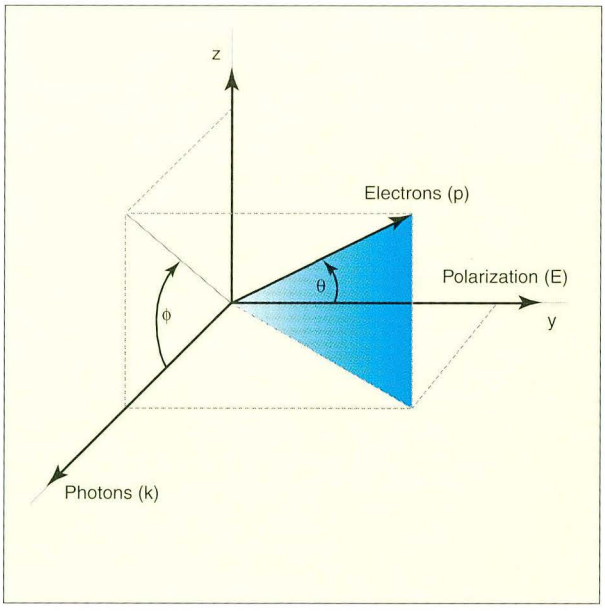

Figure 1 In the dipole approximation, a single term describes electron angular distributions as a function of the angle θ relative to the polarization, E, of the radiation. Higher-order photon interactions lead to nondipole effects, which in the experiments reported here can be described by two new parameters and a second angle, ϕ, relative to the propagation direction, k, of the radiation.

It has long been known that this approximation is not valid for high photon energies (e.g., above 5 keV), where the photon wavelength is smaller than the size of the atom or molecule. In the last few years, groups working at the ALS and elsewhere have shown that additional first-order nondipole (specifically, electric quadrupole) terms are needed in the rare gases even at lower photon energies closer to an ionization threshold. These terms involve two first-order energy-dependent parameters, $\delta(h\nu)$ and $\gamma(h\nu)$, and a new angle variable (ϕ).

At this level of approximation, the recent rare-gas experiments observed significant modifications of the photoelectron angular distributions, as compared to those expected within the dipole approximation, modifications that were in generally good agreement with the first-order calculations. However, when conducting the analysis for neon in terms of the $\gamma(h\nu)$ for 2s photoemission and $\zeta(h\nu)$ (where $\zeta = 3\delta + \gamma$) for 2p photoemission, we noticed that some discrepancy remained, particularly for neon 2p photoemission.

Theorists in our group calculated a general expression for the angle-resolved photoemission cross section including second-order contributions, which introduced four new energy-dependent nondipole factors dominated by electric-octupole and pure electric-quadrupole effects. Since no new angles were involved, the second-order corrections could then be recast in terms of effective values of $\gamma(h\nu)$ and $\zeta(h\nu)$ for comparison with their measurements on neon.

We made this comparison using four analyzers at different angular geometries. Two analyzers were at the magic angle where only nondipole terms are important but with different angles ϕ (0° and 90°), and two on a "nondipole cone" at an angle of 35.3° around the direction of the x-ray beam. The analyzers on the cone were rotated to 10 different positions on the cone, thus yielding a total of 20 geometries. Comparison of experiment with first-order theory yielded good agreement for both neon 2s and 2p photoemission for detectors on the nondipole cone, but in the magic-angle geometry, second-order corrections were needed, especially for neon 2p (Figure 2).

The complex angular dependence of the differential cross section means that which corrections to the dipole approximation are needed depends on the experimental geometry, but the new results demonstrate that researchers need to be ready to include nondipole effects through at least the second order in analyzing their results.

INVESTIGATORS

A. Derevianko and W.R. Johnson (University of Notre Dame); O. Hemmers, S. Oblad, and D.W. Lindle (University of Nevada, Las Vegas); P. Glans (Stockholm University); H. Wang (Uppsala University); S.B. Whitfield (University of Wisconsin); R. Wehlitz (University of Wisconsin); and I.A. Sellin (University of Tennessee, Knoxville).

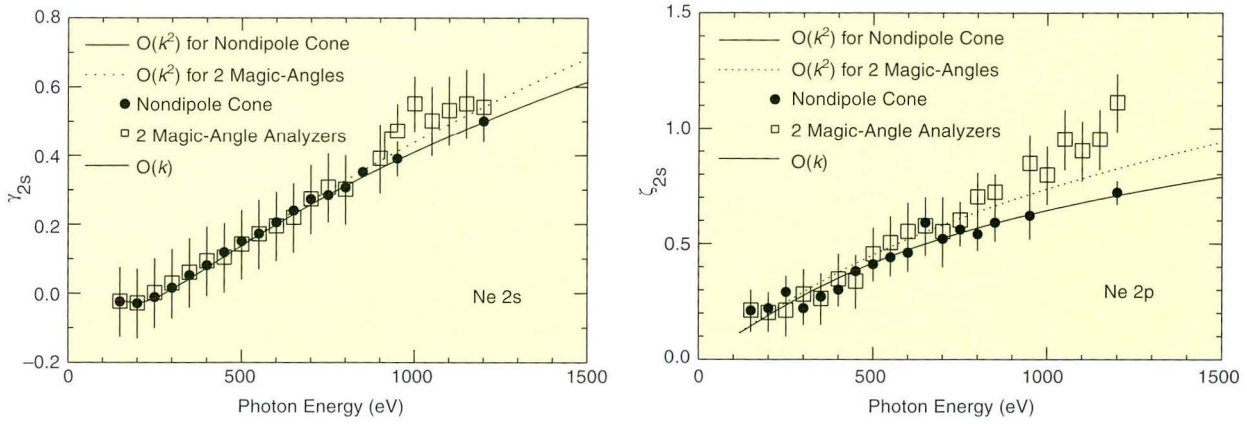

Figure 2 Experimental (*data points*) and theoretical (*lines*) values of the first-order correction terms γ_{2s} and ζ_{2p} for neon 2s (*left*) and 2p (*right*) photoemission determined in "magic-angle" and "nondipole-cone" geometries. While the experimental and theoretical values are in good agreement for the nondipole-cone geometry, second-order corrections are needed for the magic-angle geometry, especially for neon 2p.

FUNDING

National Science Foundation, EPSCor Program of the U.S. Department of Energy, and University of Nevada, Las Vegas.

PUBLICATION

1 A. Derevianko et al., "Electric-octupole and pure-electric-quadrupole effects in soft-x-ray photoemission," *Phys. Rev. Lett.* **84**, 2116 (2000).

Mirroring Doubly Excited Resonances in Argon

As compared to solid materials, isolated atoms are comparatively simple. Nonetheless, scientists cannot exactly solve the quantum-mechanical equations of motion for any atom except hydrogen with one electron, owing in part to so-called many-body effects in which the electrical interaction between negatively charged electrons causes some of the electrons to act in concert rather than as individual particles. A simple example is that in which absorption of an x ray results in energy given to two electrons simultaneously rather than one. It is up to experimentalists to search for and explore these many-body effects, which are sometimes subtle but of fundamental importance to understanding atoms. In the experiments described here, a team led by scientists from Western Michigan University reports the observation of "mirroring resonances" that exactly cancel each other out and are therefore not observable in ordinary measurements of x-ray absorption but were observed by means of state-of-the-art equipment used to make so-called partial differential cross-section measurements.

A detailed understanding of dynamic many-body interactions in atoms and molecules is fundamental to understanding the physics of clusters, nanostructures, solids, and therefore matter. Many observed phenomena in even relatively simple atomic systems still remain to be successfully treated by sophisticated *ab initio* quantum-mechanical models because of the complications introduced by many-body interactions. One manifestation of such interactions is the resonant excitation of two electrons to previously unfilled orbitals following absorption of a single photon, a clear signature of electron–electron interaction. While this process has received much successful theoretical attention for atoms such as helium and lithium, the results for more complex atoms have not been so successful, in part because of the increasing importance of relativistic effects in complex atoms.

The extent to which these effects and others play a role is difficult to assess in general, but with the aid of experimental results from third-generation synchrotron light sources such as the ALS, data can be found to guide theoretical efforts. For example, researchers who made the early measurements of the low-energy photoionization spectrum in argon were able to delineate window-like resonances due to the singly excited $3s^{-1}(np)(^1P_1)$ Rydberg series, and later they were also able to identify two low-lying, doubly excited resonances, $3s^23p^44s(^2P_{1/2,3/2})4p(^1P_1)$. Despite more than three decades of subsequent investigations, however, there has been no evidence of any other photoionization resonances in the energy region below the Ar^+ $3s^{-1}$ threshold. Now, owing to the unprecedented photon resolution from the ALS coupled with advanced differential photoelectron spectroscopy techniques, our group has been able to measure, for the first time, "mirroring" doubly excited resonances.

We used photoelectron spectroscopy to conduct the measurements at ALS Beamline 10.0.1. Our endstation is equipped with two complementary photoelectron spectrometer systems built at Western Michigan University: a system of three highly efficient time-of-flight spectrometers and a hemispherical electron analyzer. These systems allowed measurements of two-dimensional (photon energy vs. photoelectron energy) spectra at three angles from which we extracted data shown in Figures 3 and 4. We chose to conduct this work at the ALS because of the high resolution and brightness of the beamline. These resonances have not been detected in previous measurements of partial cross sections because the achievable resolution was insufficient for resolving the rather narrow features, which are less than 3 meV (FWHM).

We were motivated by recent calculations of Liu and Starace [*Phys. Rev. A* **59**, R1731 (1999)] to carry

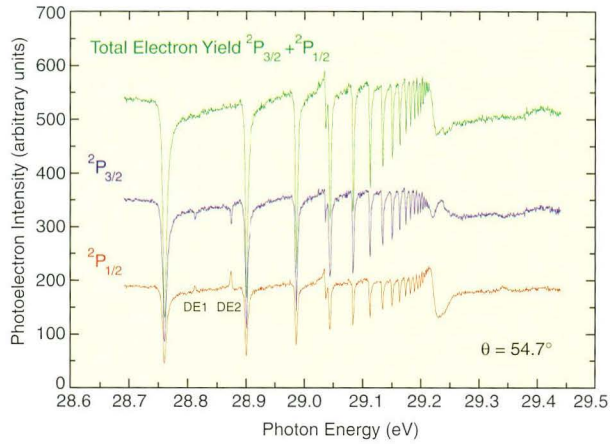

Figure 3 Partial differential cross section measured at θ = 54.7° with respect to the electric field vector of the photon beam. The mirroring resonances are the features labeled DE1 and DE2, which give equal and opposite contributions to the $^2P_{1/2}$ and $^2P_{3/2}$ partial cross sections and thus do not appear in the total cross section.

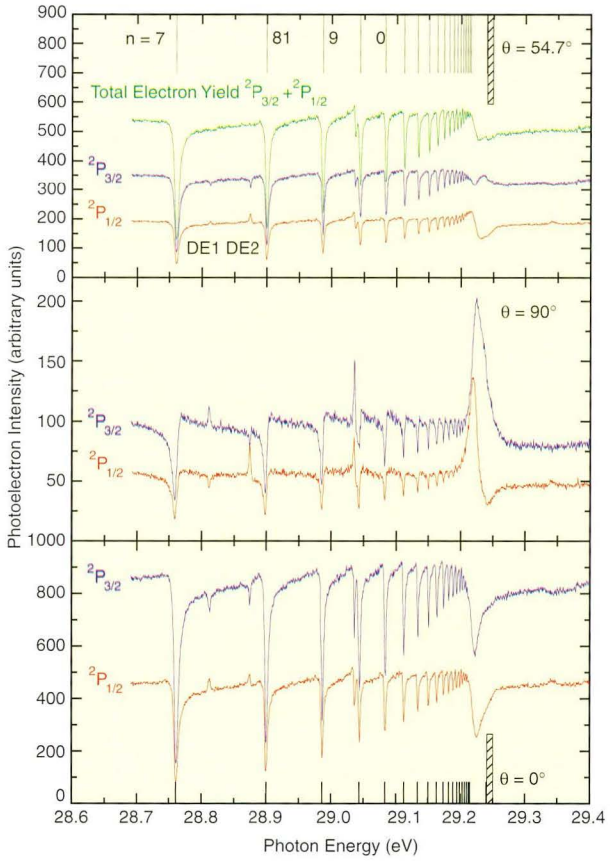

Figure 4 Partial differential cross section measured at θ = 54.7°, θ = 90°, and θ = 0° with respect to the electric field vector of the photon beam. The mirroring resonances appear in all three sets of spectra.

out, with high resolution, differential measurements of the low-lying resonances in the Ar $3p^{-1}{}_{3/2,1/2}$ continua (in the spectral range 26.4 eV ≤ $h\nu$ ≤ 29.4 eV), since their calculations predicted a new type of resonance. This quest was successful and we have indeed observed two new doubly excited resonances. They belong to a class of mirroring resonances described by Liu and Starace that give equal and opposite resonant contributions to the individual partial cross sections for $^2P_{1/2}$ and $^2P_{3/2}$ (features DE1 and DE2 in Figure 3). As a result, their net contribution to the total cross section vanishes, which is why they are not observable in photoabsorption experiments. Although no *ab initio* calculations can be carried out at the present time, these resonances are interpreted to be predominantly triplets, which are LS forbidden from the ground state.

Finally, although we focused on photoionization of atomic argon, this mirroring phenomenon should, with favorable conditions, be observable in collisional processes in atoms, ions, molecules, and solids, demonstrating that even weak relativistic effects allow forbidden pathways and can affect the partial photoionization cross sections.

INVESTIGATORS

N. Berrah, S.E. Canton-Rogan, A.A. Wills, T.W. Gorczyca, M. Wiedenhoeft, and O. Nayandin, (Western Michigan University) and C.-N. Liu (Kansas State University).

FUNDING

U.S. Department of Energy, Office of Basic Energy Sciences.

PUBLICATIONS

1. N. Berrah et al., "High-resolution angle-resolved measurements in atoms and molecules using advanced photoelectron spectroscopy at the ALS," *J. Electron Spectrosc. Relat. Phenom.* **101**, 1 (1999).
2. S.E. Canton-Rogan et al., "Mirroring doubly excited resonances in argon," *Phys. Rev. Lett.* **85**, 3113 (2000).

An Exotic Atomic System Studied by Angle-Resolved Photoelectron Spectroscopy: The Hollow Lithium Atom

Because of the mutual repulsion between them, negatively charged electrons will go to great lengths to avoid each other. In so striving, however, electrons can actually end up working together. The test bed for studying these correlation effects between electrons has been for many years the helium atom, which has just two electrons. More recently, physicists have been probing the lithium atom with three electrons, two in a tightly bound inner shell and one in a less strongly bound outer shell. Absorption of an x ray puts all the electrons in higher-energy outer shells. Since the inner shell is left empty, these highly excited lithium atoms are called "hollow" lithium. By studying the energy and direction of travel of electrons emitted from hollow lithium atoms as they lose energy on their journey back to their original condition, an international collaboration led by researchers from the University of Paris has discovered a way to disentangle some of the complexities of electron correlations in atoms.

Multiple photoexcitation of an atom is a manifestation of correlation effects between the atomic electrons. In this process, the energy of a photon incident on an atom serves to promote two electrons belonging to the same shell or belonging to two different subshells into empty outer orbitals, bringing the whole atomic system to a very energetic state whose lifetime is very short. In less than one picosecond, the highly excited system releases its energy by emitting a photon or an electron. From the early 1960s, doubly excited states of helium have provided the ideal case for studying the three-body system of two correlated electrons interacting with the nucleus.

The challenge to extend these investigations to triply excited states in neutral lithium was recently met with studies of these so-called "hollow" atoms at the ALS. The term "hollow atom" is used to describe an atomic state in which the first inner-shell has been emptied by a photon according to $1s^2 2s + h\nu \rightarrow 2s^2 2p\ ^2P$. This hollow state has a large amount of internal energy that is released by the emission of one or two electrons. More challenging angle-resolved experiments provide the potential for greater insight into the nature of the resonantly triply excited atomic state, offering a more stringent test of theory. By combining the high-resolution photon beams of the ALS with an electron spectrometer capable of simultaneously counting the electrons emitted at several different angles ϕ with respect to the polarization vector of the photons, we have been able to obtain the first angle-resolved spectra for the fragmentation of the highly excited $2s^2 2p\ ^2P$ hollow state.

In Figure 5, we show angle-resolved electron spectra measured over the photoionization energy range of the triply excited $2s^2 2p\ ^2P$ lithium resonance. The difference between the two spectra at $\phi = 0°$ and $90°$ is striking. When the hollow state decays to the metastable states $1s2s\ ^{1,3}S$ of the Li^+ ion, the electron distribution is highly asymmetric with no electrons being emitted at $90°$. However, when the Li^+ ion is left in the so-called correlation-satellite $^{1,3}P$ states, the electrons have an almost isotropic angular distribution. Spectra obtained for photon energies away from the resonance show all electron emission vanishing at $\phi = 90°$. This behavior can be easily explained physically. The process likely to be the most important for the decay of the hollow state is that one of the 2s electrons falls into one of the empty 1s orbitals, while the other 2s electron is emitted into the continuum without exchange of angular momentum, leading to an isotropic angular distribution.

The variation of the angular distribution of the emitted electrons is characterized by the angular-distribution parameter β. In Figure 6, we show the variation of β for the correlation-satellite $^{1,3}P$ states as the photon energy is scanned through the resonance, a variation that reflects the observed phenomena. The results of R-matrix calculations are qualitatively in agreement with the experimental data points. Of particular interest for experimentalists and theorists is that both theory and experiment show that the β minima occur not at the energy of the resonance but are shifted from the position of the extremum. It is important to be aware that on-resonance determinations of β do not necessarily provide a measurement of the minimum (or maximum in other cases) of β.

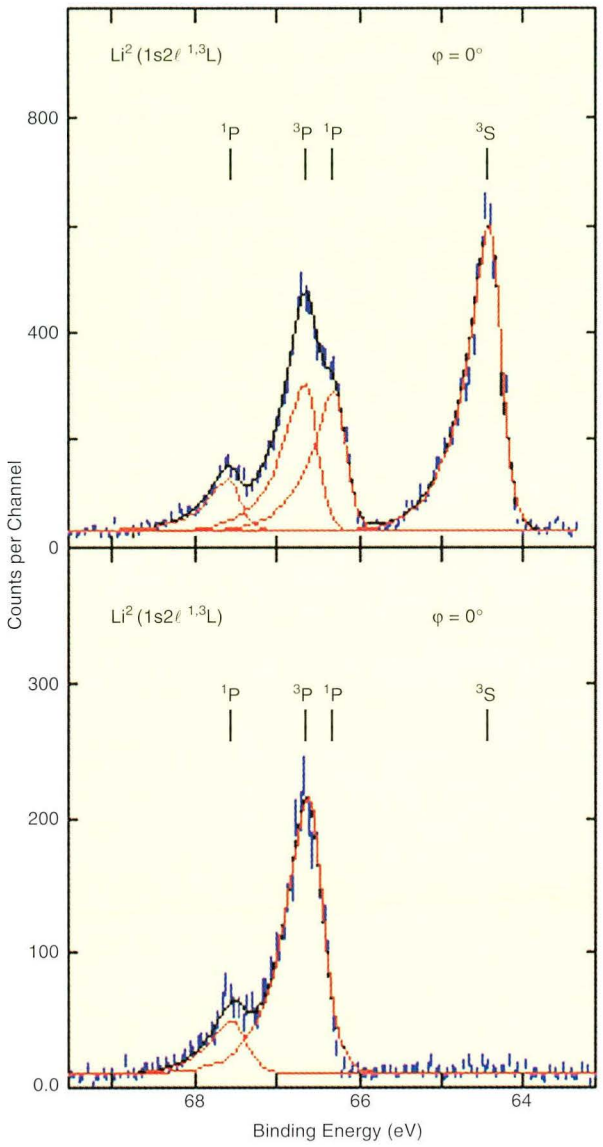

Figure 5 Angle-resolved photoelectron spectra measured over the photoionization energy range of the triply excited $2s^2 2p\ ^2P$ hollow state of lithium. The electron distribution is highly asymmetric for decay to the metastable states $1s2s\ ^{1,3}S$ with no electrons being emitted at 90°, whereas decay to the so-called correlation-satellite $^{1,3}P$ states results in electrons with an almost isotropic angular distribution.

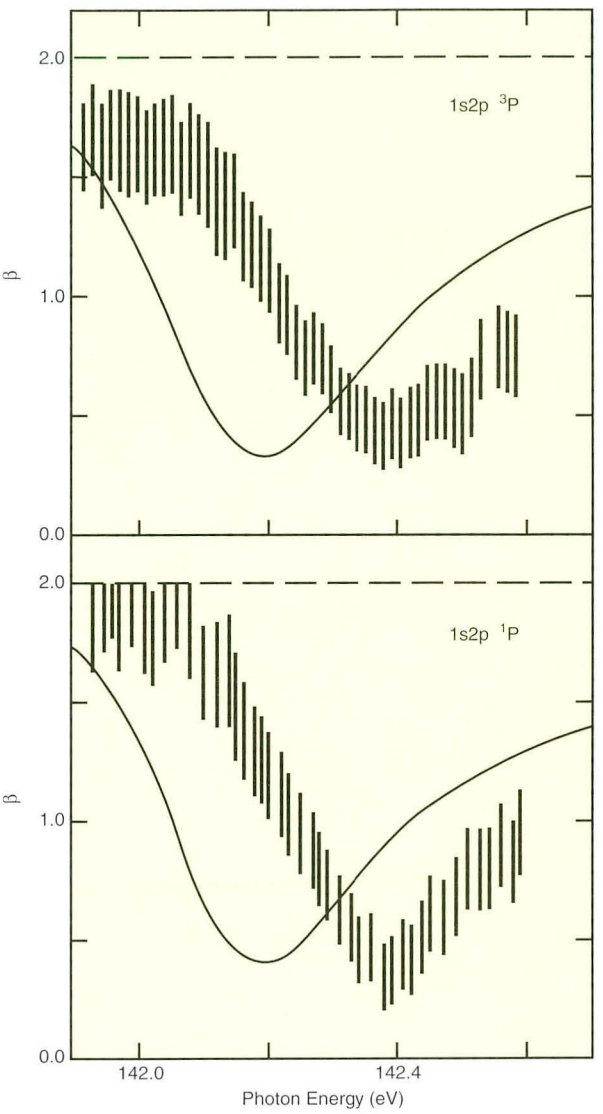

Figure 6 Variation of the angular distribution parameter β of the electrons emitted in the decay of the hollow state to the correlation-satellite $^{1,3}P$ states of the Li^+ ion. The solid lines are the result of R-matrix calculations. Note that the photon energies at which β is a minimum are higher than the resonance energy.

FUNDING

Centre National de la Recherche Scientifique; Université Paris-Sud; Centre CEA de Bruyères-Le-Châtel; Enterprise Ireland; National Science Foundation; U.S. Department of Energy, Office of Basic Energy Sciences; and U.S. National Aeronautics and Space Administration.

INVESTIGATORS

S. Diehl, D. Cubaynes, J.-M. Bizau, and F.J. Wuilleumier (CNRS and University Paris-Sud, France); E.T. Kennedy (Dublin City University, Ireland); N. Berrah (Western Michigan University); L. VoKy (Observatoire de Meudon, France); H.L. Zhou and S.T. Manson (Georgia State University); T.J. Morgan (Wesleyan University); J. Bozek (ALS); and C. Blancard (Centre CEA de Bruyères-le-Châtel, France).

PUBLICATIONS

1. S. Diehl et al., "High resolution measurements of partial photoionization cross-section in hollow lithium: A critical comparison with advanced

many-body calculations," *Phys. Rev. Lett.* **76**, 3915 (1996).
2. S. Diehl et al., "Experimental observation and theoretical calculations of Rydberg Series in hollow atomic lithium," *Phys. Rev. Lett.* **79**, 1241 (1997).
3. S. Diehl et al., "Angle-resolved photoelectron spectrometry studies of the autoionization of the $2s^2 2p\ ^2P$ triply excited state of atomic lithium: Experimental results and R-matrix calculations," *Phys. Rev. Lett.* **84**, 1677 (2000).

Chemical Dynamics

Recalibration of Proton Affinities: PFI-PEPICO Yields Key Measurements with Unprecedented Accuracy

A molecule's tendency to grab hold of a proton—its proton affinity—comes into play in reactions taking place in venues from tiny biological cells to the far reaches of interstellar space. Experimentally determined proton affinities provide feedback to theorists who need more accurate data to test their calculations. For example, whether or not a given chemical reaction proceeds is determined to a large extent by the change in energy that results as the reactants transform into the products. The dynamics of complex systems, such as flames, can involve hundreds of chemical reactions, each of which proceeds at its own rate. So workers who model complex systems rely on a knowledge of the species' thermochemical properties, such as heat of formation and proton affinity, which permit them to either calculate the unknown rates or to at least determine whether or not a reaction is feasible. Here, an academic team reports new measurements of proton affinities, ten times as accurate as previous values, that form the basis for a recalibration of the old affinity scale.

The transfer of a proton from one molecule to another is a basic chemical reaction and an important step in many biological processes. Thus, knowledge of a molecule's proton affinity is highly useful in modeling or analyzing such reactions. Over 500 molecules have proton affinities whose values are known relative to each other. However, only a few key molecules lend themselves to measurements that can establish absolute proton affinity values. We have made such measurements with unprecedented accuracy with a combination of pulsed-field ionization (PFI) and photoelectron-photoion coincidence (PEPICO) techniques at ALS Beamline 9.0.2. The results indicate that the current proton affinity scale should be shifted down by about 8 kJ/mol (Figure 1).

One of the molecules that can be used to place the proton affinity scale on an absolute footing is propene (C_3H_6). To obtain an absolute value of its proton affinity, we needed to accurately measure the energy required to ionize and dissociate a precursor molecule: propyl chloride (C_3H_7Cl). This molecule can be thought of as being made up of three components: a propyl ion ($C_3H_7^+$), a chlorine atom, and an electron. The PFI-PEPICO technique used in this study can provide a very precise measure of the minimum energy required to ionize and dissociate C_3H_7Cl (i.e., its ion dissociation threshold). With an ion energy resolution of 0.5 meV, the PFI-PEPICO method improves on previous methods by almost an order of magnitude.

PFI-PEPICO takes advantage of the multibunch time structure of the ALS storage ring (512 ns of synchrotron radiation followed by a 144-ns dark gap) (Figure 2). The ALS photons excite C_3H_7Cl molecules to energies in the vicinity of the ion

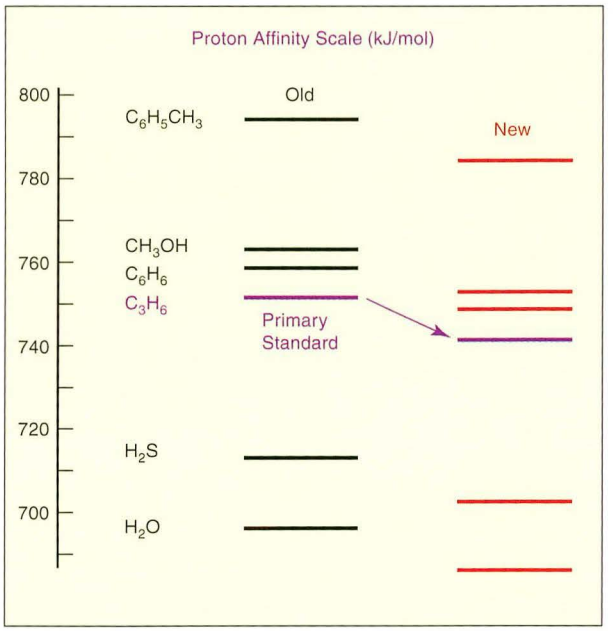

Figure 1 Energy diagram of old and new proton affinity scales, showing the readjustment of the energy scale downward by about 8 kJ/mol based on the proton affinity for the primary standard propene (C_3H_6).

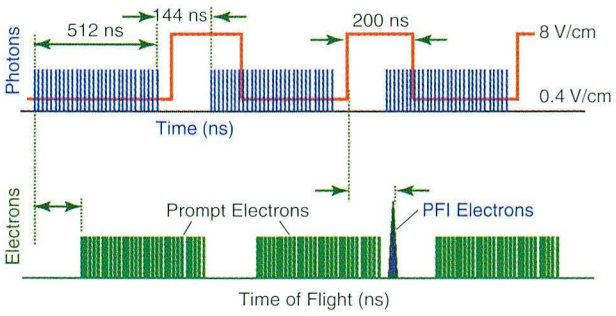

Figure 2 Schematic representation of the pulsed-field ionization technique with a "dark" gap in the train of electron bunches. The spike of electrons in the dark gap occurs when the 8-V/cm pulsed electric field ionizes photoexcited neutral molecules in high-*n* Rydberg states.

dissociation threshold. While promptly produced electrons and ions are extracted by a small electric field, some neutral molecules in high-*n* Rydberg states remain. These need just a small energy boost to become ionized. That energy is provided by a pulsed electrical field (pulsed-field ionization, or PFI) during the 144-ns dark gap. The resultant photoelectrons provide the start signal for time-of-flight measurements of the corresponding photoions (photoelectron-photoion coincidence, or PEPICO) (Figure 3). By measuring the relative abundance of $C_3H_7Cl^+$ vs. $C_3H_7^+$ over a range of photon energies, we were able to determine very precisely at what energy the abundance of $C_3H_7Cl^+$ goes to zero (i.e., where $C_3H_7Cl^+$ dissociates completely into $C_3H_7^+$ and Cl) (Figure 4).

This dissociation threshold energy represents the energy change that occurs when the parent molecule (C_3H_7Cl) splits into the products ($C_3H_7^+$ and Cl) or vice versa (in which case this energy is called the heat of formation). Because the heats of formation of C_3H_7Cl and Cl are well known, the heat of formation of $C_3H_7^+$ can now be determined with an accuracy limited by the error in the heat of formation of C_3H_7Cl. Then, because $C_3H_7^+$ is made up of C_3H_6 (propene) and H^+ (a proton), the heats of formation of $C_3H_7^+$ (from this work) and H^+ (well established) yield the change in energy involved in attaching a proton to propene (i.e., its proton affinity). As mentioned above, propene provides one of the absolute reference points for the scale of relative proton affinities.

Similar measurements and calculations were performed for ethylene (C_2H_4), another "anchor" molecule for the proton affinity scale. These more accurate heats of formation led to proton affinities of 742.3 kJ/mol for propene and 682.0 kJ/mol for ethylene, in good agreement with the latest theoretical calculations and about 8 kJ/mol lower than the previously accepted standard values. An example of

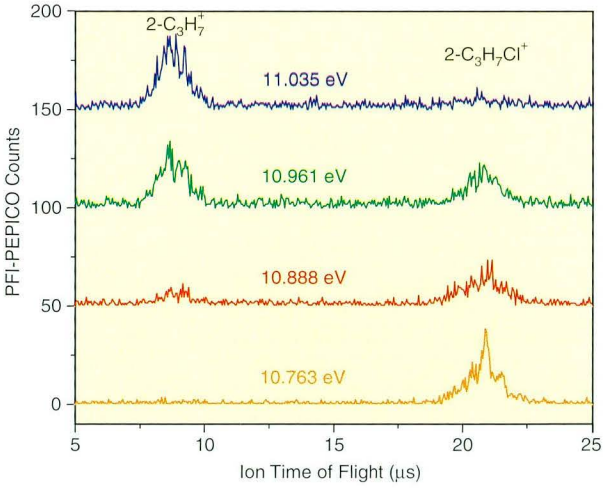

Figure 3 Time-of-flight photoelectron-photoion coincidence (PEPICO) distributions for $C_3H_7Cl^+$ and $C_3H_7^+$ at selected photon energies. From these data, the relative abundance of the ions over a range of photon energies is obtained.

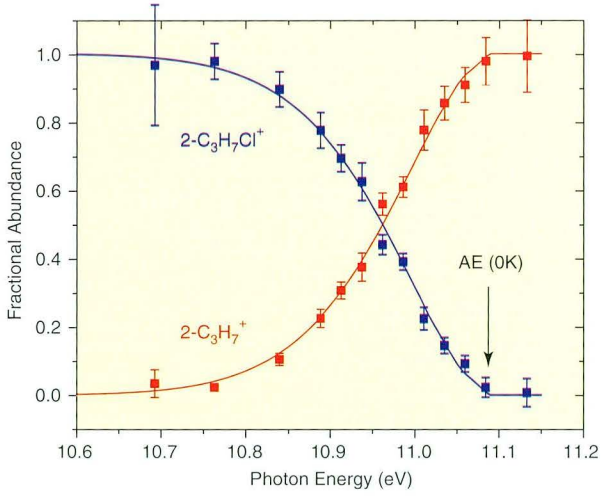

Figure 4 Relative abundance of $C_3H_7Cl^+$ vs. $C_3H_7^+$ in the vicinity of the ion dissociation threshold or "appearance energy" (AE) of $C_3H_7^+$ at 0 K. This dissociation threshold energy represents the energy change that occurs when the parent molecule (C_3H_7Cl) splits into the products ($C_3H_7^+$ and Cl) or vice versa.

the effect of these measurements for selected molecules having proton affinity values between 700 and 800 kJ/mole is shown in Figure 1.

INVESTIGATORS

T. Baer (University of North Carolina at Chapel Hill), Y. Song and C.Y. Ng (Ames Laboratory), and J. Liu and W. Chen (Berkeley Lab).

FUNDING

U.S. Department of Energy, Office of Basic Energy Sciences.

PUBLICATIONS

1. T. Baer, Y. Song, C.Y. Ng, J. Liu, and W. Chen, "The heat of formation of 2-$C_3H_7^+$ and proton affinity of C_3H_6 determined by pulsed field ionization-photoelectron photoion coincidence spectroscopy," *J. Phys. Chem. A* **104**(9), 1959 (2000).
2. T. Baer, Y. Song, J. Liu, W. Chen, and C.Y. Ng, "Pulsed field ionization-photoelectron photoion coincidence spectroscopy with synchrotron radiation: The heat of formation of the $C_2H_5^+$ ion," *Faraday Discuss.* **115**, 137 (2000).

Techniques

Femtosecond Pulses of Synchrotron Radiation: Laser Time-Slicing Will Lead to Ultrafast Time Resolution

Physical, chemical, and biological processes are by nature dynamic—that is, the atomic arrangement evolves with time. The characteristic time scale for this motion is the time scale of a molecular vibration, about 100 femtoseconds (0.1 trillionths of a second). One way to study what happens at such ultrafast time intervals is a pump-probe (or stroboscopic) technique in which the sample is illuminated with pulses of light that are shorter than the time for significant structural changes to occur. The generation of femtosecond x rays and their application for this purpose is an emerging area of scientific research. In the work reported here, a Berkeley Lab group has shown how to use a high-speed laser to "slice" out tiny slivers from the circulating electron bunches in the ALS storage ring and use them to produce pulses of synchrotron radiation lasting just 300 femtoseconds, the first step to carrying out x-ray experiments at this ultrafast time scale.

We have generated 300-femtosecond pulses of bend-magnet synchrotron radiation at the ALS with the aid of a laser "time-slicing" technique. This proof-of-principle experiment demonstrates that this technique is a viable one for producing ultrashort pulses of x rays. An ALS bend-magnet beamline is now being commissioned that will be dedicated to time-resolved x-ray diffraction, EXAFS, and other techniques capable of probing the long-range and local structure of matter on a femtosecond time scale.

Atomic motion on the fundamental time scale of a vibrational period, via the making and breaking of chemical bonds and the rearrangement of atoms, ultimately determines the course of phase transitions in solids, the kinetic pathways of chemical reactions, and even the efficiency and function of biological processes. A thorough understanding of such dynamic behavior is a first step to being able to control structural evolution, and it is expected to have important scientific applications in solid-state physics, chemistry, materials science, and biology.

X rays can provide the requisite structural information, and ultrafast x-ray science is an emerging field of research in which x-ray techniques are used in combination with femtosecond lasers to probe structural dynamics. However, the tremendous potential scientific impact of this research area is so far largely unfulfilled, owing to the lack of adequate sources. For example, the pulse length of a synchrotron x-ray source is limited by the bunch length of the electrons in the storage ring, around 30 ps at the ALS

In early 1996, Alexander Zholents and Max Zolotorev of Berkeley Lab's Center for Beam Physics proposed the laser time-slicing technique as a way to achieve effective bunch lengths in the femtosecond range. At the heart of the proposal was the use of a high-power, femtosecond laser synchronized with the electron bunches so that a pulse of laser light passed collinearly with an electron bunch through an undulator or wiggler. The high electric field of the shorter laser pulse modulated a portion of the longer electron bunch, with some electrons gaining energy and some losing energy. Subsequently, when the energy-modulated electron bunch reached a bend magnet (or other section of the storage ring with a nonzero dispersion), a transverse separation occurred. A collimator or aperture selected the synchrotron radiation from the displaced bunch slices. (See Figure 1.)

To demonstrate the laser bunch-slicing technique, we used the 16-cm-period wiggler that illuminates Beamline 5.0.2, a test chamber on bend-magnet Beamline 6.3.2, and a high-power titanium-sapphire laser. To verify the femtosecond time structure, visible light from Beamline 6.3.2 was imaged onto a nonlinear optical crystal along with a delayed 50-fs cross-correlation pulse from the laser system. Then photons were counted at the sum frequency of the two pulses as a function of

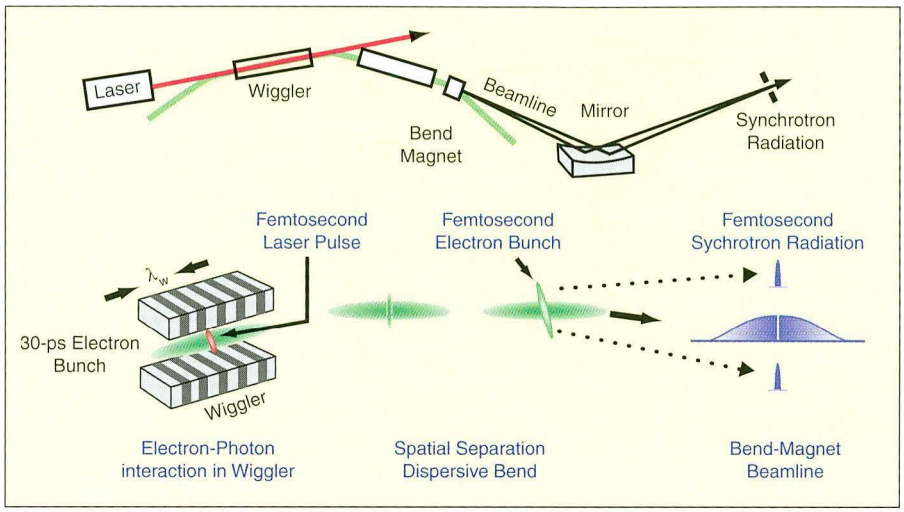

Figure 1 Schematic diagram showing how the laser bunch-slicing technique was used to produce femtosecond pulses of synchrotron radiation at the ALS. *Left*, laser/electron beam interaction in resonantly-tuned wiggler; *center*, separation of accelerated femtosecond electron slice in a dispersive bend magnet; *right*, generation of femtosecond pulses in a bend-magnet beamline.

delay between the modulating and the cross-correlation laser pulses. An adjustable knife edge located in the beamline at an intermediate image plane provided a means to select radiation from different transverse regions of the electron beam. In this way, we measured a dark 300-femtosecond hole in the central cone of the synchrotron radiation (Figure 2) and a bright 300-femtosecond peak in the wing of the synchrotron radiation (Figure 3).

As the next step in the growing femtosecond x-ray science program at the ALS, a bend-magnet beamline (Beamline 5.3.1) has been constructed with a performance goal of100-fs pulses at a repetition rate of 5 kHz with a flux of about

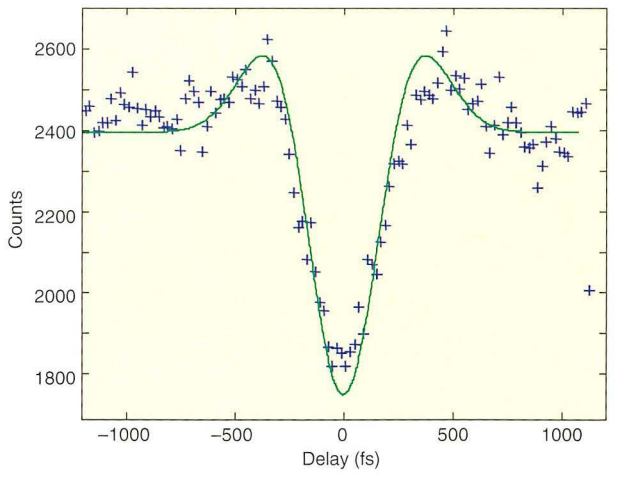

Figure 2 Cross-correlation between a delayed laser pulse and the synchrotron radiation shows light from the central cone ($\pm 3\sigma_x$) of the electron bunch has a dark femtosecond hole. Solid lines are from a model calculation of the spatial and temporal distribution of the energy-modulated electron bunch following propagation through 1.5 arc sectors at the ALS.

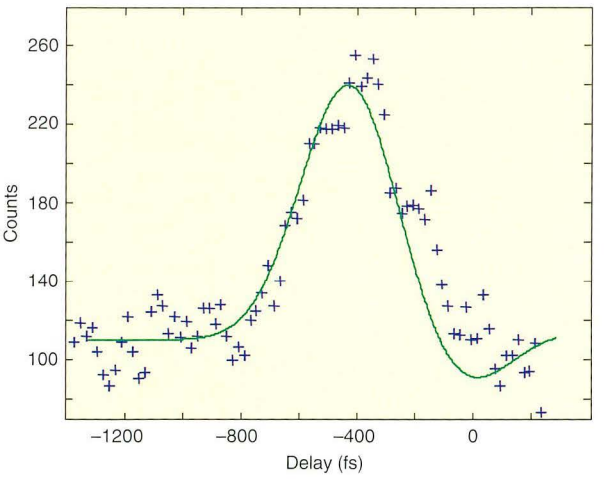

Figure 3 The cross-correlation technique also shows that light from a horizontal wing ($+3\sigma_x$ to $+8\sigma_x$) of the electron bunch exhibits a bright femtosecond peak. Solid lines are from a model calculation of the spatial and temporal distribution of the energy-modulated electron bunch following propagation through 1.5 arc sectors at the ALS.

10^5 photons/second/0.1% bandwidth and a brightness of about 10^8 photons/second/mm^2/mrad^2/0.1% bandwidth for photon energies up to 10 keV. Initial experiments include time-resolved x-ray diffraction, EXAFS, and NEXAFS (XANES).

INVESTIGATORS

R.W. Schoenlein, S. Chattopadhyay, C.V. Shank, A.A. Zholents, and M.S. Zolotorev (Berkeley Lab); H.H.W. Chong (University of California, Berkeley); and T.E. Glover and P.A. Heimann (ALS).

FUNDING

U.S. Department of Energy, Office of Basic Energy Sciences.

PUBLICATION

1. R. W. Schoenlein et al., "Generation of femtosecond pulses of synchrotron radiation," *Science* **287**, 2237 (2000).
2. R.W. Schoenlein et al., "Generation of x-ray pulses via laser-electron beam interaction," *Appl. Phys. B* **71**, 1 (2000).

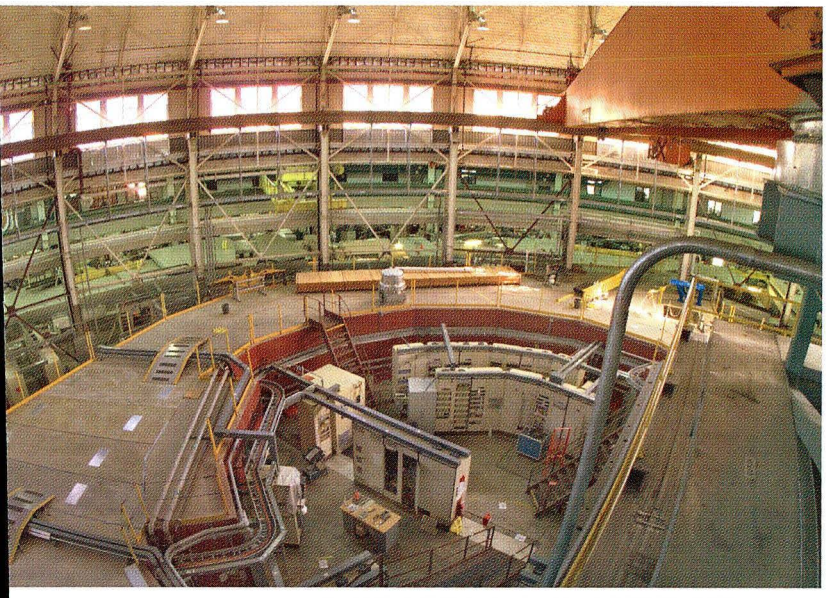

FACILITY REPORT

Operations

Ben Feinberg
Division Deputy for Operations
Terry Byrne
Accelerator Physics Group

Operations and Reliability

A reliable source of synchrotron light is a key prerequisite for a successful scientific program at the ALS. High-quality beams delivered according to a published schedule along with an efficient, effective safety program allow our researchers to make maximum use of their limited beamtime. In the year 2000, the ALS once again maintained its exemplary operations record while making continuing improvements in beam quality. In addition, the Operations groups designed, constructed, and installed new beamlines for protein crystallography and for femtosecond x-ray research. Their work also included installing focusing magnets and machining the ALS vacuum chamber in situ in preparation for the installation of the superconducting bend magnets (superbends). Figure 1 shows the setup for this work, which took place during the installation shutdown in February and March.

The research community at the ALS has become accustomed to high operational efficiency and reliability, and it was not disappointed during this period. As shown in Figure 2, the ALS delivered beam to the users more than 95% of the time scheduled for user operations in FY00, maintaining the reliability of the last several years. ALS users have also come to expect continued improvement in the quality of beams delivered. Our efforts to improve beam quality are discussed below.

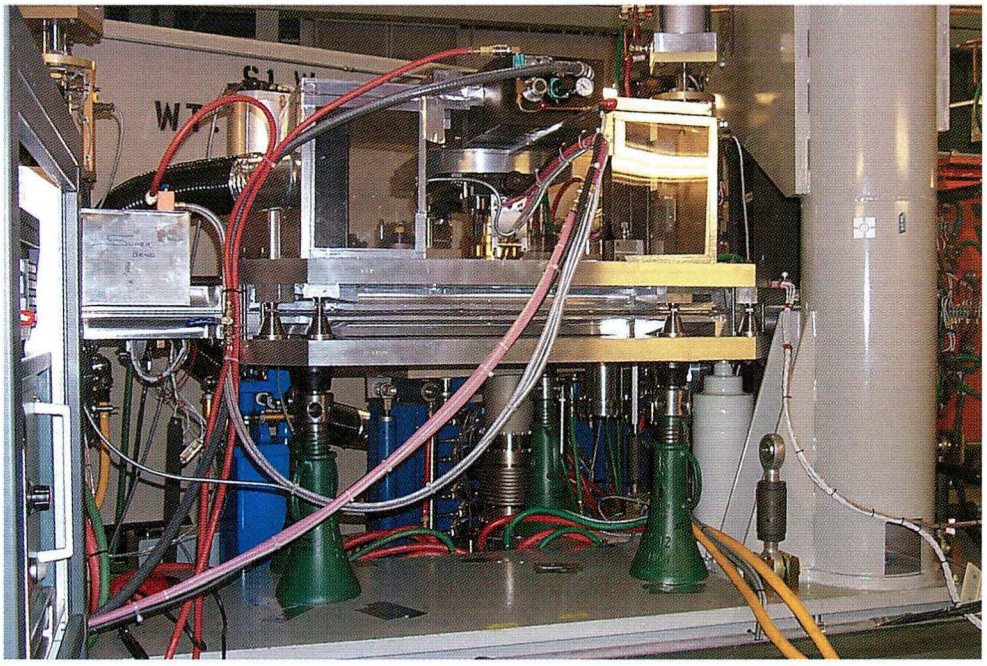

Figure 1 With this apparatus, the ALS vacuum chamber was machined in situ to prepare for the installation of superconducting bend magnets in the summer of 2001.

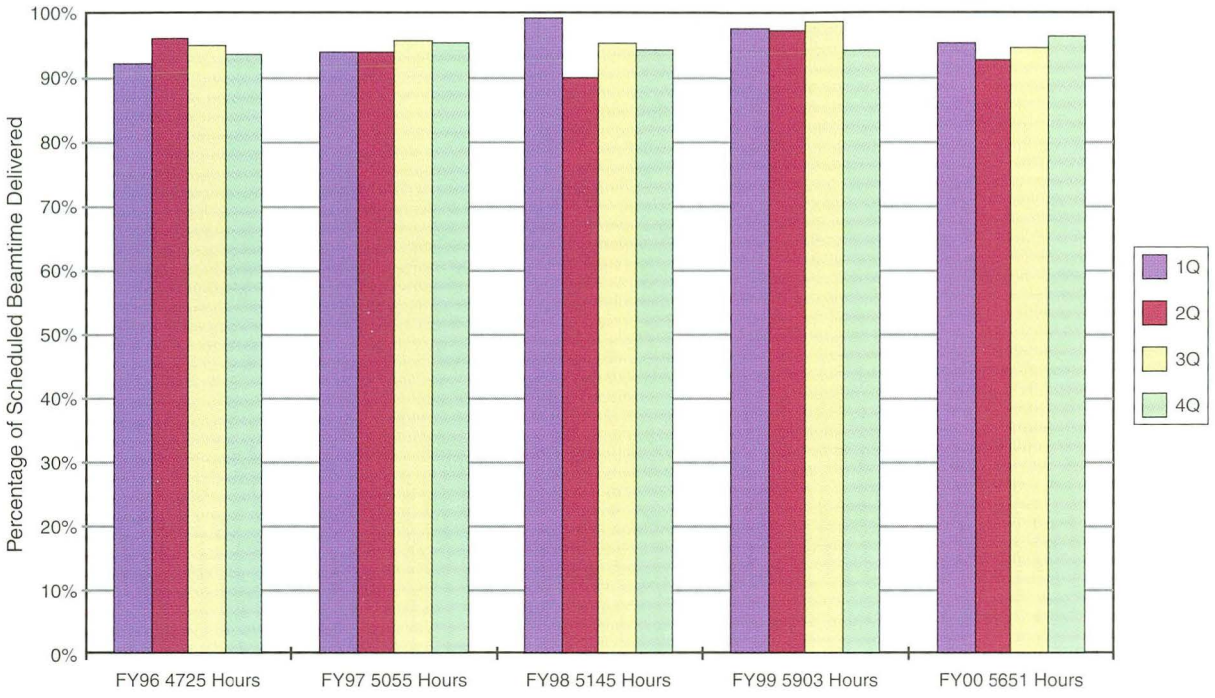

Figure 2 ALS operational reliability for FY00 (percentage of scheduled user beamtime that was actually delivered).

Changes in User and Instrument Hours

The operations schedule continued with the minimal number of maintenance and installation periods, as it has for the last several years. This has provided the maximum number of hours for user operations while allowing for needed maintenance and installation on a monthly basis. In addition to these monthly periods, this year we had one five-week installation shutdown, primarily to prepare for superbend installation. As a result of this longer installation period, the scheduled operating hours decreased from 5,903 hours in FY99 to 5,651 hours in FY00.

Even with the decrease in the number of scheduled operating hours, we were able to increase the number of instrument hours (user hours multiplied by the number of simultaneous beamlines that can accept beam), as shown in Figure 3. We finished the year with 23 beamlines operating simultaneously, up from 21 at the end of the previous year. This increase resulted in the delivery of 115,314 instrument hours, an increase of 3% over FY99.

Improvements in Beam Quality

To meet the goal of providing high-quality light to users in a consistent and reliable manner, we work very closely with the Accelerator Physics Group, which monitors the performance of the machine. To ensure high reliability and positional stability, we hold a weekly operations critique meeting, at which the performance of the accelerator over the previous week's run is reviewed. In

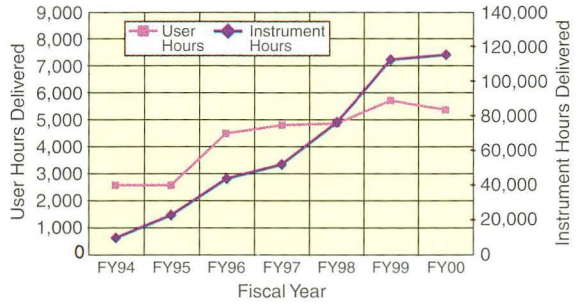

Figure 3 Number of delivered user hours (hours of beam delivered to ALS users) and instrument hours (user hours times the number of simultaneously operating beamlines) from FY94 through FY00.

particular, we look at reliability, lifetime, orbit, and beam size stability. Figures 4 through 6 show the accelerator's performance for a typical week (December 5–11, 2000). The 1.9-GeV multibunch user run lasted from 8:00 a.m. December 5 until midnight on December 10. The first third of day one and all of day seven were used for accelerator physics studies and accelerator maintenance.

RELIABILITY

The plot of beam current over time (Figure 4a) is a measure of how reliably beam has been delivered. Beam dropouts for each week are labeled and noted in the corresponding report (Figure 4b), and the causes are discussed by the group during the weekly meeting. Action is taken to correct recurring problems. In addition, statistics are compiled each week to show how reliably fills were completed. For typical 1.9-GeV operation, fills are scheduled every six hours. Each fill is categorized according to duration. At the end of the week, the data are charted to show the percentage of fills that lasted the full six hours and the fraction that ended earlier than planned (Figure 5). Our goal is to meet the scheduled six-hour fill length 95% of the time. Currently, more than 90% of the fills meet this six-hour goal.

A

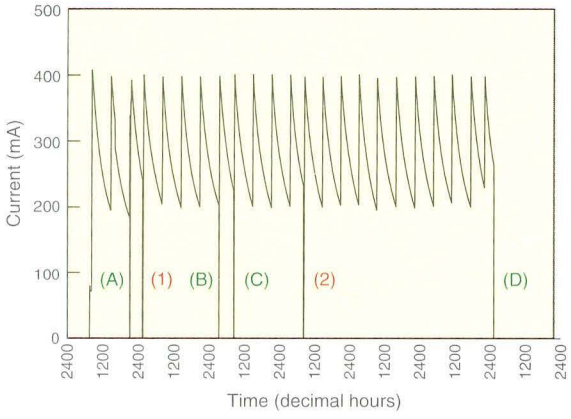

B

Drop Outs (Before Completion of Beam Delivery)

Outage	Date	Time	Description	Duration
(1)	12/6/2000	1:15	RF trip (Klystron Arc)	25min
(2)	12/8/2000	8:05	RF trip (Klystron Pwr)	25min

Controlled Access, Early Refilling, or During Refill

Outage	Date	Time	Description	Duration
(A)	12/5/2000	21:00	Lost during refill	30min
(B)	12/7/2000	3:15	Change camshaft bucket	3min
(C)	12/7/2000	8:25	Change camshaft bucket	3min
(D)	12/11/2000	1:20	End of run	

Figure 4 A typical week's operations (December 5–11, 2000) as reported in the weekly operations critique: (*A*) plot of beam current over time and (*B*) causes of beam dropouts.

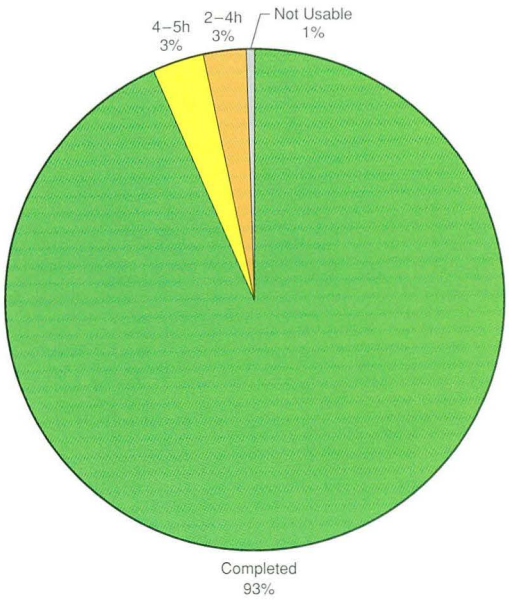

Figure 5 Fill statistics during a typical week (December 5–11, 2000), showing the percentage of fills that lasted the scheduled six hours and the percentage that ended earlier than planned.

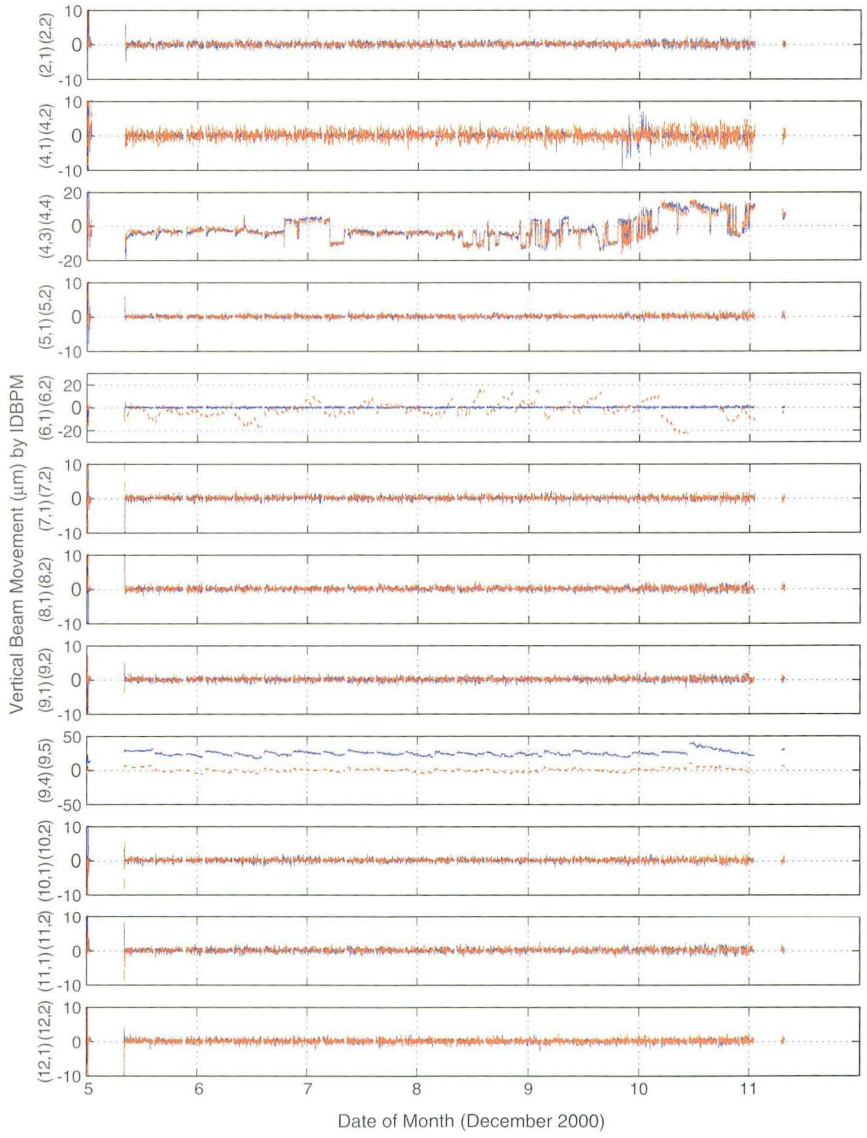

Figure 6 Vertical beam positions as measured by beam position monitors at upstream (*red*) and downstream (*blue*) ends of straight sections, in the center of the Sector 4 straight (*4,3* and *4,4*) and in the center of the Sector 9 arc (*9,4* and *9,5*) December 5–11, 2000. The BPMs with larger deviations in sectors 4, 6, and 9 were not in the correction loop. The position of the beam at the other BPMs, which were in the correction loop, remained constant within a few microns for the duration of the run.

BRIGHTNESS, LIFETIME, CURRENT, AND BEAM SIZE

The lifetime, τ, in the ALS is predominantly determined by large-angle intrabeam (Touschek) scattering. As a result, the lifetime is proportional to the transverse beam size, σ_x and σ_y, and inversely proportional to current, I:

$$\tau \propto \frac{\sigma_x \sigma_y}{I}$$

A figure of merit for brightness that we call the Touschek factor, *Tou*, is defined as

$$Tou \propto \frac{\tau I}{\sigma_x \sigma_y} \ .$$

The brightness of the beam increases with *Tou*.

During the operations critique meeting, we plot the archived beam currents and transverse beam sizes over the week as well as the calculated lifetimes and *Tou*. Sudden changes in *Tou* mean changes in the beam quality and are usually indicative of a problem with the machine (such as problems with the transverse or longitudinal feedback system). After identifying a sudden change in *Tou*, we can pinpoint the cause by looking at the histories of the beam sizes and lifetime.

We have also observed a steady increase in quality (as measured by *Tou*) over the past two years. For instance, we know that the *Tou* was 0.5 in May of 1999 (before the harmonic cavities were installed). Now it varies from 0.8 to 1.2 over a six-hour run. Since we are operating with the same transverse beam sizes, this translates into an improvement in lifetime of 1.6 (at 400 mA) to 2.4 (at 200 mA). This is a real gain in performance of the machine and comes from many sources—the harmonic cavity, increased rf power, and filling more buckets. This performance improvement in lifetime translates into an increase in halving time (time to decay from 400 mA to 200 mA) of 5 hours (May 1999) to 8 hours or more.

POSITIONAL STABILITY

In order to stabilize the beam position, the orbit of the beam in the storage ring is corrected once every second. This holds the beam position constant at the upstream and downstream ends of most of the straight sections. The performance of the correction algorithm is monitored routinely and adjusted if required to optimize performance. Figure 6 shows the stabilizing effect of the correction loop on vertical beam position during a typical week.

TUNE FEEDFORWARD AND BEAM SIZE STABILITY

The transverse beam size (particularly vertical beam size) is a function of the betatron tune (the number of free oscillations an electron makes during one circuit around the ring). Changes in insertion device gap sizes can change the betatron tune. The vertical tune is shifted higher when the gaps are closed, which moves the tune closer to the coupling resonance (where energy is transferred from one transverse plane to another). This coupling of the horizontal and vertical betatron tunes causes the beam size to increase vertically. Thus, vertical tune changes are largely responsible for changes in the vertical beam size. In mid 2000, we implemented a feedforward system to minimize this effect. Since implementing the tune correction, the change in vertical beam size associated with gap changes has been reduced from approximately 25% to 1–2%. An exception is the elliptical polarization undulator (EPU). At maximum polarization, the vertical beam size can increase up to 15% when the EPU is at minimum gap.

To illustrate the improvement in beam stability with the tune feedforward on, we have plotted tune changes and beam size changes for a day before and a day after insertion-device tune feedforward was implemented (Figure 7). As seen in the plots, before tune compensation, beam size changes correlated directly with tune changes; however, after implementation of tune feedforward, only small beam size changes could be seen.

Work is now in progress to design a tune compensation scheme for the EPU. Because of the speed and frequency with which the EPU gaps are moved, the compensation is more complicated than it is for the other insertion devices. To compensate for the EPU tune shifts without introducing large orbit changes will most likely require fast orbit compensation. We plan to implement a fast (kHz) orbit feedback system to address this in the future.

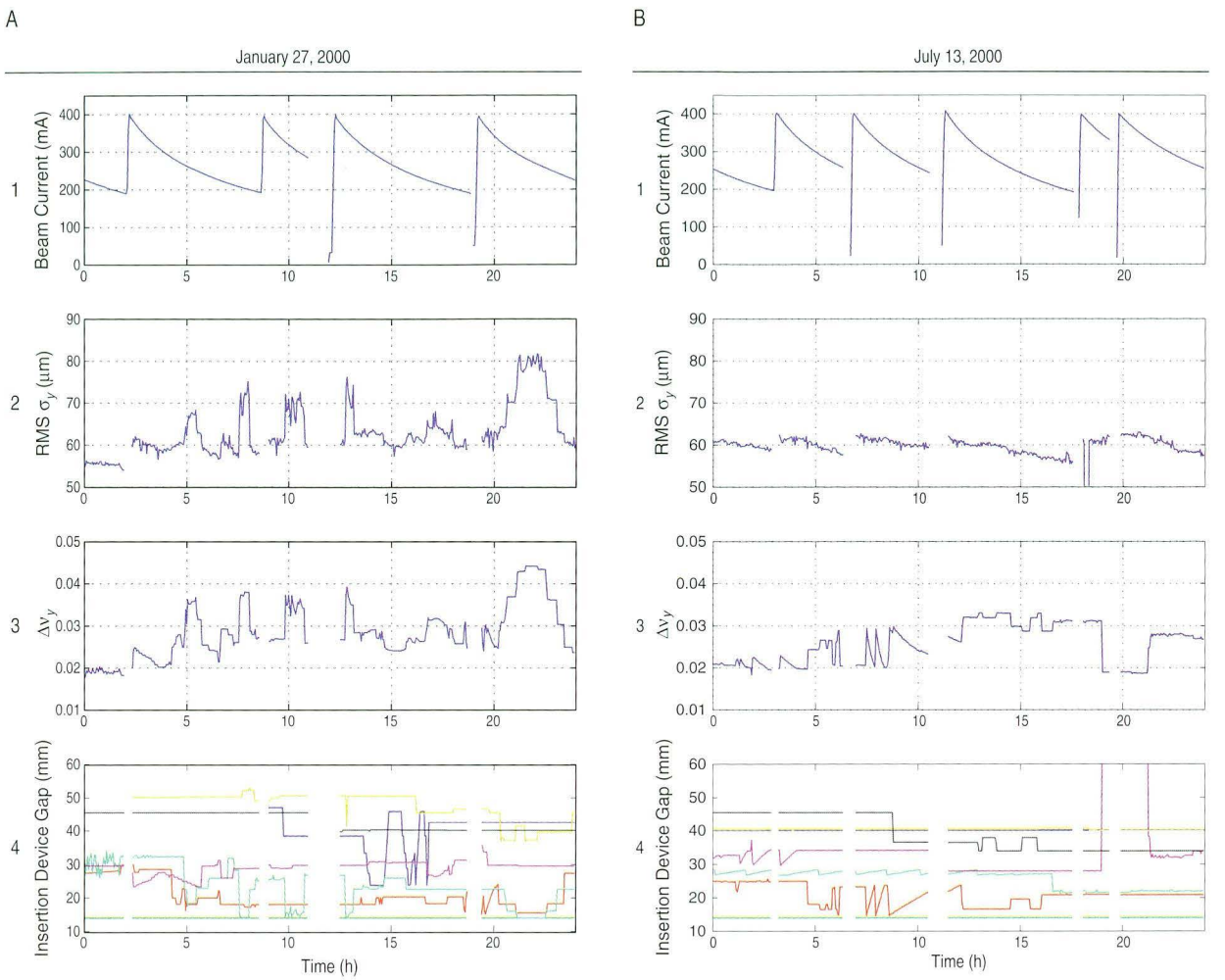

Figure 7 Beam size changes (*A*) before and (*B*) after tune feedforward was implemented. For each date, the storage ring beam current is plotted in trace 1, and the vertical beam size is plotted in trace 2. The calculated tune shifts resulting from the gap changes (excluding wiggler and EPU longitudinal tune shifts) are shown in trace 3. Changes in the insertion-device gap position are plotted in trace 4. Before tune compensation, beam size changes correlate directly with tune changes; after compensation, only small beam size changes can be seen.

Facility Growth

One major shutdown was scheduled during 2000 for the installation of new equipment. This was the February/March shutdown, in which two sections of the vacuum chamber were machined in situ in preparation for installation of the superbends during the summer of 2001. The machining was performed by Guy Pulsifer and Paul Knopp, under the general direction of Tom Henderson. Figure 8 shows one section of the vacuum chamber after machining. Also during 2000, design and construction of multiple superbend beamlines was started. This major initiative, more fully described in the Experimental Systems and Accelerator Physics sections, will greatly increase the range of science and the user base of the ALS.

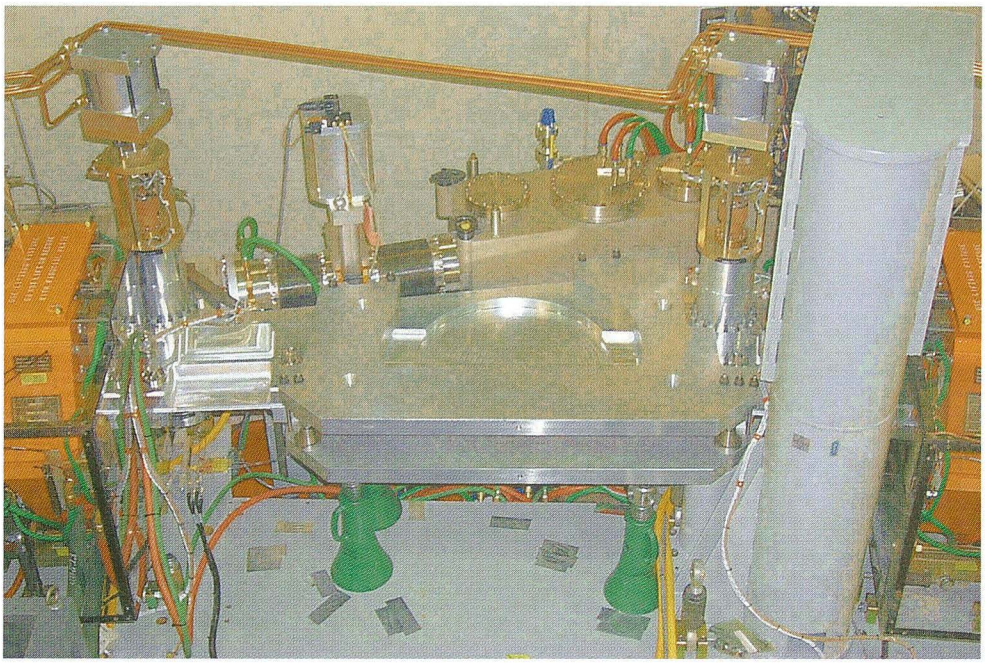

Figure 8 One of the three ALS vacuum chambers after machining in situ to prepare for superconducting bend magnet installation.

Accelerator Physics

David Robin
Accelerator Physics Group Leader

Introduction

One of the most important missions of the ALS is to provide a healthy, vibrant user facility that satisfies the needs of both the present and future user communities. To achieve the goals of this mission, the Accelerator Physics Group performs several important roles. The first is to make certain that the ALS provides high-quality beam in a reliable manner to users. The second is to strive to understand and continually improve the performance of the machine, keeping it at the forefront of synchrotron radiation sources. The third role is to ensure that machine upgrades are implemented smoothly, with minimal adverse impact to users. The fourth is to study potential upgrades to the facility that will enhance the capabilities of the ALS. In all these roles, the Accelerator Physics Group works very closely with other groups both within the ALS and elsewhere at Berkeley Lab.

Significant advances in our understanding and improvement of the machine's performance were realized in 2000, particularly in lifetime, beam size and orbit control, and injection. In lifetime, the ALS has realized a 50% improvement during normal user operation, allowing fill times to increase from four to six hours. This is primarily a result of an enhanced understanding of the interaction between the third-harmonic cavity system and other rf and feedback systems. In addition, improvements were made in understanding the momentum acceptance (the range of electron momentums that are stable in the storage ring). We expect that further improvements will allow for even longer lifetimes and run lengths.

In orbit stability, a significant improvement was made in 2000 with the commissioning of a fast (200-Hz) orbit feedforward system for the Elliptically Polarizing Undulator (EPU). This allowed us to reduce the time required to shift the device between left and right circular polarization modes from 8 to 1.6 seconds. We are now at the mechanical limit of the device. In addition, a new mode of operation of the EPU was successfully tested, where the jaws of the device can move in such a manner as to provide arbitrary-angle linear polarization. This mode of operation was not envisioned when the device was built and significantly enhances the capabilities of the device.

Our understanding of the dynamics of the injection process also improved. In particular, we developed a technique to study the matching of the injection line to the storage ring. This will be critical if we ever want to operate in a continuous top-off injection mode. Such frequent low-current filling of the storage ring would avoid the breaks in operation required for full refills.

The Accelerator Physics Group has been involved in two major projects this year: the superbend initiative and the PEEM3 project. These are detailed in separate highlights below. In addition to these projects, the group is involved in looking at future single-purpose radiation sources to enhance the capabilities of the ALS. The first is a storage ring designed for the generation of far-infrared radiation. The goal is to provide a stable, intense broadband source of infrared radiation with wavelengths from a few microns to a few millimeters. The idea would be to place this ring on the top of the booster tunnel. In addition, the group is involved in helping support Berkeley Lab's Center for Beam Physics in its efforts to generate a dedicated femtosecond radiation source for pump-probe experiments with a recirculating linac. We expect that there will be significant progress on both of these sources in 2001.

Lifetime and Dynamic Momentum Acceptance

The lifetime of a synchrotron radiation source with small emittance (like the ALS) is dominated by Touschek scattering and is limited by the momentum aperture of the ring. Touschek scattering is the large-angle scattering of two electrons (usually within an electron bunch) leading to the exchange of energy from the transverse plane to a longitudinal plane. This scattering process can cause significant changes in the energy of the scattered particles. Depending on the dispersion at the position of the scattering, it may also induce large horizontal oscillations. To achieve good lifetimes, one has to provide a sufficiently large region in phase space where the trajectories are stable. This region is the momentum aperture.

Large momentum apertures are reached by providing enough rf voltage for a large electron "bucket" size and by avoiding degradation of the dynamic momentum aperture. At the ALS, the size of the momentum aperture depends strongly on the transverse dynamics. It is very sensitive to machine conditions, such as the betatron tune (the number of transverse oscillations an electron makes in one trip around the ring) and chromaticity (the derivative of the tune with respect to energy, a measure of how strongly the global focusing changes with energy) since depending on those conditions, the Touschek-scattered particles explore different resonance regions in the phase space.

An easy way to study whether the momentum acceptance of a ring is solely determined by the voltage of the rf cavities, or whether there are dynamic effects limiting it, is to vary the rf voltage. (The bucket size, and therefore the energy acceptance of the rf, is proportional to the voltage.) Because of the energy distribution of Touschek-scattered particles, the lifetime should be a quadratic function of the rf voltage, as long as there are no dynamic effects limiting the acceptance. The turnover point, at which a deviation from the quadratic behavior occurs, provides information about the nonlinear dynamics limiting the dynamic acceptance. Figure 1 shows three scans of the rf voltage for different linear chromaticities of the ALS, set by varying the strengths of the sextupole magnets.

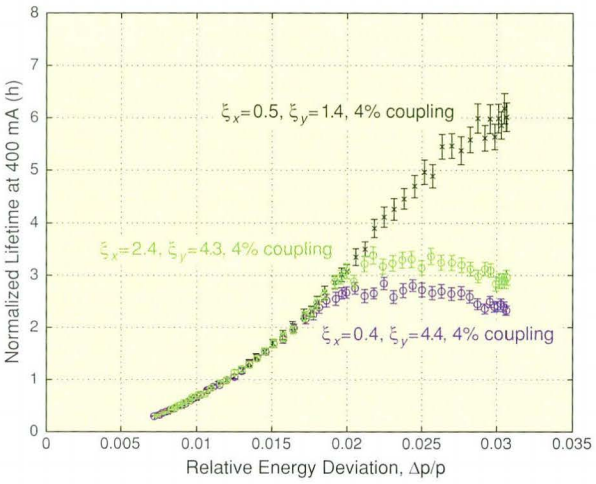

Figure 1 Scan of the energy acceptance of the rf bucket (varying the rf voltage) for three different linear chromaticities, nominal (*black*), increased vertical chromaticity (*blue*), and increased vertical and horizontal chromaticity (*green*).

As one can clearly see, the dynamic momentum acceptance, and therefore the maximum achievable lifetime, is very sensitive to the linear chromaticities. It is best for the nominal chromaticities (ξ_x = 0.5, ξ_y = 1.4), which are used in multibunch mode. It is significantly worse for a vertical chromaticity increased by 3 units (ξ_x = 0.4, ξ_y = 4.4). As seen in the figure, the maximum achievable lifetime differs in these two cases by more than a factor of two. This difference is surprisingly large, considering that the strength of the sextupoles varies by only a few percent. When both the horizontal and vertical chromaticities are increased (ξ_x = 2.3, ξ_y = 4.3), the resulting maximum lifetime is 25% larger than when just the vertical chromaticity is increased.

Unfortunately, it is sometimes necessary to operate the ring with increased vertical chromaticity. This is particularly true when operating in two-bunch mode. In such a mode, there are significantly higher single-bunch currents that require high chromaticities to damp the single-bunch instabilities. It is therefore of interest to understand the cause of this effect.

To study and understand the effects limiting the dynamic momentum acceptance, we used two single-turn "pinger" magnets together with turn-by-turn beam position monitors (BPMs). We first shifted the beam energy (by adjusting the rf frequency) and then kicked (deflected) the beam with the

pinger magnet. For each energy, we increased the horizontal kick amplitude until the beam was lost. The data sets for the three different chromaticity settings mentioned above are shown in Figure 2. The agreement between the estimated dynamic momentum acceptance of these measurements and the direct measurement using the rf-amplitude scans is very good. In addition, one clearly sees completely different structures in the shape of the loss regions in all three cases.

Using beam oscillation and beam loss data, one can use frequency map analysis to identify which resonances in tune space (lines along which coupling causes energy transfer between horizontal and vertical planes, leading to instability) cause those loss regions. The analysis (Figure 3) showed that the large difference in lifetime is not caused by a large difference in the strengths of resonances, but by the fact that different linear chromaticities cause the particles to sample completely different regions in phase space. Thus, the particles may experience completely different sets of resonances.

Figure 2 shows a large loss region on the right-hand side of graphs B and C (at positive energy deviations). In graph A, the loss region lies outside the plot on the far right side. In the cases with high vertical chromaticity, this loss turned out to be caused by the coupling resonance. Now let's look at the case where the horizontal chromaticity is increased. From Figure 1, we see that there was an improvement in lifetime of about 25%. Again, the higher horizontal chromaticity changes the area of phase space the Touschek-scattered particles probe. Comparing plots B and C in Figure 2, one can see

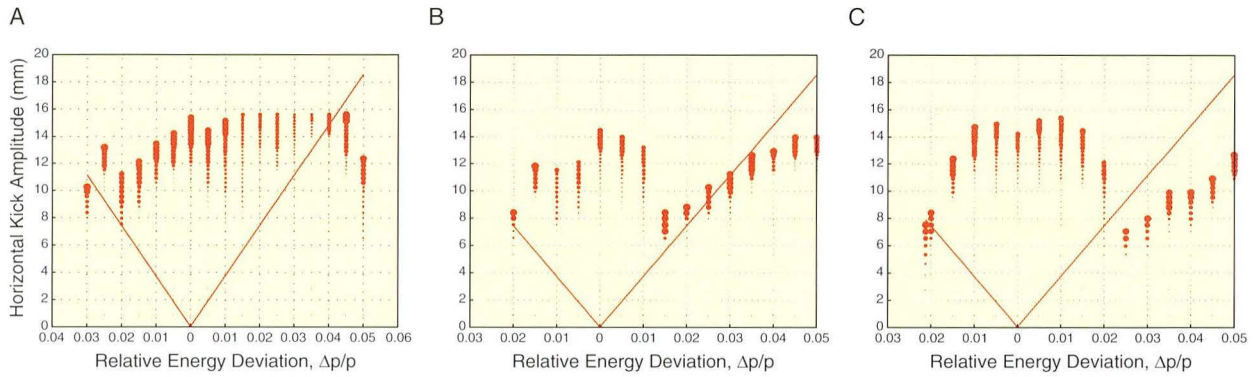

Figure 2 Beam loss data for different energy offsets (rf frequencies) verses horizontal kick amplitude at (*A*) nominal, (*B*) increased vertical, and (*C*) increased vertical and horizontal chromaticity. The thickness of a dot indicates the relative magnitude of the beam loss at that point. Red lines represent the amplitudes to which a particle will oscillate after being Touschek scattered. The intersections of these lines with the loss regions (areas with thick dots) roughly define the dynamic momentum acceptance. Particles scattered to lower energies will be stable, and particles scattered to higher energies will be lost.

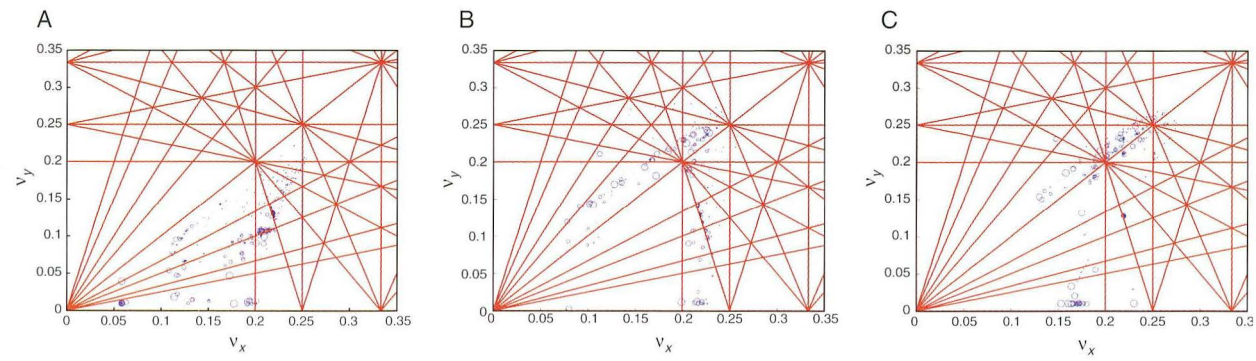

Figure 3 Beam loss data (*blue dots*) plotted in tune space for (*A*) nominal, (*B*) increased vertical, and (*C*) increased vertical and horizontal chromaticity. Resonance lines are shown in red. Because of the different chromaticities, completely different resonance regions are sampled.

that this shifted the loss region caused by the coupling resonance to the right (i.e., to larger energy deviations), leading to a larger dynamic momentum acceptance. The larger acceptance can help to increase the lifetime in two-bunch operation. Simulations based on the calibrated model of the ALS (Figure 4) are in very good agreement with these measurements.

These simple empirical tools give us real insight into beam dynamics and mechanisms for particle loss. They have helped us to diagnose problems and to tune and optimize the storage ring for maximum performance. They will be particularly important to ensure that upgrades to the machine (such as the addition of superbends and narrow-beta insertion devices) go smoothly.

This research was conducted in collaboration with Winfried Decking from DESY, Germany, and Jacques Laskar from Astronomie et Systémes Dynamiques, IMC–CNRS, France.

Progress Update on the Superbend Project

The ALS is planning to replace three of its existing 1.3-Tesla, normal conducting dipole magnets with three new 5-Tesla superconducting dipoles (superbends) in the storage ring in 2001. These magnets will be a bright source of higher-energy photons and will extend the capabilities of the ALS. Compared to the normal dipoles, the brightness and flux of the superbends are an order of magnitude higher at a photon energy of 10 keV and two orders of magnitude higher at 20 keV.

Superbends will be placed in three of the 12 sectors (4, 8, and 12), as shown in Figure 5. Figure 6 shows how the three sectors will be modified to accommodate these stronger magnets. The central dipole in each sector, B2, will be replaced by a superbend. Two new quadrupoles, QDA1 and QDA2, will be added to the lattice, and the QFA quadrupoles in a superbend sector will be put on separate power supplies. The change in the quadrupole configuration is necessary to better match the superbend sectors to the nonsuperbend sectors.

During the transition to superbend operation, we hope to minimize the amount of unscheduled operational downtime and poor operation. Therefore, the project team has adopted the strategy of precommissioning as many subsystems (with and without beam) as possible before the actual installation of the superbends. As a result, the installation activities for the superbend project are taking place in two medium-length (few-week) shutdowns rather than one long shutdown.

In the first shutdown (in March 2000), all major components of the project, excluding the actual superbend magnets, were installed. That included machining the vacuum chambers, installing the six new quadrupoles (QDAs), pulling cables for the

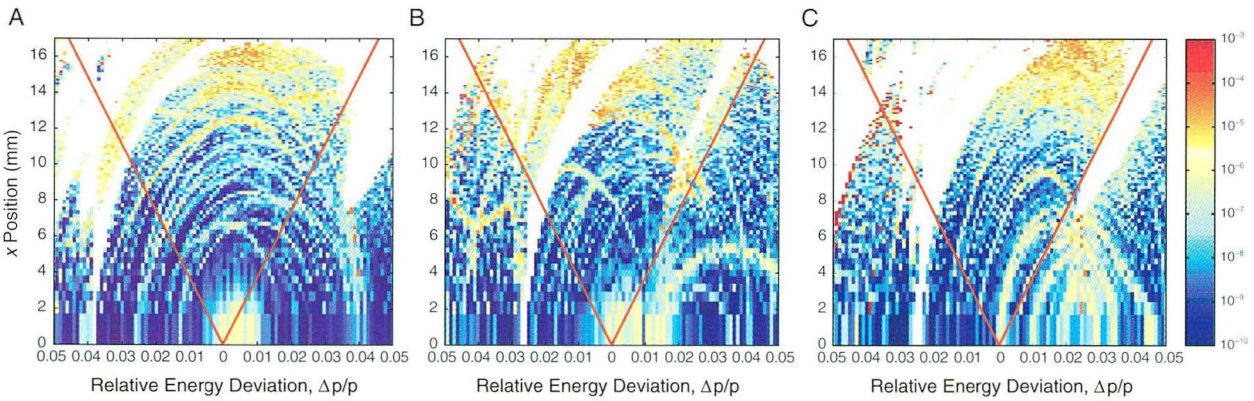

Figure 4 Simulations of electron diffusion (in configuration space) for (*A*) nominal, (*B*) increased vertical, and (*C*) increased vertical and horizontal chromaticity, based on the calibrated machine model of the ALS. The color indicates the diffusion rate, as defined by the change in transverse oscillation frequency with time. Blue areas indicate low diffusion, red areas show high diffusion (10 billion times higher than dark blue), and areas without color indicate unstable regions (where particles are lost within 1000 turns).

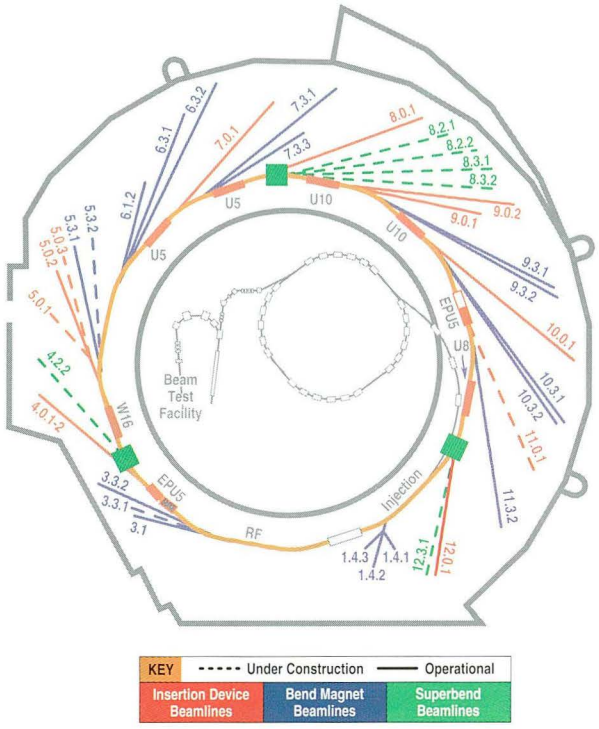

Figure 5 Locations for installation of superconducting bend magnets at the ALS.

superbend magnets, recabling the existing quadrupoles (QFAs), and moving nine magnet power supplies over to a new control system. This is the single largest modification made to the controls and the storage ring lattice since the ring was first installed. In spite of all these modifications, the shutdown and ring startup went exceedingly well, with beam being stored and ramped within several hours after startup.

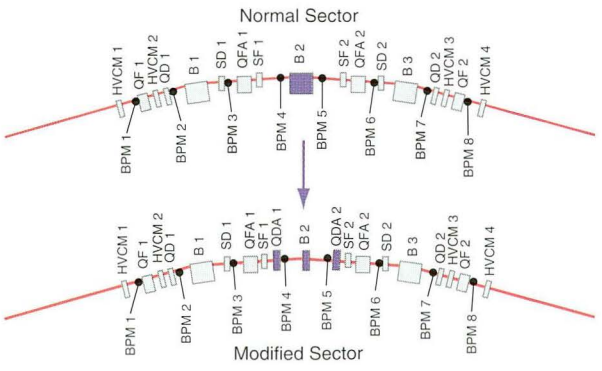

Figure 6 Changes to be made to the ALS lattice in a typical superbend sector.

There have been ongoing studies to ensure that the installation of the superbends does not have an impact on the performance of the storage ring. A particular concern was that the superbends would perturb the natural 12-fold symmetry of the storage ring and that this would excite resonances in the beam motion and a subsequent reduction in the injection efficiency and lifetime. Since the installation of the QDA quadrupoles, it has been possible to experimentally perturb the periodicity of the storage ring and simulate (to some degree) the impact of the superbends on operation. In particular, dynamic momentum acceptance measurements were made (see Lifetime and Dynamic Momentum Acceptance, above). The results so far indicate that, even with the symmetry breaking, the ALS can be operated with negligible performance degradation.

Concurrently in 2000, significant progress was realized in the construction of the four superbend magnet/cryostat assemblies. In collaboration with the ALS and the Accelerator and Fusion Research Division, Wang NMR successfully built the first of four superbend magnets. The second through fourth magnetic systems are currently under construction. The first magnet cryostat system can be seen in Figure 7. The superbend magnet has several important features. It is conduction cooled, in order to place the coils as close to the storage-ring vacuum chamber as possible, and uses a two-stage Gifford–McMahon cryocooler to make operation in the ALS as automatic, efficient, and economical as possible.

On August 24, the first superbend magnet was successfully charged. The data from that test can be seen in Figure 8. In the test, the magnet was slowly ramped from 0 A to 302 A and back down to 0 A without quenching. This was a higher current than the 291 A required for 1.9-GeV operation. In the first test, it was decided to ramp slowly (0.1 A/s) and to limit the maximum current to about 300 A. In subsequent tests, the ramping rates have been increased to 0.5 A/s, and the magnet has reached 320 A without quenching.

Other performance tests of the first superbend assembly have gone well. Preliminary measurements of the magnetic field reveal that the correlation between magnet current and integrated dipole field is very close, as predicted. Extensive vibration measurements have been carried out, and they have

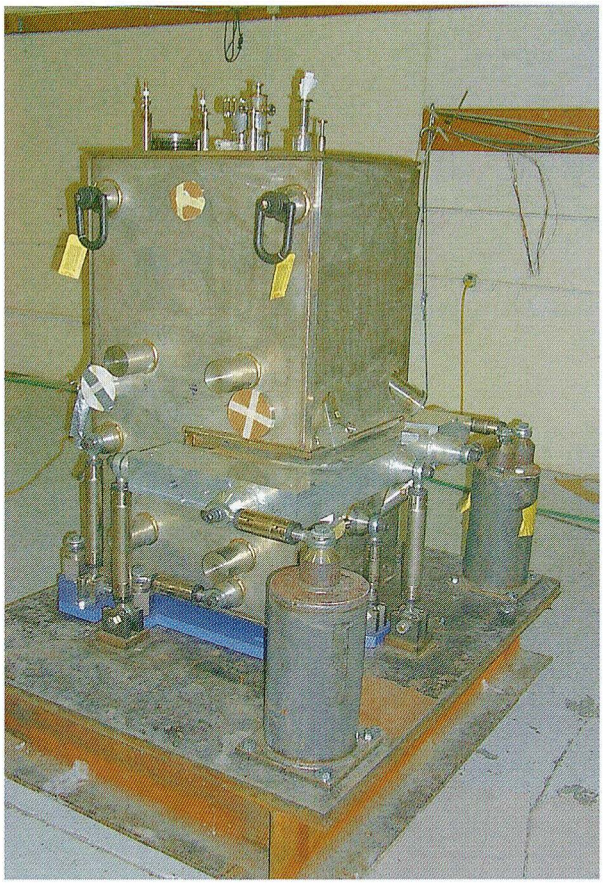

Figure 7 The first superbend magnet cryostat system.

indicated that there will be no strong increase in beam motion due to superbend vibrations. Initial thermal tests of the superbend revealed larger-than-predicted heat leaks. Modifications were therefore made that have brought the magnet's thermal performance up to the specifications. We hope to complete testing of the first magnet (magnet, power supply, control, and alignment measurements) early in 2001. The remaining three magnets will be tested upon completion.

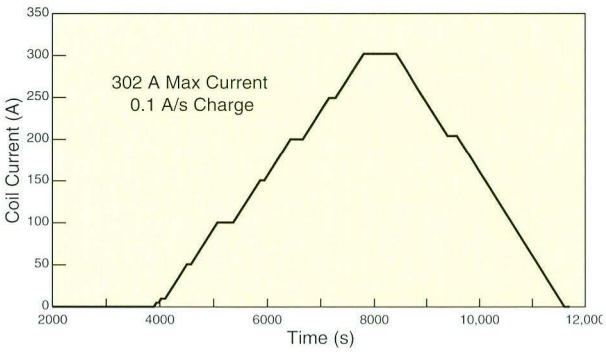

Figure 8 First successful charge of prototype superbend magnet.

Optics Design and Modeling of the PEEM3 Beam Separator

The goal of the ALS PEEM3 project is to develop a high-resolution x-ray photoemission electron microscope (PEEM) with a high transmission. In particular, the design goal is to achieve a 2-nm resolution for 1-μm samples (and 20 nm for 10-μm samples) with a reasonable flux. This microscope should also be able to deliver a much higher flux than PEEM2 (the existing ALS PEEM) does, at a resolution already demonstrated by PEEM2 (20–50 nm). The project is a collaboration between the Accelerator Physics Group, ALS Mechanical Engineering, and the Experimental Systems Group.

At first glance, it may be unclear why the Accelerator Physics Group is working on problems in electron microscopes. What does an electron microscope have in common with a high-energy particle accelerator like a TeV linear collider? The answer is "quite a lot." Both are linear particle accelerators. The principles and techniques used to reduce optics aberrations in order to achieve high resolution in an electron microscope are the same as those used to reduce optics aberrations in order to achieve small interaction spot sizes in a linear collider. Therefore, the Accelerator Physics Group is bringing its expertise to bear upon the problems of the PEEM design.

In an x-ray PEEM, the chromatic aberrations of the microscope front end (the objective lens and accelerating gap) are the main limiting factors for resolution improvement. Unlike aberration-uncompensated PEEMs such as PEEM2, PEEM3 depends on elaborate aberration correction schemes to improve the resolution of the microscope and increase the transmission at a given resolution. The beam separator is the centerpiece of the correction scheme.

The basic idea of the aberration correction scheme was proposed by a German research group and was adopted in a similar x-ray PEEM project, SMART, at the BESSY II synchrotron. In the scheme, a normal-incident-angle electron mirror is used to perform the aberration correction of the front end. The scheme requires bending elements to bend the electron trajectory from the front end to the mirror. These bending elements collectively form an electron beam separator for the microscope.

To reduce the resolution impact of the beam separator, the bending section should be designed to have minimal aberrations. A highly symmetric and compact beam separator design with two π transformations in both transverse planes is desirable. Such an optical system is free from all the second-order geometric aberrations and second-order chromatic aberrations, with the exception of the chromaticity terms. The remaining aberrations are from third and higher order terms.

The beam separator is the only magnetic element in the microscope, lacking the axial symmetry possessed by other electrostatic elements. The design goal for the separator is to make it invisible to the rest of the system, which translates to an overall aberration contribution of about 0.5 nm per pass through a quarter of the separator.

The focus of our work is to design such a highly symmetric beam separator, evaluate its performance, and improve its optics design. During the months that this report covers, we have performed the following tasks for the ALS PEEM3 project:

- developing/debugging a charged optics code for designing and modeling the beam separator (E. Forest, R. Schlueter);
- developing an electron distribution model and a simple tracking code to analyze the impact of the separator aberrations on the electron beam distribution at various locations in PEEM3 (Y. Wu, D. Robin);
- designing and analyzing two specific beam separators: a 90-cm and a 28-cm design (E. Forest, D. Robin, Y. Wu).

The initial design of the beam separator was made by M. Scheinfein and S. Anders and was rather large (90 cm). Before 2000, the impact of this separator on the resolution had not been extensively studied. The total aberration also depends on the acceleration gap voltage, the magnification of the objective lens, fine tuning of the separator, and the location of the emission point on the sample. Using the Forest/Schlueter code, we analyzed the aberrations of this version of the separator and found them to be four times larger than acceptable. We then redesigned the beam separator, reducing its size from 90 cm to 28 cm, and the aberrations were similarly reduced to acceptably small levels for a high-resolution PEEM. Figure 9 depicts the distribution of electrons after passing through the 90-cm separator and the distribution after passing through the 28-cm separator, assuming a 20-kV acceleration gap and a 20× magnification in the front end. In 2000 we began the tolerance analysis for this improved design.

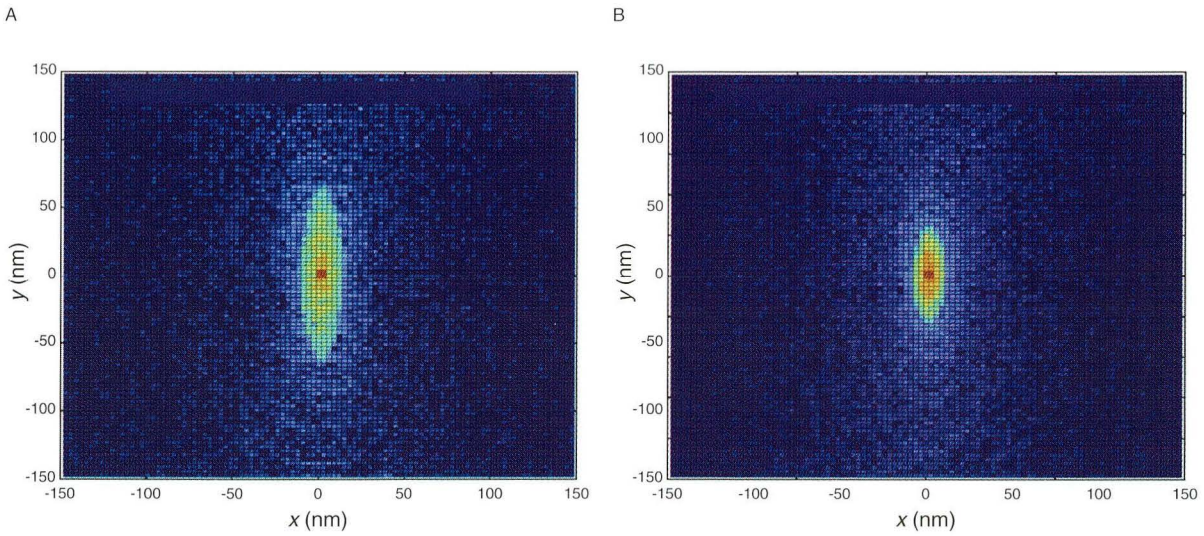

Figure 9 Distributions of electrons in PEEM3 after passing through (*A*) the 90-cm separator and (*B*) the 28-cm separator, assuming a 20-kV acceleration gap and a 20× magnification at the front end. The color scale shows intensity (red is highest).

Experimental Systems

H. A. Padmore
Experimental Systems Group Leader

Overview

The Experimental Systems Group (ESG) serves several different functions, including design of beamlines and endstations together with ALS engineers, development of the techniques of synchrotron radiation research, and scientific outreach. The latter entails making contact with potential new user groups, discussing the application of synchrotron radiation to specific problems, demonstrating custom-designed apparatus, assisting with preparation of proposals for dedicated facilities, and ultimately constructing new beamlines and endstations. Each of these functions is evident in the long list of ongoing and new projects. The past year has seen the group's highest level of activity so far, from advocacy for new projects through to scientific research on completed beamlines. Below are brief summaries of the group's activities in several areas, followed by more detailed highlights of three key projects.

A deep-etch x-ray lithography (LIGA) beamline is being constructed under contract with AXSUN Technologies, an East Coast manufacturer of optical communications equipment. Beamline 3.3.1 makes use of the existing Beamline 3.3 front end and is expected to begin commissioning in March 2001. This beamline will consist of a high-vacuum tube terminating in a cooled beryllium window, a small hutch, and a beamline control and safety system. Beamline 3.3.1 is adjacent to our existing LIGA facility (Beamline 3.3.2), which was built for

Figure 1 Experimental Systems Group members, *left to right*: *Front row*, Tony Warwick, Simone Anders, Tony Young, Feng Jun, Phil Heimann, Malcolm Howells, Bob Batterman, Sirine Fakra; *middle row*, Nobumichi Tamura, Simon Clark, Greg Morrison, Andrew Franck, Marsha Fenner, Wayne McKinney; *back row*, Rich Celestre, Steve Irick, Keith Franck, Andreas Scholl, Al Thompson, Hendrik Ohldag, Howard Padmore, Everett Harvey. Not pictured: Alastair MacDowell, Jim Patel, Ernie Glover, John Spence, Frithjof Nolting, Der-Hsin Wei, Wenbing Yun.

activities led by Sandia National Laboratory and the Jet Propulsion Laboratory. A more versatile endstation is now required by this team, so a new hutch is being constructed in conjunction with Beamline 3.3.1.

A new facility for the Molecular Biology Consortium, Beamline 4.2.2, is being constructed to take light from a superbend source for protein crystallography. The team is led by Philip Matsumura (University of Illinois at Chicago) and Edwin Westbrook (Argonne National Laboratory). The ALS is providing a front end and a collimating mirror system, including mirror, bender, and vacuum system, as well as assistance with other parts of the beamline, such as the endstation minihutch. The research team is responsible for the construction of the main

beamline components, including a sagittally focusing two-crystal monochromator and refocusing mirror system. This is due for completion in 2002. Another protein crystallography beamline (Beamline 12.3.1), combined with small-angle x-ray scattering (SAXS), is being designed and constructed for a research team led by John Tainer of the Scripps Institute and Priscilla Cooper of Berkeley Lab. The protein crystallography component is similar to that of Beamlines 8.2 and 8.3 (see highlight below), but with a second broad-bandpass monochromator using multilayer mirrors. This second monochromator will be used for SAXS studies of proteins in solution.

The femtosecond dynamics beamline (Beamline 5.3.1) consists of a single toroidal mirror to transfer light from a bend-magnet source into an x-ray hutch. The beamline offers a range of monochromators and spectrometers that can be used in conjunction with streak-camera detection for picosecond time resolution, or with an ultrafast "slicing" source (80 fs), in which a laser is used to interact with the electron beam, ultimately separating out an 80-femtosecond slice of the beam in the field of a bend magnet. This technique was invented by Sasha Zholents and Max Zolotorev of the Berkeley Lab Center for Beam Physics and demonstrated by a team led by Bob Schoenlein of the Lab's Materials Sciences Division. The beamline is complete, initial experiments are under way, and the first experiments with the slicing source are to be started in late spring 2001. Phil Heimann, leader of the beamline design team, and Ernie Glover are developing the technology and science of studying ultrafast dynamics, working closely with Bob Schoenlein, the University of California, Berkeley, (UCB) physics group of Roger Falcone, and other groups.

A research team headed by Harald Ade (North Carolina State University), Adam Hitchcock (McMaster University), and scientists from the Dow Chemical Company are constructing a scanning transmission x-ray microscope (STXM) dedicated to polymer research on Beamline 5.3.2. This microscope is similar to the STXM under development for use in molecular environmental science (see highlight below). An ALS team led by Tony Warwick has designed and constructed a bend-magnet beamline that provides optimum efficiency at the carbon K-edge and optimum coupling into the zone-plate microscope. This beamline exemplifies our philosophy of designing application-specific beamlines. These are designed to work optimally for a narrowly defined task, giving excellent performance at low cost. After optics cleaning, we expect commissioning to be complete in spring 2001.

The Beamline 8.3.2 tomography project is led by Malcolm Howells. It uses a superbend source and is being designed and constructed for a research consortium with members at the National Institute of Standards and Technology, Lawrence Livermore National Laboratory, and the University of California, San Francisco, (UCSF) medical school. The system is flexible, allowing conventional absorption tomography, phase contrast, and microtomography. It will be applied to a diverse range of problems, from failure analysis of integrated circuits to medical imaging.

Following a successful test in which a prototype system was built for micro x-ray absorption spectroscopy (μ-XAS), Beamline 10.3.2 has been rebuilt by a team led by Alastair MacDowell, Rich Celestre, and Bob Sublett. This includes a completely new optical system, a new seven-element solid-state detector, digital electronics, scanning stages, and a software control program. The system is patterned after the very successful microdiffraction system on Beamline 7.3.3. The arrangement allows a simple flux/resolution trade-off with variable spot size (from 10 μm to < 1 μm). The system is being commissioned and should be available for independent investigators after the shutdown for superbend installation in September 2001.

In collaboration with the UCB chemistry department, the ALS is constructing a dedicated small-molecule crystallography station on beamline 11.3.1. To minimize costs, a team led by Al Thompson and Keith Franck has simplified and miniaturized. That is, the optical system has been simplified to a channel-cut two-crystal monochromator and a one-to-one-focusing toroidal mirror. The mirror should produce nearly aberration-free imaging, and the monochromator, though its spectral resolution will be limited by divergence, will be adequate for small-molecule diffraction. Miniaturization is possible by bringing all the components inside the shield wall.

This also allows looser tolerances on optical components. The entire optical system is about one meter long. As only monochromatic light emerges from the shield wall, radiation shielding issues are minimized as well. The physics and engineering designs are complete, and we expect commissioning to start in fall 2001.

In addition, we have started a national synchrotron radiation detector initiative, DetectorSynch. The first step in this initiative was taken in October 2000 with a national workshop in Washington D.C. organized by Al Thompson. This resulted in seven working group reports, and a white paper submitted to the DOE Office of Basic Energy Sciences. Over the next year, DetectorSynch will develop the ideas set forth in the working group reports and the white paper and lobby for funding to support the community's aims.

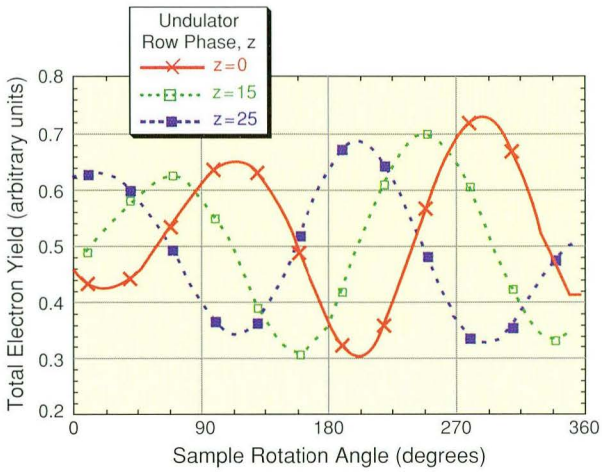

Figure 2 Generation of linearly polarized x rays at arbitrary azimuthal angles by the Beamline 4.0 EPU. Rotation of an oriented Teflon® film shows a cyclic total electron yield intensity when the *z*-phase is set to produce horizontally polarized light ($z = 0$) When the phase of the EPU is set to rotate the angle of the linear polarization by about 45 degrees ($z = 15$), the signal still has the 180-degree period, but it is shifted by 45 degrees. Finally, with the polarization rotated by 90 degrees, giving vertically polarized x rays ($z = 25$), the signal shows the same variation with sample rotation but is shifted by 90 degrees, as expected. (Experiment performed in collaboration with A. Hitchcock, McMaster University, and D. Castner, University of Washington.)

Elliptical Polarization Undulator Beamlines

Beamline 4.0.2 is the newest undulator beamline at the Advanced Light Source. Equipped with a Sasaki-type Elliptical Polarization Undulator (EPU) and a high-resolution monochromator, this facility is designed to produce high-flux beams from < 50 eV to > 1600 eV with spectral resolving powers of 5000–10,000. The EPU allows for full control of the polarization of the x rays, from linear horizontal, to helical, to linear vertical. A novel feature of the ALS EPU is the capability to rotate the angle of the linearly polarized light to any azimuthal angle. In collaboration with the ALS Accelerator Physics Group, we recently developed a fast electron-orbit correction system that allows full user control of the polarization at switching times down to 1.6 seconds between opposite helical polarizations.

The rotation of the linear polarization angle is produced by changing the *z*-phase of the EPU magnet rows in an antiparallel mode, rather than the parallel mode that produces circularly polarized light. Figure 2 illustrates this capability. This feature is critical for high-precision linear dichroism experiments. With the alternative, simply rotating the sample, the beam intensity distribution on the surface changes with rotation angle, which distorts the true dichroism. Avoiding this is even more critical in microscopy, where rotation of the sample would mean re-indexing its position to better than the resolution required to obtain a dichroic image. Rotation of the electric field vector opens a new door to high-precision dichroism experiments.

To supplement the PEEM2 photoemission electron microscope on bend-magnet Beamline 7.3.1.1, a branchline was installed on the EPU beamline this year. It consists of two mirrors: M141, a moveable, horizontally deflecting plane mirror; and M142, a horizontally deflecting cylindrical mirror. M141, the first to receive the beam, is mounted on an in-vacuum kinematic translation stage. M142 then focuses the beam to a horizontal size of 60 µm, a reduction of about 10 times compared to the horizontal size in the existing spectroscopy endstations. This arrangement allows for the rapid changeover from microscopy to spectroscopy experiments, and it allows the microscope to be in a fixed, permanent position—an important feature for high spectral resolution. Figure 3 shows the newly installed PEEM. The commercial PEEM system was provided by Boris Sinkovic (University of Connecticut), and ALS

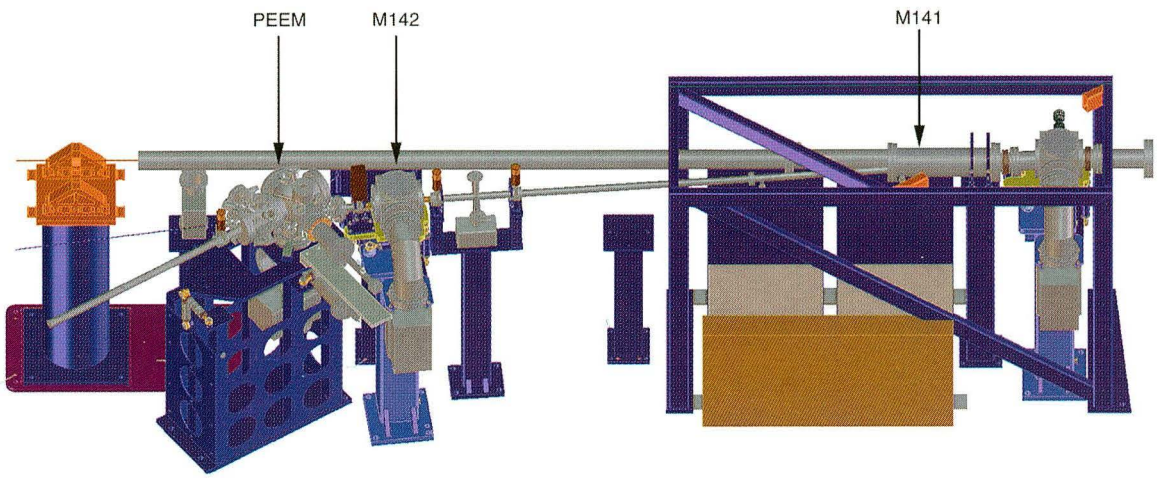

Figure 3 The newly installed PEEM endstation at Beamline 4.0.2. A portion of the existing beamline, the large tube running from right to left to the red exit slit, is also shown. When the M141 mirror is inserted into the beam, the beam is deflected into the M142 focus mirror tank and then into the PEEM.

Engineering designed and installed a new support system for the microscope. The system is now in operation, and has the advantage over PEEM2 of variable polarization at high spectral resolution, albeit with lower spatial resolution.

In 2000, work continued on another photoemission electron microscope for use with the EPU, the aberration-corrected PEEM3. The physics designs of the lens systems and magnetic separator have been completed, and the design of the electron mirror and the mechanical engineering of the system are under way. First commissioning is expected in 18 months. This microscope will ultimately receive light through a new beamline illuminated by a second EPU in Straight 4.

Molecular Environmental Science

A large soft-x-ray facility for molecular environmental science is under development in Sector 11. When complete, the beamline will have endstations for wet spectroscopy (x-ray emission and photoemission) and transmission x-ray microscopy. Completion is scheduled for 2002. The technical team is headed by Tony Warwick of ESG and Jim Comins of the Berkeley Lab Engineering Division, in collaboration with lead scientist David Shuh of the Chemical Sciences Division. The beamline will make use of an entrance slitless monochromator and a new EPU identical to that used in Straight 4.

The required energy range for this application is from 75 eV to 1500 eV, and at the low end, the monochromator thermal load will be high. Continuing developments begun by others at the BESSY synchrotron in Berlin, we have engineered a new SX700-style variable-included-angle plane-grating monochromator for these high heat loads. Our new design calls for a large silicon premirror with internal water channels 1.5 mm below the surface. This will prevent heat deformation of the premirror, thus preserving spectral resolution, while allowing the system to operate with the high thermal load that results from a low monochromator focusing parameter. (A parameter of 1.5 is most efficient for high-flux experiments at low energy.)

For this monochromator, a single grating substrate carries several ruling sets with different periods and groove profiles. The grating is changed by translating the vessel sideways. This allows any nonreproducible changes in pitch to be monitored. Coolant is introduced through lines within the drive arms, minimizing the need for couplings that flex, and the fittings are designed to transmit no load to the optics. A schematic of this system is shown in Figure 4. Fabrication has already begun, and the first testing is scheduled to take place during the next year.

A new scanning x-ray microscope (Figures 5 and 6) has been designed and built to advance the

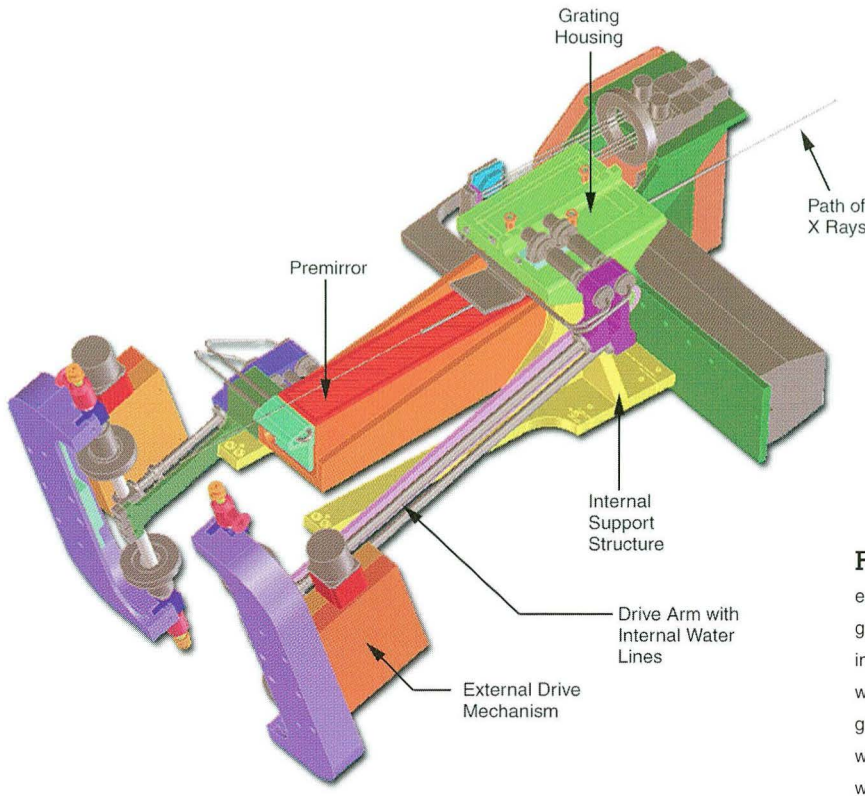

Figure 4 Schematic of the new molecular environmental science beamline's plane-grating monochromator. Key new features include the use of a single grating substrate with multiple grating rulings, change of the grating position by lateral translation of the whole monochromator, and water lines integral with the grating drive arms.

STXM technology that is now in use on Beamline 7.0. One of the important capabilities of such a microscope is to allow users to discover features by imaging, then navigate back to them and perform NEXAFS spectroscopy, scanning the energy of the incoming photons. Our new design includes interferometric measurement of the relative positions of the sample and the zone plate lens in the transverse directions (x and y). This innovation allows the control computer to lock onto spatial features against

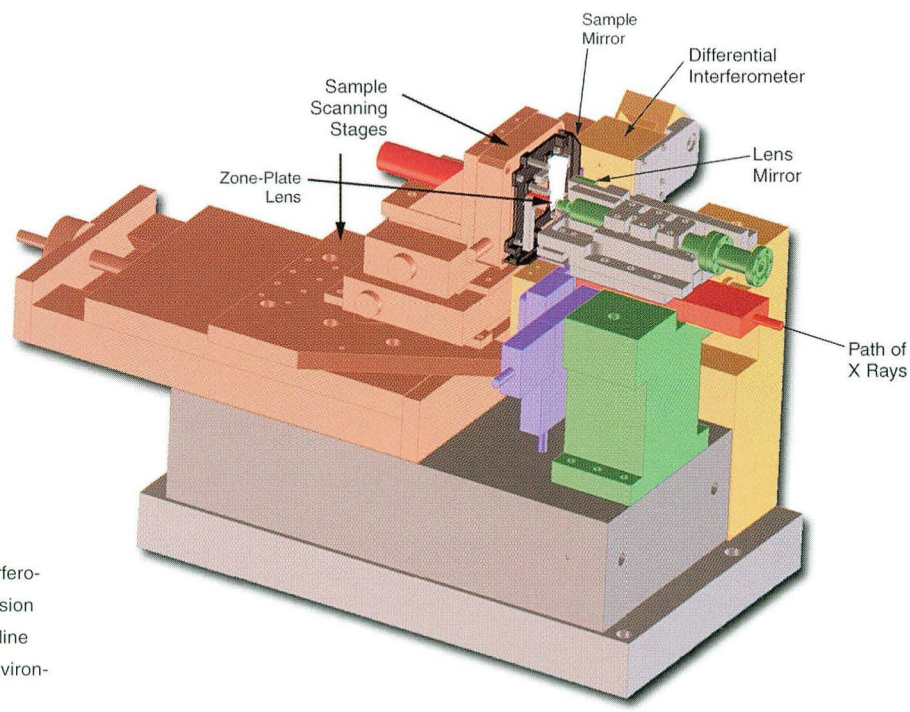

Figure 5 Diagram of the new interferometrically encoded scanning transmission x-ray microscope to be used on Beamline 7.0 and ultimately on the molecular environmental science beamline (11.0).

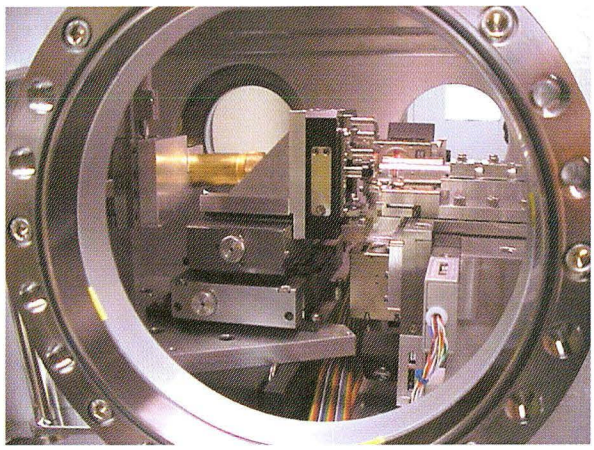

Figure 6 The scanning transmission x-ray microscope for use on Beamlines 7.0 and 11.0, under test with a focused laser source.

motions and drift for highly precise measurements. The interferometer has 0.6-nm sensitivity and will be used to navigate to about 10-nm accuracy. The resolution goal with x rays is the optical limit of the zone-plate lens, which we estimate at 20–30 nm.

The development of computer control for this instrument is an important part of the project. Coordinate values are acquired from the interferometer for each pixel. If a scan is defined with spatial oversampling, the image can be constructed by recalculating the x and y coordinates from time-based increments, and the effects of vibrations and the lack of fidelity of the scanner can be eliminated. In the test location in a fourth-floor laboratory, the ambient vibrations are seen at about ± 20 nm. Permanent installation at the ALS on a granite pedestal will be quieter by about a factor of 20, so vibrations should not be a concern unless there is activity nearby. The new instrument will be installed on Beamline 7.0 during 2001, and it will move to Beamline 11.0 in 2002. The team doing this work is led by Tony Warwick and includes Sirene Fakra, Keith Franck, and Rick Steele.

Protein Crystallography on Superbend Sources

Beamline 8.3.1 will be the first superbend beamline at the ALS. It is being designed and constructed for a UCB–UCSF consortium headed by Professor Tom Alber of the UCB Department of Molecular and Cell Biology. Beamlines 8.2.1 and 8.2.2 are nearly identical versions of Beamline 8.3.1 and are being constructed for the Howard Hughes Medical Institute. These are all state-of-the-art protein crystallography beamlines capable of multiple-wavelength anomalous diffraction (MAD). The technical project is led by Alastair MacDowell of ESG and by Dave Plate and Rob Duarte in ALS Engineering.

This project provides an excellent example of how our group works with users to develop new ALS programs. The superbend program had its genesis in developmental work that showed the viability of ALS bend-magnet beamlines for protein crystallography research. Alastair MacDowell and Rich Celestre worked with Tom Alber, James Holton, and Robert Glaeser, all of UCB, on Beamline 7.3.3. They showed that even normal conducting bend magnets at the ALS provide the necessary vertically integrated flux and horizontal brightness to collect usable MAD data. The group also determined the optics requirements that would guide the design of the superbend beamlines now under construction.

The optical layout for Beamline 8.3.1 is shown in Figure 7. It consists of a parabolic mirror (M1) that produces vertically collimated light, a flat double-crystal monochromator, and a toroidal mirror (M2) that focuses from infinity in the vertical direction and from the source in the horizontal direction with two-to-one demagnification. This arrangement is predicted to produce a focus size of 67×155 µm FWHM for a horizontal collection aperture of 1.5 mrad. The overall flux density is within a factor of

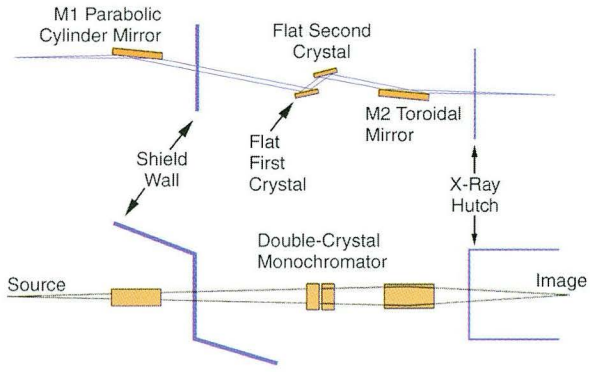

Figure 7 Optical layout of the new superbend beamlines for protein crystallography

two of a system without optical aberrations. We intensively studied a range of other options for the optical layout, such as a sagittally focusing monochromator. Although some of these produced theoretically perfect foci, the robustness of the flat crystal design, where only crystal rotation is required during MAD scanning, was preferred over the more complex alternatives.

In order to fit four beamlines on one superbend source, the four premirrors for each beamline have to be very close. This problem was solved by putting pairs of adjacent mirrors in the same vacuum tank. Even so, the lateral space between the mirrors was negligible, so the mirrors, cooling, and support structure had to be very compact. This was achieved by use of a coated nickel-plated metal (Invar) substrate with internal water cooling. The mirror is bolted to a cantilever bending mechanism to produce the required parabolic shape.

The monochromator is a standard Kohzu system with an ALS-designed, water-cooled first crystal. The power load is high enough to demand intensive cooling, but not high enough to justify the expense of the liquid nitrogen cooling now used routinely on x-ray undulator beamlines. The solution in this case was to use transverse cooling channels drilled into a silicon block such that the water-to-surface distance matched the power load at the center of the monochromator energy range. The M2 mirror is uncooled, but uses the same bending technology as the M1 mirror.

A further innovation is the use of a much smaller hutch than conventionally used, in which the operator stands outside to change samples. This gives more room for the operator, isolates the expensive endstation equipment from the user, and gives a more controlled environment.

The UCB–UCSF beamline, along with the two similar beamlines funded by the Howard Hughes Medical Institute are shown in Figure 8. The three beamlines are shown together with the three endstations, each with a further layer stripped off to show the underlying hutch construction. The first beamline will start commissioning from April 2001, and the last beamline is scheduled to start commissioning in December 2001.

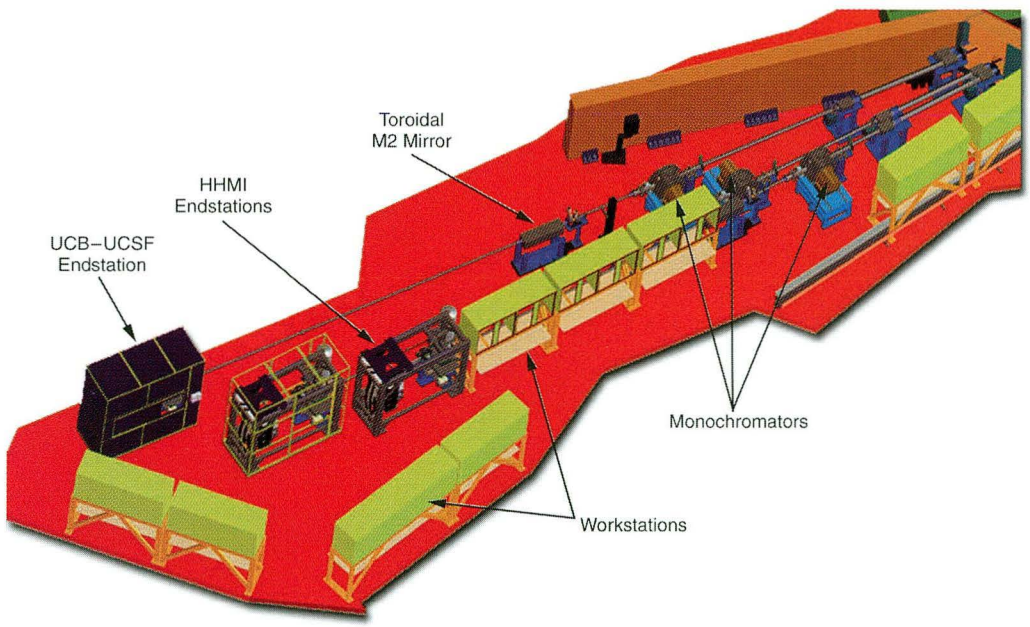

Figure 8 Overall layout of sectors 8.2 and 8.3, showing the three new protein crystallography beamlines and their corresponding endstations.

Scientific Support Group

Zahid Hussain
Scientific Support Group Leader
John Bozek
Scientific Support Group Deputy Leader

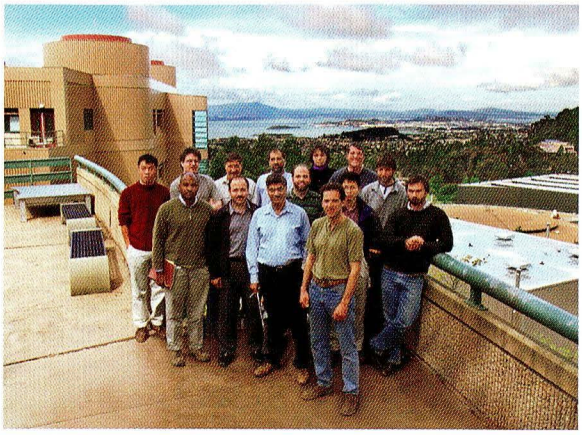

Figure 1 Scientific Support Group members, *left to right: Back row,* Xingjiang Zhou, Eli Rotenberg, Glenn Ackerman, John Bozek, Elke Arenholz, Mike Martin, John Pepper. *Front rows,* Byron Freelon, Nasser Hamdan, Zahid Hussain, Jason Akre, Bruce Rude, Yi-De Chuang, Alexei Fedorov. Not pictured: Jonathan Denlinger, George Meigs, Scot Kellar, Fred Schlachter, Wayne Stolte, Xingxiang Zhou.

Introduction

The primary mission of the Scientific Support Group (SSG) is to support the efforts of researchers at the ALS through scientific and technical collaboration and scientific outreach. Depending on the needs of the user, the degree of collaboration can range from technical assistance with the beamline to full partnership in developing new research programs and experimental endstations.

OUTREACH

The SSG strives to expand the scientific program of the ALS and broaden its user base through publications and presentations. The group organizes a variety of seminars, including the weekly ALS/CXRO seminar series and a targeted weekly lecture series. The weekly lectures focus on a topic of wide interest through a series of five to ten lectures by world-renowned scientists. The group has also initiated the quarterly ALS Colloquium, the first of which was presented by Manuel Cardona from Germany.

The group, working together with the Users' Executive Committee, also helps to organize workshops exploring new scientific opportunities and needs for new beamlines or experimental facilities. Seven such workshops were conducted during the 2000 ALS Users' Meeting. These were heavily attended by enthusiastic scientists and triggered many fruitful discussions that should spark further advances in scientific endeavors at the ALS.

SUPPORT

Members of SSG are responsible for the operation, upgrade, and maintenance of most of the facility beamlines and many of the permanent endstations at the ALS. The undulator beamlines, Beamlines 4.0.2, 7.0.1, 8.0.1, and 10.0.1, each have at least one SSG staff member responsible for their continued operation. Several improvements were made to the operation of existing beamlines in 2000. For example, installation of a sensitive photon-beam-position monitor (PBPM) on the High-Energy-Resolution Spectroscopy (HERS) endstation branch of Beamline 10.0.1 has greatly simplified the changeover from one branch of the beamline to the other. See the section on Beamline 10.0.1 (below) for more about HERS.

Several new endstations were designed, constructed, and commissioned with the help of SSG personnel in 2000. A new angle-resolved photoemission spectroscopy experimental endstation is being constructed and will be installed on Beamline 12.0.1 in early 2001. It is replacing the MAXIMUM system, which is being retired after many years of service. The new photoemission experimental endstation will utilize a Scienta SES-100 analyzer. New refocusing optics will be installed in the beamline to provide suitable focusing for the experiments. Alexei Fedorov, a scientist working jointly with Dan

Dessau at the University of Colorado at Boulder and with the ALS, is leading the effort to assemble the experimental apparatus. This endstation will expand the capabilities of the ALS to serve the large community of x-ray photoemission users on Beamlines 7.0.1, 8.0.1, and 10.0.1 and will further increase the utilization of Beamline 12.0.1. We also installed a new imaging spectrometer for photoemission work at Beamline 7.0.1. This work is further detailed in the section on Beamline 7.0.1 below.

Also this year, a new high-throughput, soft x-ray emission spectrograph utilizing a collecting mirror and a variable-line-spacing grating has been conceived and designed with the help of Jim Underwood from the Center for X-Ray Optics. This spectrograph will be used for soft x-ray inelastic scattering experiments on highly correlated materials (funded through a Laboratory Directed Research and Development project) as well as for other studies, such as work in molecular environmental science. Initial testing of the spectrometer will be carried out on beamline 12.0.1, with future deployment to other beamlines following a successful demonstration of its enhanced capabilities.

SCIENTIFIC CONTRIBUTIONS

Staff scientists within SSG are expected to maintain scientific and technical excellence in areas of synchrotron radiation research. Participation in active scientific programs is essential for such development, and all of the SSG scientists are active members of research programs at the ALS.

Beamline 1.4: Advances in Infrared Research and Instrumentation

The Fourier-transform infrared (FTIR) spectromicroscopy beamline, Beamline 1.4.3, has served many ALS users. The heaviest interest to date comes from the biological and environmental science fields. Two outstanding examples of how this beamline can be used to investigate biochemical changes within individual living human cells are described in detail in the Science Highlights Section (page 30).

In 2000, we continued our efforts to optimize the infrared spectroscopy program for biomedical applications. The funding of a DOE grant to investigators Hoi-Ying Holman, Michael Martin, and Wayne McKinney will allow the purchase of improved equipment designed with the biological scientist in mind. SSG members also carried out a test of key importance to the biological community, showing that the synchrotron infrared beam does not appreciably heat biological samples. Synchrotron infrared spectroscopy at the ALS can therefore truly be called a nondestructive technique.

The diffraction-limited spot size and high signal-to-noise ratio available on this beamline have enabled research in a wide variety of fields in addition to those mentioned above. These include subjects as diverse as development of lithium-ion batteries for use in hybrid electric vehicles, laser irradiation of dental tissues, studies of the strongly correlated material $SrRuO_3$, the chemistry of ink, and laser-driven phase transformations in fused silica. Studies were also carried out on basalt assemblages at high pressures (see Figure 2), organic matter and contaminants on sediments, fingerprints, and bacteriorhodopsin microcrystals. Other studies have involved supercooling of water, classification of cell populations with genomic data, microdistribution of trace elements in a high-boron soil, the biochemistry of bacteria attached to basalt, radiative properties of polar bear hairs, and root-derived biopolymers.

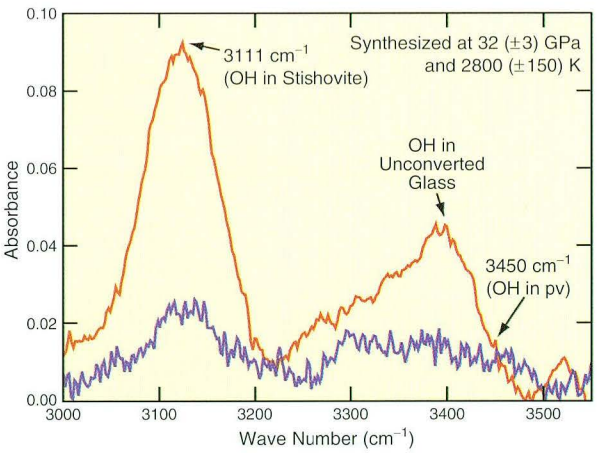

Figure 2 Comparison of a spectrum taken at Beamline 1.4.3 (*red*, 256 scans) to one taken on a lab-based spectrometer (*blue*, 60,000 scans). While both show a distinct peak at 3111 cm^{-1} corresponding to OH vibrations in stishovite, the synchrotron-based spectrum has a much better signal-to-noise ratio as well as better spatial resolution, thereby avoiding problems of sample heterogeneity. (From W.R. Panero, L.R. Benedetti, R. Jeanloz.)

Work has continued on making the infrared beamline facilities as user friendly as possible. This has included completing the installation of a four-axis active feedback system, which reduces the low-frequency noise on the beam and keeps the position of the diffraction-limited infrared spot fixed in space from day to day. Software is also being developed to aid in the analysis of the large numbers of spectra typically acquired in an infrared mapping.

Beamline 4.0.2 : Elliptical Polarization Undulator Helps Detect Dichroism

Beamline 4.0.2 is the first undulator beamline at the ALS equipped with a Sasaki-type elliptical polarization undulator (EPU). The EPU allows full control of the polarization of the x rays, from linear horizontal to helical to linear vertical, making it a unique tool to study dichroic effects, especially magnetic circular and linear dichroism. The undulator, in combination with a plane-grating, variable-included-angle monochromator, is designed to provide high-flux photon beams from 50 eV to 2000 eV. This provides full coverage of the $L_{2,3}$ edges of important magnetic transition metals (Fe, Co, Ni) and also the $M_{4,5}$ edges of magnetic rare-earth elements of interest (Gd, Tb, etc.).

Figure 3 shows some of the first measurements of small magnetic circular dichroism effects made at this facility. The sample contained alternating layers of $Co_{90}Fe_{10}$ and copper. Total-electron-yield spectra at the copper $L_{2,3}$ absorption edge were taken by switching (within two seconds) the polarization of the x rays at each photon energy, thus eliminating the influence of any long-term instabilities of the system from the dichroism signal. These experiments were performed by F. Nolting et al. (ALS, Stanford Synchrotron Radiation Laboratory).

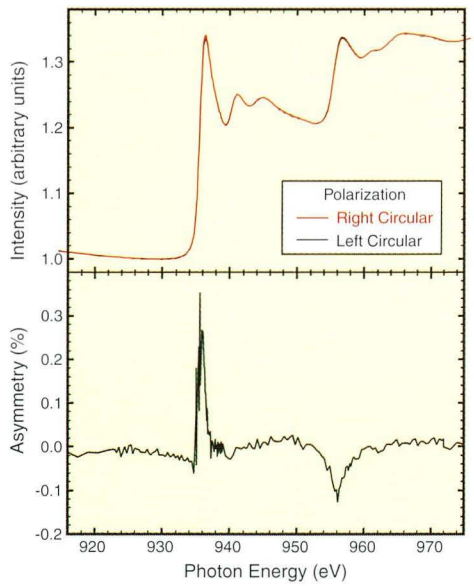

Figure 3 First measurements of dichroism at Beamline 4.0.2. Total-electron-yield spectra were obtained from a multilayer sample consisting of 10-Å-thick layers of a $Co_{90}Fe_{10}$ alloy alternating with 13-Å-thick layers of copper. The adjacent $Co_{90}Fe_{10}$ layers induce a small magnetic moment of approximately $0.01\mu_B$ in the copper spacer layer. This can be observed as a small magnetic circular dichroism effect in the copper $L_{2,3}$ absorption spectra.

Beamline 7.0.1: Investigating Novel Materials

Photoemission spectroscopy at Beamline 7.0.1 made an order-of-magnitude improvement in efficiency this year with the deployment of an SES-100 imaging spectrometer (Figure 4) to replace the

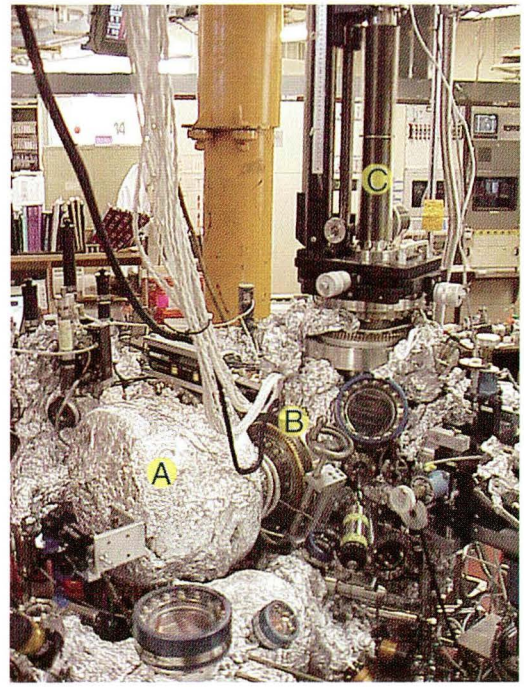

Figure 4 The upgraded high-resolution photoemission chamber on Beamline 7.0.1: (*A*) new SES-100 imaging spectrometer with (*B*) differentially pumped rotary seal around its lens; (*C*) new liquid-helium cryostat and goniometer.

original Phi Omni-IV spectrometer. The analyzer combines a two-dimensional-imaging CCD detector with ultrahigh-stability power supplies to achieve twice the energy and angle resolution of the old setup, and it offers real-time display of angle-resolved photoemission spectra. Possible applications of the new instrument include time-resolved band structure measurements (with 30-ms resolution possible). A unique feature of this installation is that the analyzer is mounted on a custom-built, heavy-duty rotary seal. This enables users to select from a wide variety of experimental geometries for probing the symmetry of valence band states. Another upgrade to the system was the addition of a liquid-helium cryostat, which was combined with a home-made azimuthal goniometer to achieve a nominal sample temperature range of 20 K to 380 K. The combination of the cryostat and new high-speed data detection opens up new frontiers in temperature-dependent electronic structure studies at Beamline 7.0.1.

Beamline 7.0.1 continues to be in great demand for novel materials science research at high resolution and flux. For example, a group led by Joseph Nordgren and colleagues (Uppsala University, Sweden) has successfully developed the ability to measure resonant soft x-ray fluorescence for liquids and solutions while making simultaneous near-edge x-ray absorption measurements. As examples, data comparing pure water, isolated water molecules in vapor, and various solutions for both x-ray absorption and resonant x-ray emission are shown in Figure 5.

An interesting field of application for this beamline is biomaterials, the basis for technologies that interface artificial structures with living organisms. An important issue in this field is biocompatibility, which is often linked to specificity in first interactions of a material with particular proteins. Research led by Adam Hitchcock (McMaster University) and carried out by Cynthia Morin, Tolek Tyliszczak, and Hiromi Ikeura-Sekiguchi has demonstrated the ability to measure—in wet conditions—the positions of monolayers of a protein (fibrinogen) on a heterogeneous polymer substrate. Figure 6 is a false-color composite image showing the ability of x-ray microscopy to locate proteins selectively adsorbed onto features of a chemically differentiated sample surface.

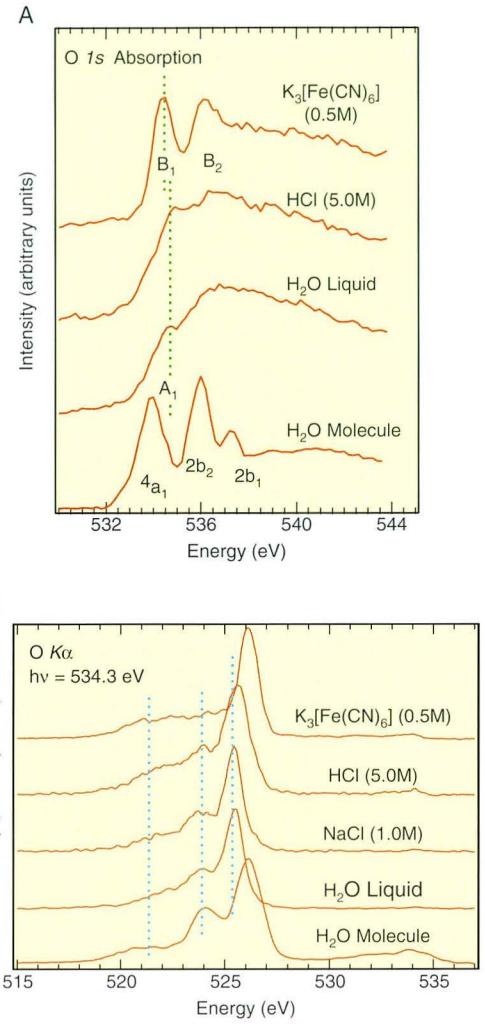

Figure 5 Simultaneous x-ray absorption and resonant x-ray emission spectra for pure water, isolated water molecules in vapor, and various solutions . The changes observed in the fine structure are directly attributable to the chemical bonding of water molecules to each other and to ions introduced into the solution. In particular, the resonant measurements at the large absorption feature (B1) in $K_3[Fe(CN)_6]$ reveal chemical-species-selected valence-band features unique to those water molecules bonded to $[Fe(CN)_6]^{3-}$ clusters.

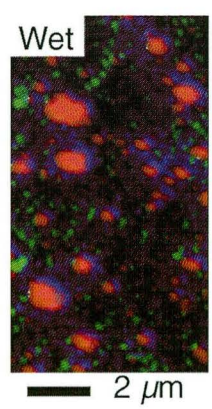

Figure 6 Studying biomaterials on Beamline 7.0.1. This false-color composite image shows the distribution of fibrinogen protein (Fg, *blue*) on a wet polyurethane substrate (*black*) containing two types of aromatic filler particles, styrene acrylonitrile (SAN, *red*) and polyisocyanate addition product (pipa, *green*). The fibrinogen is seen to selectively stick to the SAN particles, which protrude above the polymer surface from the sample preparation process. Data courtesy of Adam Hitchcock (McMaster University); polymer sample courtesy of Gary Mitchell (Dow Chemical).

Beamline 8.0.1: Photon-In–Photon-Out Spectroscopy of Materials

Various improvements to Beamline 8.0.1 have been made in the year 2000. Two of these could be placed in the category of housecleaning. The beamline floor layout, including areas for endstation control, equipment storage, and sample preparation, was significantly rearranged to fit within the border set for the new protein crystallography beamlines (8.2 and 8.3). In addition, refocus optics for each of three branchlines were UV–ozone cleaned to remove carbon contamination built up from approximately five years of use.

This year's maintenance challenges included an in-vacuum mechanical slippage of the M1 premonochromator mirror element, resulting in severe optical misalignment. This was partially compensated for by ex-situ readjustment of the mirror tank. In addition, the monochromator linear encoder for grating angle motions was mechanically realigned, and programmatic changes were made to defeat various undesirable behaviors, such as oscillatory modes and ultrafine stepping instabilities.

Several improvements to the beamline's function were undertaken this year as well. A new Labview-based beamline control and scanned-energy data acquisition program, introduced in late 1999, has been continually refined with improvements and fixes in undulator control, grating homing and scanning, exit slit positioning, signal pulse counting, and the format for saving data files. We also installed a new computer for online data analysis, centralized data archiving, and FTP access. We carefully realigned the soft x-ray emission (SXE) endstation to the optimal horizontal refocus spot, thereby gaining a closer match to the spectrometer entrance-slit width of 50 μm and increasing the detection efficiency by a factor of five. We also rewired the SXE sample cryostat temperature sensing and regulation, and we have successfully verified operation down to a temperature of 12 K.

Independent investigators at Beamline 8.0.1 are approximately evenly divided between users of the permanent SXE and ellipsoidal-mirror electron energy analyzer (EMA) endstations and users that temporarily attach their own specialized endstations. The independent investigators are also approximately evenly divided between three research areas: atomic and molecular physics, environmental science, and materials science.

One novel experiment made particularly good use of the high-vacuum SXE endstation's ability to accommodate water-based studies. In order to explore the chemical interactions of liquid water with $Cu(In,Ga)(S,Se)_2$ (CIGSSe) thin-film solar cell materials, C. Heske, U. Groh, and E. Umbach (University of Würzburg), in collaboration with Luxel, the Hahn-Meitner Institute, Siemens Solar, and Siemens AG, conducted preliminary x-ray emission experiments using a liquid sample cell assembly that was custom designed to be compatible with the SXE's transferable sample plates. By confining the liquid layer to about 1 μm, they were able to monitor an x-ray beam–induced chemical reaction at the water/CIGSSe interface. (See Figure 7.) The results of this preliminary study, along with future work on the beamline, will shed light on the effects of humidity and the presence of additional buffer layers (e.g. CdS) on the application of CIGSSe thin films in solar cells.

Beamline 10.0.1: The Atomic and Molecular Facility and the High-Energy-Resolution Spectrometer

Beamline 10.0.1 is shared by the High-Energy-Resolution Spectrometer (HERS) and the Atomic and Molecular Facility (AMF), the latter having three permanent endstations and provisions for accommodating independent investigators. The atomic and molecular physics program continues to actively produce new results. The permanent instrumentation on the AMF branchline includes a four-mirror phase retarder, to convert the polarization of the photon beam from linear to elliptical, and two endstations: one with an ion source and charge-state analyzer for studies of ion photoionization and another with a high-resolution electron spectrometer for atomic and molecular photoionization studies. Temporary endstations, such as the electron time-of-flight spectrometers used by N. Berrah (Western Michigan University), can also be accommodated on the atomic and molecular physics branches of the beamline.

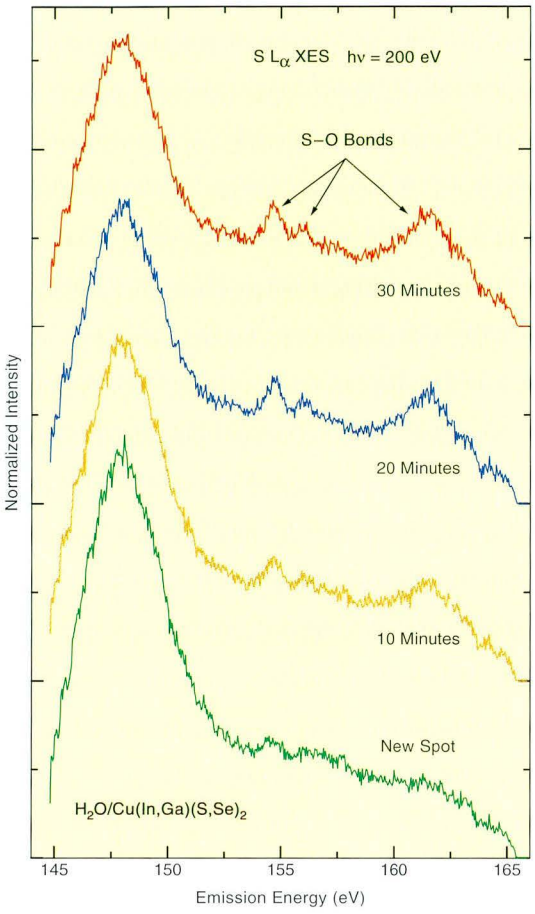

Figure 7 An x-ray-induced chemical reaction between water and a thin-film solar-cell material. Beamline 8.0.1 was used to capture sulfur L_α x-ray emission spectra of the H_2O/Cu(In,Ga)(S,Se)$_2$ liquid/solid interface. The sulfur oxidation (and hence the spectral intensity associated with S–O bonds) was enhanced with increasing x-ray exposure times. The existence of sulfur 3d-related states (around 162 eV) gives evidence that the emitting sulfur atoms are primarily bound in a sulfate-like chemical environment.

The phase retarder has been used primarily by the research group of D. Jaecks (University of Nebraska–Lincoln) to examine the partitioning of angular momentum in atomic photoionization. Ionizing circularly polarized light is used to transfer a single unit of angular momentum to an argon atom target. By measuring the polarization of visible light emitted by the argon ion, which was left in an excited state in the photoionization process, Jaecks' group was able to determine the partitioning of the angular momentum brought into the system by the circularly polarized photon. The retarder was also used to produce elliptically polarized light for spin-polarized time-of-flight electron spectroscopy of atomic barium by G. Snell and N. Berrah.

The ion beam experimental endstation was used extensively in 2000 both by the principal investigator, R. Phaneuf (University of Nevada, Reno), and by independent investigators. Extensive characterization efforts by Phaneuf's group, along with upgrades of certain key power supplies in the ion source and momentum-separating magnet, have reaped great dividends for the experiments, giving an improved signal-to-noise ratio and better resolution on a variety of singly charged target atoms. Preliminary experiments on the photoionization of molecular ions were also carried out by C. Cisneros (University of Cuernavaca, Mexico). Large changes are in store for the ion beam endstation with the commissioning of two new ion sources in early 2001, an electron cyclotron resonance source for the production of multiply charged positive ions and two negative ion sources.

The electron spectrometer endstation (referred to as the HiRAMES—High-Resolution Atomic and Molecular Electron Spectrometer) continues to be a workhorse, supporting the participating research team (PRT) and several independent-investigator programs. The endstation is equipped with a cylindrical gas cell for samples with sufficient volatilities at room temperature and a high-temperature oven to produce atomic and molecular vapors of nonvolatile samples. Photoionization studies were performed on a variety of samples in 2000, ranging from the simple three-electron atom lithium to large cluster molecules such as C_{60}. The HiRAMES is unique in the world for its combination of resolution and photon energy range, from 16 to 350 eV. These energies cover valence photoionization, multiple excitation/photoionization, and shallow core levels (i.e., the carbon K edge), with total experimental resolving powers of 10,000 achievable in many cases. This combination of flux and resolution has enabled studies of high-angular-momentum states in lithium photoionization (Figure 8) and vibrational structure in the resonant Auger spectra of CO_2, among many other examples.

The HERS endstation was designed to study highly correlated materials, including high-temperature superconductors (HTSCs), colossal magnetoresistance compounds, and heavy fermion

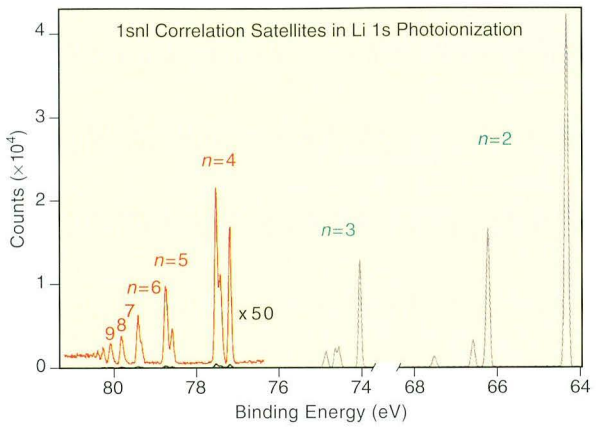

Figure 8 Photoelectron spectrum of the satellite structure accompanying the 1s main line in the photoionization of atomic lithium with 100 eV photon energy. (From W.-T. Cheng, N. Berrah, et al.)

compounds with extremely high momentum and energy resolution. The PRT members and independent users have taken advantage of this unique setup to obtain important scientific results on HTSCs and other interesting systems. By working on $(La,Nd,Sr)_2CuO_4$, a model system with static stripes, and $(La_{2-x}Sr_x)CuO_4$ (x = 0–0.3), a superconducting system with dynamic stripes, new insights have been obtained on the dual nature of the electronic structure of the stripe phase. The latter system provides a good opportunity to investigate the evolution of electronic structure from a Mott insulator to HTSCs, covering all the underdoped, optimally doped, and overdoped regions. Working on $Bi_2Sr_2CaCu_2O_8$ (optimal T_c = 92 K), and particularly lead-doped $Bi_2Sr_2CaCu_2O_8$ without superlattice complications, critical information has been obtained about the long-standing controversy over the nature of Fermi surfaces in HTSCs. Particularly significant is the observation in various HTSCs of an energy scale in the quasiparticle dispersion, which is attributed to the strong electron–phonon interaction in high-temperature superconductors. (See the science highlight on page 7.) This implies that, in addition to the strong electron–electron interaction, the electron–phonon interaction may also be an important ingredient in the mechanism of high-temperature superconductivity.

Besides the work on high-temperature superconductors, much has also been done on other interesting systems. These include $TiTe_2$, a system believed to be a model Fermi liquid; artificial one-dimensional systems like Pb(In)/Si; heavy fermion systems; ladder compounds; and nickelates.

To enhance the performance of the HERS system, a new chamber has been designed and added for sample preparation and annealing. It utilizes electron-beam heating, which can rapidly heat a sample to high temperature. This capability is essential for cleaning single crystals. The system also contains evaporators for preparing thin films and offers a low-energy electron diffraction option for surface characterization. This chamber is compatible with the original HERS setup so that a prepared sample can be transferred to the main chamber for angle-resolved photoemission measurements. As mentioned earlier, the branchline that serves this endstation was also upgraded with a photon-beam-position monitor, which makes switching between the branchlines of Beamline 10.0.1 much simpler than before.

User Services

Gary Krebs
User Services Group Leader

The User Services Group provides an interface to the facility for new and continuing users at the ALS. The group is made up of the User Services Administration, Beamline Coordination, and Technical Information sections. These groups work together to provide the users with a wide range of services. It is the goal of the ALS to continue to provide these varied services in a friendly and efficient manner.

User Services Administration

The User Services Office is located on the mezzanine floor of the ALS. The reception area at the top of the elevator provides a convenient point of contact for ALS users. The The User Services Office is staffed by the User Services Administration Section. Section members help new users through the required registration process before they begin work at the ALS. All users receive an identification card, which allows them access to the ALS experiment floor. New users also watch a short safety video that describes some of the potential safety hazards at the facility and outlines the experiment safety checkout process. New users can complete much of the processing before they arrive by preregistering on the ALS Web site (www-als.lbl.gov). Through its oversight of the registration process, the User Services Administration Section also collects data about user publications and demographics. As a national user facility, the ALS is required to report these statistics to the U.S. Department of Energy.

In another of its many functions, the User Services Administration Section coordinates the allocation of beamtime through a peer-review process. In this process, independent-investigator requests for beamtime are received through the ALS Web site twice annually. The proposals for beamtime are reviewed by the Proposal Study Panel and, under the direction of ALS Division Deputy for Science Neville Smith, beamtime is allocated based on principles and guidelines agreed upon by the ALS and the Users' Executive Committee (UEC). The UEC, elected annually by the users, is the voice of that diverse group and represents them at the ALS as an advisory body. Proposal Study Panel members are chosen in consultation with the UEC to cover the wide range of sciences represented at the ALS. The User Services Administration Section provides administrative and logistical support to both the PSP and the UEC. The proposal submission and beamtime allocation process is described in greater detail on the ALS Web site (www-als.lbl.gov/als/quickguide/independinvest.html).

For out-of-towners, the User Services Office can also be a help in finding a place to stay while working at the ALS. The office manages the ALS apartments (Figure 1), which are located near Berkeley

Figure 1 The ALS apartments provide a home away from home for visiting researchers.

Lab on the main shuttle-bus route. The apartments are available to all ALS users, and detailed information about costs and other factors can be found on the Web at www-als.lbl.gov/als/quickguide/housing.html.

The User Services Administration Section is led by Ruth Pepe and includes Bernadette Dixon, User Services Office Manager; Jeremy Coyne; Sharon Fujimura; and Barbara Phillips (Figure 2).

Figure 2 The User Services Administration Section: *left to right*, Sharon Fujimura, Barbara Phillips, Gary Krebs (User Services Group Leader), Ruth Pepe, Jeremy Coyne, and Bernadette Dixon.

Beamline Coordination

The Beamline Coordination Section serves as a point of contact for users on the experiment floor. Section members act as liaisons between users and ALS and Berkeley Lab resources. They provide shipping and receiving and storage services as well as endstation setup and safety checkout support. Ensuring that all user experiments are checked for safety is a crucial function of this group. Section members work closely with various Berkeley Lab safety specialists in the areas of electrical, mechanical, chemical, radiation, and laser safety. This safety checkout process is required in order to assure the safety of all users on the experiment floor. Upon the successful completion of the required safety checks, section members enable the beamlines for use. The Beamline Coordination Section also maintains a stock room of parts and equipment commonly needed by ALS users (Figure 3). These supplies are accessible by proximity card 24 hours a day. The Beamline Coordination Section is led by Donna Hamamoto and includes Cheryl Hauck, Gary Giangrasso, and Tony Marquez (Figure 4).

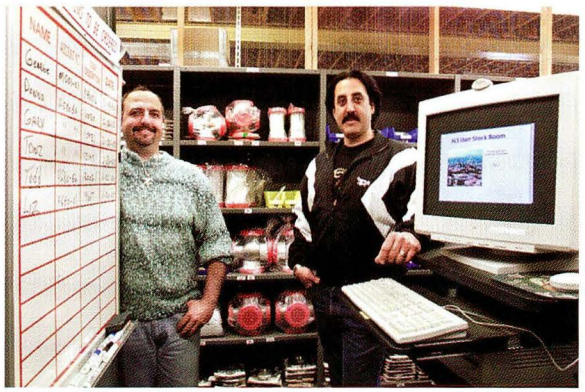

Figure 3 The User Stock Room is staffed by (*left*) Tony Marquez and (*right*) Gary Giangrasso.

Figure 4 The Beamline Coordination Section: *left to right*, Tony Marquez, Cheryl Hauck, Gary Giangrasso, and Donna Hamamoto.

Technical Information

The Technical Information Section is responsible for this Activity Report as well as the annual Compendium of User Abstracts. The group's members also prepare special brochures and create posters and announcements for countless workshops and conferences. They are responsible for the "Science Highlights" shown in the ALS lobby, around the experiment floor, and on the ALS Web site. In addition, the section maintains and develops the ALS Web site and writes and edits the

electronic newsletter, ALSNews. The section, composed of science writers along with graphics and Web experts, provides the ALS scientific community as well as the general public with information about the science carried out at the ALS. The group maintains a strong tie to the educational community, both within the state of California and internationally. In conjunction with the User Services Office, this group coordinates tours for the thousands of visitors—often from high schools, universities, and industry—who come to glimpse the ALS annually. The Technical Information section is led by Art Robinson and includes Annette Greiner, Elizabeth Moxon, Lori Tamura, and Greg Vierra (Figure 5).

Figure 5 The Technical Information Section: *left to right*, Elizabeth Moxon, Lori Tamura, Greg Vierra, Annette Greiner, and Art Robinson.

SPECIAL EVENTS

ICESS8

The Clark Kerr Campus of UC Berkeley was the site of the Eighth International Conference on Electronic Spectroscopy and Structure, held August 8–12. The conference attracted over 400 scientists from 33 countries. The well-attended plenary sessions, invited talks, and poster sessions provided participants with many opportunities to discuss experimental and theoretical aspects of laboratory- and synchrotron-radiation-based electron spectroscopy. Other topics explored during the conference included electron- and ion-beam-excited electron spectroscopy, x-ray absorption and x-ray emission spectroscopy, various forms of spectromicroscopy and microspectroscopy, and related phenomena dealing with electronic structure and dynamics, as well as their applications to surface, interface, materials, and industrial analysis.

ICESS8 attendees paused for a group portrait in the Grand Court at Clark Kerr Campus.

More than 300 posters, covering all aspects of electronic spectroscopy and its applications, were exhibited during the five-day conference.

An outdoor reception was the opportune time for informal discussions.

The daily plenary sessions filled the auditorium each morning.

2000 ALS Users' Meeting

ALS users and staff attending this year's ALS Users' Meeting were treated to a busy program of facility updates, recent science highlights, invited talks, a poster session, and workshops. This year, seven focused workshops covered topics including femtosecond x-ray science; detectors for synchrotron radiation; future directions for far-infrared sources; correlated materials systems; hard x-ray spectroscopy and holography; new research in atomic, molecular and chemical physics; and x-ray microdiffraction and its applications in materials science.

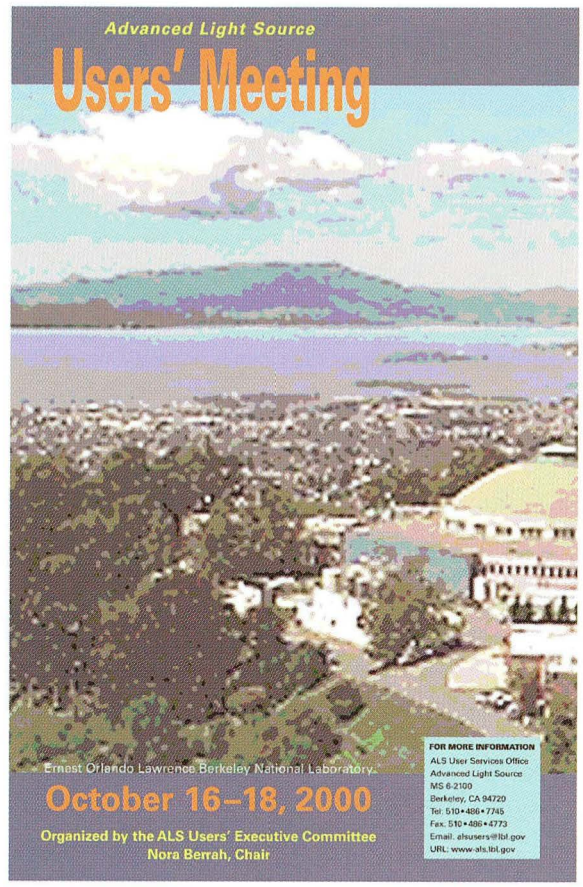

DOE Associate Director Pat Dehmer (*left*), UEC Chair Nora Berrah, and ALS Division Director Daniel Chemla answer questions from the audience during the opening session of the 2000 ALS Users' Meeting.

Meeting attendees packed the house during the popular "Highlights from Young Researchers" session.

At the evening banquet, Nora Berrah and ALS UEC Vice Chair Harald Ade (*second from right*) congratulate award recipients (*from left*) Philip Heimann, Robert Schoenlein, Thomas Earnest, and Art Robinson.

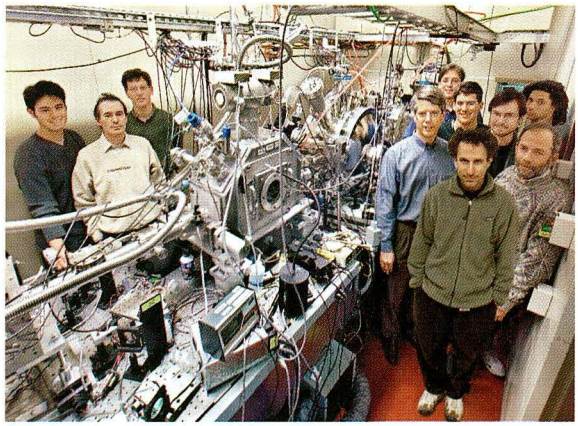

Klaus Halbach Award for Instrumentation: This award, presented annually at the ALS Users' Meeting, recognizes innovative work in instrument design and development at the ALS. Two teams shared this year's prize. One team, led by Roger Falcone, developed streak camera techniques in combination with x-ray diffraction to study the dynamics of structural phase transformations at picosecond time resolution. The other team, led by Robert Schoenlein, developed time-slicing techniques to produce subpicosecond synchrotron radiation pulses. The award recipients were, *from left*, Henry Chong, Sasha Zholents, Robert Schoenlein, Roger Falcone, Aaron Lindenberg, Steve Johnson, Philip Heimann, Marc Hertlein, Max Zolotorev, and Ernie Glover. Not pictured: Zenghu Chang.

A lively poster session was held in the early evening on the ALS patio and in an adjacent tent.

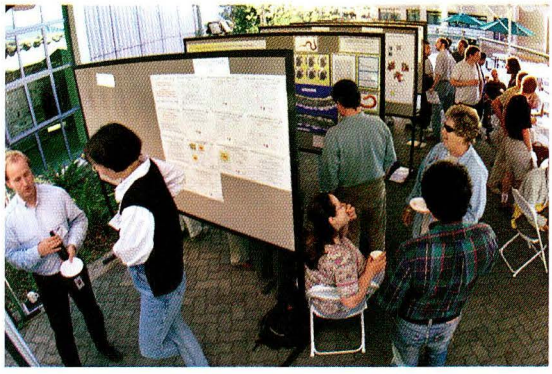

Performance Issues at Synchrotron Light Sources

Accelerator physicists and research scientists gathered at the ALS October 2–4, 2000, to discuss user needs and machine performance issues at second- and third-generation synchrotrons in Canada and the United States. Workshop topics included synchrotron user requirements, beam stability issues, methods to improve brightness, machine characterization, and the extension of beam lifetime. Working groups also explored new concepts and techniques currently attracting interest at synchrotrons, such as femtoslicing, electron recirculating (energy recovery) linacs, and dedicated, low-emittance, hard x-ray, or infrared light sources.

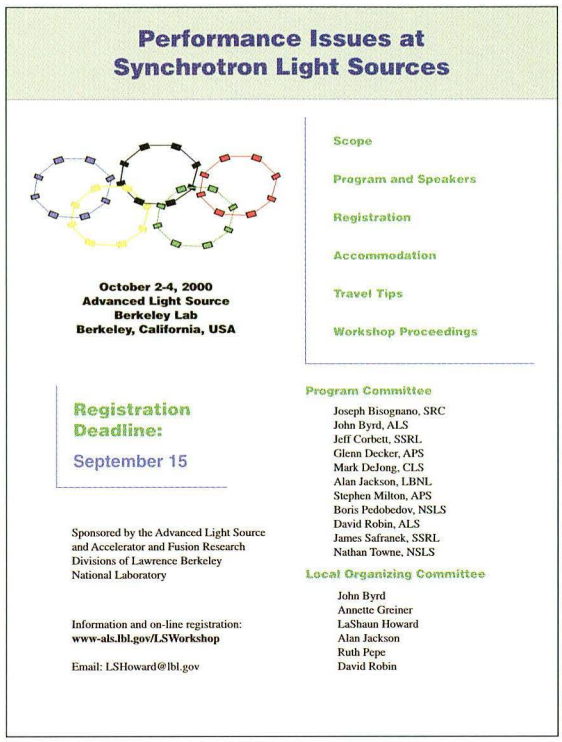

Workshop participants line up for a group photo at the banquet held in Perseverance Hall at Berkeley Lab.

Hiroshi Nishimura (*left*) and Stephen Milton take the opportunity to catch up during the banquet.

Left to right, Christoph Steier, Cecile Limborg, Nathan Towne, and Greg Portmann enjoy fine weather during an early evening reception on the ALS patio.

Distinguished Visitors

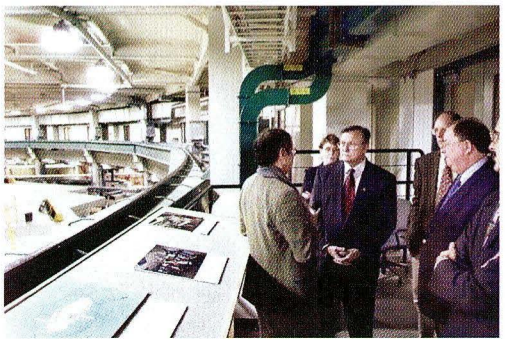

In January, U.S. Congressman Rick Smith (R-Michigan) toured the ALS during his visit of user facilities at Berkeley Lab and UC Berkeley. Representative Smith, a member of the House Budget Subcommittee and chairman of the House Science Subcommittee, was given an overview of the ALS and its scientific program by ALS Director Daniel Chemla (*left*) as Berkeley Lab Director Charles Shank (*right*) looked on.

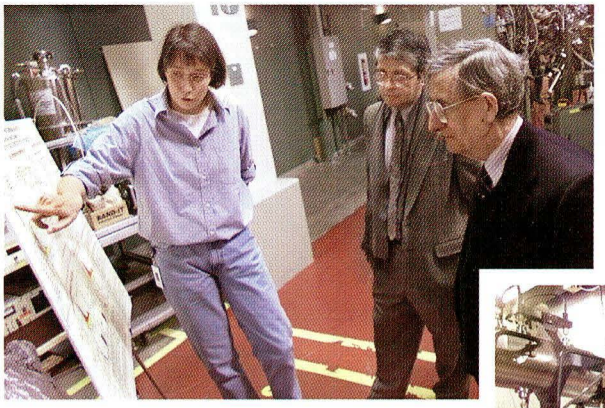

Left, renowned physicist, futurist, and author Freeman Dyson visited the ALS in March 2000. Escorted by ALS Director Daniel Chemla, Dr. Dyson (*right*) toured beamlines and spoke with several ALS researchers, including Beamline Scientist Elke Arenholz (*left*). *Below*, Dr. Dyson got the "inside story" as he toured the storage ring with ALS Division Deputy for Operations Ben Feinberg (*left*).

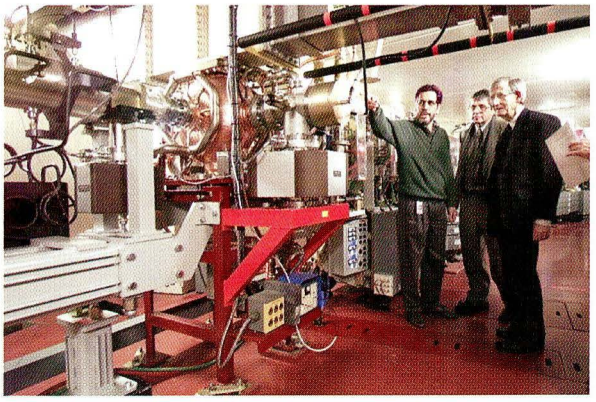

As part of her first visit to Berkeley Lab as the director of the Department of Energy's Office of Science, Mildred Dresselhaus visited the ALS. After viewing several beamlines, Director Dresselhaus (*seated, front center*) listened to a presentation by David Attwood of the Center for X-Ray Optics (*left*).

Open House

On May 6, 2000, the ALS opened its doors to the public as part of Berkeley Lab's Open House. ALS staff and scientists volunteered their time to show interested members of the public how the ALS works and examples of scientific research done at the facility. In addition to tours of the experiment floor, children and adults had the opportunity to participate in Cool Science demonstrations, or find out how things work at the Electronics Petting Zoo. Inside the ALS, visitors got hands-on experience as they temporarily became ALS surveyors and scientists.

Before going inside the ALS, visitors watched "A Light Into the Unseen," a new educational video showing how the ALS works.

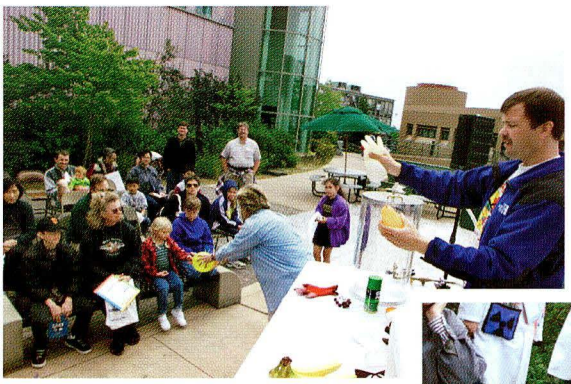

On the ALS patio, Wayne Stolte entertained Open House visitors with Cool Science demonstrations while his audience (below) awaited the outcome of his labors with anticipation.

Deborah Yager welcomed visitors to the x-ray microscope display.

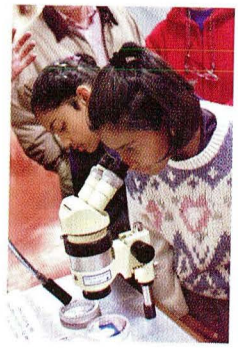

Young scientists peered into light microscopes to see cell cultures.

The Electronics Petting Zoo attracted lots of interest from visitors of all ages.

Alex Gavidia of Mechanical Engineering shows a young visitor the ropes of survey and alignment at the ALS.

Educational Outreach

Making the ALS an accessible learning resource for teachers and students at home and abroad continues to be an exciting goal for ALS staff and scientists. Locally, onsite tours and special events like the Open House and Daughters and Sons to Work Day provide opportunities for ALS volunteers to introduce the research activities of the facility to a broad audience. MicroWorlds, our interactive educational Web site, continues to provide information about synchrotron-related science to an international audience of students and educators.

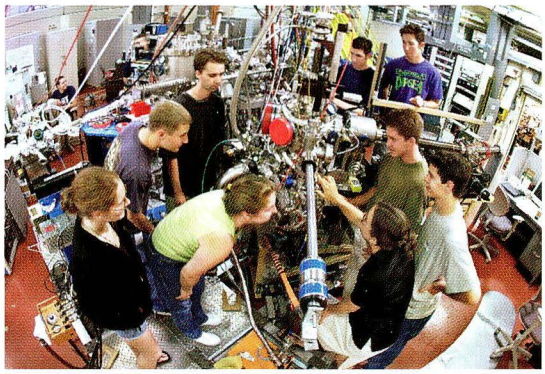

Seeing a beamline up close was a fascinating experience for these ALS summer students.

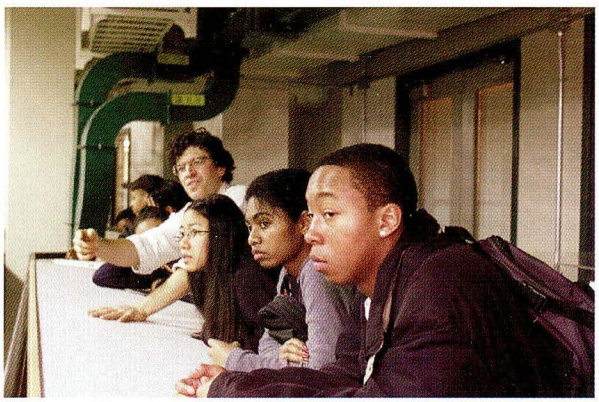

Oakland high school students get an overview of the ALS from Craig Gaines (*pointing*) of the Center for Science and Engineering Education.

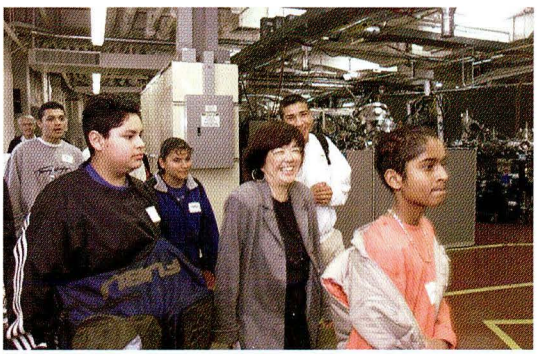

Jane Tanamachi of Berkeley Lab's Physical Biosciences Division (*center*) leads a group of students from Castlemont High School in Oakland on a tour of the ALS experiment floor.

Diversity

This year, Berkeley Lab Director Charles Shank targeted increasing workforce diversity as a goal for all Lab divisions. As part of this effort, the ALS developed a multifaceted diversity plan aimed at attracting members from underrepresented sectors of the community to scientific and technical careers at the ALS. A cornerstone of this plan is to introduce teachers and students from school districts with high minority student populations to career opportunities at the ALS by providing summer jobs and mentors. This summer, students from the Richmond High School Science and Industry Technology Partnership Academy and teachers from the Vallejo City Unified School District came to Berkeley Lab and the ALS to gain experience in the world of scientific research.

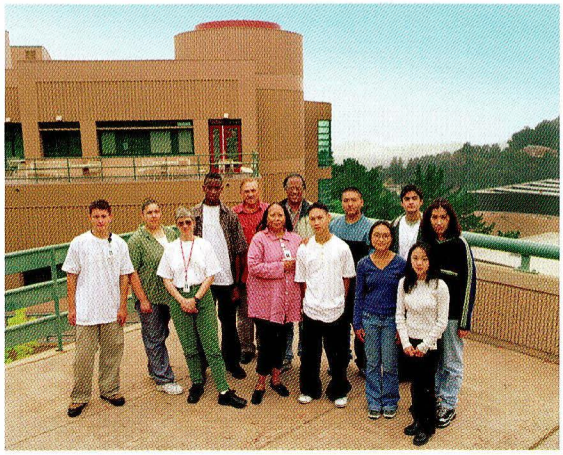

Richmond High School students posed on the ALS patio with their teacher coordinators.

Vallejo middle school teachers Lizelle Baylon and Connie Hafner-Edwards spent their summer creating curriculum materials for their students, using the ALS as the basis for a scientific discovery game.

ALS ADVISORY PANELS

Science Policy Board

Advises the Berkeley Lab Director on major policy issues concerning the ALS.

William Brinkman, Lucent Technologies/Bell Laboratories
Chien-Te Chen, Synchrotron Radiation Research Center, Taiwan
Peter Eisenberger, Columbia Earth Institute
Paul Fleury, University of New Mexico
Franz J. Himpsel, University of Wisconsin, Madison
Yuan T. Lee, Academia Sinica, Taiwan
Dr. Albert Narath, Lockheed Martin Corporation (retired)
Yves Petroff, European Synchrotron Radiation Facility
Stephen D. Kevan (ex officio), University of Oregon

Scientific Advisory Committee

Advises Berkeley Lab and ALS management on issues relating to ALS operations, resource allocation, strategic planning, and Participating Research Team proposals and research.

David Awschalom, University of California, Santa Barbara
Ernst G. Bauer, Arizona State University
James M. Berger, University of California, Berkeley
Nora Berrah, Western Michigan University
Jeffrey Bokor, University of California, Berkeley
John Carruthers, Intel Corporation
Wolfgang Eberhardt, Forschungszentrum Jülich, Germany
Charles Harris, University of California, Berkeley
Yves Idzerda, Naval Research Laboratory
Stephen D. Kevan, University of Oregon
Kate Kirby, Harvard Smithsonian Center for Astrophysics
Alain Manceau, Université Joseph Fourier, France
Zhi-xun Shen, Stanford University
Janet Smith, Purdue University
Louis J. Terminello, Lawrence Livermore National Laboratory

Users' Executive Committee

Elected by the members of the Advanced Light Source Users' Association to act as the official voice of the user community in its interactions with ALS management.

Nora Berrah (Chair), Western Michigan University
Harald Ade (Vice Chair), North Carolina State University
Charles S. Fadley, University of California, Davis
Roger Falcone, University of California, Berkeley
David L. Hansen, University of Nevada, Las Vegas
Lewis Johnson, Florida A & M University, Tallahassee
Stephen D. Kevan (Past Chairperson), University of Oregon
Carolyn A. Larabell, Life Sciences Division, Berkeley Lab
Cheuk-Yiu Ng, Iowa State University
Rupert C. Perera, Center for X-Ray Optics, Berkeley Lab
James H. Underwood, Center for X-Ray Optics, Berkeley Lab

ALS STAFF

This is a cumulative list of all those who worked at the ALS during the 2000 calendar year.

MANAGEMENT

D. Chemla
B. Feinberg
Z. Hussain
G. Krebs
J. Krupnick
H. Padmore
N. Smith

ACCELERATOR PHYSICS

J. Byrd
T. Byrne
S. DeSantis
H. Nishimura
G. Portmann
D. Robin
C. Steier
Y. Wu

ADMINISTRATION

J. Crippen
P. Epps
M. Fenner
A. Garland
L. Howard
R. Pepe
S. Rossi

BUDGET

J. Zelver

CONTROLS

A. Biocca
W. Brown, Jr.
E. Domning
K. Fowler
C. Ikami
S. Jacobson
J. McDonald
J. Meng
A. Robb
L. Shalz
J. Spring
R. Steele
C. Timossi
J. Tunis

ENVIRONMENT, HEALTH & SAFETY

R. Baker
G. Perdue
R. Statam

ELECTRICAL ENGINEERING

B. Bailey
M. Balagot
K. Baptiste
W. Barry
M. Bell
R. Benjegerdes
T. Bilstein
K. Bolin
J. Bishop
R. Calston
R. Candelario
M. Chin
J. DeVries
L. Dominguez
J. Elkins
M. Estrema
M. Fahmie
M. Foster
R. Gassaway
R. Gervasoni
A. Geyer
J. Hellmers
M. Hilburn
J. Hinkson
J. Gregor
J. Gregoire
M. Jefferson
L. Jordan
J. Julian
S. Kwiatkowski
E. Lee
A. Lindner
C.C. Lo
P. Molinari
R. Mueller
J. Nomura
F. Ottens
K. Ramos
A. Ritchie
S. Rogoff
D. Sandler
H. Sheid
R. Slater
G. Stover
B. Taylor
R. Thomas
J. Velasco
S. Warner
K. Woolfe

EXPERIMENTAL SYSTEMS

H. Ade
S. Anders
B. Batterman
R. Celestre
S. Fakra
J. Feng
E. Glover
E. Harvey
P. Heimann
M. Howells
S. Irick
D. Kilcoyne
A. Lindenberg
S. Locklin
A. MacDowell
W. McKinney
F. Nolting
H. Ohldag
J. Patel
A. Scholl
J. Spence
B. Sublett
N. Tamura
A. Thompson
A. Warwick
A. Young
W. Jun

MECHANICAL ENGINEERING

J. Akre
J. Allen
N. Andresen
R. Armstrong
W. Baldock
D. Baum
L. Bonifas
D. Calais
D. Cambie
M. Coleman
D. Colomb
J. Comins
C. Corradi
C. Cummings
D. Davis
M. Decool
R. DeMarco
R. Duarte
K. Franck
S. Gavidia
B. Gee
D. Gibson
T. Henderson
A. Hernandez
E. Hoyer
D. Hull
D. Jones
J. Y. Jung
N. Kelez
N. Kellog
S. Klingler
C. Knopf
G. Koehler
M. Kritscher
T. Lauritzen
A. Lim
B. MacDonell
D. MacGill
S. Marks
P. McKean
H. Meyer
V. Moroz
G. Morrison
V. Ngo
W. Oglesby
A. Paterson
R. Patton
J. Pepper
P. Pipersky
D. Plate
K. Rex
R. Schlueter
N. Searls
K. Sihler
T. Stevens
H. Stewart
M. Thomas
W. Thur
E. Wong
R. Zager
J. Zbasnik
F. Zucca

OPERATIONS

D. Bentsen
J. Bishop
D. Brothers
E. Diaz
O. Jones
J. McDonald
R. Miller
M. Monroy
J. Pusina
B. Samuelson
T. Scarvie
S. Stricklin
M. Wolfe

PROCEDURE CENTER

R. Jones

PROJECT MANAGEMENT

A. Catalano
J. Harkins

QUALITY ASSURANCE

E. Lampo

SCIENTIFIC SUPPORT

G. Ackerman
E. Arenholz
H. Bluhm
P. Bogdanov
J. Bozek
S. Canton
Y. D. Chuang
J. Denlinger
A. Fedorov
N. Hamdan
Z. Hasan
H. Hieslmair
S. Kellar
G. Lamble
A. Lanzara
W. Ling
M. Martin
S. McHugo
G. Meigs
E. Rotenberg
B. Rude
D. Sayer
F. Schlachter
B. Sinkovic
W. Stolte
E. Umbach
M. Van Hove
Y. Wang
W. Yang
X. Zhou
X. Zhou
W. Zhu

USER SERVICES

J. Coyne
B. Dixon
S. Fujimura
G. Giangrasso
K. Gonzalez
A. Greiner
D. Hamamoto
C. Hauck
A. Marquez
L. Moxon
R. Pepe
B. Phillips
A. Robinson
L. Tamura
G. Vierra

FACTS AND FIGURES

Using the Advanced Light Source

The ALS, a Department of Energy national user facility, welcomes researchers from universities, industry, and government laboratories. Qualified users have access either as members of participating research teams (PRTs) or as independent investigators. PRTs (groups of researchers with related interests from one or more institutions) construct and operate beamlines and have primary responsibility for experiment endstation equipment. They are entitled to a certain percentage of their beamline's operating time according to the resources contributed by the PRT. Through a peer-reviewed proposal process, the remaining beamtime is granted to independent investigators, who may provide their own endstation or negotiate access to a PRT-owned endstation.

The ALS does not charge users for beam access if their research is non-proprietary. Users performing proprietary research are charged a fee based on full cost recovery for ALS usage. All users are responsible for the day-to-day costs of research (e.g., supplies, phone calls, technical support).

The nominal operating energy of the ALS storage ring is 1.9 GeV, although it can run from 1.0 to 1.9 GeV, allowing flexibility for user operations. At 1.9 GeV, the normal maximum operating current is 400 mA in multibunch operation. The spectral range of undulator and wiggler beamlines extends from photon energies of roughly 5 eV to 21 keV. Bend magnets produce radiation from the infrared to about 20 keV.

The ALS is capable of accommodating approximately 55 beamlines and more than 100 endstations. The first user beamlines began operation in October 1993, and there were 34 operating beamlines, with several more under construction, by the end of 2000.

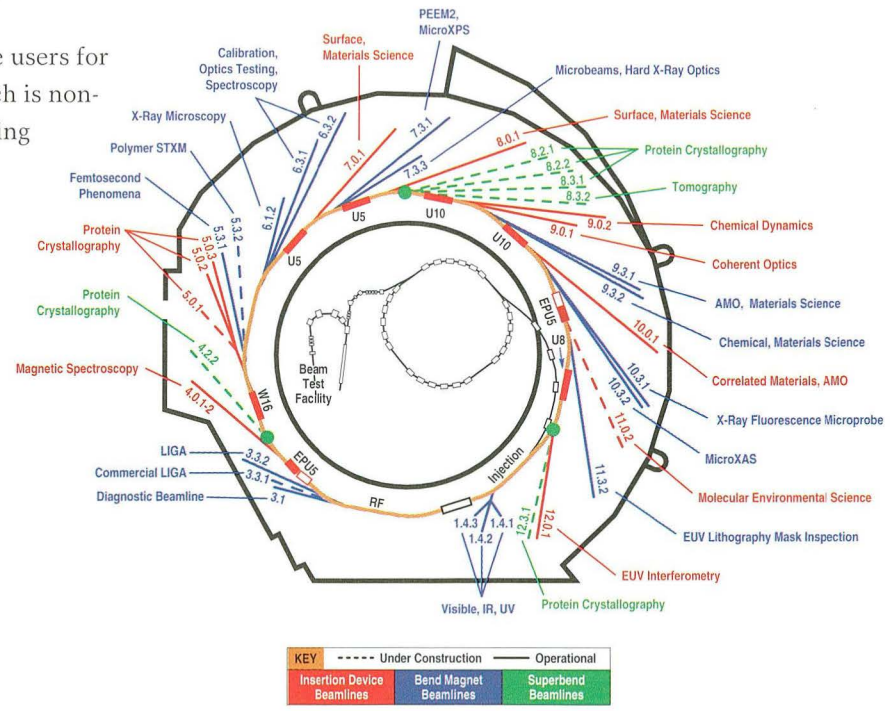

ALS BEAMLINES*

Beamline	Source	Areas of Research/Techniques	Energy Range	Monochromator	Available
BTF	ALS linac	Beam Test Facility	50 MeV (electrons)	None	Now
1.4.1	Bend magnet	Ultraviolet photoluminescence	1.6–6.2 eV	0.5 m single grating	Now
1.4.2	Bend magnet	Visible and infrared Fourier transform spectroscopy (FTIR)	0.002–3 eV (15–25,000 cm–1)	Interferometer	Now
1.4.3	Bend magnet	Infrared spectromicroscopy	0.05–1 eV (550–10,000 cm–1)	Interferometer	Now
3.1	Bend magnet	Diagnostic beamline	200–280 eV	Mirror/filter	Now
3.3.1	Bend magnet	Commercial deep-etch x-ray lithography (LIGA)	3–12 keV	None	2001
3.3.2	Bend magnet	Deep-etch x-ray lithography (LIGA)	1–20 keV	None	Now
4.0.1-2	EPU Elliptical	Magnetic spectroscopy polarization undulator	60–1800 eV	Variable-included-angle PGM	Now
4.2.2	Superbend magnet	Multiple-wavelength anomalous diffraction (MAD) and monochromatic protein crystallography	6–18 keV	Double crystal	2002
5.0.1	W16 Wiggler	Monochromatic protein crystallography	12.4 keV	Curved crystal	2001
5.0.2	W16 Wiggler	MAD and monochromatic protein crystallography	3.5–14 keV	Double crystal	Now
5.0.3	W16 Wiggler	Monochromatic protein crystallography	12.4 keV	Curved crystal	Now
5.3.1	Bend magnet	Femtosecond phenomena	0.1–12 keV	Double crystal	Now
5.3.2	Bend magnet	Polymer scanning transmission x-ray microscopy (STXM)	150–650 eV	SGM	2001
6.1.2	Bend magnet	High-resolution zone-plate microscopy	300–900 eV	Zone-plate linear	Now
6.3.1	Bend magnet	Calibration and standards, EUV/soft x-ray optics testing, solid-state chemistry	500–2000 eV	VLS-PGM	Now
6.3.2	Bend magnet	Calibration and standards; EUV optics testing; atomic, molecular, and materials science	50–1300 eV	VLS-PGM	Now
7.0.1	U5 undulator	Photoelectron spectroscopy and imaging (SPEM)	100–800 eV	SGM	Now
		Absorption-contrast near-edge x-ray absorption fine structure imaging (STXM)	180–900 eV	SGM	Now
		Spin-resolved endstation (SPIN)	60–1200 eV	SGM	Now
		High-resolution, angle-resolved photoelectron spectroscopy (UltraESCA)	60–1200 eV	SGM	Now
		Fluorescence spectroscopy	50–1200 eV	SGM	Now
7.3.1.1	Bend magnet	Magnetic microscopy, spectromicroscopy	175–1500 eV	SGM	Now
7.3.1.2	Bend magnet	Surface and materials science, micro x-ray photoelectron spectroscopy	175–1500 eV	SGM	Now
7.3.3	Bend magnet	Micro-x-ray diffraction, micro-x-ray absorption spectroscopy, hard x-ray optics testing	6–12 keV	White light, two or four crystal	Now
8.0.1	U5 undulator	X-ray photoelectron spectroscopy, angle-resolved photoelectron spectroscopy, near-edge x-ray absorption fine structure spectroscopy (EMA)	65–1400 eV	SGM	Now
		Soft x-ray fluorescence, near-edge x-ray absorption fine structure spectroscopy (SXF)	65–1400 eV	SGM	Now
8.2.1	Superbend magnet	MAD and monochromatic protein crystallography	6–18 keV	Double crystal	2001
8.2.2	Superbend magnet	MAD and monochromatic protein crystallography	6–18 keV	Double crystal	2001
8.3.1	Superbend magnet	MAD and monochromatic protein crystallography	2.4–15 keV	Double crystal	2001
8.3.2	Superbend magnet	Tomography	3–45 keV	Double crystal	2002
9.0.1	U10 undulator	Coherent optics experiments	200–800 eV	None or off-axis zone plate (available 2001)	Now
9.0.2	U10 undulator	Chemical reaction dynamics, photochemistry	5–30 eV	None	Now
		High-resolution photoelectron and photoionization spectroscopy	5–30 eV	Off-plane Eagle	Now
		Photoelectron and photoionization imaging and spectroscopy	5–30 eV	Off-plane Eagle	Now
9.3.1	Bend magnet	Time-of-flight ion mass spectroscopy, ion-ion coincidence measurements	2.2–6 keV	Double crystal	Now
		Time-of-flight photoelectron spectroscopy, electron-electron coincidence measurements	2.2–6 keV	Double crystal	Now
		Ion/anion spectroscopy	2.2–6 keV	Double crystal	Now
		X-ray emission spectroscopy in gases	2.2–6 keV	Double crystal	2002
		Absorption spectroscopy of gases or thin foils	2.2–6 keV	Double crystal	Now

Beamline	Source	Areas of Research/Techniques	Energy Range	Monochromator	Available
9.3.2	Bend magnet	Atomic and electronic structure of surfaces (AMC)	30–1400 eV	SGM	Now
10.0.1	U10 undulator	Photoemission of highly correlated materials (HERS)	17–340 eV	SGM	Now
		High-resolution atomic and molecular electron spectrometer (HiRAMES)	17–340 eV	SGM	Now
		Electron spin polarization analysis (ESP)	17–340 eV	SGM	Now
		Photoionization of ions: cross-section and excitation spectrum Measurements (IPB)	17–340 eV	SGM	Now
10.3.1	Bend magnet	X-ray fluorescence microprobe	3–20 keV	White light multilayer	Now,
10.3.2	Bend magnet	Environmental and materials science, micro x-ray absorption spectroscopy	3–17 keV	White light, four crystal	2001†
11.0.2	EPU5 undulator	Molecular environmental science (wet spectroscopy)	75–2000 eV	Variable-included-angle PGM	2002
		Molecular environmental science (STXM)	180–1000 eV	Variable-included-angle PGM	2002
11.3.2	Bend magnet	Inspection of EUV lithography masks	50–1000 eV	VLS-PGM	Now
12.0.1	U8 undulator	EUV optics testing, interferometry, coherent optics	60–320 eV	VLS-PGM	Now
		EUV optics testing, interferometry, coherent optics	60–320 eV	VLS-PGM	Now
12.3.1	Superbend magnet	MAD protein crystallography and small-angle x-ray scattering (SAXS)	6–18 keV	Double crystal and double multilayer	2002

* This table is valid as of May 2001. The most current information on ALS beamlines is available on the World Wide Web (http://www-als.lbl.gov/als/als_users_bl/bl_table.html).

† Beamline 10.3.2 is being upgraded to provide microXAS capability for environmental and materials science.

ALS INSERTION DEVICE PARAMETERS

Device	Beamline	Status	Energy Range (at 1.5 GeV)	Energy Range (at 1.9 GeV)	Period Length	Number of Periods	Operating Gap Range	Peak Effective Field Range
U5 Undulator	8.0	Operational	130–1900 eV	210–3000 eV	5.0 cm	89	1.4–4.5 cm	0.85–.10 T
U5 Undulator	7.0	Operational	50–1900 eV	80–3000 eV	5.0 cm	89	1.4–4.5 cm	0.85–0.10 T
U8 Undulator	12.0	Operational	18–1200 eV	30–1900 eV	8.0 cm	55	2.5–8.3 cm	0.80–0.07 T
U10 Undulator	9.0	Operational	5–950 eV	8–1500 eV	10.0 cm	43	2.4–11.6 cm	0.98–0.05 T
U10 Undulator	10.0	Operational	8–950 eV	12–1500 eV	10.0 cm	43	2.4–11.6 cm	0.80–0.05 T
EPU5 Elliptical Polarization Undulator	4.0	Operational	60–1000 eV*	100–1500 eV*	5.0 cm	37	1.45–5.5 cm	0.79–0.10 T (vertical field) 0.54–0.10 T (horizontal field)
W16 Wiggler	5.0	Operational	5–13 keV	5–21 keV	16.0 cm	19	1.4–18.0 cm	2.1 T

* Elliptical polarization mode

ALS STORAGE RING PARAMETERS

Parameter	Value
Beam particle	electron
Beam energy	1.0–1.9 GeV
Injection energy	1.0–1.5 GeV
Beam current	
multibunch mode	400 mA
two-bunch mode	2 × 30 mA
Filling pattern (multibunch mode)	276 to 320 bunches possibility of 10-mA "camshaft" bunch in bunch-train gap
Bunch spacing	
multibunch mode	2 ns
two-bunch mode	328 ns
Circumference	196.8 m
Number of straight sections	12
Current number of insertion devices	7
Radio frequency	499.664 MHz
Beam size in straight sections, rms	250 microns horiz. × 28 microns vert. at 1.9 GeV
Natural emittance	5.5 nm-rad at 1.9 GeV
Energy spread (ΔE/E, rms)	8×10^{-4} at 1.9 GeV

Parameter	Value at 1.5 GeV	Value at 1.9 GeV
Beam lifetime		
multibunch mode*	~3.5 hours at 400 mA	~8.0 hours at 400 mA
two-bunch mode	not used	~35 min. at 40 mA
Horizontal emittance	3.5 nm-rad	5.5 nm-rad
Vertical emittance†	0.25 nm-rad	0.2 nm-rad

*In multibunch mode, the storage ring is typically filled every six hours or as requested by our users.
† Vertical emittance is deliberately increased to improve beam lifetime.

2000 PUBLICATIONS

Beamline 1.4

Dodge, J.S., C.P. Weber, J. Corson, J. Orenstein, Z. Schlesinger, J.W. Reiner, and M.R. Beasley, "Low-frequency crossover of the fractional power-law conductivity in $SrRuO_3$," *Phys. Rev. Lett.* **85**(23), 4932–4935 (December 2000).

Geller, J.T., H.-Y. Holman, G. Su, M.E. Conrad, K. Pruess, and J.C. Hunter-Cevera, "Flow dynamics and potential for biodegradation of organic contaminants in fractured rock vadose zones," *J. Contam. Hydrol.* **43**(1), 63–90 (April 2000).

Ghosh, U., R.G. Luthy, J.S. Gillette, and R.N. Zare, "Microscale location, characterization, and association of polycyclic aromatic hydrocarbons on harbor sediment particles," *Environ. Sci. Technol.* **34**(9), 1729–1736 (April 2000).

Gomez-Vega, J.M., E. Saiz, A.P. Tomsia, T. Oku, K. Suganuma, G.W. Marshall, and S.J. Marshall, "Novel bioactive functionally graded coatings on Ti_6Al_4V," *Adv. Mater. Opt. Electr.* **12**(12), 894–898 (June 2000).

Holman, H.N., R. Goth-Goldstein, M. Martin, M.L. Russell, and W.R. McKinney, "Low-dose responses to 2,3,7,8-tetrachlorodibenzo-p-dioxin in single living human cells measured by synchrotron infrared spectromicroscopy," *Environ. Sci. Technol.* **34**(12), 2513–2517 (July 2000).

Holman, H.N., R. Goth-Goldstein, E. Blakely, K. Bjornstad, M. Martin, and W.R. McKinney, "Individual human cell responses to low doses of chemicals studied by synchrotron infrared spectromicroscopy," in *Biomedical Spectroscopy: Vibrational Spectroscopy and Other Novel Techniques*, Proceedings of SPIE Photonics West BiOS 2000 (San Jose, California, January 26, 2000).

Holman, H.N., M.C. Martin, E.A. Blakely, K. Bjornstat, and W.R. McKinney, "IR spectroscopic characteristics of cell cycle and cell death probed by synchrotron radiation based Fourier transform IR spectromicroscopy," *Biopolymers* **57**(6), 329–335 (October 2000).

Martin, M., "How to use a synchrotron for IR microscopy," *Research and Development Magazine* **42**(5), 105 (May 2000).

Zhang, X., T.J. Richardson, J.K. Pugh, and P.N. Ross, "Electrochemical and infrared studies of the reduction of organic carbonates," in *Proceedings of the 198th Meeting of the Electrochemical Society*, (Phoenix, Arizona, October 22–27, 2000).

Beamline 4.0.1

Friedrich, S., T.R. Niedermayr, O.B. Drury, M.F. Cunningham, M. L. Vandenberg, J.N. Ullom, A. Loshak, T. Funk, S. Cramer, J.D. Batteux, E. See, M. Frank, S.E. Labov, et al., "A superconducting detector endstation for high-resolution energy-dispersive SR-XRF," in *Proceedings of 7th International Conference on Synchrotron Radiation Instrumentation (SRI2000)* (Berlin, Germany, August 21–25, 2000).

Kukk, E., J.D. Bozek, T. Thomas, T.X. Carroll, L.J. Saethre, J.A. Sheehy, P.W. Langhoff, and N. Berrah, "New insights into molecular structure and dynamics using soft x-ray electron spectroscopy," in *Proceedings of the 21st International Conference on the Physics of Electronic and Atomic Collisions (ICPEAC-XXI)*(Sendai, Japan, July 21–27,1999).

Snell, G.P., B. Langer, E. Kukk, and N. Berrah, "Spin-resolved auger spectroscopy of xenon," in *Proceedings of the 21st International Conference on the Physics of Electronic and Atomic Collisions (ICPEAC-XXI)* (Sendai, Japan, July 21–27,1999).

Steier, C., G. Portmann, and A. Young, "Commissioning of the first elliptically polarizing undulator at the Advanced Light Source," in *Proceedings of the 7th European Particle Accelerator Conference (EPAC 2000)* (Vienna, Austria, June 26–30, 2000).

Beamline 5.0.2

Bard, J., A.M. Zhelkovsky, S. Helming, T.N. Earnest, C.L. Moore, and A. Bohm, "Structure of yeast poly(A) polymerase alone and in complex with 3'-dATP," *Science* **289**, 1346–1349 (August 2000).

Caruthers, J.M., E. Johnson, and D. McKay, "Crystal structure of yeast initiation factor 4A, a DEAD-box RNA helicase," *Proc. Natl. Acad. Sci. USA* **97**, 13080–13085 (November 2000).

Cramer, P., D.A. Bushnell, J. Fu, A.L. Gnatt, B. Maler-Davis, N.E. Thompson, R.R. Burgess, A.M. Edwards, P.R. David, and R.D. Kornberg, "Architecture of RNA polymerase II and implications for the transcription mechanism," *Science* **288**(566), 640–649 (April 2000).

Daniels, D., C. Mol, A. Arvai, S. Kanugula, A. Pegg, and J.A. Tainer, "Active and alkylated human AGT structures: A novel zinc site, inhibitor and extrahelical base binding," *EMBO J.* **19**(7), 1719–1730 (April 2000).

Eichman, B.F., J.M. Vargason, B.H. Mooers, and P.S. Ho, "The Holliday junction in an inverted repeat DNA sequence: Sequence effects on the structure of four-way junctions," *Proc. Natl. Acad. Sci. USA* **97**(8), 3971–3976 (April 2000).

Eigenbrot, C., M. Dennis, N. Skelton, R. Lazarus, and M.H. Ultsch, "Exosite peptide inhibitors of coagulation factor VII reveal zymogen structure," in *Proceedings of 42nd Annual Meeting of the American Society of Hematology* (San Francisco, California, December 1–5, 2000).

Eigenbrot, C., M. Dennis, N. Skelton, R. Lazarus, and M.H. Ultsch, "Structures of peptide inhibitors with FVII reveal allosteric effect and zymogen structure," in *Proceedings of 42nd Annual Meeting of the American Society of Hematology* (San Francisco, California, December 1–5, 2000).

Endrizzi, J.A., P.T. Beernink, T. Alber, and H. Schachman, "Binding of bisubstrate analog promotes large conformational changes in the unregulated catalytic trimer of aspartate transcarbamoylase: Implications for allosteric regulation," *Proc. Natl. Acad. Sci. USA* **97**(10), 5077–5082 (May 2000).

Erlandsen, H., E. Bjoro, T. Flatmark, and R.C. Stevens, "Crystal structure and site-specific mutagenesis of a pterin-bound human phenylalanine hydroxylase," *Biochemistry–US* **39**(9), 2208–2217 (March 2000).

Fu, D., A.M. Libson, L.J.W. Miercke, C. Weitzman, P.K. Nollert, J. Krucinski, and R.M. Stroud, "Structure of a glycerol conducting channel and the basis for its selectivity," *Science* **290**(5491), 481–486 (October 2000).

Galburt, E., M. Chadsey, B. Chevalie, R. Monnat, and B. Stoddard, "Conformational changes and cleavage by the homing endonuclease I-PpoI: A critical role for a leucine residue in the active site," *J. Mol. Biol.* **300**(4), 877–887 (July 2000).

Garman, S.C., B.A. Wurzburg, S.S. Tarchevskaya, J.-P. Kine, and T.S. Jardetzky, "Structure of the Fc fragment of human IgE bound to its high-affinity receptor FcεRIα," *Nature* **406**(6793) 259–266 (July 2000).

Han, B.-G., W. Nunomura, Y. Takakuwa, N. Mohandas, and B.K. Jap, "Protein 4.1R core domain structure and insights into regulation of cytoskeletal organization," *Nat. Struct. Biol.* **7**(10), 871–875 (October 2000).

Han, B.-G., W. Nunomura, H. Wu, N. Narla, and B.K. Jap, "Crystallization and preliminary x-ray crystallographic analysis of the 30 kDa membrane-binding domain of protein 4.1 from human erythrocytes," *Acta Crystallogr. D* **56**(2), 187–188 (February 2000).

Hanson, M.A., T.K. Oost, C. Sukonpan, D.H. Rich, and R.C. Stevens, "Structure basis for BABIM inhibition of botulinum neurotoxin type B protease," *J. Am. Chem. Soc.* **122**(45), 11268–11269 (November 2000).

Hanson, M., and R.C. Stevens, "Cocrystal structure of synaptobrevin-II to botulinum neurotoxin type B at 2.0 Å resolution," *Nat. Struct. Biol.* **7**(8) 687–692 (August 2000).

Hopfner, K., A. Karcher, D.S. Shin, L. Craig, L.M. Arthur, J.P. Carney, and J.A. Tainer, "Structural biology of Rad50 ATPase: ATP-driven conformational control in DNA double-strand break repair and the ABC-ATPase superfamily," *Cell* **101**, 789–800 (June 2000).

Howard, B.R., J.A. Endrizzi, and S.J. Remington, "Crystal structure of *Escherichia coli* malate synthase G complexed with magnesium and glyoxylate at 2.0 Å resolution: Mechanistic implications," *Biochemistry–US* **39**(11), 3156–3168 (March 2000).

Hung, L.W., E.L. Holbrook, and S.R. Holbrook, "The crystal structure of the Rev binding element of HIV-1 reveals novel base pairing and conformational variability," *Proc. Natl. Acad. Sci. USA* **97**(10), 5107–5112 (May 2000).

Hura, G., J.M. Sorenson, R.M. Glaeser, and T. Head-Gordon, "A high-quality x-ray scattering experiment on liquid water at ambient conditions," *J. Chem. Phys.* **113**(20), 9140–9148 (November 2000).

Jacobson, R.H., A.G. Ladurner, D.S. King, and R. Tjian, "Structure and function of a human $TAF_{II}250$ double bromodomain module," *Science* **288**(5470), 1422–1425 (May 2000).

Juers, D.H., "A structural view of beta-galactosidase in action," Ph.D. thesis, University of Oregon, 2000.

Keck, J.L., D. Roche, S. Lynch, and J.M. Berger, "Structure of the RNA polymerase domain of *E. coli* primase," *Science* **287**(5462), 2482–2486 (March 2000).

Khlebtsova, N., "Structural studies of the PDZ domain of the dishevelled protein," Ph.D. thesis, University of California, Berkeley, 2000.

Khlebtsova, N., L. Hung, R.K. Henderson, R.T. Moon, and T. Earnest, "Expression, crystallization and preliminary x-ray studies of the PDZ domain of Dishevelled protein," *Acta Crystallogr. D* **56**(2), 212–214 (February 2000).

Kim, Y., K.-H. Yoon, Y. Khang, S. Turley, and W.G.J. Hol, "The 2.0 Å crystal structure of cephalosporin acylase," *Structure* **8**, 1059–1068 (October 2000).

Liu, M., B.W. Shen, S. Nakaya, K.P. Pratt, K. Fujikawa, E.W. Davie, B.L. Stoddard, and A.R. Thompson, "Hemophilic factor VIII C1- and C2-domain missense mutations and their modeling to the 1.5-angstrom human C2-domain crystal structure," *Blood* **96**(3), 979–987 (August 2000).

Liu, J., C.L. Smith, D. DeRyckere, K. DeAngelis, G.S. Martin, and J.M. Berger, "Structure and function of Cdc6/Cdc18: Implications for origin recognition and checkpoint control," *Mol. Cell* **6**, 637–648 (September 2000).

Luecke, H., "Atomic resolution structures of bacteriorhodopsin photocycle intermediates: The role of discrete water molecules in the function of this light-driven ion pump," *Biochim. Biophys. Acta* **1460**(1), 133–156 (August 2000).

Luecke, H., B. Schobert, J.P. Cartailler, H.T. Richter, A. Rosengarth, R. Needleman, and J.K. Lanyi, "Coupling photoisomerization of retinal to directional transport in bacteriorhodopsin," *J. Mol. Biol.* **300**(5), 1239–1257 (July 2000).

Minor, D.L., Y.-F. Lin, B.C. Mobley, A. Avelar, Y.N. Jan, L.Y. Jan, and J.M. Berger, "The polar T1 interface is linked to conformational changes that open the voltage-gated potassium channel," *Cell* **102**, 657–670 (September 2000).

Mundorff, E., "Conformational effects in biological catalysis: An antibody catalyzed oxy-cope rearrangement," *Biochemistry–US* **39**(4), 627–632 (February 2000).

Parikh, S.S., "Structural and chemical biology of DNA glycosylases for base-excision repair," Ph.D. thesis, The Scripps Research Institute, 2000.

Rice, L.M., T.N. Earnest, and A.T. Brunger, "Single-wavelength anomalous diffraction phasing revisited," *Acta Crystallogr. D* **56**(11), 1413–1420 (November 2000).

Rosengarth, A.A., and H. Luecke, "Crystallization and preliminary x-ray analysis of full-length annexin I comprising the core and N-terminal domain," *Acta Crystallogr. D* **56**(11), 1459–1461 (November 2000).

Segelke, B.W., M.P. Forstner, M.S. Knapp, S.D. Trakhanov, S.S. Parkin, Y.M. Newhouse, H.D. Bellamy, K.H. Weisgraber, and B. Rupp, "Conformational flexibility in the apolipoprotein E amino-terminal domain structure determined from three new crystal forms: Implication for lipid binding," *Protein Sci.* **9**(5), 886–897 (May 2000).

Sorenson, J.M., G. Hura, R.M. Glaeser, and T. Head-Gordon, "What can x-ray scattering tell us about the radial distribution functions of water?," *J. Chem. Phys.* **113**(20), 9149-9161 (November 2000).

Sousa, M.C., C.B. Trame, H. Tsuruta, S. Wilbanks, V. Reddy, and D. McKay, "Crystal and solution structures of an HslUV protease-chaperone complex," *Cell* **103**, 633-643 (November 2000).

Sussman, D.R., J. Nix, and C. Wilson, "The structural basis for molecular recognition by the vitamin B12 RNA aptamer," *Nat. Struct. Biol.* **7**(1), 53-57 (January 2000).

Suto, R.K., M.J. Clarkson, D.J. Tremethick, and K. Luger, "Crystal structure of a nucleosome core particle containing the variant histone H2A.Z," *Nat. Struct. Biol.* **7**(12), 1121-1124 (December 2000).

van den Akker, F., X. Zhang, M. Miyagi, X. Huo, K.S. Misono, and V.C. Yee, "Structure of the dimerized hormone-binding domain of guanylyl-cyclase-coupled receptor," *Nature* **406**(6791), 101-104 (July 2000).

Beamline 6.1.2

Denbeaux, G., L.E. Johnson, and W. Meyer-Ilse, "Spectromicroscopy at the XM-1," in *X-Ray Microscopy: Proceedings of the Sixth International Conference*, edited by W. Meyer-Ilse, T. Warwick, and D. Attwood, AIP Conference Proceedings Vol. 507 (Berkeley, California, August 2-6, 1999).

Eimüller, T., R. Kalchgruber, P. Fischer, G. Schütz, P. Guttmann, G. Schmahl, M. Köhler, K. Prügl, F. Bammes, T. Schweinböck, and G. Bayreuther, "Quantative imaging of magnetization reversal in FeGd multilayers by magnetic transmission x-ray microscopy," *J. Appl. Phys.* **87**(9), 6478-6480 (May 2000).

Ford, T.W., W. Meyer-Ilse, and A.D. Stead, "Development and evaluation of cryo-imaging of unicellular algae using soft x-ray transmission microscopy: Ultrastructure and elemental analysis," in *X-Ray Microscopy: Proceedings of the Sixth International Conference*, edited by W. Meyer-Ilse, T. Warwick, and D. Attwood, AIP Conference Proceedings Vol. 507 (Berkeley, California, August 2-6, 1999).

Johnson, L.E., G. Denbeaux, and W. Meyer-Ilse, "High spatial resolution x-ray spectroscopy with the XM-1 x-ray microscope," in *Synchrotron Radiation Instrumentation: Eleventh U.S. National Conference*, edited by P. Pianetta, J. Arthur, and S. Brennan, AIP Conference Proceedings Vol. 521 (Stanford, California, 2000), pp. 35-38.

Kurtis, K.E., P.J.M. Monteiro, J.T. Brown, and W. Meyer-Ilse, "Transmission soft x-ray microscopy study of chemical additives used to control alkali-silica reaction gel expansion," in *X-Ray Microscopy: Proceedings of the Sixth International Conference*, edited by W. Meyer-Ilse, T. Warwick, and D. Attwood, AIP Conference Proceedings Vol. 507 (Berkeley, California, August 2-6, 1999).

Larabell, C.A., D. Yager, and W. Meyer-Ilse, "Localization of proteins and nucleic acids using soft x-ray microscopy," in *X-Ray Microscopy: Proceedings of the Sixth International Conference*, edited by W. Meyer-Ilse, T. Warwick, and D. Attwood, AIP Conference Proceedings Vol. 507 (Berkeley, California, August 2-6, 1999).

Larabell, C.A., D. Yager, W. Meyer-Ilse, and B. Rowning, "From dynamics to details: Live-cell light microscopy and high resolution (25 nm) soft x-ray microscopy," *Microsc. Microanal.* **6**(Suppl. 2), 84-85 (Summer 2000).

Loo, B.W., "Quantitative characterization of the protein contents of the exocrine pancreatic acinar cell by soft x-ray microscopy and advanced digital imaging methods," Ph.D. thesis, University of California, San Francisco, 2000.

Loo, B.W., W. Meyer-Ilse, and S. Rothman, "Automatic image acquisition, calibration and montage assembly for biological x-ray microscopy," *J. Microsc.-Oxford* **197**(2), 185-201 (February 2000).

Meyer-Ilse, W., G. Denbeaux, L.E. Johnson, W. Bates, A. Lucero, and E. Anderson, "The high resolution x-ray microscope, XM-1," in *X-Ray Microscopy: Proceedings of the Sixth International Conference*, edited by W. Meyer-Ilse, T. Warwick, and D. Attwood, AIP Conference Proceedings Vol. 507 (Berkeley, California, August 2-6, 1999).

Meyer-Ilse, W., D. Hamamoto, A. Nair, S.A. Lelièvre, G. Denbeaux, L. Johnson, A. Lucero, D. Yager, M.A. LeGros, and C.A Larabell, "High resolution protein localization using soft x-ray microscopy," *J. Microscopy* **201**(3), 395 (2001).

Meyer-Ilse, W., L.E. Johnson, G. Denbeaux, W.A. Bates, A. Lucero, and E.H. Anderson, "The XM-1 high resolution x-ray microscope at the Advanced Light Source," in *Synchrotron Radiation Instrumentation: Eleventh U.S. National Conference*, edited by P. Pianetta, J. Arthur, and S. Brennan, AIP Conference Proceedings Vol. 521 (Stanford, California, 2000), pp. 13–18.

Moronne, M.M., D.J. Hamamoto, L.E. Johnson, G.P. Denbeaux, and W. Meyer-Ilse, "Potential application of vanadium probes for biological x-ray microscopy," in *X-Ray Microscopy: Proceedings of the Sixth International Conference*, edited by W. Meyer-Ilse, T. Warwick, and D. Attwood, AIP Conference Proceedings Vol. 507 (Berkeley, California, August 2–6, 1999).

Beamline 6.3.2

Gota, S., M. Gautier-Soyer, and M. Sacchi, "Fe 2p absorption in magnetic oxides: Quantifying angular dependent saturation effects," *Phys. Rev. B* **62**(7), 4187–4190 (August 2000).

Grush, M.M., C.R. Horne, R.C.C. Perera, D.L. Ederer, S.P. Cramer, E.J. Cairns, and T.A. Callcott, "Correlation electronic structure with cycling performance of substituted $LiMn_2O_4$ electrode materials: A study using the techniques of soft x-ray absorption and emission," *Chem. Mater.* **12**(3), 659–664 (March 2000).

Hamad, K., "X-ray and photoelectron spectroscopy of the structure, reactivity, and electronic structure of semiconductor nanocrystals," Ph.D. thesis, University of California, Berkeley, 2000.

Kortright, J., and S. Kim, "Resonant magneto-optical properties of Fe near its 2p levels: Measurement and applications," *Phys. Rev. B* **62**(18), 12216–12228 (November 2000).

Lawniczak-Jablonska, K., T. Suski, I. Gorczyca, N.E. Christensen, K.E. Attenkofer, R.C.C. Perera, E.M. Gullikson, J.H. Underwood, D.L. Ederer, and Z. Liliental-Weber, "Electronic states in valence and conduction bands of group-III nitrides: Experiment and theory," *Phys. Rev. B* **61**(24), 16623–16632 (June 2000).

Mirone, A., M. Sacchi, and S. Gota-Goldmann, "Ligand-field atomic-multiplet calculations for arbitrary symmetry," *Phys. Rev. B* **61**(20), 13540–13544 (May 2000).

Pu, N.-W., "Picosecond ultrasonic characterization of Mo/Si multilayers for extreme ultraviolet lithography," Ph.D. thesis, University of California, Berkeley, 2000.

Robinson, A.L., "Berkeley Lab's ALS generates femtosecond synchrotron radiation," *CERN Courier* **40**(6), 31–32 (July 2000).

Sacchi, M., "Resonant magnetic scattering of polarized soft x-rays," *Surf. Rev. Lett.* **7**(1–2), 175–189 (Spring 2000).

Schoenlein, R.W., S. Chattopadhyay, H.H.W. Chong, T.E. Glover, P.A. Heimann, C.V. Shank, A. Zholents, and M. Zolotorev, "Generation of femtosecond pulses of synchrotron radiation," *Science* **287**(5461), 2237–2240 (March 2000).

Schoenlein, R.W., S. Chattopadhyay, H.H.W. Chong, T.E. Glover, P.A. Heimann, C.V. Shank, A. Zholents, and M. Zolotorev, "Generation of x-ray pulses via laser-electron beam interaction," *Appl. Phys. B–Photo.* **71**(1), 1–10 (July 2000).

Schoenlein, R.E., H. Chong, T.E. Glover, P. Heimann, C.V. Shank, A.A. Zholents, and M. Zolotorev, "Femtosecond x-ray pulses from a synchrotron," in *Ultrafast Phenomena XII*, Vol. 66, edited by T. Elsaesser, S. Mukamel, M.M. Murnane, and N.F. Scherer (Springer-Verlag, Berlin, 2000), pp. 271–275.

Schoenlein, R.W., and A.L. Robinson, "Femtosecond synchrotron radiation pulses generated in the ALS storage ring," *Synchrotron Radiation News* **13**(4), 28–32 (July 2000).

Stearns, D.G., and E.M. Gullikson, "Nonspecular scattering from extreme ultraviolet multilayer coatings," *Physica B* **283**(1–3), 84–91 (June 2000).

Takenaka, H., Y. Muramatsu, S. Hayashi, H. Ito, Y. Ueno, N. Moriya, E. Gullikson, and R.C.C. Perera, "Soft x-ray reflectivity and structure evaluation of Ni/Ti and Ni–N/Ti–N multilayers," in *X-ray Microscopy: Proceedings of the Sixth International Conference*, (Berkeley, California, August 2–6, 1999).

Wedowski, M., S. Bajt, J.A. Folta, P.A. Kearney, C. Montcalm, E.A. Spiller, E.M. Gullikson, and J.H. Underwood, "High-precision reflectometry of multilayer coatings for extreme ultraviolet lithography," in *The International Society for Optical Engineering*

Emerging Lithography, Proceedings of SPIE Conference (Santa Clara, California, February 27–March 2, 2000).

Beamline 7.0.1

Butorin, S., J.-H. Guo, N. Wassdahl, and J.E. Nordgren, "The character of doped holes in $La_{1.9}Sr_{0.1}CuO_4$: Polarization-dependent x-ray fluorescence study at the O K-edge," *J. Phys.–Condens. Mat.* **12**(28), 463–470 (July 2000).

Butorin, S., J.-H. Guo, N. Wassdahl, and J.E. Nordgren, "Tunable-excitation soft x-ray fluorescence spectroscopy of high-T_c superconductors: An inequivalent-site seeing story," *J. Electron Spectrosc.* **110–111**, 235–273 (October 2000).

Choi, H.J., E. Rotenberg, R.K. Kawakami, U. Bovensiepen, J.H. Wolfe, N.V. Smith, and Z.Q. Qiu, "Effect of interfacial roughness on the phase of quantum well states in Cu/Co(001) and Cu/Ni(001) systems," *Phys. Rev. B* **62**, 6561 (January 2000).

Denlinger, J.D., G.-H. Gweon, J.W. Allen, C.G. Olson, Y. Dalichaouch, B.W. Lee, M.B. Maple, P.C. Canfield, and P.A. Armstrong, "Advances in photoemission spectroscopy of f-electron materials," *Physica B* **281**, 716–722 (June 2000).

Eisebitt, S., and W. Eberhardt, "Band structure information and resonant inelastic soft x-ray scattering in broad band solids," *J. Electron Spectrosc.* **110**(1–3), 335–358 (October 2000).

Guo, J.-H., S. Butorin, N. Wassdahl, P.I. Skytt, J.E. Nordgren, Y. Ma, P. Berastegut, and L.-G. Johansson, "Electronic structure of $YBa_2Cu_3O_x$ and $YBa_2Cu_4O_8$ studied by soft-x-ray absorption and emission spectroscopies," *Phys. Rev. B* **61**(13), 9140–9144 (April 2000).

Guo, J.-H., and J.E. Nordgren, "Resonant C Kα x-ray emission of some carbon allotropes and organic compounds," *J. Electron Spectrosc.* **110–111**, 105–134 (October 2000).

Guo, J.-H., P.I. Skytt, N. Wassdahl, and J.E. Nordgren, "In-situ and ex-situ characterization of thin films by soft x-ray emission spectroscopy," *J. Electron Spectrosc.* **110–111**, 41–67 (October 2000).

Kortright, J.B., S. Kim, H. Ohldag, G. Meigs, and T. Warwick, "Magnetization imaging using scanning transmission x-ray microscopy," in *X-ray Microscopy: Proceedings of the Sixth International Conference* (Berkeley, California, August 2–6,1999).

Mankefors, S., P.-O. Nilsson, J. Kanski, T. Andersson, K. Karlsson, A. Agui, C. Såthe, J.-H. Guo, and J.E. Nordgren, "A theoretical investigation of the thickness dependence of soft x-ray emission from thin AlAs(100) layers buried in GaAs," *Phys. Rev. B* **61**(8) 5540–5545 (February 2000).

Moore, D.P., O. Ozturk, F.O. Schumann, S.A. Morton, and G.D. Waddill, "Ultrathin vanadium films on Cu(001): Structure and magnetism," *Surf. Sci.* **449**, 31–42 (March 2000).

Nordgren, J.E., and J.-H. Guo, "Instrumentation for soft x-ray emission spectroscopy," *J. Electron Spectrosc.* **110–111**, 1–13 (October 2000).

Rotenberg, E., J.H. Schaefer, and S.D. Kevan, "Coupling between adsorbate vibrations and an electronic surface state," *Phys. Rev. Lett.* **84**(13), 2925–2928 (March 2000).

Rotenberg, E., W. Theis, K. Horn, and P. Gille, "Quasicrystalline valence bands in decagonal AlNiCo," *Nature* **406**(6796), 602–605 (August 2000).

Saleem, F., "Characterization of thin film by soft x-ray spectroscopy," master's thesis, Uppsala University, 2000.

Schumann, F.O., and J.G. Tobin, "Magnetic properties of Fe-based alloys," *J. Appl. Phys.* **87**(9), 5460–5462 (May 2000).

Schumann, F.O., R.F. Willis, K.W. Goodman, and J.G. Tobin, "Surface-sensitive, element-specific magnetometry with x-ray linear dichroism," *J. Vac. Sci. Technol. A* **18**(4), 1259–1263 (July 2000).

Seal, S., T. Warwick, N. Sobczak, and J. Morgiel, "A scanning photoemission microscope (SPEM) to study the interface chemistry of AlTi/C system," *J. Mater. Sci. Lett.* **19**, 123–126 (January 2000).

Urquhart, S.G., H. Ade, M. Rafailovich, J.S. Sokolov, and Y. Zhang, "Chemical and vibronic effects in the high-resolution near-edge x-ray absorption fine structure spectra of polystyrene isotopomers," *Chem. Phys. Lett.* **322**(5), 412–418 (May 2000).

Xu, S.H., M. Keeffe, Y. Yang, C. Chen, M. Yu, G.J. Lapeyre, E. Rotenberg, J. Denlinger, and J.T. Yates, Jr., "Photoelectron diffraction imaging for C_2H_2 and C_2H_4 chemisorbed on Si(100) reveals a new bonding configuration," *Phys. Rev. Lett.* **84**(5), 939–942 (January 2000).

Zhang, Z.D., H.J. Choi, R.K. Kawakami, E.J. Escorcia-Aparicio, M.O. Bowen, J.H. Wolfe, E. Rotenberg, N.V. Smith, and Z. Qiu, "Magnetic interlayer coupling between Co films across $Cu/Ni_{30}Cu_{70}/Cu(100)$ doubling quantum wells," *Phys. Rev. B* **61**(1), 76–79 (January 2000).

Beamline 7.3.1

Nolting, F., A. Scholl, J. Stöhr, J.W. Seo, J. Fompeyrine, H. Siegwart, J.-P. Locquet, S. Anders, J.M. Luning, E.E. Fullerton, M.F. Toney, M.R. Scheinfein, H.A. Padmore, et al., "Direct observation of the alignment of ferromagnetic spins by antiferromagnetic spins," *Nature* **405**, 767–769 (June 2000).

Scholl, A., "Antiferromagnetism: Taking a very close look at magnetic structures," *Science* **288**(5472), 1762–1763 (June 2000).

Scholl, A., F. Nolting, J. Stöhr, J.M. Lüning, J.W. Seo, J.-P. Locquet, J. Fompeyri, S. Anders, H. Ohldag, and H.A. Padmore, "Studies of the magnetic structure at the ferromagnet-antiferromagnet interface," in *Proceedings of the 11th International Conference on X-ray Absorption Fine Structure* (Ako, Japan, July 26–31, 2000).

Scholl, A., J. Stöhr, J. Lüning, J.-P. Locquet, J. Fompeyrine, J.W. Seo, H. Siegwart, F. Nolting, S. Anders, and E. Fullerton, "Observation of antiferromagnetic domains in epitaxial thin films," *Science* **287**(5455), 1014–1016 (February 2000).

Slep, D., J. Asselta, M.A. Raffailovich, J. Sokolov, D.A. Winsett, A.P. Smith, H. Ade, and S. Anders, "Effect of an interactive surface on the equilibrium contact angles in bilayer polymer films," *Langmuir* **16**(5), 2369–2375 (March 2000).

Thomas, L., J. Lüning, J. Stöhr, S.S.P. Parkin, A. Scholl, F. Nolting, and S. Anders, "Oscillatory decay of magnetization induced by domain-wall stray fields," *Phys. Rev. Lett.* **84**(15), 3462–3465 (April 2000).

Beamline 7.3.3

Glaeser, R. , M. Facciotti, P. Wailian, S. Rouhani, J. Holton, A. MacDowell, R. Celestre, D. Cambie, and H.A. Padmore, "Characterization of conditions required for x-ray diffraction experiments with protein microcrystals," *Biophys. J.* **78**(6), 3178–3185 (June 2000).

Heimann, P.A., T. Missalla, A.M. Lindenberg, I. Kang, S. Johnson, Z. Chang, H.C. Kapteyn, R.W. Lee, R.W. Falcone, R.E. Schoenlein, T.E. Glover, A.A. Zholents, M. Zolotorev, and H.A. Padmore, "Time-resolved x-ray photoabsorption and diffraction on timescales from ns to fs," in *Proceedings of the 11th U.S. National Synchrotron Radiation Instrumentation Conference (SRI'99)* (Stanford, California, October 13–15,1999).

Hura, G., J.M. Sorenson, R.M. Glaeser, and T. Head-Gordon, "A high-quality x-ray scattering experiment on liquid water at ambient conditions," *J. Chem. Phys.* **113**(20), 9140–9148 (November 2000).

Lindenberg, A.M., I. Kang, S.L. Johnson, T. Missalla, P.A. Heimann, Z. Chang, J. Larson, P.H. Bucksbaum, H.C. Kapteyn, H.A. Padmore, R.W. Lee, J.S. Wark, and R.W. Falcone, "Time-resolved x-ray diffraction from coherent phonons during a laser-induced phase transition," *Phys. Rev. Lett.* **84**(1), 111–114 (January 2000).

MacDowell, A., R.S. Celestre, N. Tamura, R. Spolenak, B.C. Valek, W.L. Brown, J.C. Bravman, H.A. Padmore, B.W. Batterman, and J.R. Patel, "Submicron x-ray diffraction," in *Proceedings of 7th International Conference on Synchrotron Radiation Instrumentation (SRI2000)* (Berlin, Germany, August 21–25, 2000).

Sorenson, J.M., G. Hura, R.M. Glaeser, and T. Head-Gordon, "What can x-ray scattering tell us about the radial distribution functions of water?," *J. Chem. Phys.* **113**(20), 9149–9161 (November 2000).

Spolenak, R., D.L. Barr, M.E. Gross, K. Evans-Lutherodt, W.L. Brown, N. Tamura, A.A. MacDowell, R.S. Celestre, H.A. Padmore, J.R. Patel, B.C. Valek, J.C. Bravman, P. Flinn, T. Marieb, R.R. Keller, B.W. Batterman, et al., "Microtexture and strain in electroplated copper interconnects," in *Proceedings of the Materials Research Society Symposium* (San Francisco, California, April 24–28, 2000).

Tamura, N., B.C. Valek, R. Spolenak, A. MacDowell, R.S. Celestre, H.A. Padmore, W.L. Brown, T. Marieb, J.C. Bravman, B.W. Batterman, J.R. Patel, et al., "Grain orientation and strain measurements in submicron wide passivated individual aluminum test structures," in *Proceedings of the Materials Research Society Symposium* (San Francisco, California, April 24-28, 2000).

Beamline 8.0.1

Carlisle, J.A., S.R. Blankenship, L.T. Terminello, J.J. Jia, T.A. Callcott, D.L. Ederer, R.C.C. Perera, and F.J. Himpsel, "Crystal-momentum-resolved electron structure of solids using resonant soft x-ray fluorescence spectroscopy," *J. Electron Spectrosc.* **110–111**, 323-334 (October 2000).

Ederer, D.L., A. Moewes, E.Z. Kurmaev, T.A. Callcott, M.M. Grush, S. Stadler, R.P. Winarski, R.C.C. Perera, and L.J. Terminello, "Resonant raman scattering in Nd_2O_3 and the electronic structure of Sr_2RuO_4 studied by synchrotron radiation excitation," *J. Phys. Chem. Solids* **61**(3), 435-444 (March 2000).

Eich, D., "Untersuchungen zu elektronischen Volumen- und Grenzflaecheneigenschaften von II-VI-Verbindungshalbleitern mittels Roentgenspektroskopien," Ph.D. thesis, University of Würzburg, 2000.

Eich, D., "X-ray emission spectroscopy of beryllium chalcogenides," Ph.D. thesis, University of Würzburg, 2000.

Eich, D., U. Herber, U. Groth, U. Stahl, C. Heske, M. Marsi, M.P. Kiskinova, W. Riedl, R.H. Fink, and E. Umbach, "Lateral inhomogeneities of Cu(In,Ga)Se_2 absorber films," *Thin Solid Films* **361**, 258-262 (February 2000).

Föhlisch, A., P. Bennich, J. Hasselström, O. Karis, A. Nilsson, M. Nyberg, L. Triguero, and L.G.M. Pettersson, "Ground state interpretation of x-ray emission spectroscopy on adsorbates: CO adsorbed on Cu(100)," *Phys. Rev. B* **16**, 16229-16240 (Spring 2000).

Föhlisch, A., P. Bennich, J. Hasselström, O. Karis, A. Nilsson, M. Nyberg, L. Triguero, and L.G.M. Pettersson, "How CO bonds to metals," *J. Chem. Phys.* **112**, 1946-1960 (Spring 2000).

Föhlisch, A., J. Hasselström, O. Karis, A. Nilsson, M. Nyberg, L. Triguero, and L.G.M. Pettersson, "How CO adsorbs in different sites," *Phys. Rev. Lett.* **85**, 3309-3312 (Spring 2000).

Galakhov, V.R., L.D. Finkelstein, E.Z. Kurmaev, D.A. Zatsepin, A.A. Samokhvalov, S.V. Naumov, G.K. Tatarinova, M. Demeter, S. Bartkowski, M. Neumann, and A.P. Moewes, "Interaction of Cu 3d and O 2p states in $Mg_{1-x}Cu_xO$-solid solutions with the NaCl-structure: X-ray photoelectron and x-ray emission study," *Phys. Rev. B* **62**(8), 4922-4927 (August 2000).

Hart, G.L.W., W.E. Pickett, E.Z. Kurmaev, D. Hartmann, M. Neumann, A. Moewes, D.L. Ederer, R. Endo, T. Tanigushi, and S. Nagata, "Electronic structure of $Cu_{1-x}Ni_xRh_2S_4$ and $CuRh_2Se_4$: Band structure calculations, x-ray photoemission and fluorescence measurements," *Phys. Rev. B* **61**(6), 4230-4237 (February 2000).

Hellwig, O., J. B. Kortright, K. Takano, and E.E. Fullerton, "Switching behavior of Fe-Pt/Ni-Fe exchange-spring films studied by resonant soft x-ray magneto-optical Kerr effect," *Phys. Rev. B* **62**(17), 11694-11698 (November 2000).

Heske, C., D. Eich, U. Groh, R. Fink, E. Umbach, T. van Buuren, C. Bostedt, N. Franco, L.J. Terminello, M.M. Grush, et al., "Semiquantitative and non-destructive analysis of impurities at a buried interface: Na and the CdS/Cu(In,Ga)Se_2 heterojunction," *Surf. Interface Anal.* **30**(1), 459-463 (September 2000).

Heske, C., D. Eich, U. Groh, R. Fink, E. Umbach, A. Van Buuren, C.F.O. Bostedt, N. Franco Cerame, L.J. Terminello, M.M. Grush, T.A. Callcott, F.J. Himpsel, D.L. Ederer, R.C.C. Perera, W. Riedl, and F. Karg, "Self-limitation of Na content at the CdS/Cu(In,Ga)Se_2 solar cell heterojunction," *Thin Solid Films* **361**, 360-363 (February 2000).

Kakar, S., A.J. Nelson, R. Treusch, C. Heske, A. Van Buuren, I. Jimenez, P. Pagoria, and L.J. Terminello, "Electronic structure of energetic material 1,3,5-triamino-2,4,6-trinitrobenzene," *Phys. Rev. B* **62**(23), 15666-15672 (December 2000).

Karis, O., J. Hasselström, N. Wassdahl, M.G. Weinelt, A. Nilsson, M. Nyberg, L.G.M. Pettersson, J. Stöhr, and M.G. Samant, "The bonding of simple carboxylic acids on Cu(110)," *J. Chem. Phys.* **112**, 8146-8159 (Spring 2000).

Kurmaev, E.Z., V.R. Galakhov, A. Moewes, S. Shimada, K. Endo, S.S. Turner, P. Day, R.N. Lyubovskaya, D.L. Ederer, and M. Iwami, "Electronic structure of molecular superconductors containing paramagnetic 3d ions," *Physica B* **62**(17), 11380–11383 (November 2000).

Kurmaev, E.Z., V.R. Galakhov, S. Shimada, T. Otsuka, K. Endo, S. Stadler, D.L. Ederer, A. Moewes, H. Schuermann, and M. Neumann, "Soft x-ray fluorescence study of the quasi-one-dimensional Heisenberg antiferromagnet tetraphenylverdazyl," *Phys. Rev. B* **62**(23), 15660–15665 (December 2000).

Kurmaev, E.Z., A.P. Moewes, V.R. Galakhov, D.L. Ederer, and T. Koybayashi, "Ion-implantation effects in Al_2O_3: X-ray fluorescence measurements," *Nucl. Instrum. Meth. B* **168**, 395–398 (June 2000).

Kurmaev, E.Z., R.P. Winarski, J.C. Pivin, D.L. Ederer, S.N. Shamin, A.P. Moewes, K. Endo, T. Ida, G.S. Chang, and C.N. Whang, "Chemical reactions in polymers induced by ion beam mixing: Fluorescence x-ray measurements," *J. Electron Spectrosc.* **110**, 87–103 (October 2000).

Lörgen, M., "Coherent soft x-ray scattering from layered magnetic systems," master's thesis, RWTH Aachen/Forschungszentrum Jülich, 2000.

Moewes, A.P., E.Z. Kurmaev, D.L. Ederer, and T.A. Callcott, "No multiatom resonances observed in x-ray fluorescence," *Phys. Rev. B* **62**(23), 15427–15430 (December 2000).

Moewes, A.P., A.V. Postnikov, E.Z. Kurmaev, M.M. Grush, and D.L. Ederer, "Mixing of widely separated intermediate states and charge transfer at the 4d–4f resonance of La compounds," *Europhys. Lett.* **49**(5), 665–671 (March 2000).

Moewes, A.P., S. Stadler, R.P. Winarski, D.L. Ederer, and T.A. Callcott, "Soft x-ray scattering dominates emission near the giant resonance of the rare earth compounds," *J. Electron Spectrosc.* **110–111**, 189–196 (October 2000).

Muramatsu, Y., M. Grush, and R.C. Perera, "Resonant elastic x-ray scattering of graphite and diamond at the carbon K threshold," *Phys. Rev. B* **61**(4), 2393–2396 (January 2000).

Muramatsu, Y., S. Hirono, S. Umemura, T. Hayashi, and R.C.C. Perera, "Spectral features in C K x-ray emission and absorption spectra of amorphous carbon films," *Adv. X-Ray Anal.* **31**, 99–108 (January 2000).

Muramatsu, Y., H. Takenaka, Y. Ueno, E.M. Gullikson, and R.C.C. Perera, "Chemical bonding state analysis of silicon carbide layers in Mo/SiC/Si multilayer mirrors by soft x-ray emission and absorption spectroscopy," *Appl. Phys. Lett.* **77**(17), 2653–2655 (October 2000).

Muramatsu, Y., Y. Ueno, T. Hayashi, M.M. Grush, E.M. Gullikson, and R.C.C. Perera, "Soft x-ray emission and absorption spectroscopy of hydrofullerene," *J. Electron Spectrosc.* **107**(2), 177–184 (May 2000).

Muramatsu, Y., Y. Ueno, S. Hirono, S. Umemura, T. Hayashi, M.M. Grush, E.M. Gullikson, and R.C.C. Perera, "High-resolution soft x-ray emission and absorption spectra of amorphous carbon films measured using highly brilliant synchrotron radiation," in *5th International Conference on the Application of Diamond Films and Related Materials*, Proceedings of Applied Diamond Conference/ Frontier Carbon Technology Joint Conference 1999 (Tsukuba, Japan, August 31–September 3, 1999).

Nyberg, M., J. Hasselström, O. Karis, N. Wassdahl, M.G. Weinelt, A. Nilsson, and L.G.M. Pettersson, "The electronic structure and surface chemistry of glycine adsorbed on Cu(110)," *J. Chem. Phys.* **112**, 5420–5430 (Spring 2000).

Postnikov, A.V., B. Schneider, M. Neumann, D. Hartmann, H. Hesse, A. Moewes, E.Z. Kurmaev, and M. Matteucci, "Combined study for $KNbO_3$ and $KTaO_3$ by different techniques of photoelectron and x-ray emission spectroscopy," *J. Phys. Chem. Solids* **61**(2), 265–269 (February 2000).

Shirley, E., "Core and final-state excitonic effects and resonant inelastic x-ray scattering in s–p bonded solids," *J. Phys. Chem. Solids* **61**(3), 445–447 (March 2000).

Stadler, S., R.P. Winarski, J.M. McLaren, D.L. Ederer, J. van Ek, A.P. Moewes, M.M. Grush, T.A. Callcott, and R.C.C. Perera, "Electronic structures of the tungsten borides WB, W_2B, and W_2B_5," *J. Electron Spectrosc.* **110**, 75–86 (October 2000).

Stichler, M., C. Keller, C. Heske, M. Staufer, U. Birkenheuer, N. Roesch, W. Wurth, and D. Menzel, "X-ray emission spectroscopy of NO adsorbates on Ru(001)," *Surf. Sci.* **448**(2–3), 164–178 (March 2000).

Ueno, Y., and Y. Muramatsu, "Direct observation of benzene and pyridine molecules adsorbed in microporous carbon using synchrotron-radiation-excited soft x-ray emission spectroscopy," *Carbon* **38**(14), 1939–1942 (October 2000).

Ueno, Y., Y. Muramatsu, M.M. Grush, and R.C.C. Perera, "Configurations of benzene and pyridine molecules adsorbed on graphitic surface of microporous carbon," *J. Phys. Chem. B* **104**(30), 7154–7162 (August 2000).

Winarski, R.P., T. Eskildsen, S. Stadler, J. van Ek, D.L. Ederer, E.Z. Kurmaev, M.M. Grush, T.A. Callcott, and A.P. Moewes, "The effects of boron impurities on the atomic bonding and electronic stucture of Ni_3Al," *J. Electron Spectrosc.* **110**, 69–74 (October 2000).

Beamline 9.0.2

Ahmed, M., D. Peterka, and A.G. Suits, "H abstraction dynamics in crossed-beam velocity map imaging: Cl + $CH_3OH \rightarrow CH_2OH$ + HCl," *Chem. Phys. Lett.* **317**(3-5), 264–268 (February 2000).

Ahmed, M., D.S. Peterka, and A.G. Suits, "Imaging H abstraction dynamics in crossed molecular beams: Cl + ROH reactions," *Phys. Chem. Chem. Phys.* **2**(4), 861–868 (July 2000).

Baer, T., Y. Song, C.Y. Ng, J. Liu, and W. Chen, "Pulsed field ionization-phototelectron photoion coincidence spectroscopy with synchrotron radiation: The heat of formation of the $C_2H_5^+$ ion," *Faraday Discuss.* **115**, 137–145 (July 2000).

Baer, T., Y. Song, C.Y. Ng, J. Liu, and W. Chen, "The heat of formation of $C_3H_7^+$ and proton affinity of C_3H_6 determined by pulsed field ionization-photoelectron photoion coincidence spectroscopy," *J. Phys. Chem. A* **104**(9), 1959–1964 (March 2000).

Forde, N.R., L.J. Butler, B.M. Ruscic, O. Sorkhabi, F. Qi, and A.G. Suits, "Characterization of nitrogen-containing radical products from the photodissociation of trimethylamine using photoionization detection," *J. Chem. Phys.* **113**(8), 3088–3097 (August 2000).

Jarvis, G., R.C. Shiell, J. Hepburn, Y. Song, and C.Y. Ng, "Pulsed field ionization-photoion spectroscopy using two-bunch synchrotron radiation: Time-of-flight selection scheme," *Rev. Sci. Instrum.* **71**(3), 1325–1331 (March 2000).

Liu, J., W. Chen, C.-W. Hsu, M. Hochlaf, M.D. Evans, S.L. Stimson, and C.Y. Ng, "High resolution pulsed field ionization-photoelectron study of $CO_2^+(X^2\Pi_g)$ in the energy range of 13.6–14.7 eV," *J. Chem. Phys.* **112**(24), 10767–10777 (June 2000).

McGivern, W.S., O. Sorkhabi, A.H. Rizvi, A.G. Suits, and S.W. North, "Photofragment translational spectroscopy with state-selective 'Universal Detection': The ultraviolet photodissociation of CS_2," *J. Chem. Phys.* **112**(12), 5301–5307 (March 2000).

McGivern, W.S., O. Sorkhabi, A.G. Suits, A. Derecskei-Kovacs, and S.W. North, "Primary and secondary processes in the photodissociation of $CHBr_3$," *J. Phys. Chem. A* **104**(45), 10085–10091 (November 2000).

Mueller, J.A., J.L. Miller, L.J. Butler, F. Qi, O. Sorkhabi, and A.G. Suits, "Internal energy dependence of the H + Allene/H + propyne product branching from the unimolecular dissociation of 2-propenyl radicals," *J. Phys. Chem. A* **104**(48), 11261–11264 (December 2000).

Ng, C.Y., "Advances in photoionization and photoelectron studies using third generation synchrotron radiation," *J. Electron Spectrosc.* **108**(1-3), 41–45 (July 2000).

Ng, C.Y., "Advances in photoionization and photoelectron studies using third generation synchrotron radiation and UV/VUV lasers," in *Photoionization and Photodetachment*, edited by C.Y. Ng, Advanced Series in Physical Chemistry Vol. 10 (World Scientific, Singapore, 2000) pp. 394–538.

Qi, F., O. Sorkhabi, and A.G. Suits, "Evidence of triplet ethylene produced from photodissociation of ethylene sulfide," *J. Chem. Phys.* **112**(24), 10707–10710 (June 2000).

Song, Y., M.D. Evans, C.Y. Ng, C.-W. Hsu, and G.K. Jarvis, "Rotationally resolved pulsed-field ionization photoelectron bands for $O_2^+(A\ ^2\Pi_u, \upsilon^+ = 0\text{–}12)$ in the energy range of 17.0–18.2 eV," *J. Chem. Phys.* **112**(3), 1271–1278 (January 2000).

Song, Y., M.D. Evans, C.Y. Ng, C.-W. Hsu, and G.K. Jarvis, "Rotationally resolved pulsed-field ionization photoelectron bands for $O_2^+(a\ ^4\Pi_u, \upsilon^+ = 0\text{–}18)$ in the energy range of 16.0–18.0 eV," *J. Chem. Phys.* **112**(3), 1306–1315 (January 2000).

Yencha, A.J., M.C. Lopes, G.C. King, M. Hochlaf, Y. Song, and C. Ng, "Ion-pair formation observed in a pulsed-field ionization photoelectron spectroscopic study of HF," *Faraday Discuss.* **115**, 335–362 (June 2000).

Zou, P., W.S. McGivern, O. Sorkhabi, A.G. Suits, and S.W. North, "Quantum yields and energy partitioning in the ultraviolet photodissociation of 1,2 dibromo-tetrafluoroethane (Halon-2402)," *J. Chem. Phys.* **113**(17), 7149–7157 (November 2000).

Beamline 9.3.1

Doerner, R., V. Mergel, O. Jagutzki, L. Spielberger, J.H. Ullrich, R. Moshammer, and H. Schmidt-Böcking, "Cold target recoil ion momentum spectroscopy: A 'momentum microscope' to view atomic collision dynamics," *Phys. Rep.* **330**(2–3), 96–192 (June 2000).

Lindle, D.W., O.A. Hemmers, H. Wang, P. Focke, I.A. Sellin, J.D. Mills, J.A. Sheedy, and P.W. Langhoff, "Beyond the dipole approximation: Angular-distribution effects in the 1s photoemission from small molecules," in *Proceedings of the 21st International Conference on the Physics of Electronic and Atomic Collisions (ICPEAC-XXI)* (Sendai, Japan, July 21–27,1999).

Ulagappan, N., and H. Frei, "Mechanistic study of CO_2 photoreduction in Ti silicalite molecular sieve by FT-IR spectroscopy," *J. Phys. Chem. A* **104**(33), 7834–7839 (August 2000).

Beamline 9.3.2

Kortright, J., S. Kim, and H. Ohldag, "Sigmalike phase and nanoscale segregation in polycrystalline Fe_xCr_{1-x} films: An element-resolved magnetic and structural study," *Phys. Rev. B* **61**(1), 64–67 (January 2000).

Wilson, K.R., J.G. Tobin, A.L. Ankudinov, J.J. Rehr, and R.J. Saykally, "Extended x-ray absorption fine structure from hydrogen atoms in water," *Phys. Rev. Lett.* **85**(20), 4289–4292 (November 2000).

Ynzunza, R., H. Daimon, J. Palomares, E.D. Tober, Z. Wang, F.J. Garcia de Abajo, J. Morais, R. Denecke, J. Kortright, Z. Hussain, M.A. Van Hove, and C.S. Fadley, "Circular dichroism in core photoelectron emission from (1×1) oxygen on W(110): Experiment and multiple-scattering theory," *J. Electron Spectrosc.* **106**(1), 7–28 (January 2000).

Beamline 10.0.1

Berrah, N., "High-resolution angle-resolved studies of atoms and molecules using advanced electron spectroscopy at the ALS," in *Photoionization and Photodetachment*, Advanced Series in Physical Chemistry Vol. 10B (World Scientific Publishing, Singapore, 2000).

Bogdanov, P.V., A. Lanzara, S.A. Kellar, X.J. Zhou, E.D. Lu, W.J. Zheng, G. Gu, Z. Hussain, Z.-X. Shen, et al., "Evidence for an energy scale for quasiparticle dispersion in $Bi_2Sr_2CaCu_2O_8$," *Phys. Rev. Lett.* **85**(12), 2581–2584 (September 2000).

Børve, K.J., L.J. Saethre, T.D. Thomas, T.X. Carroll, N. Berrah, J.D. Bozek, and E. Kukk, "Vibronic structure in the carbon 1s photoelectron spectra of HCCH and DCCD," *Phys. Rev. A* **63**(012506), 1–14 (December 2000).

Canton, S.E., A.A. Wills, T.W. Gorczyca, M.F. Wiedenhoeft, O.Y. Nayandin, C.-N. Liu, and N. Berrah, "Mirroring doubly excited resonances in argon," *Phys. Rev. Lett.* **85**(15), 3113–3116 (October 2000).

Carroll, T.X., J. Hahne, T.D. Thomas, L.J. Saethre, N. Berrah, J. Bozek, and E. Kukk, "Carbon 1s core-hole lifetime in CO_2," *Phys. Rev. A* **61**(042503), 2503 (April 2000).

Cheng, W.T., E. Kukk, D. Cubaynes, J. Chang, G. Snell, J.D. Bozek, F.J. Wuilleumier, and N. Berrah, "Measurements and calculations of high-angular-momentum satellite transitions in Li 1s photoionization," *Phys. Rev. A* **62**(6) 1–9 (December 2000).

Derevianko, A., O. Hemmers, S.C. Oblad, P. Glans, H. Wang, S.B. Whitfield, R. Wehlitz, I.A. Sellin, W.R. Johnson, and D.W. Lindle, "Electric-octupole and pure-electric-quadrupole effects in soft-x-ray photoemission," *Phys. Rev. Lett.* **84**(10), 2116–2119 (March 2000).

Diehl, S., D. Cubaynes, H.L. Zhou, L. VoKy, F.J. Wuilleumier, E.T. Kennedy, J.M. Bizau, S.T.

Manson, T.J. Morgan, C.P. Blancard, N. Berrah, and J.D. Bozek, "Angle-resolved photoelectron spectrometry studies of the autoionization of the $2s^2 2p^2 P$ triply excited state of atomic lithium: Experimental results and R-Matrix calculations," *Phys. Rev. Lett.* **84**(8), 1677–1680 (February 2000).

Jaecks, D.H., O. Yenen, K.W. McLaughlin, and M.M. Sant Anna, "Using angular momentum sharing in atoms as a way to quantify relativistic electron–electron interactions in atoms," in *Proceedings of 31st Annual Meeting of the Division of Atomic, Molecular, and Optical Physics of the American Physical Society* (Storr, Connecticut, June 14–17, 2000).

Kukk, E., J.D. Bozek, and N. Berrah, "Angular distribution of the sulphur 2p photoemission in OCS: Variations revealed by molecular field splitting," *J. Phys. B–At. Mol. Opt.* **33**(1), 51–57 (January 2000).

Kukk, E., J.D. Bozek, and N. Berrah, "Photoexcitation and Auger decay of the Renner–Teller split C $1s^{-1}\pi^*_u$ state in CO_2," *Phys. Rev. A* **62**(032708), 2708 (September 2000).

Kukk, E., J.D. Bozek, N. Berrah, J.A. Sheehy, and P.W. Langhoff, "Angular distributions of molecular-field and spin-orbit split core levels of sulfur 2p photoemission in OCS: A sensitive probe of the molecular environment," *J. Phys. B–At. Mol. Opt.* **33**(1), 51–57 (January 2000).

McLaughlin, K.W., O. Yenen, and D.H. Jaecks, "A complete determination of photoelectron partial wave probabilities by polarization analysis of the fluorescence from an excited photoion," in *Proceedings of 31st Annual Meeting of the Division of Atomic, Molecular, and Optical Physics of the American Physical Society* (Storr, Connecticut, June 14–17, 2000).

Morin, P., M. Simon, C. Morin, N. Leclercq, E. Kukk, and N. Berrah, "Role of bending in the dissociation selective resonant inner-shell excitation as observed in CO_2," *Phys. Rev. A* **61**(050701), 1–4 (May 2000).

Snell, G., E. Kukk, B. Langer, and N. Berrah, "Angular distribution measurements of the xenon $N_{4,5}O_{2,3}O_{2,3}$ Auger electrons: Determination of alignment and intrinsic parameters," *Phys. Rev. A* **61**(042749), 324–329 (March 2000).

Snell, G., B. Langer, E. Kukk, and N. Berrah, "Spin-resolved Auger spectroscopy of Xenon," in *Proceedings of the 21st International Conference on the Physics of Electronic and Atomic Collisions (ICPEAC-XXI)* (Sendai, Japan, July 21–27,1999).

Snell, G.P., J. Viefhaus, F.B. Dunning, and N. Berrah, "Microsphere plate detectors used with a compact Mott polarimeter for time-of-flight studies," *Rev. Sci. Instrum.* **71**(6), 2608–2609 (June 2000).

Yenen, O., D.H. Jaecks, K.W. McLaughlin, and G. Snell, "Four reflector VUV quarter-wave retarder of the Beamline 10.0.1.2 of the Advanced Light Source to study angular momentum sharing in atoms," in *Proceedings of 31st Annual Meeting of the Division of Atomic, Molecular, and Optical Physics of the American Physical Society* (Storr, Connecticut, June 14–17, 2000).

Yoshida, T., M. Nakamura, A. Ino, T. Mizakawa, A. Fujimori, X.J. Zhou, S.A. Kellar, P.V. Bogdanov, E. Lu, A. Lanzara, H. Eisaki, Z. Hussain, Z.-X. Shen, T. Kakeshita, S. Uchida et al., "Nodal spectral weight and Fermi surface in $La_{2-x}Sr_xCuO_4$," *Int. J. Mod. Phys. B* **14**(29–31), 3777–3782 (December 2000).

Beamline 10.3.1

Flink, C. et al., "Out-diffusion and precipitation of copper in silicon: An electrostatic model," *Phys. Rev. Lett.* **85**, 4900 (2000).

Jones, S.D., "A characterization and assessment of the bioavailability of lead and other heavy metals in an Oakland contaminated soil," master's thesis, University of California, Berkeley, 2000.

McHugo, S., C. Flink, A.J. Mohammed, A.C. Thompson, and B. Lai, "Elemental and chemical identification of sub-micron metal precipitates in silicon using synchrotron-based x-rays," in *Proceedings of 129th Annual TMS Conference* (Nashville, Tennessee, March 12–16, 2000).

McHugo, S., A.C. Thompson, C. Flink, E.R. Weber, G.M. Lamble, R.F. Gunion, A.A. MacDowell, R. Celestre, H.A. Padmore, and Z. Hussain, "Synchrotron-based impurity mapping," *J. Cryst. Growth* **210**(1–3), 395–400 (March 2000).

Beamline 10.3.2

Manceau, A., B. Lanson, M. Schlegel, M. Musso, J.L. Hazemann, D. Chateigner, and G.M. Lamble, "Quantitative Zn speciation in smelter-contaminated soils by EXAFS spectroscopy," *Am. J. Sci.* **300**, 289–343 (June 2000).

Shin, N.S., "Theoretical detection limits of synchrotron radiation excited total reflection x-ray fluorescence analysis for silicon wafers," Ph.D. thesis, Pohang University of Science and Technology, 2000.

Beamline 12.0.1

Chang, C., P. Naulleau, E. Anderson, and D. Attwood, "Spatial coherence characterization of undulator radiation," *Opt. Commun.* **182**(1–3), 25–34 (August 2000).

Goldberg, K.A., and P. Naulleau, "In situ alignment system for phase-shifting point-diffraction interferometry," U.S. Patent No. 6,118,535 (September 12, 2000).

Goldberg, K., P. Naulleau, P. Batson, P. Denham, J. Bokor, and H.N. Chapman, "EUV interferometry of a four-mirror ring field EUV optical system," in *The International Society for Optical Engineering, Emerging Lithography,* Proceedings of the SPIE Conference (Santa Clara, California, February 27–March 2, 2000).

Naulleau, P., and K. Goldberg, "Dual domain phase-shifting point diffraction interferometer," U.S. Patent No. 6,100,978 (August 8, 2000).

Naulleau, P., and K. Goldberg, "Null test Fourier domain alignment technique for phase-shifting point diffraction interferometer," U.S. Patent No. 6,111,646 (August 29, 2000).

Naulleau, P., K. Goldberg, S. Lee, C. Chang, D. Attwood, and J. Bokor, "The EUV phase-shifting point diffraction interferometer," in *Proceedings of the 11th U.S. National Synchrotron Radiation Instrumentation Conference (SRI'99)* (Stanford, California, October 13–15,1999).

Naulleau, P., K. Goldberg, S. Lee, C. Chang, P. Batson, D. Attwood, and J. Bokor, "The PS/PDI: A high accuracy development tool for diffraction limited short-wavelength optics," in *X-Ray Microscopy: Proceedings of the Sixth International Conference*, edited by W. Meyer-Ilse, T. Warwick, and D. Attwood, AIP Conference Proceedings Vol. 507 (Berkeley, California, August 2–6, 1999).

Accelerator Physics

Byrd, J., K. Baptiste, S. De Santis, S. Kosta, C.C. Lo, D. Plate, R.A. Rimmer, M. Franks, et al., "Design of a higher harmonic rf system for the Advanced Light Source," *Nucl. Instrum. Meth. A* **439**(1), 15–25 (January 2000).

Byrd, J.M., S. De Santis, M. Georgsson, G. Stover, J.D. Fox, and D. Teytelman, "Commissioning of a higher harmonic rf system for the Advanced Light Source," *Nucl. Instrum. Meth. A* **455**(2), 271–282 (December 2000).

Console, F., S. De Santis, et al., "Measurement of the longitudinal impedance of a coaxial cavity coupled with a circular pipe through slots," in *Proceedings of the 7th European Particle Accelerator Conference (EPAC 2000)*, (Vienna, Austria, June 26–30, 2000).

De Santis, S., and A. Mostacci, "Analytical calculation of the power dissipated in the LHC liner," in *Proceedings of the U.S. Workshop on Broadband Impedance Measurement and Modeling*, (Stanford, California, February 28–March 2, 2000).

Rimmer, R.A., J.M. Byrd, and D. Li, "Comparison of calculated, measured and beam sampled impedances of a HOM-damped rf cavity," *Phys. Rev. ST Accel. Beams* **3**(102001), 1–9 (October 2000).

Robin, D., C. Steier, J. Laskar, and L.S. Nadolski, "Global dynamics of the Advanced Light Source revealed through experimental frequency map analysis," *Phys. Rev. Lett.* **85**(3), 558–561 (July 2000).

Robin, D., C. Steier, J. Safranek, and W. Decking, "Enhanced performance of the Advanced Light Source through periodicity restoration of the linear lattice," in *Proceedings of the 7th European Particle Accelerator Conference (EPAC 2000)* (Vienna, Austria, June 26–30, 2000).

Steier, C., J. Byrd, and P.M. Kuske, "Energy calibration of the electron beam of the Advanced Light Source using resonant depolarization," in

Proceedings of the 7th European Particle Accelerator Conference (EPAC 2000) (Vienna, Austria, June 26–30, 2000).

Steier, C., and D. Robin, "Fully coupled analysis of orbit response matrices at the Advanced Light Source," in *Proceedings of the 7th European Particle Accelerator Conference (EPAC 2000)*, (Vienna, Austria, June 26–30, 2000).

Steier, C., D. Robin, J. Laskar, and L.S. Nadolski, "Lattice model calibration and frequency map measurements at the Advanced Light Source," in *Proceedings of the 7th European Particle Accelerator Conference (EPAC 2000)* (Vienna, Austria, June 26–30, 2000).

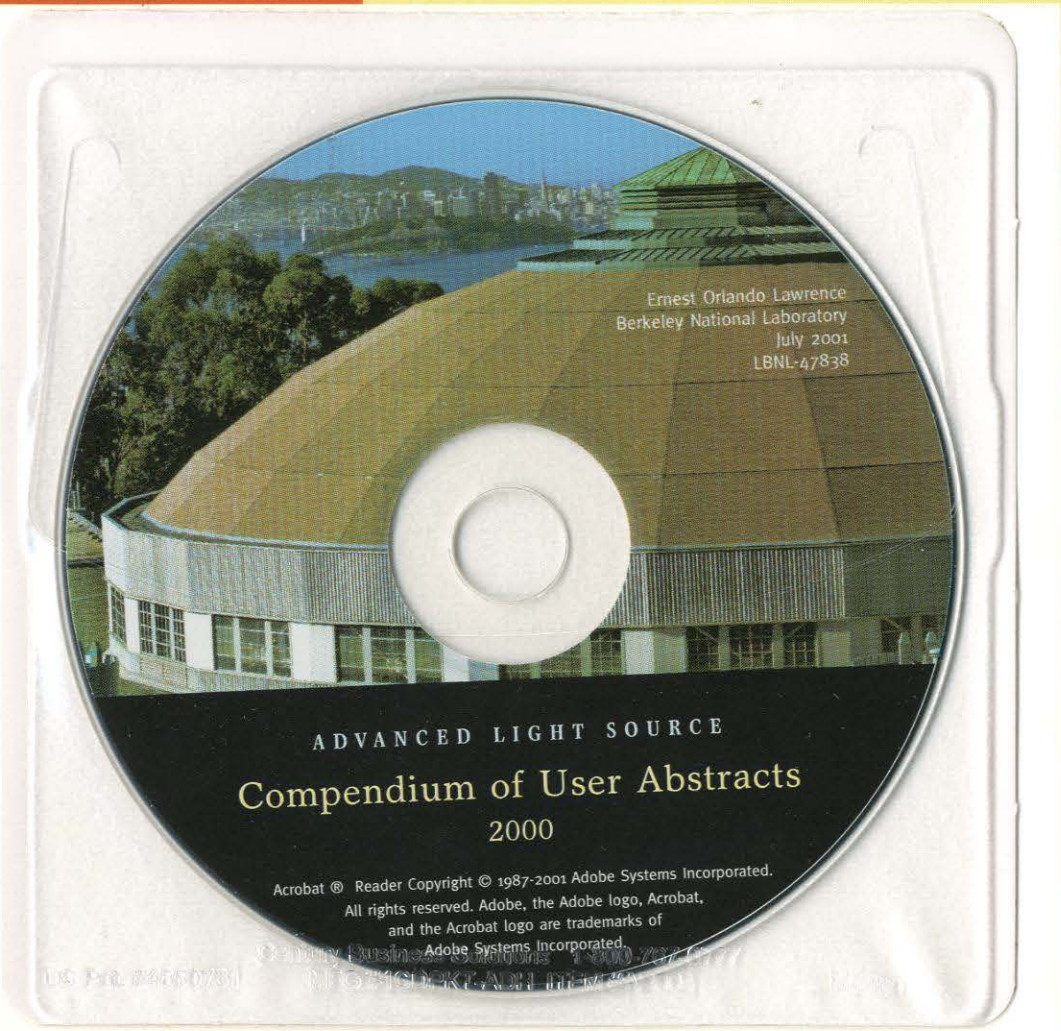

FOR INFORMATION ABOUT USING THE ALS, CONTACT:

Gary Krebs, User Services Group Leader
Advanced Light Source
Lawrence Berkeley National Laboratory
MS 6-2100, Berkeley, CA 94720
Tel: (510) 486-7727 Fax: (510) 486-4773
Email: gfkrebs@lbl.gov

FOR ALL OTHER INFORMATION CONCERNING THE ALS, CONTACT:

Bernadette Dixon, User Services Office Manager
Advanced Light Source
Lawrence Berkeley National Laboratory
MS 6-2100, Berkeley, CA 94720
Tel: (510) 486-6722 Fax: (510) 486-4773
Email: alsuser@lbl.gov

ALS HOME PAGE:

www-als.lbl.gov

ERNEST ORLANDO LAWRENCE BERKELEY NATIONAL LABORATORY
UNIVERSITY OF CALIFORNIA · BERKELEY, CALIFORNIA, 94720